SUBMITTED AS FINAL REPORT
NSG 3008, WAYNE STATE UNIV

SQT

Name: Stephen G. Borders
Major: Mechanical Engineering
Degree: Doctor of Philosophy
Date of Graduation: .....

Approved by: David Orne
Date of Approval: 10-16-79

DETERMINATION OF IN VIVO MECHANICAL PROPERTIES OF LONG BONES FROM THEIR IMPEDANCE RESPONSE CURVES

The mechanical properties of a bone are a good indicator of the health and condition of that bone, and possibly of the skeletal system as a whole. Among the better correlated mechanical properties to bone condition are stiffness properties. However, no clinical method is currently available to measure such properties noninvasively.

The long bones of the forearm and leg are the most accessible for mechanical testing. Hence, many investigators have concentrated their efforts on these bones. Various approaches have been taken involving either ultrasonics or impedance testing.

One such impedance method was developed by Thompson[1]. However, more developement is needed before this method is suitable for routine use in a clinical setting. Much of that needed developement work is presented.

A mathematical model of the vibrating forearm and leg systems is developed. Briefly, the model consists of a uniform, linear, visco-elastic, Euler-Bernoulli beam to represent the ulna or tibia of the vibrating forearm or leg system. The skin and tissue compressed between the probe and bone is represented

by a spring in series with the beam. The remaining skin and tissue surrounding the bone is represented by a visco-elastic foundation with mass.

An extensive parametric study is carried out to determine the effect of each parameter of the mathematical model on its impedance response. Two accomplishments are obtained as a result of the study. First, an increased understanding of the effects of the parameters is gained. Second, many qualitative relationships between the parameters and the characteristics of the impedance curve are derived.

A systems identification algorithm is developed, and programmed on a digital computer, to determine the parametric values of the mathematical model which best simulate the data obtained from an impedance test. The algorithm is based on minimizing the error function; a function similar in form to that of a least-squares method.

Due to the complexity of the impedance equations of the mathematical model, the error function is very nonlinear with respect to its parameters. Consequently, the system of equations obtained from a least-squares approach, is virtually impossible to solve. Hence, an iterative procedure is developed which involves the calculation of a change in each parameter which brings that parameter closer to its correct value. To start the iteration procedure, an initial guess for each parametric value is obtained using the relationships derived in the parametric study.

Data from several groups of impedance tests and experiments have been made available through personal communication with Ames Research Center. Among them are (1) *in vitro* monkey

experiments, (2) nonbiological tests, (3) Thompson's origional *in vivo*, human tests, and (4) more recent *in vivo* monkey tests.

The *in vitro* monkey experiments involve the measurement of impedance of a monkey forearm in several stages as the ulna is being excised. The mathematical model is shown to be a good representation of the physical system by using it in its appropriate form to simulate the whole set of experiments with a consistent set of parametric values. The nonbiological tests involve the measurement of impedance of two systems: a "rigid" mass and an aluminum beam. These "known" systems give an indication of the accuracy of the impedance method. The use of the computer program is demonstrated by applying it to the *in vivo* human and monkey data.

Several recommendations are given. Additional *in vitro* experiments are suggested to further understand the support conditions of the forearm and leg systems. Improvements to the testing procedure are also suggested.

The impedance testing procedure, with the recommendations taken into account, promises to be a very useful clinical tool for measuring mechanical properties of bones.

---

[1] Thompson, G. A., 1973, "*In Vivo* Determination of Bone Properties from Mechanical Impedance Measurement," abstract in Aerospace Medical Association Annual Science Meeting, Las Vegas, pp. 133-134.

DETERMINATION OF *IN VIVO* MECHANICAL PROPERTIES OF LONG BONES FROM THEIR IMPEDANCE RESPONSE CURVES

by

Stephen G. Borders

A DISSERTATION

Submitted to the Office for Graduate Studies,
Graduate Division of Wayne State University,
Detroit, Michigan
in partial fulfillment of the requirements
for the degree of

DOCTOR OF PHILOSOPHY
1979

MAJOR: MECHANICAL ENGINEERING

APPROVED BY:

David Ormsby 10-16-79
Adviser Date

Richard T.

Harry O. Hale

Paul Weiss

ACKNOWLEDGEMENTS

I would like to thank the numerous people who helped and supported me in this work. Special thanks are due to the following people.

To my advisor, Dr. David Orne, for his many hours spent in directing and supporting me.

To the members of my committee: Drs. Harry Hale, Richard Cheng and Paul Weiss.

To Dr. Donald Young, Mr. Wayne Howard and the other people at Ames Research Center for their cooperation in supplying most of the experimental data. (This work was partially supported by NASA Grant NSG-2008.)

To Kent Petersen, then a graduate student at Stanford University, for his hospitality during my visit to Ames Research Center and Stanford University.

To Sue Kulik and Ann Borders for their many hours of typing this manuscript into the computer terminal.

To my wife, Ann Borders, for her loving support and for the many, many hours of proofreading.

To my colleague, Ken Opellia, for his help in using the word processing program, *FORMAT.

To my colleague, Dan Bozek, for our many helpful, informal discussions.

And most of all, to my Lord and Savior, Jesus Christ.

LIST OF ABBREVIATIONS

BMC	bone mineral content
BMD	bone mineral density
DPMI	driving-point mechanical impedance
ERS	equivalent rotational spring
MTS	materials testing system
SDOFO	single-degree-of-freedom oscillator
SIDA	systems identification algorithm
4PM	four parameter model
6PM	six parameter model

TABLE OF CONTENTS

LIST OF TABLES

Table

LIST OF FIGURES

CHAPTER I

INTRODUCTION

A. FORWARD

1. The Need for Measurement of Bone Properties

Numerous recent studies have centered on the noninvasive measurement of mechanical properties of bones *in vivo*. Many different approaches have been taken such as impedance methods and ultrasonic methods. Some of these approaches will be discussed in Sections I.D and I.E. Most of these studies have been concerned with various kinds of stiffness measurements; usually either modulus of elasticity (E) of the material of a bone or the bending stiffness (EI) of a whole bone. These stiffness measurements have many clinical applications. Among them are the detection and the measurement of the degree of deterioration resulting from osteoporosis and other bone diseases and the measurement of the degree of fracture healing. However, relationships between stiffness measurements and bone disorders must be known to make the stiffness measurements applicable. These relationships and their clinical applications will be discussed in Section I.C. Before this discussion, however, a brief review of anatomy is appropriate.

B. ANATOMY

1. The Skeleton

The skeleton is the set of bones which form the internal framework of the body. The functions of the bones are given by Rowe (1972) as follows:

> 1. The outward form of the human body depends on the shape and size of the bones, which are the main supporting structures for other body tissues, particularly the muscles.
> 2. Some parts of the skeleton protect the vital organs; for example the bones of the cranium protect the brain and the thoracic cage protects the heart, lungs, liver and spleen.
> 3. By means of the leverage obtained through the articulation of the bones with one another at their joints, the muscles are enabled to carry out movements, including locomotion.
> 4. The calcium contained in the bones not only strengthens them against stresses and strains but also serves as a reserve from which it may be withdrawn into the blood stream should the need arise.
> 5. The red marrow contained in cancellous bone is the tissue from which red and some of the white blood cells are developed.

The skeletal system must be maintained so that these functions can operate. Many diseases are associated with the deterioration of the bones, inducing adverse effects on their functions.

Bone, like other tissues, consists of living cells and non-living intercellular substance. However, the intercellular substance (or matrix) in bone tissue, unlike other tissues, is calcified. Calcium salts impregnate the cement substance of the matrix thus giving bone its rigidity. Many bone diseases result in a loss of these calcium salts and hence a loss of bone

rigidity.

There are basically four types of bones, characterized by their size and shape: long, short, flat and irregular. Many of these bones have been studied from a variety of different points of view, in terms of monitoring bone integrity. The long bones in the limbs of the body, however, are of greatest interest for noninvasive mechanical testing. Their accessibility simplifies testing procedures and their beamlike form facilitates mathematical modeling.

2. Long Bones

The following four definitions are conventional among anatomists. The term arm refers to the portion of the upper limb between the shoulder and elbow, while the term forearm refers to the portion between the elbow and wrist. The term thigh refers to the portion of the lower limb between the hip and knee, while the term leg refers to the portion between the knee and ankle.

The bones of the arm and forearm, shown in Figure 1.1a, are the humerus, ulna and radius. Note the closeness of the ulna to the outer surface of the forearm. Little or no tissue lies between the skin and the ulna over most of its length. Thus the construction of the forearm makes the ulna conducive to noninvasive mechanical testing.

The bones of the thigh and leg, shown in Figure 1.1b, are the femur, patella (knee cap), tibia and fibula. The tibia, like the ulna, is close to the outer surface and is also suitable for noninvasive mechanical testing.

C. CLINICAL APPLICATIONS OF STIFFNESS MEASURING TECHNIQUES

1. Bone Disease

"Osteoporosis is the term used to describe a group of diseases of diverse etiology which are characterized by a reduction in the mass of bone per unit volume to a level below that required for adequate mechanical support function." (Krane, 1977). Osteoporosis results in a loss of bone strength due to the loss of bone material. Although osteoporosis is a very common metabolic disorder, often associated with other disorders, the etiology in most cases is not known. Two of the most common types of osteoporosis are disuse osteoporosis and senile osteoporosis.

Disuse osteoporosis results from a lack of stress applied to a bone. The type and degree of stress applied to a bone significantly affects the remodeling of bone. Remodeling of the bone is the continuous lifelong process of the formation and resorption of bone material. A lack of stress applied to the bone can result in a decrease of bone material (i.e., resorption will exceed formation).

Disuse osteoporosis occurs in paralytics and bedridden patients with diseases not related to the skeletal system. Many studies have been done on the effects of immobility, some as old as thirty years, e.g., Deitrick, Whedon and Shorr (1948).

Bone mineral losses have also been found to occur in astronauts after an extended period of time in a weightless

environment. The changes in calcium are clearest in the 84-day Skylab mission, see Whedon et al. (1976). Urinary calcium excretion was monitored and measurements of bone mineral content (BMC) were taken of several bones. Urinary calcium excretion increased steadily during the first few weeks in flight, and leveled off at about double the value observed during the preflight control period, with no suggestion of decline toward the end of the flight. A maximal loss of 7.9 per cent in BMC was observed in the os calcis while the radius and ulna did not change measurably. Among the implications expressed by Whedon et al. (1977) is the following:

> Since mineral is lost differentially in greater total amounts from trabecular areas of bone, one must consider the possibility that in very long space flights local area losses of mineral of a degree equivalent to osteoporosis, visible by ordinary X-ray would take place and that the strength of critical bones would be endangered.

Hence, during longer space flights such as a flight to Mars (1.5 to 3 years duration), significant changes are expected to occur in the long bones such as the radius or ulna and particularly in the weight bearing tibia.

Whedon et al. (1977) also points out that "urinary calcium inflight increased steadily to a plateau in virtually the same pattern and degree as previously seen in bedrest studies." Hence, one would expect that results from such studies are a good indication of the effect of weightlessness. Ongoing investigations are being conducted to study this effect over long periods of restraint (six months or more). See Young and Tremor (1978).

Senile osteoporosis is an osteoporosis associated with aging. Although the exact mechanisms which act to induce this

osteoporosis are not known, it is believed to be at least partially caused by hormonal imbalances which occur with age, particularly with post-menopausal changes in women.

Other diseases such as rickets and osteomalacia also result in a decrease in strength in bone. These two diseases are associated with a defective mineralization of bone material.

2. Bone Strength

Each of the bone diseases discussed above results in a decrease in bone strength, the force required to fracture the bone. Therefore, a measuring technique would be valuable. However, bone strength can not be measured directly except by methods which entail destruction of the specimen. Therefore a noninvasive method for inferring bone strength is needed. If correlations can be found between stiffness and bone strength, then the stiffness measurements, mentioned in Section I.A, will be very useful. Once correlations are established to the point that bone strength can be accurately inferred then the stiffness measurements can be used to: (1) diagnose bone diseases, (2) determine the extent of the deterioration caused by the disease, (3) prescribe treatment and (4) caution patients to avoid activities which will induce dangerous stress levels in their bones.

3. Correlation Studies

Although bone diseases usually affect all of the bones in the skeletal system, long bones are more accessible for testing. Thus most of the studies have been concerned with long bones.

Mather (1967a) (1967b) was among the first to correlate bone

strength to other material and geometric properties of the bone. He ran simple bending tests on fresh, excised, human long bones and found strong correlations between bone strength and such "measureable" quantities as age, modulus of elasticity and bone geometry.

Further correlation studies have been performed to relate bone strength to bending stiffness of long bones. Borders, Petersen and Orne (1977) tested fifty-six excised, fresh, canine long bones (ulnae, radii and tibiae) in three and four point bending. Jurist and Foltz (1977) tested forty-five excised, embalmed, human ulnae in three-point bending. In each case, the force versus deflection was recorded while the bone was loaded to fracture. Statistical correlations were found between bone strength and various mechanical properties of the bones.

These two independent investigations were parallel although the specimens used in each were substantially different. Their findings and conclusions support one another. In particular, very strong correlations were found between bone strength and bending stiffness for the normal bones tested. BMC was also measured near the center of each bone tested. Both studies indicate a substantial correlation between BMC and both bone strength and bending stiffness.

Thus, correlations have been well established between bone strength and bending stiffness for healthy bones. Further correlation studies involving various kinds of diseased bones are needed to establish the effect of these diseases. It is reasonable to expect that good correlations can be found for diseased bones, since they exist for healthy bones. A reliable method for measuring bending stiffness would then be very useful

as a non-invasive indicator of bone strength.

4. Fracture Healing

Another potential use of stiffness measurements is the determination of the extent of fracture healing. A few recent studies have already been done in this area. Among the first to investigate the feasibility of such an application were Campbell and Jurist (1971). They made impedance measurements on an excised, intact human femur and further measurements on the same bone in various injurious conditions, concluding that methods of this type are indeed feasible. Further studies were carried out by Harkey and Jurist (1974) and Hoeksema and Jurist (1977) in which resonant frequency was correlated to fracture healing. Bourgis and Burny (1972) performed a theoretical study to show the effect of a partially healed section on the mechanical response of a bone. Abendschein and Hyatt (1972) made ultrasonic measurements to obtain the modulus of elasticity of bones in guinea pigs at various stages in the healing process, thereby demonstrating its variation with healing.

In measuring bone properties for the purpose of monitoring the healing process of a fracture, it would be advantageous to know what the bone properties were before the fracture occurred. This, of course, is not possible in a clinical setting. However, Borders, Petersen and Orne (1977) found, in the case of healthy canine bones that paired bones (right and left bones of the same type from one animal) have virtually identical mechanical properties. If this paired bone relationship holds true for the human skeleton as well, then measurements taken on a partially healed bone can be compared to corresponding measurements on its

paired bone to determine the extent of healing.

5. Cadaver Evaluation

Still another potential use of *in vivo* stiffness measurements is the skeletal status evaluation of cadavers. Human cadavers are used quite extensively for impact safety studies. A noninvasive screening technique would be very useful in determining the suitability of a cadaver to represent a specific population in such a test. Although this approach to cadaver evaluation is presently not in widespread use, the concept was introduced and discussed in detail by Orne (1976).

D. OTHERS WORK

1. Ultrasonics

It was shown in the last section that bone conditon is related to the mechanical properties of the bone. Many investigators have attempted, with varying degrees of success, to measure these properties *in vivo*. Two major types of approaches have been taken: ultrasonics and impedance testing.

Craven, Costinini, Greenfield and Stern (1973) investigated the plausibility of measuring the speed of sound in ulnae *in vivo* using a pulse-echo technique. They showed a significant difference in their measurements for bones of two extreme groups of subjects: young healthy males and older (post-menopausal) females. Further investigations using this method were carried out by Greenfield et al. (1975). They deduced the modulus of elasticity from the speed of sound, measurements of geometry and

bone mineral content.

Abendschein and Hyatt (1970) measured the longitudinal wave speed of standardized specimens of human femoral and tibial diaphyseal cortices. In this preliminary *in vitro* study, they found correlations between wave speed and a few physical properties including modulus of elasticity. Selle and Jurist (1966) made similar measurements on whole excised ulnae and on ulnae *in vivo*. The *in vivo* tests were conducted on osteoporotic, diabetic and normal subjects. Saha and Lakes (1977) investigated the effect of the soft tissue on the measurement of wave speed in long bones. They concluded that the presence of soft tissue has a significant effect on these measurements and therefore must by considered.

In each of the ultrasonic methods discussed above, geometrical measurements were required to deduce the modulus of elasticity of the bone being tested. These measurements can be very difficult to obtain accurately *in vivo* and may even be impossible in a clinical setting. A technique for measuring bending stiffness EI such as impedance testing is a more sensitive indicator of bone condition than measurements of either the modulus of elasticity E, or geometric properties such as I since both are usually affected by a bone disorder. Furthermore, bending stiffness was shown in the last section to be well correlated with bone strength.

2. Impedance

A variety of experimental procedures and apparatus have been used to measure the mechanical impedance of excised long bones and intact limbs. Most of those who have attempted to

model their system at all have used relatively simple models which do not account for all of the significant characteristics of the impedance curves. Entrekin and Abrams (1976) measured the mechanical impedance of the human forearm but did not attempt to model it. Jurist (1970), Jurist and Kianian (1973) and Speigl and Jurist (1975) measured the mechanical impedance of a similar system but used it only as a method of measuring the resonant frequency which they then related to the mechanical properties of the ulna. Doherty, Bovill and Wilson (1974) made impedance-like measurements on three excised tibia. They concluded that "stiffness K, or dynamic mass M, are more sensitive to changes in the physical state of the human long bone than is resonant frequency F, due to the functional relationship of these parameters", i.e., F is proportional to $\sqrt{K/M}$.

Garner and Blackketter (1975) used a finite element model to simulate their impedance data from a human forearm. This procedure involves many X-rays of the forearm and very careful measurement to determine its geometry.

Thompson (1973) measured the driving-point mechanical impedance of a forearm near the middle of the ulna. He modeled it with a fair amount of success as a simple single-degree-of-freedom oscillator over a frequency range from 65 to 1000 Hz. Thompson's procedure and apparatus will be discussed further in the next section. Orne (1974) presented an improved model consisting of a viscoelastic beam in series with a three-parameter solid to represent the skin. Orne and Mandke (1975) and Thompson, Orne and Young (1976) improved the model further by including a few different kinds of viscoelastic foundations with mass to represent the tissue surrounding the ulna. This

model has potential but more examination and modification is required before it can be used effectively for clinical application.

E. VIBRATION TESTS AT AMES RESEARCH CENTER

1. Apparatus and Procedure

A noninvasive method for measuring the driving-point mechanical impedance[1] of an *in vivo* human ulna was developed by Thompson (1973). The same procedure and apparatus has since been modified and used on monkey ulnae and tibiae, (Peterson, 1977).

The forearm (or leg) is suspended across two aluminum supports as shown in Figure 1.2. An aluminum block is placed over the wrist (ankle) and secured by two screws. A downward force is applied through the humerus (femur) to hold the proximal end of the ulna (tibia) in place.

Specially formed plaster pads were made by Thompson for each subject he tested. The plaster pads were formed to the subject's wrist and elbow to maximize comfort while maintaining rigidity of the supports. Petersen substituted the plaster pads with a firm putty (duct seal) to increase comfort of the subject, but with questionable results.

A Wilcoxon Research Impedance Head (model Z-11) mounted on the vibrating shaft of a Ling Altec electro-magnetic shaker is

---

[1] Driving-point mechanical impedance is precisely defined in Section II.B. Briefly, it is the ratio of the amplitude of the force to the amplitude of the velocity of the driving-point of a system.

applied to the ulna (tibia) through a cylindrical probe. The shaker is mounted on one end of a lever with counter weights applied to the opposite end. Various sized weights are used to apply and control a constant preload force on the ulna (tibia). Preloads ranging from 200 to 600 gram-force (196×10^3 to 589×10^3 dyne) are used.

A schematic diagram of the impedance-measuring system is shown in Figure 1.3. A sinusoidal electrical input signal is generated by an audio oscillator and fed through an audio amplifier to the electro-magnetic shaker. The shaker, which works on the same principal as a loud speaker, converts the electrical signal to a mechanical vibration of the impedance head and probe. The probe, when placed against a forearm (leg), forces the ulna (tibia) to vibrate at the frequency at which the audio oscillator is set.

The force and acceleration signals from the impedance head are fed through operational amplifiers and high pass filters to a Hewlett-Packard gain-phase meter (model 3565A). The gain-phase meter displays the gain (in decibels) and the phase (in degrees) of the force signal, in digital form, using the acceleration signal as a reference. Traces of the force and acceleration signals are also displayed on an oscilloscope.

The forcing frequency and the two readings from the gain-phase meter are recorded by the operator at many different frequencies over a specified frequency range. Thompson made measurements in the range from 65 to 1000 Hz. Later measurements were taken in the range from 100 to 3000 Hz.

2. Processing the Raw Data

The gain reading from the gain-phase meter is in units of decibels. A gain measurement in bels is defined as the common logarithm of the ratio of the power P, of the electrical signal being measured, to the power P_o, of a reference signal. Therefore in decibels, the gain is

$$G = 10 \log P/P_o \qquad (1.1)$$

Since for a given resistance, power is proportional to the square of the voltage

$$G = 10 \log V^2/V_o^2 = 20 \log V/V_o \qquad (1.2)$$

where V is the voltage of the signal being measured and V_o is the voltage of the reference signal. The gain reading from the gain-phase meter is the gain of the force signal relative to the acceleration signal. Since the force and acceleration are each proportional to their respective signals, the gain reading is

$$G = 20 \log cF/c_o a = 20 \log F/a - 20 \log c/c_o \qquad (1.3)$$

where c and c_o are the constants of proportionality and F and a are the force and acceleration amplitudes, respectively. The quantity, $-20 \log c/c_o$, is not known. Therefore the impedance-measuring system must be calibrated in order to convert the gain reading to an impedance.

A small calibration mass is attached to the impedance head in place of the probe. A gain reading for the mass is taken at 100 Hz. This reading should be independent of frequency (at least for relatively low frequencies) since F/a in this case is the mass m, a constant. Equation (1.3) applied to the calibration mass is

$$G_m = 20 \log m - 20 \log c/c_o \qquad (1.4)$$

where G_m is the gain reading for the mass. The result of

subtracting equation (1.4) from equation (1.3) is

$$G - G_m = 20 \log F/a - 20 \log m \qquad (1.5)$$

Solve equation (1.5) for F/a

$$F/a = m \text{ antilog } (G-G_m)/20 \qquad (1.6)$$

Equation (1.6) is the ratio of the amplitude of force to the amplitude of the acceleration. Impedance, however, is the ratio of the amplitude of the force to the amplitude of the velocity. Since the input force (and hence the motion, if the system is linear) is harmonic, the relationship between the velocity and acceleration amplitudes is

$$a = vp \qquad (1.7)$$

where p is the forcing frequency. Therefore the impedance is

$$Z = F/v = mp \text{ antilog } (G-G_m)/20 \qquad (1.8)$$

A computer program was developed by Thompson to carry out the above computations. The calibration mass and its gain reading are entered into the computer followed by each test frequency and its corresponding gain-phase readings. The gain reading at each frequency is converted to an impedance using equation (1.8). The phase reading at each frequency is adjusted by 90° to account for the difference between the acceleration and velocity, i.e.,

phase of impedance = phase of F/a + 90°

Finally, the results are tabulated and plotted, e.g., see Figures 1.4 and 1.5.

F. THE PURPOSE AND DIRECTION OF THIS WORK

1. Interpretation of Impedance Measurements

The mechanical impedance response of a given system contains information about the mechanical properties of that system. Hence, Thompson's impedance measuring technique described in the last section is potentially a very powerful clinical tool for determining bone properties. However, it alone is not enough. Thompson's procedure produces an impedance plot which must be interpreted to extract the mechanical properties of the bone being tested. Two major concepts must be developed: (1) an appropriate mathematical model and (2) a systems identification technique.

A mathematical model which accounts for the predominant characteristics of the system must be developed. Expressions for the mechanical impedance of the model must be derived and studied in detail to gain an understanding of its behavior. Several versions of the model must be considered to determine the importance of each of its parameters.

A systems identification technique must be developed to determine the values of the parameters in the mathematical model for any given test. When the values are correct, the model will generate an impedance plot which matches the impedance plot of the system (i.e., the data from the test) over the frequency range of the test. The technique must uniquely determine that set of values. Furthermore, it must be systematic enough to

program on a digital computer. A user oriented program will be written to eliminate the need for a trained operator.

A set of *in vitro* impedance tests will be discussed and analysed using the systems identification technique. These tests will establish some verification of the modeling.

The ultimate goal, of course, is to achieve a working scheme to determine bone properties. The scheme will be applied to sets of data from several impedance tests to show how it works.

CHAPTER II

MATHEMATICAL MODELS

A. THE NEED FOR MATHEMATICAL MODELS

1. Construction and Application

Real physical systems can be extremely complicated and difficult to study. It is therefore advantageous to make some simplifying assumptions about the system to be studied which are approximately correct, thereby constructing a model which represents the system. The model can then be studied to gain an understanding of the system. Useful relationships between parts of the system can be discovered as an outcome of the model studies.

It is often of interest to make a specific measurement on a part of the system being studied. Unfortunately, however, many physical systems, especially biological systems, cannot be disassembled to make that measurement without destroying the system. Therefore, if a reasonable model of the system can be constructed with sufficient correlations established between it and the system, then noninvasive measurements can be made on the system which infer the measurement of interest through the model.

The accuracy of the assumptions made in constructing the model has significant effects on both the outcome of the model studies and the accuracy to which a measurement can be inferred. Therefore, these assumptions should be accurate to construct a reasonable model.

The measurement of interest here is the stiffness of a long bone. The noninvasive measurement being modeled is the mechanical impedance which will be defined more precisely in the next section. A mathematical model of the forearm and leg will be derived, studied and applied to the measurement of bone stiffness in the chapters that follow.

B. IMPEDANCE

1. Definition

In general, impedance is the ratio of input to output of a linear system. A linear system is one in which the output is in the same proportion to the input, regardless of the amplitude of that input. Hence, impedance is independent of amplitude. If the input to a linear system is harmonic, then the output will also be harmonic, possibly with some phase shift. Impedance then, is the ratio of the amplitudes of the harmonic input and harmonic output and, mathematically, must be a complex quantity to account for the phase shift. If the output is taken to be the physical response of a specific point in the system then the impedance is said to be the impedance of that point.

In a mechanical system, the input is usually a force.[2] The corresponding output is the velocity of the point in the system at which the impedance is being considered. If the point under consideration is the point in the system at which the force is being applied then the impedance is known as the driving-point mechanical impedance (DPMI).

For a linear system, the DPMI is independent of the amplitude of the input force.

2. Justification

The three types of idealized mechanical elements are: mass, damper and spring. The behavior of any linear mechanical system can be simulated (over a small enough frequency range) using one or some combination of these elements. Therefore, in order to clearly define the behavior of a system, the three basic elements must be distinguishable on the response curve of that system in what ever form it is presented. The response curve can be presented in a number of ways. It can be presented as the ratio of force to acceleration, velocity or displacement. Furthermore, it can be plotted on either a linear or a log plot.

The equation of motion for a force f, applied to each of the basic elements is given in Tabel 2.1. If the input force is harmonic, then the response will be harmonic, and the following relationships hold between the amplitudes of the acceleration a, velocity v, and displacement δ

$$a = p^2\delta \qquad v = p\delta \qquad (2.1)$$

---

[2] In other types of mechanical systems the input might be, for example, a torque or a hydraulic pressure. The corresponding outputs in these cases are an angular velocity and a fluid flow rate, respectively.

where p is the forcing frequency. The ratios of the amplitudes of the force to the acceleration, velocity and displacement are easily derivable from equations (2.1) and the equation of motion for each element. These ratios are also listed in Table 2.1.

Note that each of the ratios is proportional to an integer power of the forcing frequency p. Therefore, a log-log plot of one of the ratios versus the forcing frequency is a straight line. The slope of the straight line is equal to the power of p. For example, the ratio of the force to acceleration for a spring is

$$F/a = kp^{-2} \tag{2.2}$$

Taking the log of equation (2.2) yields

$$\log F/a = -2 \log p + \log k \tag{2.3}$$

Equation (2.3) is a straight line with a slope of -2 on a plot of log F/a versus log p, i.e., the line makes an angle of arctan (-2) = -63.4° with the horizontal. In a similar manner, the slope of the straight line produced by plotting each of the other ratios is calculated and listed in in Table 2.1.

To maximize the distinguishability between the response of the mass, damper and spring, the response curve must be presented in such a way to maximize the difference in the slopes of the response of each of the three basic elements. The slopes in each case listed in Table 2.1 reveal that this can be accomplished by presenting the response curve in the form of F/v (impedance) rather than F/a or F/δ.

C. THE RELATIONSHIP BETWEEN THE MATHEMATICAL MODEL AND THE PHYSICAL SYSTEM

1. Background

In modeling a mechanical system, the model used must, in some sense, resemble the actual physical system. This resemblance must be evident to give physical meaning to the parameters of the model. The physical parameters associated with the material characteristics, as well as those associated with the geometrical characteristics, must be accounted for in as much detail as the investigator is willing to deal with. It is often appropriate to start with a model which accounts for the most obvious physical parameters to gain an understanding of the system, and then to progress to other models which account for some of the finer details of the physical system.

Modeling of the forearm system associated with the impedance-measuring procedure developed by Thompson (1973) (discussed in Section I.E) was first attempted by Orne (1974). Orne modeled the ulna as a uniform, linear, visco-elastic, simply-supported, Euler-Bernoulli beam. The skin which is compressed between the ulna and the probe was represented by a tri-parameter solid in series with the beam. The harmonically varying load applied by the probe is represented by a concentrated force applied to the beam through the tri-parameter solid as shown in Figure 2.1. Orne and Mandke (1975) improved this model by including a one-degree-of-freedom mass

with elastic and viscous resistance, uniformly distributed along the beam to represent the tissue surrounding the ulna. This refinement produced the capability of the model to account for the sub-resonances that are evident in the otherwise smooth impedance curves. A further refinement was made by Thompson, Orne and Young (1976) in which the one-degree-of-freedom tissue model was replaced by a continuous tissue model. Additional refinements involving the boundary conditions of the beam will be presented here. These models will also be applied, with some modification, to the leg system as well.

2. The Bone

Several assumptions have been made in modeling the bone as a uniform, linear, visco-elastic, simple-supported, Euler-Bernoulli beam. First of all, a uniform Euler-Bernoulli beam is a beam which is based on the following two assumptions: (1) the cross section of the beam does not change along its length, and (2) the beam is slender enough that shear deformation is small compared to bending deformation. The first assumption is obviously not true of bones and will be investigated in detail in Chapter IV. The second assumption was shown to be true by Piziali, Wright and Nagel (1976). The beam is also assumed to be linear. This assumption was verified by Thompson when he showed that the DPMI is independent of amplitude of the driving force provided that amplitude is small. Finally the beam is assumed to be visco-elastic. This is a reasonable assumption since the structure of bone material, on the microscopic level, is a fluid-filled matrix.

3. The Supports

Orne (1974) reasons that the supports at the ends of the ulna are such that the resisting moment is negligible and the transverse rigidity is much greater than that of the bone, therefore the bone is simply-supported. However, other aspects of the conditions at the supports have not been considered. The transverse rigidity of the supports when the plaster pads are replaced by putty is questionable. A possible misalignment between the downward force applied through the humerus with the support point of the elbow can conceivably cause an effective resistance to rotation at the support.

Several different classical and non-clasical beam boundary conditions are proposed as possibilities for representing the motion of the bone at the joints. These include various combinations of translational and rotational springs at the supports. One special case is considered in which the beam is extended past the support to a translational spring to represent the possible misalignment of the humerus over the support.

4. The Skin and Tissue

It is advantageous at this point to propose two definitions. The skin and the thin layer of tissue which are compressed between the bone and the probe will be referred to as the skin. All of the musculature, skin and other tissue surrounding the bone will be refered to as the tissue. The lack of consistency of these definitions in the literature can be a source of misinterpretation. Therefore, the proposed definitions will be used here to insure clarity.

The tissue model is presented by Thompson, Orne and Young

(1976) as "an infinite series of one-dimensional visco-elastic rods attached to and vibrating with the ulna and rigidly attached to and restrained against motion at their opposite ends by the radius." This model is conceptually identical to the classical problem of a beam on an elastic foundation. The difference is that the classical foundation includes only a stiffness element, whereas the tissue model includes stiffness, damping and mass elements. The tissue model will often be referred to as a visco-elastic foundation with mass, or simply as the "foundation." The shear coupling between adjacent fibers of the foundation is neglected. The fixed-end boundary condition is replaced by a free-end boundary condition when modeling the tibia.

The skin is represented in Orne's model by a tri-parameter solid, as shown in Figure 2.1. This may seem like a reasonable representation since one would expect the skin to exhibit damping as well as stiffness characteristics. However, a typical set of impedance data from a piece of skin shown in Figure 2.2 indicates springlike behavior over the entire frequency range. (Recall from Section II.B that the DPHI of a spring is a straight line with a -45 degree slope.) Therefore the skin will be represented here by a simple spring, as shown in Figure 2.3.

D. THE BEHAVIOR OF THE MATHEMATICAL MODEL

1. Impedance Equations and Parametric Study

The mathematical model described in the last section is to be studied to gain an understanding of the system. In order to conduct this study, equations for the DPMI of the model must derived. These equations will contain, as one of their parameters, the quantity to be measured, i.e., the bending stiffness of the bone. The equations will be nondimensionalized to reduce the number of independent parameters and then plotted. The nondimensionalized plots will facilitate the study of the mathematical model.

These plots can be used to study the model in a number of ways. They will be used to determine the effects that each of the model parameters have on the plots. Further use of the plots will be more productive if the effects of each parameter are known.

Quantitatively, they will be used in generating approximate, semi-empirical relationships between the parameters of the mathematical model and the characteristics of the DPMI plot of that model. Relationships of this type will be useful in obtaining approximations for the values of the parameters of the system directly from its DPMI plot.

Qualitatively, the plots will be used to aid in determining which parameters to include in the model of the system. This is accomplished by comparing the DPMI plot of the system to the

model plots to distinguish between the parameters which are essential to obtain an appropriately shaped DPMI plot and those which are not.

The DPMI equations and their plots will be the subjects of the next two chapters.

CHAPTER III

IMPEDANCE EQUATIONS

A. THE GENERAL METHOD FOR DERIVING IMPEDANCE EQUATIONS

1. Background

Driving-point mechanical impedance (DPMI) is the mechanical impedance of the point in the system at which the driving force is being applied. To derive the DPMI of a mathematical model, one must solve the equations of motion, evaluate the steady-state solution for the velocity at the driving-point and take the ratio of the force to the velocity. The method for deriving the DPMI of the mathematical model described in Section II.C is presented in this section.

Orne (1974) and Orne and Mandke (1975) have derived the DPMI of a simply-supported beam on a one-degree-of-freedom visco-elastic-foundation-with-mass. The analysis presented here is more general in that the boundary conditions are not restricted to simply-supported. Six different sets of boundary conditions are considered; the simply-supported case and five nonclassical cases. A diagram of each case is shown in Figure 3.1. The visco-elastic-foundation-with-mass is continuous and two types of boundary conditions on the foundation are allowed.

2. The Derivation

A convenient way to define a coordinate system on the beam is shown in Figure 3.2. $y_1(x,t)$ and $y_2(z,t)$ are the deflection functions defined for $0<x<a$ and $0<z<b$, respectively, shown positive in the figure, where the concentrated force is applied at $x = a$ $(z = b)$. The equations of motion are

$$EI\,\partial^4 y_1/\partial x^4 + \eta I\,\partial^5 y_1/\partial x^4\partial t + \mu\,\partial^2 y_1/\partial t^2 = p_1(x,t),\quad 0<x<a$$

$$EI\,\partial^4 y_2/\partial z^4 + \eta I\,\partial^5 y_2/\partial z^4\partial t + \mu\,\partial^2 y_2/\partial t^2 = p_2(z,t),\quad 0<z<b \tag{3.1}$$

where

E is the modulus of elasticity of the beam material

I is the area moment of inertia of the cross section

η is the damping coefficient of the beam material

μ is the mass per unit length of the beam

p_1, p_2 are the force per unit length of the beam due to the reaction of the foundation. These equations are based on the visco-elastic uni-axial stress-strain law, i.e., $\sigma = E\varepsilon + \eta\dot{\varepsilon}$. To determine the DPMI, the steady state solutions to equations (3.1) are required. These solutions are of the form

$$y_1(x,t) = Y_1(x)\exp ipt$$
$$y_2(z,t) = Y_2(z)\exp ipt \tag{3.2}$$

(i.e., every point in the system is vibrating at the same frequency) where p is the forcing frequency and $Y_1(x)$ and $Y_2(z)$ are complex amplitudes of the beam vibration. Upon substitution of equations (3.2) into equations (3.1), the following ordinary differential equations are obtained

$$E^*I\,d^4Y_1/dx^4 - \mu p^2 Y_1 = P_1(x),\quad 0<x<a$$
$$E^*I\,d^4Y_2/dz^4 - \mu p^2 Y_2 = P_2(z),\quad 0<z<b \tag{3.3}$$

where

$$E^* = E(1 + \eta ip/E) = E(1 + 2i\zeta p/\omega)$$

$$P_1(x,t) = P_1(x) \exp ipt$$

$$P_2(z,t) = P_2(z) \exp ipt \qquad (3.4)$$

$$\omega = (\pi/L)^2 \sqrt{EI/\mu}$$

$$\zeta = \omega\eta/2E$$

In the cases where the foundation is not included, $P_1(x) = P_2(z) = 0$. In cases where the foundation is included

$$P_1(x) = \mu_f^* p^2 Y_1(x)$$

$$P_2(z) = \mu_f^* p^2 Y_2(z) \qquad (3.5)$$

where μ_f^* is the complex, frequency-dependent quantity obtained by solving the foundation wave equation

$$E_f \, \partial^2 u/\partial\xi^2 + \eta_f \, \partial^3 u/\partial\xi^2 \partial t - \rho_f \, \partial^2 u/\partial t^2 = 0 \qquad (3.6)$$

with the appropriate boundary conditions, as indicated in Figure 3.3, where

E_f is the modulus of elasticity of the foundation material

η_f is the damping coefficient of the foundation material

ρ_f is the density of the foundation material

$u(\xi,t)$ is the displacement function of the foundation

and the shear stresses in the foundation are neglected. For the fixed foundation

$$\mu_f^* = -\mu_f \cot\Psi / \Psi \qquad (3.7)$$

for the free foundation

$$\mu_f^* = \mu_f \tan\Psi/2 / \Psi/2 \qquad (3.8)$$

where

$$\Psi = p\pi/\omega_f \, / \sqrt{1 + 2i\zeta_f p/\omega_f}$$

μ_f is the mass per unit length of the foundation

ω_f is the fundamental frequency of the foundation

ζ_f is the damping ratio of the foundation.

The result of substituting equation (3.5) into equation (3.3) is

$$E^*I\, d^4Y_1/dx^4 - \mu^*p^2Y_1 = 0$$
$$E^*I\, d^4Y_2/dz^4 - \mu^*p^2Y_2 = 0 \qquad (3.9)$$

where $\mu^* = \mu + \mu^*_f$. The solutions to these equations are

$$Y_1(x) = A_1 \sin\lambda x + B_1 \cos\lambda x + C_1 \sinh\lambda x + D_1 \cosh\lambda x$$
$$Y_2(z) = A_2 \sin\lambda z + B_2 \cos\lambda z + C_2 \sinh\lambda z + D_2 \cosh\lambda z \qquad (3.10)$$

where $\lambda^4 = \mu^*p^2/E^*I$

and A_1, B_1, C_1, D_1, A_2, B_2, C_2 and D_2 are eight unknown constants which depend on the boundary and matching conditions. The deflection, slope, bending moment and shear force functions are found by using equations (3.2), (3.10) and the following

$$\theta_1(x,t) = \partial y_1/\partial x \qquad \theta_2(z,t) = \partial y_2/\partial z$$
$$M_1(x,t) = E^*I\, \partial^2 y_1/\partial x^2 \qquad M_2(z,t) = E^*I\, \partial^2 y_2/\partial z^2 \qquad (3.11)$$
$$V_1(x,t) = E^*I\, \partial^3 y_1/\partial x^3 \qquad V_2(z,t) = E^*I\, \partial^3 y_2/\partial z^3$$

These functions are evaluated at the point of load application ($x = a$ and $z = b$) and substituted into the following matching conditions

$$y_1(a,t) + y_2(b,t) = 0 \qquad M_1(a,t) + M_2(b,t) = 0 \qquad (3.12)$$
$$\theta_1(a,t) - \theta_2(b,t) = 0 \qquad V_1(a,t) - V_2(b,t) = P \exp ipt$$

These are four of the eight equations required to solve for the eight unknown constants in equations (3.10). The remaining four equations are obtained by evaluating the appropriate functions at $x = 0$ or $z = 0$ and substituting them into the boundary conditions listed for each case in Table 3.1.

For the case where the beam is extended a distance e, past the left support, a third deflection function with an additional four constants is required on the interval $-e<x<0$. To determine the twelve constants for this case, an additional four equations are required. They are obtained from the following matching conditions at $x = 0$

$$y_1(0,t) = 0 \qquad \theta_1(0,t) - \theta_3(0,t) = 0$$
$$y_3(0,t) = 0 \qquad M_1(0,t) - M_3(0,t) = 0 \tag{3.13}$$

The deflection amplitude δ, at the point where the load is applied is determined by evaluating $Y_1(x)$ at $x = a$ or $Y_2(z)$ at $z = b$ in equation (3.10). The DPMI of the beam is obtained from

$$Z_b^* = F/ip\delta \tag{3.14}$$

For the case where a transverse translational spring is in series with the beam, the DPMI of the system is given by

$$Z^* = (Z_b^{*-1} + ip/k)^{-1} \tag{3.15}$$

For the case where the spring is not included in the model, $Z^* = Z_b^*$.

The DPMI associated with each set of boundary conditions in Table 3.1 is listed in Appendix A. In each case, the diagrams of Figure 3.1, the boundary conditions of Table 3.1 and the equations of Appendix A are each numbered correspondingly. One sample DPMI derivation (case 2) is presented in the following section to show how the DPMI equations of Appendix A have been derived from the general method presented in this section.

B. A SPECIFIC EXAMPLE

1. Rotational Spring on One End

Case 2 was chosen as an example to demonstrate the method used in deriving the DPMI. The support at $x = 0$ is perfectly rigid with respect to translation while the resisting moment is proportional to the rotation at that support. The support at $z = 0$ is a simple support, i.e., perfectly rigid with respect to translation and no resistance to rotation. These conditions are

listed in mathematical form in Table 3.1.

The general solutions to the beam equations (3.1) were found in the last section to be given by equations (3.2) and (3.10), i.e.,

$$y_1(x,t) = [A_1 \sin\lambda x + B_1 \cos\lambda x + C_1 \sinh\lambda x + D_1 \cosh\lambda x] \exp ipt \quad (3.16)$$

$$y_2(z,t) = [A_2 \sin\lambda z + B_2 \cos\lambda z + C_2 \sinh\lambda z + D_2 \cosh\lambda z] \exp ipt$$

The slope, bending moment and shear force functions are obtained from the deflection functions (3.16) using equations (3.11). These functions are substituted into matching conditions (3.12) to obtain the following four equations

$$A_1 \sin\lambda a + B_1 \cos\lambda a + C_1 \sinh\lambda a + D_1 \cosh\lambda a + A_2 \sin\lambda b + B_2 \cos\lambda b + C_2 \sinh\lambda b + D_2 \cosh\lambda b = 0 \quad (3.17)$$

$$A_1 \cos\lambda a - B_1 \sin\lambda a + C_1 \cosh\lambda a + D_1 \sinh\lambda a - A_2 \cos\lambda b + B_2 \sin\lambda b - C_2 \cosh\lambda b - D_2 \sinh\lambda b = 0 \quad (3.18)$$

$$-A_1 \sin\lambda a - B_1 \cos\lambda a + C_1 \sinh\lambda a + D_1 \cosh\lambda a - A_2 \sin\lambda b - B_2 \cos\lambda b + C_2 \sinh\lambda b + D_2 \cosh\lambda b = 0 \quad (3.19)$$

$$-A_1 \cos\lambda a + B_1 \sin\lambda a + C_1 \cosh\lambda a + D_1 \sinh\lambda a + A_2 \cos\lambda b - B_2 \sin\lambda b - C_2 \cosh\lambda b - D_2 \sinh\lambda b = F / E*I\lambda^3 \quad (3.20)$$

These equations each contain all eight of the unknown constants. With several algebraic steps, four new equations can be generated from these four equations. Each new equation contains only three of the unknown constants. Add and subtract equations (3.17) and (3.19). Add and subtract equations (3.18) and (3.20). Divide each of the four results by two to obtain respectively

$$C_1 \sinh\lambda a + D_1 \cosh\lambda a + C_2 \sinh\lambda b + D_2 \cosh\lambda b = 0 \quad (3.21)$$

$$A_1 \sin\lambda a + B_1 \cos\lambda a + A_2 \sin\lambda b + B_2 \cos\lambda b = 0 \quad (3.22)$$

$$C_1 \cosh\lambda a + D_1 \sinh\lambda a - C_2 \cosh\lambda b - D_2 \sinh\lambda b = P / 2E^*I\lambda^3 \quad (3.23)$$

$$A_1 \cos\lambda a - B_1 \sin\lambda a - A_2 \cos\lambda b + B_2 \sin\lambda b = -P / 2E^*I\lambda^3 \quad (3.24)$$

Multiply equation (3.21) by $\sinh\lambda b$, multiply equation (3.23) by $\cosh\lambda b$ and add the two results

$$C_1 (\sinh\lambda a \sinh\lambda b + \cosh\lambda a \cosh\lambda b) + D_1 (\cosh\lambda a \sinh\lambda b + \sinh\lambda a \cosh\lambda b) + C_2 (\sinh^2\lambda b - \cosh^2\lambda b) = P \cosh\lambda b / 2E^*I\lambda^3 \quad (3.25)$$

Recall the following hyperbolic identities

$$\cosh^2 B - \sinh^2 B = 1$$

$$\cosh A \cosh B + \sinh A \sinh B = \cosh(A+B)$$

$$\cosh A \sinh B + \sinh A \cosh B = \sinh(A+B)$$

Noting that $a + b = L$, equation (3.25) reduces to

$$C_1 \cosh\lambda L + D_1 \sinh\lambda L - C_2 = P \cosh\lambda b / 2E^*I\lambda^3 \quad (3.26)$$

In a similar manner, multiply equation (3.21) by $\sinh\lambda a$, multiply equation (3.23) by $\cosh\lambda a$ and subtract the second result from the first. Then again using the hyperbolic identities given above, the result reduces to

$$-C_1 + C_2 \cosh\lambda L + D_2 \sinh\lambda L = -P \cosh\lambda a / 2E^*I\lambda^3 \quad (3.27)$$

Multiply equation (3.22) by $\sin\lambda b$, multiply equation (3.24) by $\cos\lambda b$ and subtract the second result from the first

$$A_1 (\sin\lambda a \sin\lambda b - \cos\lambda a \cos\lambda b) + B_1 (\cos\lambda a \sin\lambda b + \sin\lambda a \cos\lambda b) + A_2 (\sin^2\lambda b + \cos^2\lambda b) = P \cos\lambda b / 2E^*I\lambda^3 \quad (3.28)$$

Recall the following trigonometric identities

$$\cos^2 B + \sin^2 B = 1$$

$$\cos A \cos B - \sin A \sin B = \cos(A+B)$$

$$\cos A \sin B + \sin A \cos B = \sin(A+B)$$

Again noting that a + b = L, equation (3.28) reduces to

$$-A_1 \cos\lambda L + B_1 \sin\lambda L + A_2 = F \cos\lambda b / 2E^*I\lambda^3 \qquad (3.29)$$

In a similar manner, multiply equation (3.22) by $\sin\lambda a$, multiply equation (3.24) by $\cos\lambda a$ and add the two results. Then again using the trigonometric identities given above, the result reduces to

$$A_1 - A_2 \cos\lambda L + B_2 \sin\lambda L = -F \cos\lambda a / 2E^*I\lambda^3 \qquad (3.30)$$

Equations (3.26), (3.27), (3.29) and (3.30), which contain only three of the unknown constants each, apply to any beam since they have been generated without use of the boundary conditions.

Substitute the deflection, slope and bending moment functions into the boundary conditions listed in Table 3.1 for case 2 to produce the following four equations

$$B_1 + D_1 = 0 \qquad (3.31)$$

$$-B_1 + D_1 = k_1 (A_1 + C_1) / E^*I\lambda \qquad (3.32)$$

$$B_2 + D_2 = 0 \qquad (3.33)$$

$$-B_2 + D_2 = 0 \qquad (3.34)$$

The equations above are easily solved for B_1, D_1, B_2 and D_2 in terms of A_1 and C_1. The results are

$$B_1 = -k_1 (A_1 + C_1) / 2E^*I\lambda \qquad (3.35)$$

$$D_1 = k_1 (A_1 + C_1) / 2E^*I\lambda \qquad (3.36)$$

$$B_2 = 0 \qquad (3.37)$$

$$D_2 = 0 \qquad (3.38)$$

Substitute equations (3.35), (3.36), (3.37) and (3.38) into equations (3.26), (3.27), (3.29) and (3.30) and combine the terms which have the same unknown constant

$$C_1 (\cosh\lambda L + k_1 \sinh\lambda L / 2E^*I\lambda) \qquad (3.39)$$

$$+ A_1 k_1 \sinh\lambda L / 2E^*I\lambda - C_2 = F \cosh\lambda b / 2E^*I\lambda^3$$

$$C_1 = C_2 \cosh\lambda L + F \cosh\lambda a / 2E^*I\lambda^3 \qquad (3.40)$$

$$-A_1(\cos\lambda L + k_1 \sin\lambda L / 2E^*I\lambda) \tag{3.41}$$

$$-C_1 k_1 \sin\lambda L / 2E^*I\lambda + A_2 = P\cos\lambda b / 2E^*I\lambda^3$$

$$A_1 = A_2\cos\lambda L - P\cos\lambda a / 2E^*I\lambda^3 \tag{3.42}$$

Substitute equations (3.40) and (3.42) into equations (3.39) and (3.41) and again combine terms which have the same unknown constant and transfer all known terms to the right hand side of the equations

$$A_2 k_1/2E^*I\lambda \cos\lambda L \sinh\lambda L$$

$$+ C_2(\cosh^2\lambda L + k_1/2E^*I\lambda \sinh\lambda L \cosh\lambda L - 1)$$

$$= P/2E^*I\lambda^3 [\cosh\lambda b - \cosh\lambda a \cosh\lambda L \tag{3.43}$$

$$- k_1/2E^*I\lambda \sinh\lambda L (\cosh\lambda a - \cos\lambda a)]$$

$$-A_2(\cos^2\lambda L + k_1/2E^*I\lambda \sin\lambda L \cos\lambda L - 1)$$

$$- C_2 k_1/2E^*I\lambda \cosh\lambda L \sin\lambda L$$

$$= P/2E^*I\lambda^3 [\cos\lambda b - \cos\lambda a \cos\lambda L \tag{3.44}$$

$$- k_1/2E^*I\lambda \sin\lambda L (\cos\lambda a - \cosh\lambda a)]$$

The last two sets of substitutions have been carried out in such a way to reduce the set of eight equations and eight unknowns to a set of two equations and two unknowns.

Again, recall hyperbolic and trigonometric identities, but this time in a slightly different form, i.e.,

$$\cosh^2(A+B) - 1 = \sinh^2(A+B)$$

$$\cos^2(A+B) - 1 = -\sin^2(A+B)$$

$$\cosh B - \cosh(A+B)\cosh A = -\sinh(A+B)\sinh A$$

$$\cos B - \cos(A+B)\cos A = \sin(A+B)\sin A$$

Apply these identities to equations (3.43) and (3.44) with $a + b = L$ to obtain

$$A_2\, k_1/2E^*I\lambda \cos\lambda L \sinh\lambda L + C_2(\sinh^2\lambda L + k_1/2E^*I\lambda \sinh\lambda L \cosh\lambda L) = P/2E^*I\lambda^3 [-\sinh\lambda a \sinh\lambda L - k_1/2E^*I\lambda \sinh\lambda L (\cosh\lambda a - \cos\lambda a)] \quad (3.45)$$

$$A_2(\sin^2\lambda L - k_1/2E^*I\lambda \sin\lambda L \cos\lambda L) - C_2\, k_1/2E^*I\lambda \cosh\lambda L \sin\lambda L = P/2E^*I\lambda^3 [\sin\lambda a \sin\lambda L - k_1/2E^*I\lambda \sin\lambda L (\cos\lambda a - \cosh\lambda a)] \quad (3.46)$$

Put equations (3.45) and (3.46) into matrix form

$$[A]\{C\} = \{B\} \quad (3.47)$$

where

$$[A] = \begin{bmatrix} k_1/2E^*I\lambda \cos\lambda L \sinh\lambda L & \sinh^2\lambda L + k_1/2E^*I\lambda \sinh\lambda L \cosh\lambda L \\ \sin^2\lambda L - k_1/2E^*I\lambda \sin\lambda L \cos\lambda L & -k_1/2E^*I\lambda \cosh\lambda L \sin\lambda L \end{bmatrix}$$

$$\{C\} = \begin{Bmatrix} A_2 \\ C_2 \end{Bmatrix} \quad \text{and}$$

$$\{B\} = P/2E^*I\lambda^3 \begin{Bmatrix} -\sinh\lambda a \sinh\lambda L - k_1/2E^*I\lambda (\cosh\lambda a - \cos\lambda a) \\ \sin\lambda a \sin\lambda L - k_1/2E^*I\lambda (\cos\lambda a - \cosh\lambda a) \end{Bmatrix}$$

Matrix equation (3.47) can now be solved for A_2 and C_2 using Cramers rule. The determinant of matrix [A] is

$$D = -k_1/2E^*I\lambda \cos\lambda L \sinh\lambda L\, k_1/2E^*I\lambda \cosh\lambda L \sin\lambda L - (\sinh^2\lambda L + k_1/2E^*I\lambda \sinh\lambda L \cosh\lambda L)(\sin^2\lambda L - k_1/2E^*I\lambda \sin\lambda L \cos\lambda L) \quad (3.48)$$

Multiply out equation (3.48) and combine like terms. The determinant then reduces to

$$D = \sinh\lambda L \sin\lambda L \left[k_1/2E^*I\lambda \right. \tag{3.49}$$
$$\left. (\sinh\lambda L \cos\lambda L - \sin\lambda L \cosh\lambda L) - \sinh\lambda L \sin\lambda L\right]$$

The solution to matrix equation (3.47), with the determinant D of matrix [A] defined by equation (3.49), is

$$A_2 = P/2E^*I\lambda^3 D$$
$$\{-k_1/2E^*I\lambda \cosh\lambda L \sin\lambda L \tag{3.50}$$
$$[-\sinh\lambda a \sinh\lambda L - k_1/2E^*I\lambda \sinh\lambda L (\cosh\lambda a - \cos\lambda a)]$$
$$- (\sinh^2\lambda L + k_1/2E^*I\lambda \sinh\lambda L \cosh\lambda L)$$
$$[\sin\lambda a \sin\lambda L - k_1/2E^*I\lambda \sin\lambda L (\cos\lambda a - \cosh\lambda a)]\}$$

$$C_2 = P/2E^*I\lambda^3 D$$
$$\{k_1/2E^*I\lambda \cos\lambda L \sinh\lambda L \tag{3.51}$$
$$[\sin\lambda a \sin\lambda L - k_1/2E^*I\lambda \sin\lambda L (\cos\lambda a - \cosh\lambda a)]$$
$$- (\sin^2\lambda L - k_1/2E^*I\lambda \sin\lambda L \cos\lambda L)$$
$$[-\sinh\lambda a \sinh\lambda L - k_1/2E^*I\lambda \sinh\lambda L (\cosh\lambda a - \cos\lambda a)]\}$$

The constants A_2, B_2, C_2 and D_2 are now known from equations (3.50), (3.37), (3.51) and (3.38), respectively. The deflection amplitude δ, can be calculated from either $-Y_1(x=a)$ or $Y_2(z=b)$. Therefore if Y_2 is used then the constants A_1, B_1, C_1 and D_1 are not needed to calculate δ. (The calculation of δ using Y_1 has been made as a means of checking the following calculations but it is not presented here.)

Substitute equations (3.50), (3.37), (3.51) and (3.38) into the second of equations (3.10) and evaluate the result at $z = b$

$$\delta = P/2E^*I\lambda^3D$$

$$\{-k_1/2E^*I\lambda \sin\lambda b \cosh\lambda L \sin\lambda L$$

$$[-\sinh\lambda a \sinh\lambda L - k_1/2E^*I\lambda \sinh\lambda L (\cosh\lambda a - \cos\lambda a)]$$

$$-\sin\lambda b (\sinh^2\lambda L + k_1/2E^*I\lambda \sinh\lambda L \cosh\lambda L)$$

$$[\sin\lambda a \sin\lambda L - k_1/2E^*I\lambda \sin\lambda L (\cos\lambda a - \cosh\lambda a)]$$

$$+ k_1/2E^*I\lambda \sinh\lambda b \cos\lambda L \sinh\lambda L \qquad (3.52)$$

$$[\sin\lambda a \sin\lambda L - k_1/2E^*I\lambda \sin\lambda L (\cos\lambda a - \cosh\lambda a)]$$

$$-\sinh\lambda b (\sin^2\lambda L - k_1/2E^*I\lambda \sin\lambda L \cos\lambda L)$$

$$[-\sinh\lambda a \sinh\lambda L - k_1/2E^*I\lambda \sinh\lambda L (\cosh\lambda a - \cos\lambda a)]\}$$

After several steps of algebra, equation (3.52) reduces to

$$\delta = P/2E^*I\lambda^3D \sinh\lambda L \sin\lambda L$$

$$\{[\sinh\lambda a + k_1/2E^*I\lambda (\cosh\lambda a - \cos\lambda a)]$$

$$[\sinh\lambda b \sin\lambda L - k_1/2E^*I\lambda$$

$$(\sinh\lambda b \cos\lambda L - \sin\lambda b \cosh\lambda L)] \qquad (3.53)$$

$$- [\sin\lambda a + k_1/2E^*I\lambda (\cosh\lambda a - \cos\lambda a)]$$

$$[\sin\lambda b \sinh\lambda L - k_1/2E^*I\lambda$$

$$(\sinh\lambda b \cos\lambda L - \sin\lambda b \cosh\lambda L)]\}$$

Define the following three constants

$$\alpha = k_1/2E^*I\lambda (\cosh\lambda a - \cos\lambda a)$$

$$\beta = k_1/2E^*I\lambda (\sin\lambda b \cosh\lambda L - \sinh\lambda b \cos\lambda L) \qquad (3.54)$$

$$\gamma = k_1/2E^*I\lambda (\sin\lambda L \cosh\lambda L - \sinh\lambda L \cos\lambda L)$$

Substitute the expression for the determinant D, from equation (3.49) into equation (3.53) and replace the appropriate terms with α, β and γ according to equations (3.54)

$$\delta = P/2E^*I\lambda^3$$

$$[-(\sinh\lambda a + \alpha)(\sinh\lambda b \sin\lambda L + \beta) \qquad (3.55)$$

$$+ (\sinh\lambda a + \alpha)(\sin\lambda b \sinh\lambda L + \beta)]$$

$$/(\sinh\lambda L \sin\lambda L + \gamma)$$

Finally, substitute equation (3.55) into equation (3.14) to

obtain the expression for the DPMI

$$Z^* = 2E^*I\lambda^3/ip$$
$$\{[-(\sinh\lambda a + \alpha)(\sinh\lambda b \sin\lambda L + \beta) \quad (3.56)$$
$$+ (\sin\lambda a + \alpha)(\sin\lambda b \sinh\lambda L + \beta)]$$
$$/(\sinh\lambda L \sin\lambda L + \gamma)\}^{-1}$$

Equations (3.54) and (3.56) are the expressions given in Appendix A for case 2.

C. NON-DIMENSIONALIZATION OF IMPEDANCE EQUATIONS

1. Non-dimensionalization

The most effective way of studying the role of each parameter in a mathematical model is to first nondimensionalize the equations associated with that model, and then perform the parametric study. The set of variables and parameters are grouped together in a natural way to form a set of nondimensional variables and parameters, thereby reducing the number of parameters to be studied.

One very natural and convenient way to nondimensionalize the DPMI of a beam is to form the ratio $Z\omega/K$, where Z is the magnitude of the DPMI, ω is the fundamental frequency of a uniform simply-supported beam of the same length and K is the static stiffness

$$K = 48EI/L^3 \quad (3.57)$$

of that same simply-supported beam when centrally loaded. The nondimensionalized DPMI will be plotted versus the nondimensional frequency ratio p/ω where p is the forcing frequency. The nondimensional parameters are listed in Table 3.2

with their definitions.

The general form of the DPMI equation is given in Appendix A as

$$Z^* = 2EI\lambda^3 (1 + 2i\zeta p/\omega) / ipf(\lambda L) \qquad (3.58)$$

where E^* has been replaced by $E(1 + 2i\zeta p/\omega)$ according to equation (3.4), and $f(\lambda L)$ is a function of λL involving trigonometric and hyperbolic functions and nondimensional spring constants. From equations (3.7), (3.8) and (3.10), λL can be written as

$$\lambda L = [(\rho + \mu_f g(\Psi))p^2 / EI(1 + 2i\zeta p/\omega)]^{1/4} L \qquad (3.59)$$

where

$$g(\Psi) = \begin{cases} -1/\Psi \cot\Psi & \text{for a fixed foundation} \\ 2/\Psi \tan \Psi/2 & \text{for a free foundation} \\ 0 & \text{for no foundation} \end{cases}$$

and

$$\Psi = \pi p/\omega_f / \sqrt{1 + 2i\zeta_f p/\omega_f}$$

A few steps of algebra will produce the following equivalent expressions in terms of the nondimensional parameters

$$\begin{aligned} \lambda L &= \pi \sqrt{p/\omega}\ (1 + 2i\zeta p/\omega)^{-1/4}\ (1 + Bg(\Psi))^{1/4} \\ \Psi &= \pi\ p/\omega\ B\ (1 + 2i\zeta_f Bp/\omega)^{-1/2} \end{aligned} \qquad (3.60)$$

Multiply equation (3.58) by ω and divide by equation (3.57). After some simplification, the result reduces to

$$Z\omega/K = -\pi^3 i/24 \sqrt{p/\omega}\ (1 + 2i\zeta p/\omega)^{1/4}\ (1 + Bg(\Psi))^{3/4}\ f^{-1}(\lambda L) \qquad (3.61)$$

If the spring in series with the beam is included, then multiplying the impedance equation by ω/K will simply change the additional term from ip/k to $i(p/\omega)/(k/K)$.

If the boundary conditions of the beam are nonclassical, then terms involving spring constants will appear in the

function $f(\lambda L)$. The terms that appear are

$$2k/E^*I\lambda^3 \qquad \text{and} \qquad k/2E^*I\lambda$$

for translational and rotational springs, respectively (see Appendix A). In terms of the nondimensional parameters, these terms reduce to

$$\begin{aligned} 2k/E^*I\lambda^3 &= T / (\lambda L)^3 (1 + 2i\zeta p/\omega) \\ k/2E^*I\lambda &= R / (\lambda L)(1 + 2i\zeta p/\omega) \end{aligned} \tag{3.62}$$

For case 6 (see Appendix A) the length of the extended part of the beam e, also appears in the function $f(\lambda L)$. However, everywhere e appears in the function, L also appears. Therefore the ratio e/L is taken as the nondimensional parameter ε.

It is also possible to include damping in the nonclassical supports. This is done by adding an imaginary, frequency-dependent term to the appropriate spring constant. Thus k would be replaced by k + ipc. In terms of nondimensional parameters, T or R would be replaced by

$$T(1 + iC_T p/\omega) \quad \text{or} \quad R(1 + iC_R p/\omega)$$

respectively, where the new nondimensional parameter is

$$C_T = c_T\omega/k \quad \text{or} \quad C_R = c_R\omega/k$$

In the next chapter, the nondimensionalized DPMI equations are plotted for several values of the nondimensional parameters. The plots will be studied and many relationships between the parameters will be determined.

CHAPTER IV

PARAMETRIC STUDY

A. THE BASIC SIMPLY-SUPPORTED BEAM

1. The Beam

The bone of a vibrating forearm or leg system is represented by a visco-elastic beam. Ideally, this beam is assumed to be simply-supported. This is an incorrect assumption for many driving-point mechanical impedance (DPMI) tests and experiments. However, the simply-supported beam will be investigated here first and the effect of changing the boundary conditions will be deferred to the next section.

Figure 4.1 is the DPMI plot of such a beam with the driving force applied at its center. The curves were generated, allowing the beam damping to take on five different values. The parametric values used to generate this and all other nondimensional plots presented in this chapter, are listed in Table 4.1.

Comparing Figure 4.1 to a typical DPMI data plot shown in Figure 1.5, it can be seen that the beam alone does not produce all of the characteristics neccessary to model a vibrating forearm or leg system. Other elements must be added to the beam

to produce these characteristics. However, it is beneficial to study and understand the beam itself before adding on these other elements.

At low frequencies, the curves in Figure 4.1 are predominately springlike (i.e., the slope of the curve is virtually negative one) with a stiffness equal to the static stiffness of the beam. Thus the magnitude of the DPMI in this region can be approximated by

$$Z_{Low} = K/p_{Low} \tag{4.1}$$

where (p_{Low}, Z_{Low}) is any point on the curve in the low frequency range and K, in this case, is

$$K = 48EI/L^3 \tag{4.2}$$

The minimum points of the curves appear to occur right at the fundamental frequency of the beam for all values of the beam damping. The magnitude of the DPMI at that frequency, however, does depend on the beam damping. To aid in determing the nature of that dependence, the concept of an equivalent single-degree-of-freedom oscillator is introduced.

2. The Equivalent Single-Degree-of-Freedom Oscillator

A single-degree-of-freedom oscillator (SDOFO) is a model which consists of a mass connected to the "ground" by a linear spring and a linear viscous damper as shown in Figure 4.2. Its DPMI plot, shown in Figure 4.3, was generated, allowing the damping to take on five different values.

Note that Figures 4.1 and 4.3 are identical for frequencies almost an order of magnitude above their fundamental frequency. Define an "equivalent" SDOFO of a beam as the SDOFO whose static stiffness K, fundamental frequency ω, and damping ratio ζ, are

equal to those of the beam. Then it can be said that a centrally-loaded simply-supported beam behaves in the same manner (i.e., has the same magnitude and phase angle of its DPMI) as its equivalent SDOFO up to frequencies almost an order of magnitude above their fundamental frequency.

The concept of an equivalent SDOFO is the key to deriving some of the relationships between the parameters of the beam and the characteristics of its DPMI plot. The relative simplicity of the DPMI equation of a SDOFO facilitates the derivations. A relationship derived between the parameters of the SDOFO and the characteristics of its DPMI plot will be a good approximation for any beam that behaves in a similar manner to its equivalent SDOFO in the appropriate frequency range. The relationship must be expressed in terms of K, ω and ζ and these parameters must be interpreted properly. One such relationship is the dependance of the minimum point of the DPMI plot on the beam damping. Its derivation follows.

The DPMI of a SDOFO is

$$Z^* = c + i(mp - K/p) \tag{4.3}$$

In terms of K, ω and ζ the DPMI is

$$Z^* = K/\omega \left[2\zeta + i(p/\omega - \omega/p) \right] \tag{4.4}$$

The magnitude of the DPMI is

$$Z = K/\omega \sqrt{4\zeta^2 + (p/\omega - \omega/p)^2} \tag{4.5}$$

To find the frequency at which the DPMI is minimum, take the derivative with respect to the forcing frequency p, and set it equal to zero

$$dZ/dp = K/\omega^2 \, (p/\omega - \omega/p) \, (1 + \omega^2/p^2) \, / \sqrt{4\zeta^2 + (p/\omega - \omega/p)^2} = 0 \tag{4.6}$$

The only real positive solution equation (4.6) is

$$p_{MIN} = \omega \qquad (4.7)$$

i.e., the minimum point of the curve does in fact occur at the fundamental frequency regardless of the amount of damping present. The magnitude of the DPMI at that frequency, according to equation (4.5), is

$$Z_{MIN} = 2\zeta K/\omega \qquad (4.8)$$

Equations (4.7) and (4.8) hold true for a centrally-loaded simply-supported beam with K interpreted according to equation (4.2).

More traditional frequency response curves are given in terms of a ratio of deflection δ, to static deflection F/K, rather than force to velocity, i.e.,

$$\delta K/F = 1 \; / \; \sqrt{(1 - p^2/\omega^2)^2 + (2\zeta p/\omega)^2}$$

For example, see Thompson (1972). In this case, the maximum point occurs at

$$p = \sqrt{1 - 2\zeta^2}$$

Hence, the frequency at which the maximum occurs is dependent on the damping. It was shown above that the minimum point of a DPMI curve of a SDOFO occurs right at the fundamental frequency, regardless of the damping. This is an additional advantage of presenting the response of a system as an impedance.

3. The Location of the Driving Force

Figure 4.4 is the DPMI plot of a simply-supported beam with the driving force applied at four different locations along the length of the beam.

Each of the curves have the same shape up to frequencies of at least two times the fundamental frequency. The upward shift in the curves is due to the increase in the static stiffness K

of the beam, as the driving force is moved away from the center. One might expect that equations (4.1), (4.7) and (4.8) are still valid in this case provided K is interpreted properly, i.e.,

$$K = 3EIL/a^2b^2 \qquad (4.9)$$

A few calculations to compare these equations to the appropriate points on the DPMI plot indicate that they are, indeed, good approximations.

In the high frequency range of Figure 4.4, a second resonance appears at about four times the fundamental frequency. The centrally-loaded beam does not exhibit such a resonance since the anti-symmetric modes of vibration are not excited under a symmetric loading.

B. THE EFFECT OF THE BOUNDARY CONDITIONS

1. Qualitative Effects

Ideally, the bone of a vibrating forearm or leg system is assumed to vibrate as a simply-supported beam. A discussion presented by Orne (1974) indicates that this is in fact true of the system involved in the test procedure developed by Thompson (1973) (discussed in Section I.E). However, subsequent modifications to this test procedure may have altered the simply-supported condition of the bone. Therefore, it is important to investigate the effect of various boundary conditions on the DPMI of a beam.

Figures 4.5 through 4.9 are the DPMI plots of a beam with five different, nonclassical boundary conditions: a rotational spring on one end, a rotational spring on each end, a

translational spring on one end, a translational spring on each end and a translational spring on an extended beam, respectively. In each case, the nondimensional spring constant was allowed to take on five different values while holding the damping in the beam and supports at a constant value.

A simple support on the end of a beam has infinite resistance to translation and no resistance to rotation. The DPMI of a simply-supported beam was presented in the last section, Figure 4.1.

Adding a rotational spring to a support introduces some resistance to the rotation which can occur at that support. The effect on the system is to stiffen it as indicated by the shift upward and to the right of the DPMI curves of Figures 4.5 and 4.6.

Adding a translational spring to a support relaxes some of the resistance to the translation which can occur at that support. The effect on the system is to reduce its over all stiffness as indicated by the shift downward and to the left of the DPMI curves of Figures 4.7 and 4.8.

Extending the beam past its left support and adding a translational spring to its end introduces a non-zero bending moment at the left support. This bending moment offers some resistance to the rotation which can occur there just as does a rotational spring. Hence, an expression for an equivalent rotational spring (ERS) constant was derived by equating the bending moment at the left support of the extended beam to the moment caused by the same rotation applied to the ERS. The expression is

$$R = 3\varepsilon^3 T / (12 + 2\varepsilon^3 T) \qquad (4.10)$$

where the nondimensionalized parameters are as follows (see Table 3.2)

R the ERS constant

T the translational spring constant of the spring at the end of the extended beam

ε length of the beam extension

The result of solving equation (4.10) for T is

$$T = 12R / (3\varepsilon^2 - 2\varepsilon^3 R) \qquad (4.11)$$

The set of four values of R used to generate Figure 4.5 were used in equation (4.11) to produce an equivalent set of values for T. These values were used to generate Figure 4.9. The DPMI curves of Figures 4.5 and 4.9 are virtually identical. Therefore, any system which can be modeled as an extended beam with a translational spring on its end can be modeled equally well as a beam with a rotational spring on one end provided the parameters of two models are related according to equation (4.10).

2. Re-nondimensionalization

It is apparent that the curves of Figures 4.5 through 4.8 are similar in shape regardless of the boundary conditions of the beam. The location of each curve on its plot, however, is affected by the boundary conditions. To investigate this further, Figures 4.10 and 4.11 are generated. Figure 4.10 is generated by choosing one curve from each of Figures 4.1 and 4.5 through 4.8 and re-nondimensionalizing it with respect to its own static stiffness and fundamental frequency. (Recall that all curves thus far have been nondimensionalized with respect to the static stiffness and fundamental frequency of a centrally-

loaded, simply-supported beam.) Figure 4.11 is generated by changing the damping value used for Figure 4.10 to a lower value.

Expressions for the static stiffness of a beam with various boundary conditions have been derived and are listed in Table 4.2. The fundamental frequency in each case is obtained by solving the appropriate characteristic equation. The natural frequencies of a system occur when the DPMI goes to zero for the case of no damping. For a beam, this occurs when the function $f(\lambda L)$ goes to infinity. Hence, the characteristic equation to be solved for each set of boundary conditions is obtained by setting the denominator of $f(\lambda L)$ equal to zero[3] (See Appendix A). The lowest value found for λL is then used in the following equation to obtain the fundamental frequency

$$\omega_1 = (\lambda L)^2/L^2 \sqrt{EI/\mu} = (\lambda L/\pi)^2 \omega \qquad (4.12)$$

where ω_1 is the fundamental frequency of the beam in question and ω is the fundamental frequency of a simply supported beam.

The five curves in each of Figures 4.10 and 4.11 are virtually identical up to frequencies of at least two times the fundamental frequency. Hence, two conclusions can be drawn.

First, recall that equations (4.1), (4.7) and (4.8) hold for a simple-supported beam. Then these equations also hold for (or are at least very good approximations for) beams with other boundary conditons provided K is interpreted according to Table 4.1 and ω and ζ are interpreted as fundamental frequencies and damping ratios of the beams.

Secondly, the shape of the DPMI curve (in the frequency

---

[3] Characteristic equations obtained in this way are in agreement with Gorman (1975).

range of interest, i.e., up to frequencies of at least two times the fundamental frequency of the beam) is determined by the damping ratio and the location of the DPMI curve on the plot is determined by the static stiffness and fundamental frequency of the beam. The stiffness of the boundaries of the beam affect each of these three quantities in the same way as does the bending stiffness of the beam. Therefore the bending stiffness and the boundary stiffness have the same effect on the DPMI plot of a beam up to frequencies of at least two times the fundamental frequency of the beam. At very high frequencies, the curves begin to deviate from one another. However, the deviation is only significant if the damping is relatively low. Therefore, the effects of the bending stiffness and the stiffness of the supports of a beamlike structure (i.e., an ulna or a tibia) are not easily distinguishable on its DPMI data plot.

C. THE EFFECT OF TAPER

1. Qualitative Effects

It can be seen from Figure 1.1 that long bones are not uniform. Some long bones, such as the ulna, have very severe tapers. It is, therefore, worthwhile to investigate the effect of taper on the DPMI plot of a beam.

A method of computing the DPMI of a tapered beam is given in Appendix B. This method was used to generate DPMI plots for beams with two different types of tapers: a linear taper which roughly approximates an ulna and a quadratic taper which roughly approximates a tibia (see Figure 4.12).

The nondimensionalized DPMI plot in each case turned out to be identical to that of a uniform beam. Apparently, DPMI data only provides information about the overall stiffness of a beamlike structure and not about its distribution. Therefore, no information concerning the nature of the taper of a bone can be extracted from its DPMI plot alone. However, using a model in which the bone is assumed to be uniform, the average bending stiffness is determined. This is the same average bending stiffness which was measured and correlated to breaking strength in the investigations by Borders, Petersen and Orne (1977) and Jurist and Foltz (1977). These correlations provide a means of inferring breaking strength from a measurement of bending stiffness. Thus, knowlege of the exact geometry is not needed.

D. THE EFFECT OF THE FOUNDATION

1. Qualitative Effects

The tissue surrounding the bone of a vibrating forearm or leg system is represented by a visco-elastic foundation with mass. The boundary of the foundation is either fixed or free as discussed in Section II.C. Figures 4.13 and 4.14 are DPMI plots of a simply-supported beam on a fixed foundation while Figures 4.15 and 4.16 are DPMI plots of a simply-supported beam on a free foundation. Figures 4.13 and 4.15 were generated with the damping in the foundation held constant while allowing the mass per unit length of the foundation to take on five different values. Figures 4.14 and 4.16, on the other hand, were generated with the mass per unit length of the foundation held constant

while alloving the damping in the foundation to take on four different values. In each case, the stiffness of the foundation is chosen to produce a fundamental subresonant frequency for the foundation of one-half the fundamental frequency of the beam. The arbitrary factor of one-half sufficiently seperates the subresonant frequency of the foundation from the resonant frequency of the beam to distinguish their effects.

The foundation exhibits two major effects on the DPMI curves. First, the damping in the foundation smooths out the DPMI in much the same way as the damping in the beam. The minimum point of the curve moves upward as damping increases regardless of the source of the damping (beam or foundation). Secondly, the DPMI curve changes drastically in the region around the subresonant frequency. This disturbance in the otherwise smooth curve is evident in many of the data sets from DPMI tests. It is therefore essential to include a foundation in the mathematical model.

2. Quantification of the Effect on the Minimum Point

Note from Figures 4.13 through 4.16 that the magnitude of the DPMI at the minimum point of the curves is very dependent on both the mass per unit length μ_f, and the damping ratio ζ_f, of the foundation. This dependence, expressed in mathematical form, can be used to determine approximate values for these parameters for a forearm of leg system directly from its DPMI data plot.

The fundamental frequency ω_f, of the foundation also affects the minimum point. However, it will be useful later to have relationships expressing the dependence of μ_f and ζ_f on the minimum DPMI while holding ω_f constant. The disturbance which

appears in many data sets occurs at approximately one half the fundamental frequency of the beam. Therefore, the relationship to be derived will be based on a frequency ratio ω/ω_f, of two.

Due to the complexity of the DPMI equations, the exact expression for the dependence of μ_f and ζ_f on the minimum DPMI can not be determined. Therefore, approximate relationships are derived. The details of the derivation are given in Appendix C. The relationships expressing the dependence of μ_f and ζ_f on the minimum DPMI are

$$Z_{MIN}\omega/K = 2\zeta + 0.25\ \zeta_f^{1/3}\ \mu_f/\mu \qquad (4.13)$$

$$Z_{MIN}\omega/K = 2\zeta + 0.75\ \zeta_f^{1/2}\ \mu_f/\mu \qquad (4.14)$$

for the fixed and free foundation, respectively. Since these relationships are approximate, it is beneficial to demonstrate their accuracy. This is done in Figure 4.17. The minimum DPMI's tabulated in Table 4.2 are shown as squares on the plot while equations (4.13) and (4.14) are shown as solid lines. The approximation is quite accurate for the range of values under consideration.

E. THE EFFECT OF THE SPRING-IN-SERIES

1. Qualitative Effects

The skin of the vibrating forearm or leg system is represented by a transverse spring in series with the beam. DPMI plots of a simply-supported beam with the spring in place are given in Figures 4.18 and 4.19. Figure 4.18 was generated with the damping of the beam held constant while allowing the spring stiffness to take on five different values. Figure 4.19, on the

other hand, was generated with the spring stiffness held constant while allowing the damping of the beam to take on five different values.

At very low frequency, the curves are predominantely springlike (i.e., the slope of the curve is virtually negative one). The apparent stiffness is simply the combined static stiffnesses of the beam and spring in series. At very high frequency, the curves are again springlike. However, the apparent stiffness is higher than the apparent stiffness in the low frequency range. In the high frequency range, the beam DPMI is predominantely masslike (see Figure 4.1) while the spring, of course, is still springlike. Thus, the beam DPMI is much higher than that of the spring. Recall that DPMI's in series add according to

$$Z^* = (1/Z_1^* + 1/Z_2^*)^{-1} \qquad (4.15)$$

The lower of the two DPM 's, the DPMI of the spring in this case, dominates the overall DPMI. Therefore, at very high frequency the overall DPMI is simply the DPMI of the spring. In other words, the beam, due to its mass and damping, does not vibrate at high frequency.

The apparent stiffness at low and high frequencies have often been used to approximate the bone and skin stiffnesses of forearm or leg systems directly from the DPMI plots. A data point is chosen from each of the (low and high) frequency ranges and used in the following formulas

$$k = Z_{HIGH} P_{HIGH} \qquad (4.16)$$

$$K = (1/Z_{LOW} P_{LOW} - 1/k)^{-1} \qquad (4.17)$$

Where k = skin stiffness

K = bone stiffness (eg., $3EIL/a^2b^2$ for a simply-supported beam)

(P_{HIGH}, Z_{HIGH}) = a data point from the high frequency range

(P_{LOW}, Z_{LOW}) = a data point from the low frequency range (see Figure 4.20)

However, large errors are easily introduced with improper choices of the data points. Recall that the data points must be taken from sections of the data plot where the frequency is low enough or high enough to indeed produce a slope which is virtually negative 45 degrees. This stipulation does not present a problem in the low frequency range. However, the data from most DPMI tests have not been taken in a frequency range high enough to attain the required negative 45 degree slope. However, a new relationship has been discovered which allows the skin stiffness to be approximated using the maximum point (see Figure 4.20) which occurs just before the high frequency negative slope on the data plot. This eliminates the need for the high frequency data.

2. Quantification of the Effect on the Maximum Point

It can be seen from Figures 4.18 and 4.19 that the maximum point is severely affected by the spring. Although the maximum value of the DPMI has a significant dependence on the damping of the beam, the frequency at which it occurs does not. Therefore, an approximate relationship between the stiffness of the spring and the frequency at which the maximum DPMI occurs can be derived which is independent of the damping in the beam.

To find this relationship, two simplifications are

introduced to facilitate the analysis. First, replace the beam by its equivalent single-degree-of-freedom oscillator (SDOFO). Recall from Sections IV.A and IV.B that a beam, regardless of its boundary conditions, behaves in the same manner as its equivalent SDOFO up to frequencies of at least two times their fundamental frequency. In many cases the similarity in behavior extends to as high as an order of magnitude above the fundamental frequency. Recall further that at high frequency, the DPMI of a spring-in-series dominates the total DPMI. Therefore, a spring in series with a beam behaves in the same manner as a spring in series with a SDOFO at any frequency provided the spring is soft enough.

Secondly, since the frequency of interest is assumed to be independent of the damping, set the damping equal to zero. Then the frequency which makes the DPMI maximum will actually be the frequency which makes the DPMI approach infinity. Thus, the model to be analysed is that which is shown in Figure 4.21 with $\zeta = 0$.

The DPMI's of the SDOFO and the spring are, respectively

$$Z_1^* = mip + K/ip \qquad (4.18)$$

$$Z_2^* = k/ip \qquad (4.19)$$

where p is the forcing frequency. The overall DPMI, according to equation (4.15) is

$$Z^* = [\,1/(mip + K/ip) + 1/(k/ip)\,]^{-1} \qquad (4.20)$$

After replacing m by K/ω^2 and performing several steps of algebra, equation (4.20) becomes

$$Z^* = -iK/\omega \; (k/K)/(p/\omega) \; (1 - p^2/\omega^2) \; / \; (1 + k/K - p^2/\omega^2) \qquad (4.21)$$

The DPMI approaches infinity when the denominator of equation (4.21) approaaches zero

$$1 + k/K - p^2_{MAX}/\omega^2 = 0 \qquad (4.22)$$

Therefore the frequency at which the DPMI is maximum is given by

$$p^2_{MAX}/\omega^2 = 1 + k/K \qquad (4.23)$$

Solve equations (4.17) and (4.23) simultaneously for k and K

$$k = Z_{LOW} P_{LOW} p^2_{MAX}/\omega^2 \qquad (4.24)$$

$$K = Z_{LOW} P_{LOW} p^2_{MAX}/\omega^2 \; / \; (p^2_{MAX}/\omega^2 - 1) \qquad (4.25)$$

Equations (4.24) and (4.25) can now be used to approximate the bone and skin stiffnesses without the use of equation (4.16), i.e., without the use of a data point from the very high frequency range.

Figures 4.18 and 4.19 show that the location of the minimum point is only slightly affected by the presence of the spring. This indicates that the relationships discussed in Section IV.A and IV.B (equations 4.7 and 4.8) which relate the minimum point to the damping ratio and the fundamental frequency are still approximately valid in the presence of the spring. This is also verified by considering the frequency which makes equation (4.21) go to zero, i.e., set the numerator equal to zero

$$1 - p^2_{MIN}/\omega^2 = 0 \qquad (4.26)$$

or

$$p^2_{MIN}/\omega^2 = 1 \qquad (4.27)$$

Since equations (4.23) and (4.27) were obtained by considering the case where $\zeta = 0$, they are approximations which are independent of the beam damping. To investigate the accuracy of these approximations, the minimum and maximum points of the DPMI of the model of Figure 4.21 can be found without setting the beam damping equal to zero. Although this analysis is nearly impossible in closed form, the first few terms of a Taylor series solution can be found. This very lengthy analysis is

outlined in Appendix D. The first three terms of the solutions are

$$\beta^2_{MAX} = S + 1 + 2/S\ (2+S)/(1+S)\ \zeta^2 - 2/S^3\ (2+S)/(1+S^3)\ (4+16S+13S^2+4S^3)\ \zeta^4 + \ldots \quad (4.28)$$

$$\beta^2_{MIN} = 1 - 4/S\ \zeta^2 + 8/S^3\ (2+3S)\ \zeta^4 - \ldots \quad (4.29)$$

where $S = k/K$ and $\beta = p/\omega$. Both series converge for $0<\zeta<1$ and $S>1$ which is the range of values of interest.

Several typical values of ζ and S have been tried in equations (4.28) and (4.29) and compared to the results from equations (4.23) and (4.27), respectively. For example, with ζ = 0.2 and S = 5, equation (4.28) yields β_{MAX} = 2.453 while equation (4.23) yields β_{MAX} = 2.449. This and many other sets of values indicate that equations (4.23) and (4.27) are indeed very good approximations.

CHAPTER V

THE SYSTEMS IDENTIFICATION ALGORITHM

A. THE NEED FOR A SYSTEMATIC METHOD

1. The Need

Each of the parameters of the mathematical model corresponds to one (or some combination) of the geometrical or material properties of the vibrating forearm or leg system. The driving-point mechanical impedance (DPMI) of the system is measured in a vibration test (Section I.E). The DPMI of the model is calculated and depends on the values chosen for its parameters (Section III.A). Therefore, the set of parametric values for the model which generates a DPMI curve that closely coincides with the DPMI data points of the system infers the geometrical and material properties of that syatem. A method for finding this set of parametric values is needed.

2. Requirements

To obtain a consistent interpretation of the DPMI data, the method used to find the parametric values (hence forth referred to as "the method") must be repeatable and systematic. The method must be repeatable in the sense that each time it is

applied to a given set of DPMI data it must produce the same results. The method must be systematic enough to program on a digital computer for on-line analysis.

Although computers are capable of performing tremendous amounts of computation, they are incapable of making subjective decisions. The method must be completely objective in nature and expressible in mathematical form.

Finally, the computer program which employs the method must be set up in a user-oriented fashion. The user in a clinical situation should not need extensive computer experience in order to easily obtain results.

B. THE ERROR FUNCTION

1. Definition

The first step in developing the method is to define an error function which quantifies the difference between the measured DPMI data and the calculated DPMI of the mathematical model. The parametric values of the model will then be chosen in a systematic way to minimize the error function. This is accomplished using a systems identification algorithm (SIDA) which is analogous to the classical least-squares approach to curve fitting.

The error e_n, at frequency p_n, is the difference between the measured DPMI $\hat{Z}_n$, and the DPMI calculated using the model $Z_n(P_i)$, as shown in Figure 5.1a. The error function E, is the finite sum over all the discrete test frequencies of the squares of the percentage errors $e_n/\hat{Z}_n$, divided by the number of data

points. The percentage error is used rather than the error itself because of the wide range of absolute values which the DPMI can take in a single DPMI test. The division by the number of data points normalizes the error function so that a comparison of its value from two sets of data with different numbers of data points is meaningful. The error, and hence the error function, is a function of the parameters of the model since it depends on the DPMI of the model. An example of an error function as a function of one of the model parameters, represented by P_i, is shown in Figure 5.1b.

2. Analysis

Mathematically, the error function is expressed as

$$E = 1/N \sum_{n=1}^{N} [(\hat{Z}_n - Z_n(P_i)) / \hat{Z}_n]^2 \qquad (5.1)$$

where N is the number of data points. To obtain the parametric values using a classical least-squares approach, one would set the derivatives of the error function with respect to each of the parameters equal to zero. The resulting equations would then be solved directly for the parametric values. Due to the complexity of the function which represents the DPMI of the model, however, this approach is impractical if not impossible.

Since the DPMI of the model is a continuous function of the model parameters, it can be expanded in a Taylor series.

$$E = 1/N \sum_{n=1}^{N} 1/\hat{Z}_n^2 \left[\hat{Z}_n - \left(Z_n + \sum_{i=1}^{M} dZ_n/dP_i \ \Delta P_i \right) \right]^2 \qquad (5.2)$$

where M is the number of model parameters. Higher order terms of the series have been neglected and the function which represents the DPMI of the model and its derivatives are evaluated at some initial set of estimated parametric values.

Using this form of the error function, changes in the

parametric values ΔP_i, rather than the parametric values themselves, can be chosen to minimize the error function. To accomplish this, set the derivatives of the error function with respect to the changes in the parametric values equal to zero

$$dE/d\Delta P_j = -2/N \sum_{n=1}^{N} 1/\hat{Z}_n^2 \left[\hat{Z}_n - \left(Z_n + \sum_{i=1}^{M} dZ_n/dP_i \ \Delta P_i \right) \right] dZ_n/dP_j$$
$$= 0 \ ; \quad j = 1,2...M \tag{5.3}$$

After a few steps of algebra, equation (5.3) becomes

$$dE/d\Delta P_j = -2/N \left[\sum_{n=1}^{N} (\hat{Z}_n - Z_n)/\hat{Z}_n^2 \ dZ_n/dP_j \right. \tag{5.4}$$
$$\left. - \sum_{i=1}^{M} \sum_{n=1}^{N} 1/\hat{Z}_n^2 \ dZ_n/dP_i \ dZ_n/dP_i \ \Delta P_i \right] = 0; \ j = 1,2...M$$

Therefore the equations to be solved are

$$[A] \{\Delta P\} = \{B\} \tag{5.5}$$

Where the components of the matrices are

$$A_{ij} = \sum_{n=1}^{N} 1/\hat{Z}_n^2 \ dZ_n/dP_i \ dZ_n/dP_j \tag{5.6}$$

and $$B_j = \sum_{n=1}^{N} (\hat{Z}_n - Z_n)/\hat{Z}_n^2 \ dZ_n/dP_j \tag{5.7}$$

The derivatives of the DPMI of the model with respect to each of the parameters is given in Appendix E.

3. Application

Since changes in the parametric values are calculated rather than the parametric values themselves, the procedure is iterative. The components of the A and B matrices are calculated using the parametric values obtained from previous iteration. The changes in the parametric values are calculated from

$$\{\Delta P\} = [A]^{-1} \{B\} \tag{5.8}$$

and added to the old set of parametric values to obtain a new set. Each succesive set of parametric values will reduce the value of the error function. The procedure is repeated as many times as necessary to obtain an acceptable set of parametric values.

To begin the iterations, an initial set of parametric values must be chosen which will facilitate quick convergence.

C. CONVERGENCE AND THE INITIAL GUESS

1. Definition

Convergence is said to have occurred in an iteration scheme when further iterations no longer improve the result. In terms of the SIDA, convergence has ocurred when the relative change in any given parameter becomes smaller than a specified amount, e.g., 0.1 percent. The characteristics of the error function have a considerable effect on the convergence of the SIDA. Therefore, some control must be maintained over the error function to insure convergence for the DPMI data from any forearm or leg vibration test.

2. Restrictions on the Mathematical Model

When two parameters of a given mathematical model have very similar effects on its DPMI curve, the effect of changing one parametric value may cancel an opposite effect in the other to produce no net effect in either the DPMI curve or the value of the error function. In this case, the error function may contain an infinite number of minimum points along some curve in the error function space. There is no way to distinguish between these minimum points. Therefore the DPMI data does not contain enough information itself to uniquely define all of the parameters of the model, and the SIDA will diverge. This problem has ocurred with the boundary conditions of the beam and with

the damping. To eliminate the problem, something more must be known about one of the two parameters. A constant value can then be assigned to it, allowing the rest of the parameters to be determined by the SIDA.

It was shown in Section IV.B, that the static stiffness of a beam, and hence its DPMI, is affected in much the same way by the bending stiffness of the beam itself as by the stiffness of the boundaries. Therefore, if the model includes a spring at one or both ends of the beam. Then the DPMI data does not contain enough information to determine all of the parametric values. Therefore, the characteristics of the supports of the forearm or leg must be known a priori. One way to avoid the necessity of determining the support characteristics is to always place the forearm or leg in the fixture in such a way to insure that the supports are virtually simply-supported.

The sharp peaks of the minimum and maximum points of the DPMI curve of an undamped beam are rounded-off when damping is added. The extent of the rounding-off depends on the amount of damping present but not on its location, i.e., in the beam or foundation, as was shown in Section IV.D. Since both the bone and the tissue contribute to the overall damping of the system, the DPMI data does not contain enough information to determine all of the parametric values. A constant value will be assigned to one of the damping ratios, thus allowing the other to be determined by the SIDA. It will be seen in Section VI.A that the tissue contributes much more to the overall damping than does the bone. Consequently, the DPMI is relatively insensitive to the value chosen for the damping ratio of the beam. Therefore, it will be held constant at five percent of critical damping in

the fundamental mode, a reasonable value.

With the boundary conditions being specified and the damping in the beam held constant, the model has six parameters to be determined by the SIDA. They are the bending stiffness EI, and the fundamental frequency ω, of the beam; the mass per unit length μ_f, the fundamental frequency ω_f, and the damping ratio ζ_f, of the foundation and the stiffness k, of the spring. This version of the model will be referred to as the six-parameter model (6PM).

3. The Initial Guess

Even if all of the parameters are such that their effects on the DPMI curve are independent, it is possible that more than one set (but not and infinite number of sets) of parametric values exist which will minimize the error function for the DPMI data from any given vibration test. One of these referred to as the correct solution, is the set of parametric values corresponding to the true geometric and material properties of the forearm or leg system being tested.

Several successive iterations of the SIDA can produce a set of parametric values associated with one of the local minimum or maximum points of the error function. To illustrate this concept, an error function is shown in Figure 5.1b. Only one of these minimum points represents the correct solution, and it appears to be the only one in which all of the parametric values are positive. The initial values chosen for the parameters to start the iterations, referred to as the initial guess, determine whether or not the SIDA will converge and to which minimum or maximum point. Therefore, the initial guess must be

close enough to the correct solution to allow the SIDA to converge to it.

The means for acquiring the initial guess is provided by the relationships established in the parametric study (Chapter IV). The initial guess is calculated from a few key data points using these relationships. In many cases, the intial guess is close enough to the correct solution. However, if one or more of the key data points happens to contain an excessive amount of experimental error then the initial guess will not be close enough. This problem is overcome by temporarily simplifying the model.

The model is simplified by eliminating the foundation. The damping effect that the tissue has on the bone is accounted for by a higher than normal damping in the beam. The simplified model has only four parameters to be determined by the SIDA. They are the bending stiffnes EI, the fundamental frequency ω, and the damping ratio ζ, of the beam and the stiffness k, of the spring. This version of the model will be referred to as the four-parameter model (4PM).

A reduction in the number of parameters in the model is accompanied by a reduction in the number of minimum and maximum points in the error function. This increases the chance for convergence to the correct solution when applying the SIDA. The results from applying the SIDA to the 4PM are used as part of an improved initial guess for the 6PM, thus increasing the chance for convergence when applying the SIDA to the 6PM. The process described herein occurs in three phases. The SIDA is applied in a different way in each phase.

In phase one, the SIDA is applied to the 4PM. The initial

guess is determined by solving equations (4.7), (4.8), (4.28) and (4.29) for the four parameters

$$EI = a^2b^2/3L\phi \; Z_{LOW}P_{LOW} \; (P_{MAX}/P_{MIN})^2 \; / \; [\,(P_{MAX}/P_{MIN})^2 - 1\,] \qquad (5.9)$$

$$\omega = P_{MIN} \qquad (5.10)$$

$$\zeta = 1/2 \; Z_{MIN}P_{MIN}/Z_{LOW}P_{LOW} \; [\,(P_{MAX}/P_{MIN})^2 - 1\,] \; / \; (P_{MAX}/P_{MIN})^2 \qquad (5.11)$$

$$k = Z_{LOW}P_{LOW} \; (P_{MAX}/P_{MIN})^2 \qquad (5.12)$$

where (P_{LOW}, Z_{LOW}), (P_{MIN}, Z_{MIN}) and (P_{MAX}, Z_{MAX}) are the key data points as shown in Figure 4.20, and ϕ is a constant which depends on the boundary conditions of the beam (see Table 4.2).

In phase two, the SIDA is applied to the 6PM. However, only the foundation parameters are allowed to vary. The bending stiffness and the fundamental frequency of the beam and the stiffness of the spring are held constant at the values determined from phase one. The damping ratio of the beam is reduced to the reasonable value of 0.05 as mentioned earlier. Phase two allows the values of the foundation parameters to be improved without disturbing the beam and spring parameters. The initial guess is partially based on experience with simulating DPMI data "by hand" and partially based on equation (4.16). The fundamental frequency and damping ratio are guessed from experience to be one-half of those of the beam. The mass per unit length is calculated by solving equation (4.16). Thus the initial guess is calculated from

$$\mu_f = \pi^4/L^4 \; EI/\omega^2 \; 2(\zeta - 0.05)/A(\zeta/2)^n \qquad (5.13)$$

$$\omega_f = \omega/2 \qquad (5.14)$$

$$\zeta_f = \zeta/2 \qquad (5.15)$$

In phase three, the SIDA is again applied to the 6PM. All six parameters are allowed to vary. The initial guess is simply the results of phases one and two. The SIDA converges to the

correct solution for the DPMI data from almost any reasonable forearm or leg vibration test. Examples will be given in Chapters VI and VII.

D. THE COMPUTER PROGRAM

1. The Program

A Fortran computer program was written to carry out the process described in the last section. Due to the complexity of the DPMI functions being evaluated, the program is written in double precision. A listing of the program is given in Appendix F.

The computer program is divided into three phases of the total process. Each phase is similar in structure. A general flow chart of the program is shown in Figure 5.2 and a more detailed flow chart of one phase is shown in Figure 5.3. Control passes through the main loop of each phase of the program until the iterations are terminated by the passing of one of the four tests as indicated in the diamond shaped boxes in the flow chart.

The first test is to determine whether or not a negative value was obtained for one of the parameters in the previous iteration. Unlike the other three tests, the consequence of passing this test depends on the phase. In phase one, the parameters are returned to their old values. In phase two, the tissue parametric values are returned to their initial guess. In phase three, the 6PM is disregarded and the parametric values obtained for the 4PM are recalled.

The second test is to determine whether or not the value of the error function has increased in the last iteration. If it has, then this is an indication that the parametric values are either moving away from the correct minimum point of the error function toward a maximum point or that the SIDA has overstepped the minimum point. In either case, the old set of parametric values are closer to the correct solution than the new set. Therefore, the parameters are returned to their old values.

The third test is to determine whether or not convergence has occurred. Convergence is considered to have occurred when all of the percentage changes in the parameters have become less than one-tenth of a percent.

The fourth test is to determine whether or not ten iterations have occurred. A limit of ten iterations is placed on each phase to insure that the iterations will not go on indefinitely.

If all four tests fail in a given iteration, then control is transferred back to the top of the loop and another iteration is carried out.

2. The Matrix Equation

Within each iteration of the SIDA, a matrix equation of the form

$$[A]\{\Delta P\} = \{B\} \tag{5.5}$$

is generated. The solution is to be obtained within the computer progam using the subroutine DGELG from the IBM Scientific Subroutine Package (*SSP). DGELG solves the matrix equation using Gaussian elimination.

Accuracy of the calculations is an important factor since it can influence convergence of the SIDA. Matrix A, however, is an ill-formed matrix, i.e., its elements vary in absolute value as much as ten to twenty orders of magnitude. Ill-formed matrices are very difficult to solve accurately. Therefore, equation (5.5) will be modified to eliminate the ill-formedness of matrix A.

Consider matrix equation (5.5) in component form

$$\sum_{i=1}^{M} A_{ij} \Delta P_i = B_j \; ; \quad j = 1,2...M \tag{5.16}$$

Equation (5.16) represents M linear algegraic equations, where M is the number of parameters to be determined by the SIDA. Each of the algebraic equations can be multiplied by a constant without altering the solution.

$$\sum_{i=1}^{M} (C_i A_{ij}) \Delta P_i = (C_j B_j) \; ; \quad j = 1,2...M \tag{5.17}$$

where C_j, $j = 1,2...M$ is a set of M constants. Furthermore, the coefficients of each unknown can be multiplied by a constant if that unknown is divided by the same constant. Using the same set of M constants, the symetry of matrix A is preserved.

$$\sum_{i=1}^{M} (C_i C_j A_{ij}) \; (\Delta P_i / C_i) = (C_j B_j) \; ; \quad j = 1,2...M \tag{5.18}$$

thus the new matrix equation is

$$[\hat{A}] \; [\hat{\Delta P}] = [\hat{B}] \tag{5.19}$$

where

$$\begin{aligned} \hat{A}_{ij} &= C_i C_j A_{ij} \\ \hat{\Delta P}_i &= \Delta P_i / C_i \\ \hat{B}_j &= C_j B_j \end{aligned} \tag{5.20}$$

Refering to the definitions of A_{ij} and B_j given in equations (5.6) and (5.7), the orders of magnitude of each of the quantities in equation (5.16) are as follows:

A_{ij} has order $P_i^{-1} \; P_j^{-1}$

ΔP_i has order P_i

B_j has order P_j^{-1}.

The difference in the orders of magnitude of ΔP_i, $i = 1,2...M$ results in the ill-formedness of matrix A. However, matrix $\hat{A}$ will be well-formed if the constants are chosen so that each element of matrix $\hat{A}$ is of order one. This can be accomplished by choosing

$$C_i = 1/B_i \; ; \quad i = 1,2...M \tag{5.21}$$

Then the new matrix equation becomes

$$[\hat{A}]\,\{\hat{\Delta P}\} = \{I\} \tag{5.22}$$

where

$$\hat{A}_{ij} = A_{ij}/(B_i B_j) \qquad \hat{\Delta P}_i = B_i \Delta P_i \tag{5.23}$$

and all of the components of the column matrix I are unity.

Matrix equation (5.22) can be solved without loss of accuracy because matrix $\hat{A}$ is well-formed. The solution, however, is different from the solution to matrix equation (5.5). The relationship between the two solutions is known from equation (5.23). Hence the solution to equation (5.5) is calculated from the solution to equation (5.22) by

$$\Delta P_i = \hat{\Delta P}_i / B_i \; ; \quad i = 1,2...M \tag{5.24}$$

3. Input

To make the computer program user oriented, the input required to run it has been simplified as much as possible. Only four lines of information are required in addition to the data points themselves. The input is checked by the computer program and error messages are printed out to inform the user if it is not in proper form. An example of input is given in Figure 5.4.

The first line is a title. The user can insert anything he

wishes with a limit of sixty characters. The title is printed on both the output and the plot.

The second line contains the support length of the forearm and the length-to-probe location ratio. This ratio is the distance between the left support and the driving point divided by the support length. The ratio must be a number between zero and one. If it is not, then an error message is printed. The length and ratio are read in free format.[4]

The first two columns of the third line contain an integer.[5] A negative integer indicates that the specimen is an ulna and a positive integer indicates that the specimen is a tibia. Recall that the boundary condition on the foundation of the model is either free or fixed depending on the type of specimen being represented. This is the only indication given to the program concerning the type of specimen. The data is interpreted according to the value given on this line regardless of what information is entered in the title. If a zero appears on this line, then the foundation is not included in the model.

The fourth line contains the number of the data points. This number must also appear as an integer in the first two columns. At least eight but no more than sixty data points are alloved. An error message is printed if this is violated.

Starting with line five, the remaining lines contain the data points, one per line. The forcing frequency, magnitude of

---

[4] Free format: There is no restrictions on the form of the number, i.e., with or without a decimal point, with or without scientific notation. A comma and/or at least one space must appear between each entry.

[5] Integer: Decimal points and scientific notation are not alloved. Note, a one-digit number with no sign must appear in column two.

the DPMI and the phase angle of the DPMI must appear in order and in free format.

The only other restriction on the input concerns units. Frequencies and phase angles are entered in Hertz (cycles per second) and degrees, respectively. All other quantities must have consistent units. No conversion factors have been written into the program. The CGS system is suggested, i.e., all quantities are expressed in terms of centimeters, grams, seconds and dynes.

4. Output

To make the program user oriented, the output must be easy to read and interpret. An example of output is given in Figure 5.5. The corresponding computer plot is given in Figure 5.6.

The title, given by the user on the first line of the input, is printed at the top of the output page followed by the length and ratio. The parameters of the model are listed with their values. The data points and their corresponding DPMI's of the model are tabulated. Finally the value of the error function is given.

A computer plot is also generated as part of the output. The squares represent the DPMI data points. The solid line represents the DPMI of the model, calculated using the final parametric values, determined by the SIDA. Both the magnitude and the phase angle of the DPMI are plotted to visualize the quality of the simulation.

CHAPTER VI

VERIFICATION OF THE MATHEMATICAL MODEL

A. IN VITRO MONKEY EXPERIMENTS

1. Proposed Experiments

A series of experiments was proposed by Orne and Mandke (1975) to verify the mathematical model. These experiments are designed to isolate the effects of the various components of the vibrating forearm system. The experiments involve the application of the test procedure, described in Section I.E., to a monkey arm under three different conditions.

The anatomy of the arm and forearm of a monkey is quite similar that of a human arm and forearm. There are, of course, some minor differences but the similarity is strong enough so that the results of these experiments will provide and indication of the validity of the application of the mathematical model to experiments done with either species.

A few modifications, including the addition of a fourth condition, were introduced before the experiments were conducted by Peterson (1977). A description of the experiments (in modified form) is given here.

The arm of a sacrificed monkey is disarticulated at the

shoulder and immediately frozen to maintain freshness until the experiments could be performed. The specimen was thawed and allowed to come to room temperature before testing. The following experiments were then performed as quickly as possible.

The monkey arm is positioned in the test fixture. A weight is placed at the top of the humerus to represent the downward force applied through the humerus by the live subject, as shown in Figure 6.1. This first condition should resemble an *in vivo* test as much as possible. The driving-point mechanical impedance (DPMI) of this system is measured.

A small piece of skin is removed from the forearm to allow the probe to be applied directly to the ulna. This is the second condition. The DPMI is again measured.

All of the tissue surrounding the bones between the supports is removed. The joints and the tissue surrounding the joints at the supports is left intact. Care is taken that the support conditions are not altered between the first three conditions. A third set of DPMI data is taken.

Finally, the ulna is completely excised. Holes are drilled in the ends of the ulna to accommodate small steel pins. Care is taken in drilling the holes so that the orientation of the ulna is not changed between the third and fourth conditions. The pins are supported in brackets as shown in Figure 6.1. The fourth set of DPMI data is taken.

2. The Mathematical Model

The DPMI plots produced by the experiments are to be used to verify the mathematical model described in Section II.E. To

do this, the DPMI plots are simulated using the mathematical model in its appropriate form. The validity of the mathematical model is verified by demonstrating its capability to accurately simulate each of the DPMI plots produced by the experiments. Furthermore, each parametric value obtained by the simulations must be within a range of reasonable values and, of course, must be non-negative.

In the fourth condition (excised ulna), the ulna is supported by a pin and bracket at each end. The pins, which are made of steel are smooth and relatively rigid. The smoothness of the pins produces essentially no resistance to rotation while their rigidty provides essentially infinite resistance to translation.[6] Therefore the excised ulna can be modeled as a simply-supported beam. For each successive condition, in reversed order, the element is added to the mathematical model which corresponds to the component of the system which was removed in obtaining the previous condition.

The third condition (musculature removed) differs from the excised-ulna condition only in the manner in which the ulna is supported. Ideally, the joints provide simple supports for the ends of the ulna, yielding identical DPMI plots for the two conditions. If the two DPMI plots are not identical, however, then the DPMI plot of the arm in the musculature-removed condition will provide and indication of the true boundary conditions of a live forearm.

The second condition (probe on ulna) has all of the tissue

---

[6] The relative rigidity of the pins was verified by calculating the static stiffness of a pin and comparing it to a typical value of static stiffness of a bone. A difference of two to three orders of magnitude was found.

surrounding the ulna and radius in place. The layer of skin between the probe and ulna in this case has been removed. Therefore the mathematical model includes the foundation but not the spring-in-series.

Finally, the first condition (intact arm) is modeled according to the mathematical model description given in Section II.C. Since all of the components of the vibrating forearm system are present, all of the elements of the mathematical model are present.

The form of the mathematical model for each successive condition (in reversed order) contains all of the parameters present in the previous condition together with one or more additional parameters. The parametric values obtained for the previous condition are preserved while values for the additional parameters are obtained using the systems identification algorithm (SIDA) described in Chapter V. This consistent building-block approach to modeling the intact arm gives greater confidence that the model actually represents the physical system and that arbitrary curve-fitting is reduced to a minimum.

3. Application of the Systems Identification Algorithm

A set of computer programs was written to carry out the simulations discussed above using the SIDA. These computer programs are each similar to a "one-phase" version of the computer program described in Section V.D. The most significant modification is that the derivatives, calculated within each iteration of the SIDA, are replaced by finite differences, i.e.,

$$dZ_n/dP_i = [Z_n(P_i + \delta P_i) - Z_n(P_i)]/\delta P_i \qquad (6.1)$$

where the finite increment in the parameter δP_i, is taken to be one percent of the current value of the parameter.

Early on in the development of the SIDA, some sets of data were simulated using the SIDA both with exact derivatives and with the derivatives approximated by finite differences. The values of the derivatives and the finite differences were printed out by the computer programs so that they could be compared. Their values were found to be in agreement within at least two, and often within three decimal places. Hence, accuracy of the finite differences does not present a problem.

A trade-off exists between the effort spent in deriving exact expressions for the derivatives of the DPMI function with respect to each parameter of the mathematical model and computer time spent in calculating the finite difference approximations to those derivatives. The set of computer programs used to simulate the <u>in vitro</u> experiments must be very adaptable. Several versions of the mathematical model are use in an attempt to produce good simulations, but each corresponding version of the program is run only a few times. When finite differences are used rather than exact derivatives, much less effort is required to change the computer program and employ a different version of the mathematical model. Therefore, the extra computer time spent to calculate the finite differences is justified by their adaptability and convenience. On the other hand, the computer program which was developed to simulate <u>in vivo</u> tests is to be run many times without changes. The same program is used with many different sets of data. The effort spent in deriving exact expressions for the derivatives required for this computer program is justified by the saving of much computer time.

Another important difference is that the set of "one-phase" computer programs is not as user-oriented as the computer program described in Section V.D. Adaptability is required not only in the mathematical model but also in the method of establishing the initial guess. Therefore, the initial guess is calculated "by hand" and read in at the beginning of the computer program. This adaptability is more important than the simplicity of the input in this case.

4. Results From Monkey 663

The series of experiments, described earlier in this section, were performed on the forearms of three monkeys, identified by their numbers, 659, 663 and 665. The DPHI data produced by these experiments were simulated by the set of computer programs discussed above, using the various versions of the mathematical model. The resulting DPHI plots associated with Monkey 663 are shown in Figures 6.2 through 6.5. The solid lines represent the DPHI of the mathematical model while the boxes represent the data points generated in the experiments. The corresponding parametric values are listed in Table 6.1.

Figure 6.2 is the DPHI plot of the ulna in its excised state. As expected, the DPHI data is well simulated as a simply-supported beam. Therefore the value obtained for the bending stiffness is the best possible estimate of its true value.

Figure 6.3 is the DPHI plot of the same ulna with the musculature removed but with the joints left intact. It is easily seen that the excised-ulna and musculature-removed plots are quite different from one another other. The excised ulna is virtually simply-supported. Therefore, since no other parameters

C-2

were changed between the excised-ulna and musculature-removed cases, the support conditions of the ulna when the joints are intact must be something other than simply-supported.

The bone parametric values determined from the excised-ulna case were used for the musculature-removed case; holding them constant while determining values for the boundary condition parameters that will best simulate the data. The boundary conditions which produce the best results were found to be a rotational spring on one end of the beam and simply-supported on the other. Damping was also included at both ends of the beam.

Based on the parametric studies of Section IV.B, a significant amount of resistance to rotation can be created if the downward force applied through the humerus is not directly in line with the support as shown in Figure 6.6. Hence, this is most likely the major cause of the resistance to rotation at the support in these experiments, but experimental verification is necessary.

Figure 6.4 is the DPMI plot of the arm in which the layer of skin between the probe and ulna is removed but the rest of the tissue is left intact. The major difference between the musculature-removed and probe-on-ulna plots is the increase in damping in the latter case, i.e., the region around the minimum point of the DPMI plot is moved upward. The tissue, in fact, contributes much more to overall damping than does the bone.

Figure 6.5 is the DPMI plot of the intact arm. The major difference between the probe-on-ulna and intact-arm plots is an overall decrease in DPMI. This is to be expected since the skin between the probe and the bone is in series with the bone. The DPMI of the whole system is less than the DPMI of either part

alone.

A slightly better fit is obtained using Orne's three-parameter model for the skin (see Section II.C) rather than the spring alone. However, the skin, when tested alone, does behave as a simple spring, see Figure 2.2. These experiments would have to be rerun to include higher frequencies to better define this behavior.

Since the mathematical model has all of the capabilities necessary to simulate the entire set of in vitro experiments, it is a good representation of the physical system. In dealing with an in vivo test, however, the support conditions of the physical system must be evaluated. The parametric values obtained from a simulation in this case, will be valid only if the boundary conditions of the mathematical model are a good representation of the support conditions of the physical system.

5. Results From Monkey 665

The experiments run on Monkey 663, as discussed above, were also run on Monkey 665. The data was simulated using the SIDA and the same versions of the mathematical model. The resulting DPMI plots are shown in Figures 6.7 through 6.10. The corresponding parametric values are listed in Table 6.2.

Again, the excised-ulna data of Figure 6.7 is well simulated as a simply-supported beam. The remainder of the data sets, however, are not simulated as well. A disturbance, occurring at about 200 Hz, in the musculature removed plot becomes progressively more pronounced in the probe-on-ulna and intact-arm plots. This disturbance is similar in appearance to that which is expected from the tissue surrounding the bone.

However, the tissue is not the cause of the disturbance in this case since it also appears in the musculature-removed plot. The true origin of the disturbance in this data set is not known. It is not likely, however, that it is a true characteristic of the vibrating forearm system, since it does not appear in the data from the other two monkeys.

The disturbance found to occur in most of the data from human subjects is still thought to be a result of the tissue surrounding the bone. This situation does not occur in the monkey data, since the monkey has less tissue on his bones. Similar experiments on a human cadaver arm must be run to verify this effect.

6. Results From Monkey 659

The DPMI plots of Monkey 659 are shown in Figures 6.11 through 6.15. The corresponding parametric values are listed in Table 6.3. Two major differences exist between the procedure of these experiments and that of Monkeys 663 and 665. First, DPMI data for the ulna in its excised state was not taken until two months after the other DPMI data. During that time, the ulna was stored in a refrigerator. Second, DPMI measurements were taken on the intact arm at both a 400 and 600 gram-force preload.

As in the other two cases, the excised-ulna data of Figure 6.11 is well simulated as a simply-supported beam. The musculature-removed data of Figure 6.12, however, could not be simulated directly using the same boundary conditions in the mathematical model as those used for Monkeys 663 and 665. Recall that the excised-ulna data was obtained two months after the other data. Although the attempt was made to maintain freshness,

significant deterioration had occurred. In fact, the SIDA indicates a thirty-two percent decrease in the bending stiffness of the ulna over that time. With this change in bending stiffness taken into account, a good simulation was obtained for the musculature-removed plot.

The probe-on-ulna data of Figure 6.13 is well simulated by the mathematical model.

Figures 6.14 and 6.15 are DPMI plots of the intact arm with 400 and 600 gram-force preloads, respectively. As with the data from Monkeys 663 and 665, the presence of the skin between the probe and bone has the effect of decreasing the DPMI. This decrease is less for the 600 than for the 400 gram-force preload, as expected. If the preload could be made high enough without destroying the ulna, the decrease in DPMI would eventually disappear altogether.

B. BENDING TESTS

1. Procedure

The DPMI technique and its analysis described herein, results in a value measured for the bending stiffness of a long bone. To verify that this measurement is valid, the bending stiffness of an excised long bone, which has been measured using the DPMI technique, was measured using another independent technique. Each technique should give the same result. The alternate technique involves a simple three-point bending test from which a load-deflection curve is generated.

The ulna of Monkey 659 was tested in each of four

conditions described in the last section. After the tests were completed, it was wrapped in gauze, soaked in Ringer's solution and frozen to maintain as much freshness as possible. The ulna was then mailed from Stanford University, California to Wayne State University, Michigan, where it was again frozen. Just prior to testing, the ulna was brought to room temperature by soaking it in a jar of Ringer's solution.

A Material Testing System (MTS) machine was used to perform the bending tests. The ulna, already pinned from the DPMI test, was placed in the bending fixture as shown in Figure 6.16. The MTS machine was programmed to apply a constant deflection rate to the center of the ulna. Several different deflection rates, ranging from 0.5×10^{-3} to 0.5 in/s (1.27×10^{-3} to 1.27 cm/s) were used. These deflection rates are slow enough so that mass and damping effects are not present. The maximum deflection, approximately one-half centimeter, produced stresses which are within the elastic range. The load-deflection curve, shown in Figure 6.17, was generated on an x-y recorder, using the force and displacement signals from the MTS machine.

The static stiffness of the ulna is determined from the load-deflection curve using the relation

$$K = \Delta F/\Delta \delta \qquad (6.2)$$

where ΔF and $\Delta \delta$ are shown in Figure 6.17. The bending stiffness of the ulna, using a uniform beam model, is then determined from the relation

$$EI = KL^3/48 \qquad (6.3)$$

The ulna was allowed to dry for a period of two months. The value of the bending stiffness was then remeasured.

2. Results and Evaluation

A summary of the measurements described above is given in Table 6.4. Note that the value obtained for the bending stiffness from each successive test is significantly lower than that obtained from the previous test.

Although the attempt was made to keep the ulna as fresh as possible, it had deteriorated to some degree. Table 6.4 suggests a trend towards lower values of bending stiffness as the ulna deteriorates. Therefore, higher values would be expected if the bending tests had been performed immediately after the DPMI tests. The percent difference would then be reduced, if not eliminated all together.

With the effect of deterioration taken into account, the bending stiffness values measured by the two independent techniques are fairly consistent. Hence, these results support the validity of the DPMI tests.

C. NON-BIOLOGICAL TESTS

1. The Systems

To verify that the equipment is actually measuring the DPMI properly, the DPMI of two non-biological systems is measured. Non-biological systems can be constructed in such a way that their mechanical response is much more predictable than that of a biological system. Furthermore, the components of that system can be made of materials whose mechanical properties are well known. In particular, the two systems at hand are made of common

metals.

The first system is simply the calibration mass discussed in Section I.E. The second system consists of a uniform beam, machined from a bar of aluminum, and supported by pins near its ends.

2. Calibration Mass

The calibration mass is cylindrical in shape, is made of brass and has a mass of 98.4 grams. The magnitude of the DPMI of a pure mass is (see Table 2.1)

$$Z = mp \tag{6.4}$$

Therefore, a log-log plot of the DPMI data should form a straight line on a +45° angle. However, this is true only for relatively low frequencies. At very high frequencies the mass deforms. Therefore, the DPMI curve should go through a series of resonant and anti-resonant points.

DPMI data, taken for the calibration mass up to a frequency of 3000 Hz, is shown in Figure 6.18. The calibration mass vibrates as a pure mass up to a frequency of about 1000 Hz. It then approaches its first anti-resonant point at approximately 2800 Hz.

The system is modeled as a simple one-dimensional continuous rod with a harmonic force applied to its base. The DPMI of such a model is

$$Z^* = imp \tan\Psi / \Psi \tag{6.5}$$

where

$\Psi = \pi p/\omega$

m = mass

ω = fundamental frequency

p = forcing frequency

The mathematical model was used with the SIDA, described in Chapter V, to determine that the fundamental frequency of the system is 5519 Hz (i.e., the first anti-resonant point is $\omega/2$ = 2760 Hz). The DPMI of the model is shown as a solid line in Figure 6.18.

The modulus of elasticity and density of brass are known quantities and the height and diameter of the calibration mass are easily measured. The fundamental frequency, estimated from

$$\omega = \pi/L \sqrt{E/\rho} \qquad (6.6)$$

is found to be on the order of 60,000 Hz, with a corresponding anti-resonant point at 30,000 Hz.

Since the anti-resonant frequency determined from the DPMI data is a whole order of magnitude lower than the expected value, it must be a sub-anti-resonant[7] point. If the frequency range of the DPMI data could be extended beyond 3000 Hz, sub-resonant and more sub-anti-resonant points would be observed. These points may be due to the deformation of the screw connection between the impedance head and the calibration mass.

3. Aluminum Beam

The aluminum beam and its support brackets are shown with their dimensions in Figure 6.19. The purpose of the aluminum beam is to provide a standard to insure that the impedance equipment is operating properly each time it is used. Metal, unlike biological materials, remains unchanged over a long

[7] "Sub-anti-resonant" point refers to a local disturbance whose source is outside the system of interest; analogous to "sub-resonant" point, see Section IV.D.

period of time. Therefore the true DPMI of the aluminum beam will remain unchanged. The DPMI plot of the aluminum beam should be generated prior to each use of impedance equipment. If any deviation appears in this data then the equipment should be checked for malfunctioning.

The aluminum beam was designed to have a static stiffness and fundamental frequency in the same range as a typical monkey ulna. Unfortunately, it is not possible to produce a uniform beam with these properties and with a cross section large enough to accomodate rigid support pins. Therefore, it was necessary to make the ends of the beam larger in cross section than the mid-portion. Only a very small effect on the DPMI data plot due to the enlarged ends is anticipated.

A typical set of DPMI data from the aluminum beam was simulated using uniform, simply-supported beam model with the SIDA. Its DPMI plot is shown in Figure 6.20.

The modulus of elasticity E, and density ρ, of aluminum is known[8] and the dimensions of the beam are given in Figure 6.19. The bending stiffness and fundamental frequency are calculated using

$$EI = E\pi d^4/64 \tag{6.7}$$

$$\omega = (\pi^2/L^2)\sqrt{EI/\rho A} = (\pi^2 d/4L^2)\sqrt{E/\rho} \tag{6.8}$$

An area-moment method of analysis and a Rayleigh method analysis were carried out to determine the effect of the enlarged ends on the bending stiffness and fundamental frequency, respectively. These values, together with those determined from the DPMI data are listed in Table 6.5.

---

[8] $E = 7\times10^{11}$ dyne/cm^2, $\rho = 2.7$ g/cm^3, e.g., see Faires (1965).

It is seen from Table 6.5 that significant differences are apparent between the predicted values of the bending stiffnes and fundamental frequency and their values determined from the DPMI data. Some, but not all, of that difference is accounted for by including the effect of the enlarged ends of the beam. The only other possible source of the discrepancy (assuming, of course, the impedance equipment is functioning properly) is in the boundary conditions. It was shown in Section IV.B, that resistance to rotation at an otherwise simple support of a beam tends to move the DPMI curve upward and to the right. Therefore, there might be and excessive amount of friction in the pins which support the beam. A light oil should be applied to the pins to eliminate this friction.

It is seen from Figure 6.20 that the DPMI data and the DPMI of the mathematical model are well correlated up to a frequency of about 1000 Hz. The anti-resonant point of the mathematical model, however, is a few hundred Hz higher than the anti-resonant point of the system.

Recall that a sub-anti-resonant point was observed near this frequency in the DPMI data of the calibration mass, most likely due to deformations in the screw connection at the impedance head. It is possible that a similar sub-anti-resonant point is occurring due to the screw connection between the impedance head and the probe. This sub-anti-resonant point may or may not be exactly the same frequency as the previous one. Since the sub-anti-resonant point is relatively close to the anti-resonant point of the beam, the observed anti-resonant point is a combination of the two.

CHAPTER VII

APPLICATION TO EXISTING DATA

A. THOMPSON'S ORIGINAL DATA

1. Results

Thompson measured the driving-point mechanical impedance (DPMI) of the forearm of several human subjects using the impedance measuring equipment which he developed (see Section I.E). The tests were performed over a frequency range from 50 to 1000 Hz using three different preload forces. The systems identification algorithm* (SIDA) was then used to determine parametric values for the mathematical model which best simulate the data for eight of these subjects. The DPMI plots from one of these subjects, Subject TT, are shown in Figures 7.1, 7.2 and 7.3. The solid lines represent the DPMI of the mathematical model while the boxes represent the data points generated by Thompson. The DPMI plots of the remaining seven subjects are

* The computer program which incorporates the SIDA is similar to the one presented in Section V.D. The only difference is that the computer program used here has the capability of simulating three sets of data simultaneously, thus determining the three values for the spring-in-series; one corresponding to each preload.

presented in Appendix G. The corresponding parametric values for all eight subjects are listed together with other available information in Table 7.1.

2. Discussion

The parametric values listed in Table 7.1 are good approximations of the geometrical and material properties of the physical system provided the mathematical model is a good representation of that physical system. Therefore, to investigate the validity of these values, it is necessary to evaluate the support conditions. All other aspects of the mathematical model were shown in previous chapters to be very good approximations of the vibrating forearm system.

When positioning the subject's forearm in the fixture, Thompson carefully lined up the humerus with the support "by eye". The misalignment (discussed in Section VI.A) may not be perfectly eliminated but it is certainly significantly reduced. Thus the supports are relatively free from rotational resistance.

Thompson made the supports as rigid as possible with respect to translation by forming plaster pads under both the wrist and elbow. He demonstrated the rigidity of the supports by showing that the DPMI was independent of both the clamping force at the wrist and the downward force applied through the humerus at the elbow.

Based on the discussion above, the supports are virtually simply-supported. The parametric values listed in Table 7.1 were obtained using the SIDA and the mathematical model with simply-supported boundary conditions. Therefore these values are very

good approximations to the actual geometrical and material properties of the vibrating forearm system for each subject. Furthermore, the simulations appear to give accurate results. The error functions associated with each plot are within two percent and about half of them are within one percent.

The mass per unit length of the bone μ, is calculated by solving equation (3.4)

$$\mu = (\pi/L)^4 \, EI/\omega^2 \qquad (7.1)$$

where L is the support length, EI is the bending stiffness and ω is the fundamental frequency. This value represents the <u>total</u> mass per unit length of the bone. Measurements of bone mineral content (BMC) were also taken for each subject using a Norland-Cameron Bone Mineral Analyzer. This value represents the <u>mineral</u> mass per unit length of the bone. Values for μ and BMC for each subject are also listed in Table 7.1. It is reasonable to expect these two quantities to correlate quite well since all bones tested are bones of healthy, young adults. The correlation coefficient r is in fact 0.81, a reasonably high value.

Strong correlations have been found to exist between bending stiffness and BMC. (see Borders, Peterson and Orne, 1977 and Jurist and Foltz, 1977). Since the existence of this correlation is well established, it is reasonable to expect a similar correlation between the values of bending stiffness and BMC listed in Table 7.1 provided the values for bending stiffness are valid. The correlation coefficient r, of such a correlation, was found to be 0.87, a value comparable to findings of Borders, Petersen and Orne (1977) and Jurist and Foltz (1977).

Each of the points discussed above support the validity of

parametric values listed in Table 7.1.

B. MONKEY DATA

1. Results

Since the development of Thompson's impedance measuring equipment, DPMI data has been generated on a routine basis for the forearms and legs of monkeys at Ames Research Center. Ninety-four sets of such data from twenty-six different monkeys have been made available through personal communication. These tests were run over a frequency range from 100 to 2000 or 3000 Hz. The preload force in most cases was 600 gram-force (589 x 10^3 dyne), although some tests were run with both a 600 and a 300 gram-force (294 x 10^3 dyne) preload.

The computer program presented in Section V.D was used to determine parametric values and generate a DPMI plot for each of these sets of data. A representative set of six of these DPMI plots are presented in Figures 7.4 through 7.9. They are from the tests run on the leg and forearm of Monkeys 2, 16 and 17. The corresponding parametric values are listed with other available information in Table 7.2.

2. Discussion

The DPMI plots of the legs appear to indicate that the simulations are quite accurate. The DPMI plots of the forearms, however, indicate that the simulations are not accurate. Furthermore, the SIDA did not converge when applied to two of these data sets (forearms of Monkeys 2 and 16) using the six-

parameter model[10] (6PM). This trend is present throughout most of the data.

To investigate the validity of the parametric values listed in Table 7.2, it is necessary to perform two evaluations. First, the cause of the difference between the leg data and the forearm data must be determined. Second, the support conditions must be evaluated.

Form the ratio k/K using the parametric values listed in Table 7.2, where

$K = 3EIL/a^2b^2$ = the spring constant of the bone

$= 48EI/L^3$ for the probe at the center (tibia)

$= 625EI/12L^3$ for the probe at .6L (ulna)

k = spring constant of the skin

The value of k/K is also listed in Table 7.2 for each limb. Since k/K is the ratio of the spring constants of the skin and bone, it is a major factor in determining the magnitudes of the DPMI data. The stiffness of the skin k, is made as high as possible by increasing the preload force on the electromagnetic shaker to a tolerable limit. If it were possible to increase k to infinity, then the resulting DPMI plot would be that of the system without the skin. If k is relatively low, such that k/K is equal to 2 or 3, then most of the characteristics of the underlying system will be "masked" by the presence of the skin. Therefore, k/K must be high enough to "expose" all of the characteristics of the rest of the system.

In view of these comments, examine the values of k/K listed

---

[10] The results obtained from applying the SIDA with the four-parameter model (4PM) are presented in these cases. For an explanation of the 4PM and the 6PM, see Section V.C.

for each limb in Table 7.2. Note that in general, k/K is much higher for the forearm than for the leg. In particular, note the extremely high values for the forearm of Monkeys 16 and 17. k is relatively constant since the preload is the same for all bones. Hence, it is reasonable to expect this large variation in k/K because the bone stiffness K, varies significantly with the size of the bone. Table 7.2 shows that K is almost an order of magnitude larger for the tibiae than for the ulnae. Therefore the data which best exhibits the characteristics of the system (the bone, tissue and supports) are those of the forearms because k/K is greater. Furthermore, the most revealing forearm data is from Monkeys 16 and 17.

Referring to Figures 7.8 and 7.9, it can be seen that there is an additional relative minimum in the DPMI data at about 1200 Hz which the simply-supported beam model can not account for. This is typical of the sets of data which have a high k/K value. Based on the above discussion regarding the masking effect of a low k/K value, it is reasonable to suspect that this additional relative minimum is characteristic of most of the limbs but that it is hidden by the low k/K value in many cases, particularly with the legs.

In Section IV.B, it was shown that although the boundary conditions do not affect the shape of the DPMI curve at low frequency, they can affect it at high frequency. A DPMI curve with a general shape similar to that of the DPMI data in Figures 7.8 and 7.9 can be generated if the boundary conditions of the beam are those of case 5, i.e., a translational spring (and damper) at each end. This is further demonstrated by the non-dimensionalized DPMI plot shown in Figure 7.10. This figure was

generated using the following non-dimensional parametric values:

$\zeta = 0.1$

$T_1 = 2k_1 L^3/EI = 10$

$T_2 = 2k_2 L^3/EI = 10$

$C_{T1} = c_1\omega/k_1 = 2$

$C_{T2} = c_2\omega/k_2 = 2$

$k/K = 20$

Furthermore, the masking effect of a low value of k/K is accounted for in this model as demonstrated by Figure 7.11, where its value was reduced from 20 to 2. Knowing the type of boundary conditions which can possibly produce the kind of DPMI data in Figures 7.8 and 7.9, speculations can be made on the cause of such data.

At some point in the development of the impedance measuring procedure, the plaster pads at the supports (discussed in Section VII.A) were replaced by putty. Most putty exhibits both springlike and damperlike behavior. Therefore, it is very likely that the putty is a major factor in producing the second relative minimum in the DPMI data. Furthermore, it is difficult to rigidly support the tibia at the ankle. The soft tissue surrounding the tibia may also be contributing to the springlike and damperlike behavior of the support.

The boundary conditions of the mathematical model used to obtain the parametric values listed in Table 7.2 are simply-supported. Since the support conditions of the forearms and legs for the DPMI tests discussed above are not simply-supported, the parametric values are not accurate.

CHAPTER VIII

CONCLUSION

A. SUMMARY

1. Overview

A brief summary of the research project as a whole is given, followed by a summary of the contributions of this work. It is important to consider the relationship between this work and the work of other investigators involved in the research project and to give them appropriate credit.

The impedance measuring equipment and procedure were developed by Thompson (1973). He measured the driving-point mechanical impedance (DPMI) *in vivo* of the forearm of several healthy, young, adult, human subjects. Thompson also used a single-degree-of-freedom oscillator (SDOFO) in series with a spring as a mathematical model to interpret his data.

Orne (1974) proposed a visco-elastic beam model to better simulate the DPMI data. Orne and Mandke (1975) further improved the mathematical model to account for some of the finer details of the DPMI data. They also proposed a series of experiments to be run on a monkey forearm to verify the mathematical model.

Petersen (1977) performed the experiments which Orne

proposed.[11] One of the ulnae from these experiments was also tested statically in three-point bending on a Materials Testing System (MTS) machine.

A series of experiments involving the measurement of breaking strength of excised canine long bones was performed; see Borders, Petersen and Orne (1977). Bending tests were conducted on an MTS machine and correlations were established between the various parameters measured in these tests.

Petersen (1977) made some modifications to Thompson's test procedure and applied it in vivo to both the forearm and leg of monkeys. DPMI data has since been collected for monkey forearms and legs on a routine basis by Howard (personal communication) at Ames Research Center.

Concurrently, the mathematical model was further developed. An extensive parametric study was made using the mathematical model. A systems identification algorithm (SIDA) was developed and applied to the data obtained during the experiments and tests mentioned above.

2. Parametric Study

A parametric study has been carried out (Chapter IV) to determine the effect of each parameter of the mathematical model on its DPMI response. Two accomplishments were attained as a result of the study. First, an increased understanding of the effects of the parameters was gained. Second, many qualitative relationships between the parameters and the characteristics of

---

[11] These experiments were rerun with a wider frequency range on both the forearm and leg of a monkey. However, the impedance measuring equipment was not functioning properly and the DPMI data could not be interpreted.

the DPMI curve were derived. A brief description of the mathematical model followed by a summary of some of the major findings is given here.

The ulna of the vibrating forearm system is represented by a uniform, linear, visco-elastic, Euler-Bernoulli beam. The skin and tissue compressed between the probe and bone is represented by a spring in series with the beam. The remaining skin and tissue surrounding the bone is represented by a visco-elastic foundation with mass.

A linear beam model, regardless of its boundary conditions, generates a DPMI curve which is identical in shape to that of a SDOFO up to a frequency of at least two times, and often as much as ten times the fundamental frequency. This is demonstrated by the figures presented in Chapter IV for several different types of non-classical boundary conditions. The only parameter affecting the shape of the curve is the damping ratio. Furthermore, the position of the curve on the plot is entirely determined by the static stiffness and fundamental frequency of the beam.

None of the boundary conditions discussed in Chapter IV produce a rigid body mode of vibration, i.e., produce a zero fundamental frequency. In fact there exists only two cases of boundary conditions which will produce a rigid body mode: free-free and pinned-free. The DPMI curve in these two cases is identical, up to three or four times the first antiresonant frequency, to a SDOFO with the driving force applied to its base.

A few approximate relationships between the parameters of the beam and the characteristics of its DPMI curve have been

derived. They are useful for obtaining a first approximation for the parameters directly from a set of DPMI test data.

A transfer matrix method of analysis was developed to study the effect of taper (Appendix B). This method allows any parameter which is varying along the length of the beam to be approximated by a series of step functions constant within each element of the beam. The transfer matrix is generated from the exact solution of the beam within each element. (Note: the equations which make up the matrix could also be rearranged to form a stiffness matrix, thus producing a finite element representation of the beam.)

The conclusion drawn from applying the transfer matrix method to a calculation of the DPMI is that the taper does not affect the DPMI in the frequency range of the DPMI tests. A uniform beam and a tapered beam with the same static stiffness each produce a DPMI curve which is identical up to frequencies of at least an order of magnitude above the fundamental frequency.

A visco-elastic foundation with mass has two effects on the DPMI curve of a beam. First, it produces a subresonant disturbance in the otherwise smooth curve. This disturbance is present in many DPMI data sets. Second, the foundation produces a damping effect, similar to the damping in the beam. Hence, the minimum point of the DPMI curve is affected by the parameters of the foundation. This effect could not be quantified in close form due to the complexity of the DPMI equations. However, approximate relationships were derived which are valid for some range of parametric values.

A spring in series with a beam has its major effect in the

high frequency range. The total DPMI of two systems in series is dominated by whichever system has a lower DPMI. Thus, the spring dominates the total DPMI in the high frequency range where its DPMI is low. The high frequency data from a DPMI test has been used in the past to approximate the stiffness of the spring. However, data is not available in a high enough frequency range to completely eliminate the effect of the beam. Hence, this approach led to significant errors in estimating the spring stiffness, which in turn led to errors in estimating the stiffness of the beam. An alternate approach has been developed which is much more accurate. The approach is based on the location of the maximum point of the DPMI curve which occurs due to the spring. This eliminates the need for the high frequency data, otherwise required to make the estimate.

3. The Systems Identification Algorithm

A SIDA has been developed to determine the parametric values of the mathematical model which best simulate the data obtained from a DPMI test (Chapter V). The SIDA is based on minimizing the error function; a function similar in form to that used in a classical least-squares method.

Due to the complexity of the DPMI equations of the mathematical model, the error function is very nonlinear with respect to its parameters. Consequently, a system of equations obtained by setting the derivative with respect to each parameter equal to zero, is virtually impossible to solve. Rather than solving for the parametric values directly, an iterative procedure was developed which involves the calculation of a change in each parametric value which will bring that

parameter closer to its correct value.

The expression for the DPMI of the mathematical model was replaced by the first two terms of its Taylor series expansion about the point associated with the current value of each parameter. Then differentiating the error function with respect to changes in the parametric values leads to a system of equations which are linear in these changes. To start the iteration procedure, an initial guess for each parametric value is obtained using the relationships derived in the parametric study.

4. Evaluation of Existing Experiments and Tests

Data from several groups of DPMI tests and experiments have been made available through personal communication with Ames Research Center. Among them are (1) in vitro monkey experiments, (2) nonbiological tests, (3) Thompson's original in vivo tests and (4) more recent in vivo monkey tests.

The in vitro monkey experiments, discussed in Section VI.A, involve the measurement of DPMI of a monkey forearm in several stages as the ulna is being excised. The mathematical model was shown to be a good representation of the physical system by using it in its appropriate form to simulate the whole set of experiments with a consistent set of parametric values. Bending tests were performed on one of the ulnae which were excised during the experiments (Section VI.B). These tests verify the value obtained for the bending stiffness of that ulna. The experiments, however, revealed that a problem exists in the consistency of the support conditions of the specimen. This problem will be summarized in the next section.

DPMI tests were run on two nonbiological systems: a "rigid" mass and an aluminum beam. The data from these tests were studied, making use of some simple mathematical models (Section VI.C). The results indicate that the impedance measuring system is, in fact, measuring the DPMI properly over most of the frequency range.

Thompson, the developer of the impedance measuring equipment, measured the DPMI *in vivo* of the forearm of several human subjects. The mathematical model was used with the SIDA to determine the parametric values (Section VII.A). The results indicate that both the impedance measuring equipment and the analysis procedure are working well. Values were obtained for bending stiffness of the ulna of each subject.

The impedance measuring procedure has since been modified and applied to forearms and legs of monkeys *in vivo* (Section VII.B). These tests revealed a further problem with the support conditions of the specimen and is also summarized in the next section.

B. RECOMMENDATIONS

1. Problems Revealed by Experiments

In simulating the *in vitro* experiments of Section VI.A, only a few parametric values were determined from each set of data. In particular, the bone parameters and the support parameters were determined from two different DPMI data plots. However, when simulating an *in vivo* test, values for the whole set of parameters must be determined simultaneously from a

single set of data. If this set of parameters contains stiffnesses of both the bone and supports, then the number of parameters will be too great. It is impractical to use a mathematical model which has too many stiffness parameters since it is impossible to identify each parameter individually. On the other hand, the boundary conditions of the mathematical model must be a good representation of the support conditions of the physical system. The only way to solve this dilemma is to have some control over the support conditions in the in vivo tests.

Ideally, the support conditions in the in vivo tests should be made simply-supported. To do this, all sources of lateral translation and resistance to rotation at the supports must be eliminated. A systematic procedure should be developed which consistently produces support conditions which are virtually simply-supported.

In practice, it may not be possible to consistently attain the simply-supported support condition. However, even if this is the case, a systematic procedure is needed for positioning the specimen in the test fixture. Two requirements must be imposed on this procedure. First, the procedure must produce support conditions which are as nearly simple-supported as possible (or practical). The purpose in striving for such a support condition is to maximize the strength of the dependence of the DPMI of the vibrating forearm or leg system on the bone stiffness, thus maximizing the sensitivity of the DPMI to changes in the bone stiffness. Secondly, the procedure must produce support conditions which are repeatable. If the support conditions are not to be known, then they must at least be consistent from one test to the next. In this case, the value of bone stiffness

inferred through the mathematical model will be an index of the true bone stiffness rather than an absolute measure.

2. Further Suggested Experiments

Based on the parametric studies of Section IV.B, a significant amount of resistance to rotation can be created if the downward force applied through the humerus is not directly in line with the support as shown in Figure 6.6. It is believed, therefore, that this is a major cause of the rotational resistance that was found to be present at one of the supports in the *in vitro* monkey forearm experiments. This speculation can be tested by running additional *in vitro* monkey forearm experiments. In these experiments, the support is to be positioned in several different locations in the vicinity of the elbow, thus varying the degree of misalignment. A value can be obtained for the bending stiffness of the ulna using the simply-supported beam model and the SIDA in each case. Then excising the ulna, the true value of the bending stiffness can be determined. A comparison of this value with the former values will reveal whether or not the misalignment is the only cause of the rotational resistance at the support, and which positioning will minimize or eliminate it. Several sets of such experiments will aid in establishing a standard, systematic method of positioning for all future *in vivo* monkey forearm tests.

The *in vitro* experiments suggested in this section, as well as those discussed in Section VI.A should also be performed on monkey tibiae, human cadaver ulnae and any other type of specimen to be routinely tested *in vivo*. Although the modeling concepts applied to the forearm of a monkey are also applicable

to monkey legs and human forearms, the geometry of the supports in each case is quite different. A standard, systematic method of positioning is also needed in these cases.

3. Suggested Modifications to the Test Procedure

The impedance measuring procedure currently being used at Ames Research Center has one major flaw: the support conditions of the specimen are not being controlled. Since the DPMI is just as sensitive to the support conditions as it is to the bending stiffness of the bone, the support conditions must be known in order to determine the bending stiffness. If the boundary conditions of the mathematical model are not a good representation of the support conditions of the physical system, then the value obtained for the bending stiffness will be in error, possibly as much as an order of magnitude.

Two modifications to the impedance measuring procedure are recommended. First, the positioning procedure to be established by the experiments suggested above should be adopted as part of the procedure for each DPMI test. This will reduce, if not completely eliminate the resisitance to rotation at the supports. Second, Thompson's procedure, involving the use of plaster pads under the wrist and elbow should be readopted. This will eliminate the translation allowed by the putty at the supports (Section VII.B). The result of adopting these modifications is that the support conditions will be sufficiently controlled to obtain repeatable accurate results.

One further recommendation which may prevent the production of meaningless DPMI data is suggested. A standard, such as the aluminum beam (Section VI.B), should be used to insure that the

impedance measuring equipment is operating properly over the frequency range of the test. Each time DPMI tests are conducted, the DPMI of the standard should be measured and the data briefly examined. For example, using the aluminum beam shown in Figure 6.19, with the pins lubricated with a light oil, the general shape of the DPMI data should be as shown in Figure 6.20. The minimum point should occur at approximately 450 Hz and the maximum point at approximately 2800 Hz. The static stiffness should be 5.35 x 10^7 dyne/cm which corresponds to a DPMI of 8.5 x 10^4 dyne s/cm at 100 Hz. If these specifications are not met to within a few percent, then the impedance measuring equipment should be further checked for malfunctioning.

4. Concluding Remarks

The impedance measuring procedure developed by Thompson (Section I.E), with recommended modifications discussed above, can be used to generate an accurate, repeatable set of DPMI data for a forearm or leg. A systematic, user oriented analysis procedure has been developed and programmed on a digital computer. The computer program, listed in Appendix F, employs the mathematical model, developed in Chapters III and IV, and the SIDA, developed in Chapter V. The mathematical model consists of a uniform, linear, visco-elastic, simply-supported Euler-Bernoulli beam to represent the bone; a visco-elastic foundation with mass to represent the tissue surrounding the bone; and a spring between the beam and driving force to represent the skin between the bone and probe. The SIDA determines values for the mathematical model which best simulate the DPMI data using an iteration scheme to minimize an error

function. The error function is similar to that which is used in a classical least-squares curve fit. Due to the resemblance between the mathematical model and the physical system, the parametric values which produce a good simulation of the DPMI will infer the material and geometrical properties of the physical system.

One of these properties, the bending stiffness of the bone, was shown to correlate quite well with its breaking strength, at least for normal bones (Borders, Petersen and Orne, 1977; Jurist and Poltz, 1977). Breaking strength is a good measure of bone integrity and therefore may be a good indicator for many bone disorders such as osteoporosis. However, more correlation studies are needed to determine the effects of various bone disorders on the stiffness and strength of bones.

Bone mineral content (BMC) is currently being used in ongoing experiments to monitor changes in the bones of monkeys during prolonged hypodynamic restraint (Young and Tremor, 1978). Impedance testing is the only feasible technique currently available as a possible countermeasure to BMC. The impedance measuring and analysis procedures presented here can be used in conjunction with measurements of BMC to better define the condition of the bone being examined.

Young and Tremor (1978) report an average of 3.5 percent loss in femoral BMC in ten restrained monkeys over the relatively short time period of one month. Whedon et al. (1976) reports changes in BMC of 7.9 percent in the os calcis of astronauts after 84 days in a weightless environment, in spite of a rigorous exercise program. These changes are significant although they occurred during a relatively short period of time.

Much larger changes are expected to occur over longer periods of weightlessness, e.g., during a 1.5 to 3 year trip to Mars, or in a severe case of bone disease such as osteoporosis.

Although the percent changes in bending stiffness which occur with various bone disorders have not been measured, they are expected to be at least as great as those found in BMC. Bending stiffness is proportional to the fourth order of the cross sectional dimensions while BMC is proportional only to the second order, i.e.,

$$EI = E\, c_1\, d^4 \qquad BMC = BMD\ A = BMD\ c_2 d^2 \qquad (8.1)$$

where BMD is the bone mineral density,

A is the area of the cross section,

d is a cross sectional dimension,

and c_1, c_2 are constants of proportionality.

Therefore, the bending stiffness is more sensitive than the BMC is to changes in geometry. If percent changes in modulus of elasticity are of the same order of magnitude as percent changes in BMD, then bending stiffness will actually be a more sensitive indicator than BMC. Hence, the expected percent changes in bending stiffness are greater than those cited above for BMC and greater yet for more severe cases. With the recommendations discussed above taken into account, the impedance measuring procedure is accurate and repeatable enough to detect and measure these changes.

A technician in the clinical setting, can carry out the impedance testing procedure and run the computer program to determine the bending stiffness of a bone and interpret the result in terms of a particular bone disorder, all with a minimum of training. The test takes only a few minutes and is

entirely noninvasive. Two developments are needed to ascertain the feasibility of this technique. They are: (1) to develop a systematic positioning procedure, and (2) to develop the correlations between BMC, bending stiffness and various bone disorders. Both of these are quite achievable.

CHAPTER IX

APPENDIX

A. IMPEDANCE EQUATIONS

The driving-point mechanical impedance (DPMI) of a single-degree-of-freedom oscillator is

$$Z^* = c + i(mp - K/p)$$

The DPMI of a beam is of the form

$$Z^* = 2E^*I\lambda^3/[\,ipf(\lambda L)\,]$$

where

$$\lambda^4 = \mu^* p^2/E^*I$$

and $f(\lambda L)$ is a function which depends on the boundary conditions. For each set of boundary conditions listed in Table 3.1, $f(\lambda L)$ is as follows:

1. Simply-supported

$$f(\lambda L) = \sin\lambda a \sin\lambda b/\sin\lambda L - \sinh\lambda a \sinh\lambda b/\sinh\lambda L$$

2. Rotational spring on one end

$$f(\lambda L) = [\,(\sin\lambda a + \alpha)(\sin\lambda b \sinh\lambda L + \beta) - (\sinh\lambda a + \alpha)(\sinh\lambda b \sin\lambda L + \beta)\,]/(\sin\lambda L \sinh\lambda L + \gamma)$$

where

$$\alpha = k_1(\cosh\lambda a - \cos\lambda a)/2E^*I\lambda$$

$$\beta = k_1(\sin\lambda b \cosh\lambda L - \sinh\lambda b \cos\lambda L)/2E^*I\lambda$$

$$\gamma = k_1(\sin\lambda L \cosh\lambda L - \sinh\lambda L \cos\lambda L)/2E^*I\lambda$$

3. Rotational spring on each end

$$f(\lambda L) = [\,(\sin\lambda a + \alpha)(\sin\lambda b + \beta)(\sinh\lambda L + \gamma + \delta_2) - (\sinh\lambda a + \alpha)(\sinh\lambda b + \beta)(\sin\lambda L - \gamma - \delta_1) - (\sin\lambda b + \beta)(\sinh\lambda a + \alpha)(\gamma + \delta_4) - (\sin\lambda a + \alpha)(\sinh\lambda b + \beta)(\gamma + \delta_3)\,]/[\,(\sin\lambda L - \gamma - \delta_1)(\sinh\lambda L + \gamma + \delta_2) + (\gamma + \delta_3)(\gamma + \delta_4)\,]$$

where $\alpha = k_1(\cosh\lambda a - \cos\lambda a)/2E^*I\lambda$

$\beta = k_2(\cosh\lambda b - \cos\lambda b)/2E^*I\lambda$

$\gamma = k_1 k_2(\sinh\lambda L + \sin\lambda L)/(2E^*I\lambda)^2$

$\delta_1 = (k_1 + k_2)\cos\lambda L/2E^*I\lambda$

$\delta_2 = (k_1 + k_2)\cosh\lambda L/2E^*I\lambda$

$\delta_3 = (k_1\cos\lambda L + k_2\cosh\lambda L)/2E^*I\lambda$

$\delta = (k_2\cos\lambda L + k_1\cosh\lambda L)/2E^*I\lambda$

4. Translational spring on one end

$$f(\lambda L) = \sin\lambda a\sin\lambda b/\sin\lambda L - \sinh\lambda a\sinh\lambda b/\sinh\lambda L - \beta^2/\delta$$

where $\beta = \sin\lambda b/\sin\lambda L + \sinh\lambda b/\sinh\lambda L$

$\delta = \cosh\lambda L/\sinh\lambda L - \cos\lambda L/\sin\lambda L - 2k_1/E^*I\lambda^3$

5. Translational spring on each end

$$f(\lambda L) = \sin\lambda a\sin\lambda b/\sin\lambda L - \sinh\lambda a\sinh\lambda b/\sinh\lambda L - (\beta^2\delta_2 + \alpha^2\delta_1 + 2\alpha\beta\gamma)/(\delta_1\delta_2 - \gamma^2)$$

where $\alpha = \sin\lambda a/\sin\lambda L + \sinh\lambda a/\sinh\lambda L$

$\beta = \sin\lambda b/\sin\lambda L + \sinh\lambda b/\sinh\lambda L$

$\gamma = 1/\sinh\lambda L - 1/\sin\lambda L$

$\delta_1 = \cosh\lambda L/\sinh\lambda L - \cos\lambda L/\sin\lambda L - 2k_1/E^*I\lambda^3$

$\delta_2 = \cosh\lambda L/\sinh\lambda L - \cos\lambda L/\sin\lambda L - 2k_2/E^*I\lambda^3$

6. Translational spring on an extended beam

$$f(\lambda L) = \sin\lambda a \sin\lambda b/\sin\lambda L - \sinh\lambda a \sinh\lambda b/\sinh\lambda L$$
$$-\beta^2/[(\gamma + k\varepsilon)/(\varepsilon - k) - \delta]$$

where $\beta = \sinh\lambda b/\sinh\lambda L - \sin\lambda b/\sin\lambda L$

$\gamma = 2(\cos\lambda e \cosh\lambda e + 1)/\sin\lambda e \sinh\lambda e$

$k = 2k_3/E^*I\lambda^3$

$\varepsilon = \cosh\lambda e/\sinh\lambda e - \cos\lambda e/\sin\lambda e$

$\delta = \cosh\lambda L/\sinh\lambda L - \cos\lambda L/\sin\lambda L$

B. IMPEDANCE OF TAPERED BEAMS

An exact, closed-form solution for a vibrating beam with an arbitrary taper does not exist. Therefore, an approximate method for calculating the driving-point mechanical impedance (DPMI) of such a beam is developed here.

Divide the beam into n elements such that one of the nodes corresponds to the point of application of the driving force, as shown in Figure B.1. Approximate the taper as a series of step functions[12] so that all geometrical properties of the beam are constant within each element. The exact solution to each element in transfer matrix form is

$$\{Y_i\} = [T_i]\{Y_{i-1}\}$$

where

$$[T_i] = \begin{bmatrix} (\cosh\lambda_i\Delta + \cos\lambda_i\Delta)/2 & (\sinh\lambda_i\Delta + \sin\lambda_i\Delta)/2\lambda_i & (\cosh\lambda_i\Delta - \cos\lambda_i\Delta)/2E^*I_i\lambda_i^2 & (\sinh\lambda_i\Delta - \sin\lambda_i\Delta)/2E^*I_i\lambda_i^3 \\ (\sinh\lambda_i\Delta - \sin\lambda_i\Delta)\lambda_i/2 & (\cosh\lambda_i\Delta + \cos\lambda_i\Delta)/2 & (\sinh\lambda_i\Delta + \sin\lambda_i\Delta)/2E^*I_i\lambda_i & (\cosh\lambda_i\Delta - \cos\lambda_i\Delta)/2E^*I_i\lambda_i^2 \\ (\cosh\lambda_i\Delta - \cos\lambda_i\Delta)E^*I_i\lambda_i^2/2 & (\sinh\lambda_i\Delta - \sin\lambda_i\Delta)E^*I_i\lambda_i/2 & (\cosh\lambda_i\Delta + \cos\lambda_i\Delta)/2 & (\sinh\lambda_i\Delta + \sin\lambda_i\Delta)/2\lambda_i \\ (\sinh\lambda_i\Delta + \sin\lambda_i\Delta)E^*I_i\lambda_i^3/2 & (\cosh\lambda_i\Delta - \cos\lambda_i\Delta)E^*I_i\lambda_i^2/2 & (\sinh\lambda_i\Delta - \sin\lambda_i\Delta)\lambda_i/2 & (\cosh\Delta + \cos\Delta)/2 \end{bmatrix}$$

$$\{Y_i\} = \begin{Bmatrix} Y_i \\ \theta_i \\ M_i \\ V \end{Bmatrix} \begin{matrix} \text{(deflection)} \\ \text{(slope)} \\ \text{(bending moment)} \\ \text{(shear force)} \end{matrix} \qquad \text{and} \qquad \lambda_i = (\mu_i^* p^2/E^*I_i)^{1/4}$$

---

[12] The method is being applied here to a case of non-uniform geometry. The same method could also be applied to a case of non-uniform material properties or both simultaneously.

The transfer equation across the driving force is

$$\{Y_k^{(+)}\} = \{Y_k^{(-)}\} + \{F\}$$

where $$\{F\} = \begin{Bmatrix} 0 \\ 0 \\ 0 \\ P \end{Bmatrix}$$

and the (+) and (-) superscripts refer to the state variables just to the right and left of the driving force applied at the kth node. Let

$$[U] = [T_k][T_{k-1}]\cdots[T_2][T_1]$$

$$[V] = [T_n][T_{n-1}]\cdots[T_{k+2}][T_{k+1}]$$

$$[S] = [V][U]$$

then the following two matrix equations are obtained by successive substitutions from one transfer matrix equation to the next

$$\{Y_k^{(-)}\} = [U]\{Y_o\}$$

$$\{Y_n\} = [S]\{Y_o\} + [V]\{F\}$$

These two matrix equations represent eight algebraic equations of twelve state variables. Four of the state variables must be known from the boundary conditions leaving eight unknown state variables.

Any set of classical or non-classical boundary conditions can be applied to these eight equations. The simply-supported boundary condition states that

$$y_o = y_n = 0 \qquad M_o = M_n = 0$$

After applying these, the first, fifth and seventh equations are

$$y_k = U_{12}\theta_o + U_{14}V_o$$

$$0 = S_{12}\theta_o + S_{14}V_o + V_{14}P$$

$$0 = S_{32}\theta_o + S_{34}V_o + V_{34}P$$

The solution for y_k, after eliminating θ_o and V_o from these

three equations is

$$y_k = P\,[\,U_{12}(V_{34}S_{14} - V_{14}S_{34}) + U_{14}(V_{14}S_{32} - V_{34}S_{12})\,]/(S_{12}S_{34} - S_{14}S_{32})$$

Finally, the DPMI is

$$Z^* = P/ipy_k$$

or

$$Z^* = (-i/p)\,(S_{12}S_{34} - S_{14}S_{32})/[\,U_{12}(V_{34}S_{14} - V_{14}S_{34}) + U_{14}(V_{14}S_{32} - V_{34}S_{12})\,]$$

Since the exact solution for each element was used, the accuracy of the total solution is as good as the accuracy of the step function approximation of the taper.

C. DEPENDENCE OF THE FOUNDATION PARAMETERS ON THE MINIMUM POINT OF AN IMPEDANCE PLOT

The minimum driving-point mechanical impedance (DPMI) is to be determined for various combinations of the values of the mass per unit length p_f, and the damping ratio γ_f, of the foundation. Several DPMI plots, similar to those of Figures 4.13 through 4.16 were generated.

DPMI plots are generated by evaluating the DPMI equations at a finite number of points and joining those points with a sequence of straight line segments. A large enough number of points are taken to give the DPMI plots the appearance of smooth curves. The values of the DPMI and the forcing frequency for each point are listed in the computer printout associated with each plot. The true minimum point may not occur precisely at one of these points. In such a case, the true minimum point occurs at some frequency between the frequencies of the lowest DPMI listed and an adjacent point. The true minimum DPMI is lower than either of these points. See Figure C.1. A good approximation to the true minimum DPMI is obtained from the values of the DPMI and forcing frequency of the lowest point listed and its two adjacent points as follows:

Let (x_0, y_0) describe the coordinates of the true minimum point, i.e.,

$$x_0 = p_{min}/\omega \qquad y_0 = Z_{min}\omega/K$$

Similarly, let (x_2, y_2), (x_1, y_1) and (x_3, y_3) describe the coordinates of the lowest listed point and its two adjacent points, respectively. See Figure C.1. Approximate the DPMI

equation by a quadratic equation in the region around these points

$$y = A + Bx + Cx^2$$

A, B and C are constants which can easily be found by solving

$$y_1 = A + Bx_1 + Cx_1^2$$

$$y_2 = A + Bx_2 + Cx_2^2$$

$$y_3 = A + Bx_3 + Cx_3^2$$

The minimum point frequency is found by seting the derivative of the DPMI equations equal to zero

$$y' = B + 2Cx = 0$$

$$x_o = -B/2C$$

The minimum DPMI is obtained by replacing x with the expression for x_o

$$y_o = A - B^2/4C$$

The minimum DPMI was determined in this way for several DPMI plots, each generated with a different combination of values of μ_f and ζ_f. The results are tabulated in Table C.1.

For the case where $\mu_f = 0$ and $\zeta_f = 0$ (i.e., no foundation), the minimum DPMI is given by

$$Z_{min}\omega/K = 2\zeta$$

(see Sections IV.A and IV.B). Therefore a reasonable form to assume for the minimum DPMI is

$$Z_{min}\omega/K = 2\zeta + f(\mu_f, \zeta_f)$$

where $f(\mu_f, \zeta_f)$ is a function of μ_f and ζ_f whose value is zero at $\mu_f = 0$ and $\zeta_f = 0$. Values of this function are found from values of the minimum DPMI by subtracting 2ζ. The results are tabulated in Table C.2.

Note that the values of $f(\mu_f, \zeta_f)$ seem to increase linearly with μ_f/μ. Assume that the dependence of μ_f on $f(\mu_f, \zeta_f)$ is in

fact linear, i.e., assume

$$Z_{min}\omega/K = 2\zeta + \mu_f/\mu \; g(\zeta_f)$$

where $g(\zeta_f)$ is a function of ζ_f whose value is zero at $\zeta_f = 0$. Values of this function are found from values of $f(\mu_f, \zeta_f)$ by dividing by their respective values of μ_f/μ. The results are tabulated in Table C.3.

To determine the form of the function $g(\zeta_f)$, its values were plotted on a log-log grid. All points were found to lie very close to a straight line. Therefore $g(\zeta_f)$ is of the form of a power of ζ_f, i.e.,

$$Z_{min}\omega/K = 2\zeta + \mu_f/\mu \; A \; \zeta_f^n$$

where n is one-third for a fixed foundation and one-half for a free foundation. To find the values of A, a least-squares technique was employed. The best values for A were found to be one-fourth for a fixed foundation and three-fourths for a free foundation.

The relationships which approximate the dependence of μ_f and ζ_f on the minimum DPMI are

$$Z_{min}\omega/K = 2\zeta + 1/4 \; \mu_f/\mu \; \zeta_f^{1/3}$$

and

$$Z_{min}\omega/K = 2\zeta + 3/4 \; \mu_f/\mu \; \zeta_f^{1/2}$$

for a fixed and free foundation, respectively. These relationships can be used to determine approximate values for the tissue parameters of a vibrating forearm or leg system directly from its DPMI data plot. Such an approximation is necessary to establish the initial guess for the systems identification algorithm discussed in Section V.C.

D. THE MINIMUM AND MAXIMUM POINTS OF AN IMPEDANCE PLOT

Expressions for the minimum and maximum points of the driving-point mechanical impedance (DPMI) plot are to be found. The lengthy analysis will be outlined briefly here.

The DPMI of a single-degree-of-freedom oscillator in series with a spring (see Figure 4.21) with $\zeta \neq 0$ is

$$Z^* = [1/(mip + c + K/ip) + 1/(k/ip)]^{-1}$$

After replacing m by K/ω^2, c by $2K\zeta/\omega$ and performing several steps of algebra, this equation becomes

$$Z^* = K/\omega \frac{2\zeta S(\beta^2-1) - 2\zeta S\beta(\beta^2-1-S) - i[4\zeta^2 S\beta + S(\beta^2-1)(\beta^2-1-S)]}{(\beta^2-1-S)^2 + 4\zeta^2\beta}$$

where $S = k/K$ and $\beta = p/\omega$. The magnitude of the DPMI is

$$Z = K/ \frac{\sqrt{[2\zeta S(\beta^2-1) - 2\zeta S\beta(\beta^2-1-S)]^2 + [4\zeta^2 S\beta + S(\beta^2-1)(\beta^2-1-S)]^2}}{\beta(\beta^2-1-S)^2 + 4\zeta^2\beta}$$

To find the minimum and maximum points, take the derivative of the magnitude of the DPMI and set it equal to zero.

$$dZ/dp = K/^2 \frac{\begin{array}{l}[\beta(\beta^2-1-S)^2 + 4\zeta^2\beta] \\ \times\{[4\zeta S\beta - 2\zeta S(\beta^2-1-S) - 4\zeta S\beta^2] \\ \times[2\zeta S(\beta^2-1) - 2\zeta S\beta(\beta^2-1-S)] \\ +[4\zeta^2 S + 2S\beta(2\beta^2-2-S)] \\ \times[4\zeta^2 S\beta + S(\beta^2-1)(\beta^2-1-S)]\} \\ -\{(\beta^2-1-S)^2 + 4\beta^2(\beta^2-1-S) + 4\zeta^2\} \\ \times\{[2\zeta S(\beta^2-1) - 2\zeta S\beta(\beta^2-1-S)]^2 \\ +[4\zeta^2 S\beta + S(\beta^2-1)(\beta^2-1-S)]^2\}\end{array}}{\begin{array}{l}[\beta(\beta^2-1-S)^2 + 4\zeta^2\beta] \\ \times\sqrt{[2\zeta S(\beta^2-1) - 2\zeta S\beta(\beta^2-1-S)]^2 + [4\zeta^2 S\beta + S(\beta^2-1)(\beta^2-1-S)]^2}\end{array}} = 0$$

The denominator is positive and therefore non-zero for all positive values of β, ζ and S. Therefore the numerator must be set equal to zero. The expression in the numerator, when

multiplied out, is a sixth order polynomial in ζ^2. As an alternative to the difficult task of solving it, Taylor series expansions of β^2 with respect to ζ^2 can be found which satisfy the sixth order polynomial equation.

Assume that the solutions for β^2 exist and are of the form

$$\beta_{MAX}^2 = S + 1 + \sum_{n=1}^{\infty} a_n \zeta^{2n}$$

$$\beta_{MIN}^2 = 1 + \sum_{n=1}^{\infty} b_n \zeta^{2n}$$

where $\beta_{MAX} = p_{MAX}/\omega$ and $\beta_{MIN} = p_{MIN}/\omega$. These equations will produce the correct solutions for $\zeta = 0$ according to equations (4.23) and (4.27). Substitute the assumed form of the solutions into the numerator of the equation. The coefficients of the constant term and the ζ^2 and ζ^4 terms are each set equal to zero. In each case, the constant term was found to be identically equal to zero, indicating that equations (4.23) and (4.27) are actually the correct first order approximations to the solutions. The equations obtained from the ζ^2 and ζ^4 terms are solved to obtain the first two unknown coefficients of each of the Taylor series. Hence, the first three terms of each of the Taylor series are found to be

$$\beta_{MAX}^2 = S + 1 + 2/S\ (2+S)/(1+S)\ \zeta^2 - 2/S^3\ (2+S)/(1+S^3)\ (4+16S+13S^2+4S^3)\ \zeta^4 + \ldots$$

$$\beta_{MIN}^2 = 1 - 4/S\ \zeta^2 + 8/S^3\ (2+3S)\ \zeta^4 - \ldots$$

E. DERIVATIVES OF THE IMPEDANCE

The driving-point mechanical impedance (DPMI) equation to be differentiated is

$$Z^* = \{ipf(\lambda L)/[2EI(1 + 2i\zeta p/\omega)\lambda^3] + ip/k\}^{-1}$$

where

$$f(\lambda L) = \sin\lambda a \sin\lambda b/\sin\lambda L - \sinh\lambda a \sinh\lambda b/\sinh\lambda L$$

$$\lambda = [\pi^4/L^4\ p^2/\omega^2 + p^2\mu_f/EI\ g(\Psi)]^{1/4}\ (1 + 2i\zeta p/\omega)^{-1/4}$$

$$\Psi = p\pi/\omega_f\ /\ \sqrt{1 + 2i\zeta_f p/\omega_f}$$

and the function $g(\Psi)$, depends on the type of foundation included in the model. Three cases are considered. Case A: no foundation. The function $g(\Psi)$, is zero and λ reduces to

$$\lambda = \pi/L\ (p/\omega)^{1/2}\ (1 + 2i\zeta p/\omega)^{-1/4}$$

Case B: fixed foundation

$$g(\Psi) = -\cot\Psi\ /\ \Psi$$

Case C: free foundation

$$g(\Psi) = \tan\Psi/2\ /\ \Psi/2$$

Define X and Y as the real and imaginary parts of the inverse of the complex DPMI, respectively, i.e.,

$$Z^* = (X + iY)^{-1}$$

The magnitude of the DPMI is

$$Z = (X^2 + Y^2)^{-1/2}$$

The derivative of the magnitude of the DPMI with respect to one of the model parameters is

$$dZ/dP = -(X^2 + Y^2)^{-3/2}\ (X\ dX/dP + Y\ dY/dP)$$

or $$dZ/dP = -Z^3\ (X\ dX/dP + Y\ dY/dP)$$

where P represents any one of the model parameters. The value of

X, Y and their derivatives are calculated from[13]

$$X = \text{Real}(1/Z^*) \qquad dX/dP = \text{Real}[d(1/Z^*)/dP]$$

$$Y = \text{Imag}(1/Z^*) \qquad dY/dP = \text{Imag}[d(1/Z^*)/dP]$$

Since the DPNI is a function of EI, ω, ζ, k and λ; and λ is a function of EI, ω, ζ, μ_f, ω_f and ζ_f; the derivatives are of the form

$$d(1/Z^*)/dEI = \partial(1/Z^*)/\partial\lambda \; d\lambda/dEI + \partial(1/Z^*)/\partial EI$$

$$d(1/Z^*)/d\omega = \partial(1/Z^*)/\partial\lambda \; d\lambda/d\omega + \partial(1/Z^*)/\partial\omega$$

$$d(1/Z^*)/d\zeta = \partial(1/Z^*)/\partial\lambda \; d\lambda/d\zeta + \partial(1/Z^*)/\partial\zeta$$

$$d(1/Z^*)/d\mu_f = \partial(1/Z^*)/\partial\lambda \; d\lambda/d\mu_f$$

$$d(1/Z^*)/d\omega_f = \partial(1/Z^*)/\partial\lambda \; d\lambda/d\omega_f$$

$$d(1/Z^*)/d\zeta_f = \partial(1/Z^*)/\partial\lambda \; d\lambda/d\zeta_f$$

$$d(1/Z^*)/dk = \partial(1/Z^*)/\partial k$$

The partial derivatives are

$$\partial(1/Z^*)/\partial EI = -ipf(\lambda L)\,[2(EI)^2(1 + 2i\zeta p/\omega)\lambda^3]^{-1}$$

$$\partial(1/Z^*)/\partial\omega = -p^2 f(\lambda L)\,[\omega^2 EI(1 + 2i\zeta p/\omega)^2\lambda^3]^{-1}$$

$$\partial(1/Z^*)/\partial\zeta = p^2 f(\lambda L)\,[\omega EI(1 + 2i\zeta p/\omega)^2\lambda^3]^{-1}$$

$$\partial(1/Z^*)/\partial k = -ip/k^2$$

$$\partial(1/Z^*)/\partial\lambda = -3ipf(\lambda L)\,[2EI(1 + 2i\zeta p/\omega)\lambda^4]^{-1} + ip\, df/d\lambda\,[2EI(1 + 2i\zeta p/\omega)\lambda^3]^{-1}$$

where

---

[13] Since X and Y are real continuous functions, and $i = \sqrt{-1}$ is a constant, the distributive property of the derivative holds, i.e.,

$$d(X + iY)/dP = dX/dP + i\, dY/dP$$

Hence $\text{Real}[d(X + iY)/dP] = dX/dP$

and $\text{Imag}[d(X + iY)/dP] = dY/dP$

$$Df/d\lambda = [a \cos\lambda a \sin\lambda b + b \sin\lambda a \cos\lambda b - L \sin\lambda a \sin\lambda b \cos\lambda L/\sin\lambda L] / \sin\lambda L - [a \cosh\lambda a \sinh\lambda b + b \sinh\lambda a \cosh\lambda b - L \sinh\lambda a \sinh\lambda b \cosh\lambda L/\sinh\lambda L] / \sinh\lambda L$$

Since λ is a function of EI, ω, ζ, μ_f and Ψ; and Ψ is a function of ω_f and ζ_f; the derivatives of λ are of the form

$$d\lambda/dEI = \partial\lambda/\partial EI \qquad d\lambda/d\mu_f = \partial\lambda/\partial\mu_f$$

$$d\lambda/d\omega = \partial\lambda/\partial\omega \qquad d\lambda/d\omega_f = \partial\lambda/\partial\Psi \; d\Psi/d\omega_f$$

$$d\lambda/d\zeta = \partial\lambda/\partial\zeta \qquad d\lambda/d\zeta_f = \partial\lambda/\partial\Psi \; d\Psi/d\zeta_f$$

The partial derivatives of are

Case A

$$\partial\lambda/\partial EI = 0$$

$$\partial\lambda/\partial\omega = -\pi/2\omega L \; (p/\omega)^{1/2} \; (1 + 2i\zeta p/\omega)^{-1/4} + \pi i\zeta p/2L\omega^2 \; (p/\omega)^{1/2} \; (1 + 2i\zeta p/\omega)^{-5/4}$$

$$\partial\lambda/\partial\zeta = -\pi ip/2\omega L \; (p/\omega)^{1/2} \; (1 + 2i\zeta p/\omega)^{-5/2}$$

Cases B and C

$$\partial\lambda/\partial EI = -p^2\mu_f/4(EI)^2 \; g(\Psi) \; (1 + 2i\zeta p/\omega)^{-1/4} \; [\pi^4/L^4 \; p^2/\omega^2 + p^2\mu_f/EI \; g(\Psi)]^{-3/4}$$

$$\partial\lambda/\partial\omega = -1/2\omega \; \pi^4/L^4 \; p^2/\omega^2 \; (1 + 2i\zeta p/\omega)^{-1/4} \; [\pi^4/L^4 \; p^2/\omega^2 + p^2\mu_f/EI \; g(\Psi)]^{-3/4} + i\zeta p/2\omega^2 \; (1 + 2i\zeta p/\omega)^{-5/4} \; [\pi^4/L^4 \; p^2/\omega^2 + p^2\mu_f/EI \; g(\Psi)]^{1/4}$$

$$\partial\lambda/\partial\zeta = -ip/2\omega \; (1 + 2i\zeta p/\omega)^{-5/4} \; [\pi^4/L^4 \; p^2/\omega^2 + p^2\mu_f/EI \; g(\Psi)]^{1/4}$$

$$\partial\lambda/\partial\mu_f = p^2/4EI \; g(\Psi) \; (1 + 2i\zeta p/\omega)^{-1/4} \; [\pi^4/L^4 \; p^2/\omega^2 + p^2\mu_f/EI \; g(\Psi)]^{-3/4}$$

$$\partial\lambda/\partial\Psi = p^2\mu_f/4EI \; dg/d\Psi \; (1 + 2i\zeta p/\omega)^{-1/4} \; [\pi^4/L^4 \; p^2/\omega^2 + p^2\mu_f/EI \; g(\Psi)]^{-3/4}$$

where

$$dg/d\Psi = [\Psi \csc^2\Psi + \cot\Psi]/\Psi^2 \qquad \text{(case B)}$$

$$dg/d\Psi = 1/2\,[\Psi/2 \sec^2\Psi/2 - \tan\Psi/2]/(\Psi/2)^2 \qquad \text{(case C)}$$

The derivatives of Ψ are

$$d\Psi/d\omega_f = -1/\omega_f\ p\pi/\omega_f\ (1 + 2i\zeta_f p/\omega_f)^{-1/2}$$
$$-i\zeta_f p/\omega_f{}^2\ p\pi/\omega_f\ (1 + 2i\zeta_f p/\omega_f)^{-3/2}$$

$$d\Psi/d\zeta_f = -ip/\omega_f\ p\pi/\omega_f\ (1 + 2i\zeta_f p/\omega_f)^{-3/2}$$

F. THE COMPUTER PROGRAM

A listing of the Fortran computer program which determines the parametric values of the mathematical model used to simulate a set of driving-point mechanical impedance data from a forearm or leg vibration test is given. All of the function subroutines required by the program are not available in double precision. Therefore, five function subroutines have been written to accommodate the main program. They are also listed. The subroutine DGELG from the IBM Scientific Subroutine Package (*SSP) is used to solve the system of linear algebraic equations within each iteration of the systems identification algorithm. A listing of DGELG can be found in IBM (1968).

```
C     THIS PROGRAM EMPLOYS AN ITERATIVE PROCEDURE TO CONVERGE ON THE
C     CORRECT VALUES OF THE PARAMETERS IN A VIBRATING LONG BONE
C     EXPERIMENT, BY MINIMIZING THE PERCENTAGE ERROR IN THE MAGNITUDE
C     OF THE IMPEDANCE.
C
C     THE INPUT DATA MUST BE ARRANGED AS FOLLOWS:
C          CARD 1     TITLE                                   15A4
C          CARD 2     LENGTH AND LENGTH-TO-PROBE-
C                          LOCATION RATIO                     FREE
C          CARD 3     BOUNDARY CONDITION OF TISSUE            I2
C          CARD 4     NUMBER OF DATA CARDS TO FOLLOW          I2
C     THE REST OF THE CARDS CONTAIN THE FREQUENCY AND THE MAGNITUDE AND
C     PHASE ANGLE OF THE IMPEDANCE, ONE POINT PER CARD, IN FREE FORMAT.
C
C     THE SIX PARAMETERS IN THIS MODEL ARE:
C          BEI        STIFFNESS OF THE BONE
C          BWN        NATURAL FREQUENCY OF THE BONE
C          TMU        MASS PER UNIT LENGTH OF THE TISSUE
C          TWN        NATURAL FREQUENCY OF THE TISSUE
C          TZETA      DAMPING RATIO OF THE TISSUE
C          K          STIFFNESS OF THE SKIN
C     BZETA, THE DAMPING RATIO OF THE BONE, IS HELD AT A CONSTANT
C     VALUE.
C
C     THE FOUNDATION IN THE MODEL, WHICH REPRESENTS THE TISSUE, CAN
C     HAVE EITHER A FIXED OR FREE BOUNDARY DEPENDING ON THE VALUE ON
C     CARD 3.  -1 CORRESPONDS TO A FIXED BOUNDARY.  1 CORRESPONDS TO A
C     FREE BOUNDARY.
C
C     THIS PROGRAM CONTAINS ROUTINES WHICH 'LOOK' AT THE DATA AND
C     CHOOSE INITIAL SETS OF PARAMETER VALUES.
C
C     THE ITERATIONS ARE CARRIED OUT IN THREE PHASES:
C     1.   A FOUR PARAMETER MODEL IS EMPLOYED TO OBTAIN A GOOD
C     APPROXIMATION TO THE BONE AND SKIN PARAMETERS.
C     2.   THESE ARE HELD FIXED WHILE A GOOD APPROXIMATION TO THE
C     TISSUE PARAMETERS IS OBTAINED FOR A SIX PARAMETER MODEL.
C     3.   ALL SIX PARAMETERS ARE ALLOWED TO VARY TO OBTAIN THE FINAL
C     SET OF PARAMETERS FOR THE SIX PARAMETER MODEL.
C
C     DECLARATION STATEMENTS.
C
      COMPLEX*16 DCMPLX,CDSQRT,CDTAN,CDSINH,CDSIN,CDABS,CDCOSH,CDCOS
      COMPLEX*16 DZI(6)
      COMPLEX*16 ARG,LAMDA,ZA,ZB,ZL,ZBI,ZTI,ZC,BQ,TQ,Q,
     1 ZBI1,ZBI2,DZIDL,COT,CSCS,SECS
      REAL*8 DBLE,DREAL,DIMAG,DATAN,DABS
      REAL*8 W(60),P(60),ZE(60),PHIE(60),Z(60),PHI(60),DZ(60,6),DP(6),
     1 A6(6,6),A4(4,4),A3(3,3),B(6),DP6(6),DP4(4),DP3(3),DX(6),DY(6)
      REAL*8 PI,BL,BRATIO,BA,BB,BEI,BWN,BPN,BZETA,
     1 TMU,TWN,TPN,TZETA,K,KK,ZMIN,ZMAX,WMIN,WMAX,X,Y,ERROR,ERROLD,
     2 SBEI,SBWN,SBZETA,SK,STMU,STWN,STZETA,A
      REAL*8 FMT(1)/'*'/
      INTEGER TITLE(15)
      REAL WP(60),ZP(60),PHIP(60),ZEP(60),PHIEP(60)
```

```
C
C       READ IN DATA.
C
        PRINT74
        PI=3.14159D0
        READ(5,5) TITLE
    5   FORMAT(15A4)
        READ(5,FMT) BL,BRATIO
        BL=DABS(BL)
        IF(BRATIO.LE.0.D0.OR.BRATIO.GE.1.D0)GO TO 6
        GO TO 8
    6   PRINT7
    7   FORMAT('      THE VALUE GIVEN TO THE LENGTH-TO-PROBE-LOCATION'/
       1       '      RATIO MUST BE BETWEEN ZERO AND ONE.'/)
        STOP
    8   CONTINUE
        BA=BL*BRATIO
        BB=BL-BA
        READ(5,20) IBC
        IF(IBC.EQ.0)GO TO 16
        IBC=ISIGN(1,IBC)
        IF(IBC.EQ.-1)PRINT12
   12   FORMAT('      THE BOUNDARY OF THE FOUNDATION IS FIXED (ULNA).'/)
        IF(IBC.EQ.1)PRINT13
   13   FORMAT('      THE BOUNDARY OF THE FOUNDATION IS FREE (TIBIA).'/)
        GO TO 18
   16   PRINT17
   17   FORMAT('      THE FOUNDATION IS NOT INCLUDED IN THE MODEL'/)
   18   CONTINUE
        READ(5,20) N
   20   FORMAT(I2)
        IF(N.LT.8)GO TO 21
        IF(N.GT.60) GO TO 23
        GO TO 25
   21   PRINT22
   22   FORMAT('      A MINIMUM OF EIGHT DATA POINTS IS REQUIRED.'/)
        STOP
   23   PRINT24
   24   FORMAT('      A MAXIMUM OF SIXTY DATA POINTS IS REQUIRED.'/)
        STOP
   25   CONTINUE
        DO 26 I=1,N
        READ(5,FMT) W(I),ZE(I),PHIE(I)
        W(I)=DABS(W(I))
        ZE(I)=DABS(ZE(I))
   26   P(I)=W(I)*2.D0*PI
        PRINT74
C
C       PHASE 1
C
C       DETERMINE INITIAL SET OF PARAMETERS.
C
        KK=0.D0
        DO 27 I=1,4
   27   KK=KK+ZE(I)*P(I)
```

```
56                KK=KK/4.D0
57                NN=N/2
58                WMAX=W(NN-1)
59                ZMAX=ZE(NN-1)
60                DO 30 I=NN,N
61                IF(ZE(I).GT.ZMAX)GO TO 29
62                GO TO 30
63            29  ZMAX=ZE(I)
64                WMAX=W(I)
65            30  CONTINUE
66                NN=N/4
67                NNN=3*N/4
68                WMIN=W(NN-1)
69                ZMIN=ZE(NN-1)
70                DO 32 I=NN,NNN
71                IF(ZE(I).LT.ZMIN)GO TO 31
72                GO TO 32
73            31  ZMIN=ZE(I)
74                WMIN=W(I)
75            32  CONTINUE
76                K=KK*(WMAX/WMIN)**2
77                KK=1.D0/((1.D0/KK)-(1.D0/K))
78                BEI=(BA*BB)**2/3.D0/BL*KK
79                BWN=WMIN
80                BZETA=ZMIN*PI*BWN/KK
81                PRINT33
82            33  FORMAT(/'      THE INITIAL SET OF PARAMETERS IS:'/)
83                PRINT77
84                PRINT78,BEI,BWN,BZETA,K
                  C
                  C       THIS IS THE BEGINNING OF THE OUTSIDE LOOP.  EACH RUN THROUGH THIS
                  C       LOOP CONSTITUTES ONE ITERATION.
                  C
85                ERROR=1.D20
86                MM=0
87            34  MM=MM+1
                  C
                  C       CHECK EACH PARAMETER FOR THE NON-NEGATIVITY CONDITION.
                  C
88                IF(BEI.LT.0.D0)GO TO 35
89                IF(BWN.LT.0.D0)GO TO 35
90                IF(BZETA.LT.0.D0)GO TO 35
91                IF(K.LT.0.D0)GO TO 35
92                GO TO 37
93            35  MMM=MM-1
94                PRINT36,MMM
95            36  FORMAT(/5X,'A NEGATIVE VALUE WAS OBTAINED FOR ONE OR MORE'/5X,
                    1 'OF THE PARAMETERS ON ITERATION NUMBER ',I2,'.'/5X,
                    2 'THE CURRENT PARAMETER VALUES ARE:'/)
96                PRINT77
97                PRINT78,BEI,BWN,BZETA,K
98                GO TO 48
99            37  CONTINUE
                  C
                  C       CALCULATE Z AT EACH FREQUENCY.
```

```
      C
      BPN=BWN*2.D0*PI
      DO 45 I=1,N
      BQ=DCMPLX(1.D0,2.D0*BZETA*P(I)/BPN)
      LAMDA=DCMPLX(PI/BL,0.D0)*CDSQRT(DCMPLX(P(I)/BPN,0.D0)/CDSQRT(BQ))
      ZA=LAMDA*DCMPLX(BA,0.D0)
      ZB=LAMDA*DCMPLX(BB,0.D0)
      ZL=LAMDA*DCMPLX(BL,0.D0)
      ZBI1=DCMPLX(0.D0,-.5D0*P(I)/BEI)/LAMDA**3/BQ
      ZBI2=CDSINH(ZA)*CDSINH(ZB)/CDSINH(ZL)
     1 -CDSIN(ZA)*CDSIN(ZB)/CDSIN(ZL)
      ZBI=ZBI1*ZBI2
      ZTI=DCMPLX(0.D0,P(I)/K)
      ZC=ZTI+ZBI
      X=DREAL(ZC)
      Y=DIMAG(ZC)
      ZC=DCMPLX(1.D0,0.D0)/ZC
      Z(I)=CDABS(ZC)
      C
      C     CALCULATE THE DERIVITIVES OF Z AT EACH FREQUENCY.
      C
      DZIDL=(DCMPLX(BA,0.D0)*CDCOSH(ZA)*CDSINH(ZB)
     2      +DCMPLX(BB,0.D0)*CDSINH(ZA)*CDCOSH(ZB)
     3      -DCMPLX(BL,0.D0)*CDSINH(ZA)*CDSINH(ZB)
     4          *CDCOSH(ZL)/CDSINH(ZL))/CDSINH(ZL)
      DZIDL=DZIDL-(DCMPLX(BA,0.D0)*CDCOS(ZA)*CDSIN(ZB)
     2            +DCMPLX(BB,0.D0)*CDSIN(ZA)*CDCOS(ZB)
     3            -DCMPLX(BL,0.D0)*CDSIN(ZA)*CDSIN(ZB)
     4                *CDCOS(ZL)/CDSIN(ZL))/CDSIN(ZL)
      DZIDL=DZIDL*ZBI1+DCMPLX(-3.D0,0.D0)/LAMDA*ZBI
      Q=DZIDL*DCMPLX(-.25D0,0.D0)*LAMDA/BQ-ZBI/BQ
      DZI(1)=-ZBI/DCMPLX(BEI,0.D0)
      DZI(2)=Q*DCMPLX(0.D0,-2.D0*BZETA*P(I)/BPN**2)
     1 +DZIDL*DCMPLX(-.5D0/BPN,0.D0)*LAMDA
      DZI(3)=Q*DCMPLX(0.D0,2.D0*P(I)/BPN)
      DZI(4)=-ZTI/DCMPLX(K,0.D0)
      DZI(2)=DZI(2)*DCMPLX(2.D0*PI,0.D0)
      DO 45 J=1,4
      DX(J)=DREAL(DZI(J))
      DY(J)=DIMAG(DZI(J))
   45 DZ(I,J)=-Z(I)**3*(DX(J)*X+DY(J)*Y)
      C
      C     CALCULATE AND PRINT THE ERROR FUNCTION.
      C
      ERROLD=ERROR
      ERROR=0.D0
      DO 46 I=1,N
   46 ERROR=ERROR+((ZE(I)-Z(I))/ZE(I))**2
      ERROR=ERROR/N
      PRINT47,MM,ERROR
   47 FORMAT(/'     THE ERROR FUNCTION BEFORE ITERATION NUMBER',
     1 I2,' IS',F12.8,'.')
      IF(ERROR.LT.ERROLD)GO TO 49
   48 BEI=BEI-DP4(1)
      BWN=BWN-DP4(2)
```

```
9                 BZETA=BZETA-DP4(3)
0                 K=K-DP4(4)
1                 GO TO 75
2           49    CONTINUE
          C
          C       SET UP AND SOLVE THE SYSTEM OF LINEAR EQUATIONS.
          C
3                 DO 55 J=1,4
4                 B(J)=0.D0
5                 DO 50 I=1,N
6           50    B(J)=B(J)+(ZE(I)-Z(I))*DZ(I,J)/ZE(I)**2
7                 DO 55 JJ=1,4
8                 A4(J,JJ)=0.D0
9                 DO 55 I=1,N
0           55    A4(J,JJ)=A4(J,JJ)+DZ(I,J)*DZ(I,JJ)/ZE(I)**2
1                 DO 58 J=1,4
2                 DP4(J)=1.0D0
3                 DO 58 JJ=1,4
4           58    A4(J,JJ)=A4(J,JJ)/B(J)/B(JJ)
5                 CALL DGELG(DP4,A4,4,1,1.E-14,IER)
6                 DO 59 J=1,4
7           59    DP4(J)=DP4(J)/B(J)
8                 PRINT60,IER
9           60    FORMAT(/'      THE ERROR CODE FOR THE MATRIX INVERSION IS ',
                  1 I2,'.')
          C
          C       ADJUST THE VALUES OF THE PARAMETERS.
          C
)                 BEI=BEI+DP4(1)
1                 BWN=BWN+DP4(2)
2                 BZETA=BZETA+DP4(3)
3                 K=K+DP4(4)
          C
          C       CHECK WHETHER OR NOT ANOTHER ITERATION IS NECESSARY.
          C
                  DP(1)=DP4(1)/BEI
                  DP(2)=DP4(2)/BWN
                  DP(3)=DP4(3)/BZETA
                  DP(4)=DP4(4)/K
                  JJ=0
                  DO 70 J=1,4
           70     IF(DABS(DP(J)).GT.1.D-3)JJ=1
                  IF(JJ.EQ.1) GO TO 71
                  PRINT73,MM
                  GO TO 75
           71     IF(MM.LT.10)GO TO 34
                  PRINT72,(DP(J),J=1,4)
           72     FORMAT(/'      10 ITERATIONS HAVE OCCURED WITHOUT CONVERGENCE.'/
                  1 '      THE PERCENT CHANGES IN THE PARAMETERS ARE:'
                  2 //5X,4D14.5/)
           73     FORMAT(/'      CONVERGENCE OCCURED ON ITERATION NUMBER',I3,'.')
           74     FORMAT('1')
           75     CONTINUE
                  PRINT74
          C
```

```
      C     SAVE PARAMETERS FOR THE FOUR PARAMETER MODEL.
      C
1           SBEI=BEI
2           SBWN=BWN
3           SBZETA=BZET'
4           SK=K
      C
      C     PHASE 2
      C
      C     DETERMINE INITIAL SET OF PARAMETERS.
      C
5           BZETA=.05D0
6           TZETA=SBZETA/2.D0
7           TWN=BWN/2.D0
8           IF(IBC)129,236,130
9       129 A=.25D0
0           NE=3
1           GO TO 132
2       130 A=.75D0
3           NE=2
4       132 TMU=BEI/2.D0*(PI/BWN/BL**2)**2*(SBZETA-BZETA)/A/TZETA**(1.D0/NE)
5           PRINT33
6           PRINT77
7           PRINT78,BEI,BWN,BZETA,K
8           PRINT79
9           PRINT80,TMU,TWN,TZETA
      C
      C     SAVE INITIAL SET OF TISSUE PARAMETERS.
      C
0           STMU=TMU
1           STWN=TWN
2           STZETA=TZETA
      C
      C     THIS IS THE BEGINNING OF THE OUTSIDE LOOP.  EACH RUN THROUGH THIS
      C     LOOP CONSTITUTES ONE ITERATION.
      C
3           ERROR=1.D20
4           MM=0
5       134 MM=MM+1
      C
      C     CHECK EACH PARAMETER FOR THE NON-NEGATIVITY CONDITION.
      C
6           IF(TMU.LT.0.D0)GO TO 135
7           IF(TWN.LT.0.D0)GO TO 135
8           IF(TZETA.LT.0.D0)GO TO 135
9           GO TO 137
0       135 MMM=MM-1
1           PRINT36,MMM
2           PRINT77
3           PRINT78,BEI,BWN,BZETA,K
4           PRINT79
5           PRINT80,TMU,TWN,TZETA
6           TMU=STMU
7           TWN=STWN
8           TZETA=STZETA
```

```
      GO TO 175
  137 CONTINUE
C
C     CALCULATE Z AT EACH FREQUENCY.
C
      BPN=BWN*2.D0*PI
      TPN=TWN*2.D0*PI
      DO 145 I=1,N
      BQ=DCMPLX(1.D0,2.D0*BZETA*P(I)/BPN)
      TQ=DCMPLX(1.D0,2.D0*TZETA*P(I)/TPN)
      ARG=DCMPLX(P(I)*PI/TPN,0.D0)/CDSQRT(TQ)
      IF(IBC.EQ.1)ARG=ARG/DCMPLX(2.D0,0.D0)
      COT=DCMPLX(1.D0,0.D0)/CDTAN(ARG)
      LAMDA=CDSQRT(CDSQRT((DCMPLX(((PI/BL)**2*P(I)/BPN)**2,0.D0)+
     1 DCMPLX(P(I)**2*TMU/BEI,0.D0)/ARG/COT**IBC*IBC)/BQ))
      ZA=LAMDA*DCMPLX(BA,0.D0)
      ZB=LAMDA*DCMPLX(BB,0.D0)
      ZL=LAMDA*DCMPLX(BL,0.D0)
      ZBI1=DCMPLX(0.D0,-.5D0*P(I)/BEI)/LAMDA**3/BQ
      ZBI2=CDSINH(ZA)*CDSINH(ZB)/CDSINH(ZL)
     1 -CDSIN(ZA)*CDSIN(ZB)/CDSIN(ZL)
      ZBI=ZBI1*ZBI2
      ZTI=DCMPLX(0.D0,P(I)/K)
      ZC=ZTI+ZBI
      X=DREAL(ZC)
      Y=DIMAG(ZC)
      ZC=DCMPLX(1.D0,0.D0)/ZC
      Z(I)=CDABS(ZC)
C
C     CALCULATE THE DERIVITIVES OF Z AT EACH FREQUENCY.
C
      IF(IBC.EQ.1)GO TO 138
      CSCS=DCMPLX(1.D0,0.D0)/CDSIN(ARG)**2
      DZI(1)=DCMPLX(-P(I)**2/BEI/4.D0,0.D0)*COT/ARG/LAMDA**3
      DZI(2)=DCMPLX(-TMU*P(I)**2/TPN/BEI/4.D0,0.D0)/LAMDA**3*
     1 (DCMPLX(1.D0,0.D0)-DCMPLX(0.D0,TPN*TZETA/P(I)/PI**2)*ARG**2)
     2 *(CSCS+COT/ARG)
      DZI(3)=DCMPLX(0.D0,-TMU*P(I)*TPN/PI**2/BEI/4.D0)*ARG/LAMDA**3
     1 *(COT+ARG*CSCS)
      GO TO 139
  138 CONTINUE
      SECS=DCMPLX(1.D0,0.D0)/CDCOS(ARG)**2
      DZI(1)=DCMPLX(P(I)**2/BEI/4.D0,0.D0)/COT/ARG/LAMDA**3
      DZI(2)=DCMPLX(-TMU*P(I)**2/TPN/BEI/4.D0,0.D0)/LAMDA**3*
     1 (DCMPLX(1.D0,0.D0)-DCMPLX(0.D0,4.D0*TPN*TZETA/P(I)/PI**2)*ARG**2)
     2 *(SECS-DCMPLX(1.D0,0.D0)/COT/ARG)
      DZI(3)=DCMPLX(0.D0,-TMU*P(I)*TPN/PI**2/BEI)*ARG/LAMDA**3
     1 *(ARG*SECS-DCMPLX(1.D0,0.D0)/COT)
  139 CONTINUE
      DZIDL=(DCMPLX(BA,0.D0)*CDCOSH(ZA)*CDSINH(ZB)
     2       +DCMPLX(BB,0.D0)*CDSINH(ZA)*CDCOSH(ZB)
     3       -DCMPLX(BL,0.D0)*CDSINH(ZA)*CDSINH(ZB)
     4            *CDCOSH(ZL)/CDSINH(ZL))/CDSINH(ZL)
      DZIDL=DZIDL-(DCMPLX(BA,0.D0)*CDCOS(ZA)*CDSIN(ZB)
     2             +DCMPLX(BB,0.D0)*CDSIN(ZA)*CDCOS(ZB)
```

```
     3                -DCMPLX(BL,0.D0)*CDSIN(ZA)*CDSIN(ZB)
     4                    *CDCOS(ZL)/CDSIN(ZL))/CDSIN(ZL)
6              DZIDL=DZIDL*ZBI1+DCMPLX(-3.D0,0.D0)/LAMDA*ZBI
7              DO 140 J=1,3
8        140   DZI(J)=DZI(J)/BC*DZIDL
9              DZI(2)=DZI(2)*DCMPLX(2.D0*PI,0.D0)
0              DO 145 J=1,3
1              DX(J)=DREAL(DZI(J))
2              DY(J)=DIMAG(DZI(J))
3        145   DZ(I,J)=-Z(I)**3*(DX(J)*X+DY(J)*Y)
         C
         C     CALCULATE AND PRINT THE ERROR FUNCTION.
         C
4              ERROLD=ERROR
5              ERROR=0.D0
6              DO 146 I=1,N
7        146   ERROR=ERROR+((ZE(I)-Z(I))/ZE(I))**2
8              ERROR=ERROR/N
9              PRINT47,MM,ERROR
0              IF(ERROR.LT.ERROLD)GO TO 149
1        148   TMU=TMU-DP3(1)
2              TWN=TWN-DP3(2)
3              TZETA=TZETA-DP3(3)
4              GO TO 175
5        149   CONTINUE
         C
         C     SET UP AND SOLVE THE SYSTEM OF LINEAR EQUATIONS.
         C
6              DO 155 J=1,3
7              B(J)=0.D0
8              DO 150 I=1,N
9        150   B(J)=B(J)+(ZE(I)-Z(I))*DZ(I,J)/ZE(I)**2
0              DO 155 JJ=1,3
1              A3(J,JJ)=0.D0
2              DO 155 I=1,N
3        155   A3(J,JJ)=A3(J,JJ)+DZ(I,J)*DZ(I,JJ)/ZE(I)**2
4              DO 158 J=1,3
5              DP3(J)=1.0D0
6              DO 158 JJ=1,3
7        158   A3(J,JJ)=A3(J,JJ)/B(J)/B(JJ)
8              CALL DGELG(DP3,A3,3,1,1.E-14,IER)
9              DO 159 J=1,3
0        159   DP3(J)=DP3(J)/B(J)
1              PRINT60,IER
         C
         C     ADJUST THE VALUES OF THE PARAMETERS.
         C
2              TMU=TMU+DP3(1)
3              TWN=TWN+DP3(2)
4              TZETA=TZETA+DP3(3)
         C
         C     CHECK WHETHER OR NOT ANOTHER ITERATION IS NECESSARY.
         C
5              DP(1)=DP3(1)/TMU
6              DP(2)=DP3(2)/TWN
```

```
                DP(3)=DP3(3)/TZETA
                JJ=0
                DO 170 J=1,3
          170   IF(DABS(DP(J)).GT.1.D-3)JJ=1
                IF(JJ.EQ.1)GO TO 171
                PRINT73,MM
                GO TO 175
          171   IF(MM.LT.10)GO TO 134
                PRINT172,(DP(J),J=1,3)
          172   FORMAT(/'      10 ITERATIONS HAVE OCCURED WITHOUT CONVERGENCE.'/
               1'      THE PERCENT CHANGES IN THE PARAMETERS ARE:'
               2//5X,3D14.5/5X,3D14.5/)
          175   CONTINUE
                PRINT74
          C
          C     PHASE 3
          C
          C     DETERMINE INITIAL SET OF PARAMETERS.
          C
                PRINT33
                PRINT77
                PRINT78,BEI,BWN,BZETA,K
                PRINT79
                PRINT80,TAU,TWN,TZETA
          C
          C     THIS IS THE BEGINNING OF THE OUTSIDE LOOP.  EACH RUN THROUGH THIS
          C     LOOP CONSTITUTES ONE ITERATION.
          C
                ERROR=1.D20
                MM=0
          234   MM=MM+1
          C
          C     CHECK EACH PARAMETER FOR THE NON-NEGATIVITY CONDITION.
          C
                IF(BEI.LT.0.D0)GO TO 235
                IF(BWN.LT.0.D0)GO TO 235
                IF(TAU.LT.0.D0)GO TO 235
                IF(TWN.LT.0.D0)GO TO 235
                IF(TZETA.LT.0.D0)GO TO 235
                IF(K.LT.0.D0)GO TO 235
                GO TO 237
          235   MMM=MM-1
                PRINT36,MMM
                PRINT77
                PRINT78,BEI,BWN,BZETA,K
                PRINT79
                PRINT80,TAU,TWN,TZETA
          236   BEI=SBEI
                BWN=SBWN
                BZETA=SBZETA
                TAU=0.D0
                TWN=0.D0
                TZETA=0.D0
                K=SK
                GO TO 275
```

```
      237  CONTINUE
C
C     CALCULATE Z AT EACH FREQUENCY.
C
           BPN=BWN*2.D0*PI
           TPN=TWN*2.D0*PI
           DO 245 I=1,N
           BQ=DCMPLX(1.D0,2.D0*BZETA*P(I)/BPN)
           TQ=DCMPLX(1.D0,2.D0*TZETA*P(I)/TPN)
           ARG=DCMPLX(P(I)*PI/TPN,0.D0)/CDSQRT(TQ)
           IF(IBC.EQ.1)ARG=ARG/DCMPLX(2.D0,0.D0)
           COT=DCMPLX(1.D0,0.D0)/CDTAN(ARG)
           LAMDA=CDSQRT(CDSQRT((DCMPLX(((PI/BL)**2*P(I)/BPN)**2,0.D0)+
          1 DCMPLX(P(I)**2*TMU/BEI,0.D0)/ARG/COT**IBC*IBC)/BQ))
           ZA=LAMDA*DCMPLX(BA,0.D0)
           ZB=LAMDA*DCMPLX(BB,0.D0)
           ZL=LAMDA*DCMPLX(BL,0.D0)
           ZBI1=DCMPLX(0.D0,-.5D0*P(I)/BEI)/LAMDA**3/BQ
           ZBI2=CDSINH(ZA)*CDSINH(ZB)/CDSINH(ZL)
          1 -CDSIN(ZA)*CDSIN(ZB)/CDSIN(ZL)
           ZBI=ZBI1*ZBI2
           ZTI=DCMPLX(0.D0,P(I)/K)
           ZC=ZTI+ZBI
           X=DREAL(ZC)
           Y=DIMAG(ZC)
           ZC=DCMPLX(1.D0,0.D0)/ZC
           Z(I)=CDABS(ZC)
C
C     CALCULATE THE DERIVITIVES OF Z AT EACH FREQUENCY.
C
           IF(IBC.EQ.1)GO TO 238
           CSCS=DCMPLX(1.D0,0.D0)/CDSIN(ARG)**2
           DZI(1)=DCMPLX(TMU/4.D0*(P(I)/BEI)**2,0.D0)*COT/ARG/LAMDA**3
           DZI(2)=DCMPLX(-P(I)/BPN**2/2.D0,0.D0)/LAMDA**3*
          1 (DCMPLX(P(I)/BPN*(PI/BL)**4,0.D0)-DCMPLX(0.D0,BZETA)*LAMDA**4)
           DZI(3)=DCMPLX(-P(I)**2/BEI/4.D0,0.D0)*COT/ARG/LAMDA**3
           DZI(4)=DCMPLX(-TMU*P(I)**2/TPN/BEI/4.D0,0.D0)/LAMDA**3*
          1 (DCMPLX(1.D0,0.D0)-DCMPLX(0.D0,TPN*TZETA/P(I)/PI**2)*ARG**2)
          2 *(CSCS+COT/ARG)
           DZI(5)=DCMPLX(0.D0,-TMU*P(I)*TPN/PI**2/BEI/4.D0)*ARG/LAMDA**3
          1 *(COT+ARG*CSCS)
           GO TO 239
      238  CONTINUE
           SECS=DCMPLX(1.D0,0.D0)/CDCOS(ARG)**2
           DZI(1)=DCMPLX(-TMU/4.D0*(P(I)/BEI)**2,0.D0)/COT/ARG/LAMDA**3
           DZI(2)=DCMPLX(-P(I)/BPN**2/2.D0,0.D0)/LAMDA**3*
          1 (DCMPLX(P(I)/BPN*(PI/BL)**4,0.D0)-DCMPLX(0.D0,BZETA)*LAMDA**4)
           DZI(3)=DCMPLX(P(I)**2/BEI/4.D0,0.D0)/COT/ARG/LAMDA**3
           DZI(4)=DCMPLX(-TMU*P(I)**2/TPN/BEI/4.D0,0.D0)/LAMDA**3*
          1 (DCMPLX(1.D0,0.D0)-DCMPLX(0.D0,4.D0*TPN*TZETA/P(I)/PI**2)*ARG**2)
          2 *(SECS-DCMPLX(1.D0,0.D0)/COT/ARG)
           DZI(5)=DCMPLX(0.D0,-TMU*P(I)*TPN/PI**2/BEI)*ARG/LAMDA**3
          1 *(ARG*SECS-DCMPLX(1.D0,0.D0)/COT)
      239  CONTINUE
           DZIDL=(DCMPLX(BA,0.D0)*CDCOSH(ZA)*CDSINH(ZB)
```

```
     2        *DCMPLX(BB,0.D0)*CDSINH(ZA)*CDCOSH(ZB)
     3        -DCMPLX(BL,0.D0)*CDSINH(ZA)*CDSINH(ZB)
     4            *CDCOSH(ZL)/CDSINH(ZL))/CDSINH(ZL)
7    DZIDL=DZIDL-(DCMPLX(BA,0.D0)*CDCOS(ZA)*CDSIN(ZB)
     2              *DCMPLX(BB,0.D0)*CDSIN(ZA)*CDCOS(ZB)
     3              -DCMPLX(BL,0.D0)*CDSIN(ZA)*CDSIN(ZB)
     4                  *CDCOS(ZL)/CDSIN(ZL))/CDSIN(ZL)
8    DZIDL=DZIDL*ZBI1+DCMPLX(-3.D0,0.D0)/LAMDA*ZBI
9    DO 240 J=1,5
0  240 DZI(J)=DZI(J)/BQ*DZIDL
1    DZI(1)=DZI(1)-ZEI/DCMPLX(BEI,0.D0)
2    DZI(2)=DZI(2)+ZEI/BQ*DCMPLX(0.D0,2.D0*BZETA*P(I)/BPN**2)
3    DZI(6)=-ZTI/DCMPLX(K,0.D0)
4    DZI(2)=DZI(2)*DCMPLX(2.D0*PI,0.D0)
5    DZI(4)=DZI(4)*DCMPLX(2.D0*PI,0.D0)
6    DO 245 J=1,6
7    DX(J)=DREAL(DZI(J))
8    DY(J)=DIMAG(DZI(J))
9  245 DZ(I,J)=-Z(I)**3*(DX(J)*X+DY(J)*Y)
     C
     C     CALCULATE AND PRINT THE ERROR FUNCTION.
     C
0    ERROLD=ERROR
1    ERROR=0.D0
2    DO 246 I=1,N
3  246 ERROR=ERROR+((ZE(I)-Z(I))/ZE(I))**2
4    ERROR=ERROR/N
5    PRINT47,MN,ERROR
6    IF(ERROR.LT.ERROLD)GO TO 249
7  248 BEI=BEI-DP6(1)
8    BWN=BWN-DP6(2)
9    TMU=TMU-DP6(3)
0    TWN=TWN-DP6(4)
1    TZETA=TZETA-DP6(5)
2    K=K-DP6(6)
3    GO TO 275
4  249 CONTINUE
     C
     C     SET UP AND SOLVE THE SYSTEM OF LINEAR EQUATIONS.
     C
6    DO 255 J=1,6
7    B(J)=0.D0
8    DO 250 I=1,N
9  250 B(J)=B(J)+(ZE(I)-Z(I))*DZ(I,J)/ZE(I)**2
0    DO 255 JJ=1,6
1    A6(J,JJ)=0.D0
2    DO 255 I=1,N
3  255 A6(J,JJ)=A6(J,JJ)+DZ(I,J)*DZ(I,JJ)/ZE(I)**2
4    DO 258 J=1,6
5    DP6(J)=1.0D0
6    DO 258 JJ=1,6
7  258 A6(J,JJ)=A6(J,JJ)/B(J)/B(JJ)
8    CALL DGELG(DP6,A6,6,1,1.E-14,IER)
9    DO 259 J=1,6
0  259 DP6(J)=DP6(J)/B(J)
```

```
0                PRINT60,IER
                 C
                 C       ADJUST THE VALUES OF THE PARAMETERS.
                 C
1                BEI=BEI+DP6(1)
2                BWN=BWN+DP6(2)
3                TMU=TMU+DP6(3)
4                TWN=TWN+DP6(4)
5                TZETA=TZETA+DP6(5)
6                K=K+DP6(6)
                 C
                 C       CHECK WHETHER OR NOT ANOTHER ITERATION IS NECESSARY.
                 C
7                DP(1)=DP6(1)/BEI
8                DP(2)=DP6(2)/BWN
9                DP(3)=DP6(3)/TMU
0                DP(4)=DP6(4)/TWN
1                DP(5)=DP6(5)/TZETA
2                DP(6)=DP6(6)/K
3                JJ=0
4                DO 270 J=1,6
5            270 IF(DABS(DP(J)).GT.1.D-3)JJ=1
6                IF(JJ.EQ.1)GO TO 271
7                PRINT73,MM
8                GO TO 275
9            271 IF(MM.LT.10)GO TO 234
0                PRINT172,(DP(J),J=1,6)
1            275 CONTINUE
2                PRINT74
                 C
                 C       PRINT THE FINAL PARAMETER VALUES.
                 C
3                PRINT76,TITLE,EL,BRATIO
4             76 FORMAT(5X,15A4//5X,'BONE LENGTH',5X,'PROBE LOCATION'/F9.1,F15.1/)
5                PRINT77
5                PRINT78,BEI,BWN,BZETA,K
7                PRINT79
8                PRINT80,TMU,TWN,TZETA
9             77 FORMAT(5X,'BONE STIFFNESS',5X,'BONE NAT FREQ',5X,
                1 'BONE DAMPING',5X,'SKIN STIFFNESS')
0             78 FORMAT(D16.5,F13.1,F19.4,D22.5/)
1             79 FORMAT(5X,'TISSUE MASS/LENGTH',5X,'TISSUE NAT FREQ',5X,
                1 'TISSUE DAMPING')
2             80 FORMAT(F10.2,F23.1,F21.4/)
3                PRINT 81
4             81 FORMAT(31X,'EXPERIMENTAL',14X,'THEORETICAL'/41X,'PHASE',21X,
                1 'PHASE'/15X,'FREQ',8X,'IMPEDANCE',5X,'ANGLE',7X,'IMPEDANCE',
                2 5X,'ANGLE'/)
                 C
                 C       RECALCULATE THE IMPEDANCE.
                 C
5                BPN=BWN*2.D0*PI
5                TPN=TWN*2.D0*PI
7                DO 85 I=1,N
3                BQ=DCMPLX(1.D0,2.D0*BZETA*P(I)/BPN)
```

```
                IF(TMU.EQ.0.D0)GO TO 82
                TQ=DCMPLX(1.D0,2.D0*TZETA*P(I)/TPN)
                ARG=DCMPLX(P(I)*PI/TPN,0.D0)/CDSQRT(TQ)
                IF(IBC.EQ.1)ARG=ARG/DCMPLX(2.D0,0.D0)
                COT=DCMPLX(1.D0,0.D0)/CDTAN(ARG)
                LAMDA=CDSQRT(CDSQRT((DCMPLX(((PI/BL)**2*P(I)/BPN)**2,0.D0)*
               1DCMPLX(P(I)**2*TMU/BEI,0.D0)/ARG/COT**IBC*IBC)/BQ))
                GO TO 83
           82   LAMDA=DCMPLX(PI/BL,0.D0)*CDSQRT(DCMPLX(P(I)/BPN,0.D0)/CDSQRT(BQ))
           83   ZA=LAMDA*DCMPLX(BA,0.D0)
                ZB=LAMDA*DCMPLX(BB,0.D0)
                ZL=LAMDA*DCMPLX(BL,0.D0)
                ZBI=DCMPLX(0.D0,-.5D0*P(I)/BEI)/LAMDA**3/BQ*
               1(CDSINH(ZA)*CDSINH(ZB)/CDSINH(ZL)-CDSIN(ZA)*CDSIN(ZB)/CDSIN(ZL))
                ZTI=DCMPLX(0.D0,P(I)/K)
                ZC=DCMPLX(1.D0,0.D0)/(ZTI+ZBI)
                Z(I)=CDABS(ZC)
                PHI(I)=DATAN(DIMAG(ZC)/DREAL(ZC))*180.D0/PI
          C
          C     PRINT THE IMPEDANCE.
          C
           85   PRINT86,I,W(I),ZE(I),PHIE(I),Z(I),PHI(I)
           86   FORMAT(I7,F13.2,D16.4,F10.2,D16.4,F10.2)
          C
          C     CALCULATE AND PRINT THE ERROR FUNCTION.
          C
                ERROR=0.D0
                DO 87 I=1,N
           87   ERROR=ERROR+((ZE(I)-Z(I))/ZE(I))**2
                ERROR=ERROR/N
                PRINT88,ERROR
           88   FORMAT(/'     THE ERROR FUNCTION FOR THIS SET OF PARAMETERS IS',
               1F12.8,'.'/)
                PRINT 74
          C
          C     PLOT THE IMPEDANCE.
          C
                DO 90 I=1,N
                WP(I)=SNGL(W(I))
                ZEP(I)=SNGL(ZE(I))
                PHIEP(I)=SNGL(PHIE(I))
                ZP(I)=SNGL(Z(I))
           90   PHIP(I)=SNGL(PHI(I))
                CALL PLTOFS(1.,1./2.,3.,1./2.,1.5,4.5)
                CALL PLGAXS(1.5,4.5,'FREQUENCY',-9,6.,0.,1.,1./2.)
                CALL PLGAXS(1.5,4.5,'IMPEDANCE',9,6.,90.,3.,1./2.)
                CALL PGRID(1.5,4.5,2.,2.,3,3)
                CALL PLTLOG(3)
                CALL PLINE(WP(1),ZP(1),N,1,0,0,1)
                CALL PLINE(WP(1),ZEP(1),N,1,-1,0,1)
                CALL PLTREC
                CALL PLTOFS(1.,1./2.,-90.,90.,1.5,1.5)
                CALL PLGAXS(1.5,1.5,'FREQUENCY',-9,6.,0.,1.,1./2.)
                CALL PAXIS(1.5,1.5,'PHASE ANGLE',11,2.,90.,-90.,90.,.25)
                CALL PGRID(1.5,1.5,2.,1.,3,2)
```

```
      CALL PLTLOG(2)
      CALL PLINE(WP(1),PHIP(1),N,1,0,0,1)
      CALL PLINE(WP(1),PHIEP(1),N,1,-1,0,1)
      CALL PLTREC
      CALL PGRID(0.,0.,8.5,11.,1,1)
      CALL PSYMB(1.5,.5,.125,TITLE(1),0.,60,0)
      CALL PLTEND
      END
TIONS IN EFFECT*  ID,EBCDIC,SOURCE,NOLIST,NODECK,LOAD,NOMAP
TIONS IN EFFECT*  NAME = MAIN     , LINECNT =      57
ATISTICS*     SOURCE STATEMENTS =      509,PROGRAM SIZE =    35900
ATISTICS*  NO DIAGNOSTICS GENERATED
ES IN MAIN
```

```
1                REAL FUNCTION DREAL*8(X)
2                COMPLEX*16 X,DCMPLX
3                REAL*8 Y,CDABS,DBLE
4                DREAL=CDABS((X+DCONJG(X))/DCMPLX(2.D0,0.D0))
5                Y=DBLE(REAL(X))
6                DREAL=DSIGN(DREAL,Y)
7                RETURN
8                END
PTIONS IN EFFECT*  ID,EBCDIC,SOURCE,NOLIST,NODECK,LOAD,NOMAP
PTIONS IN EFFECT*  NAME = DREAL    , LINECNT =      57
TATISTICS*    SOURCE STATEMENTS =        8,PROGRAM SIZE =      524
TATISTICS*  NO DIAGNOSTICS GENERATED
ORS IN DREAL
```

```
1                REAL FUNCTION DIMAG*8(X)
2                COMPLEX*16 X,DCMPLX
3                REAL*8 Y,CDABS,DBLE
4                DIMAG=CDABS((X-DCONJG(X))/DCMPLX(2.D0,0.D0))
5                Y=DBLE(AIMAG(X))
6                DIMAG=DSIGN(DIMAG,Y)
7                RETURN
8                END
PTIONS IN EFFECT*  ID,EBCDIC,SOURCE,NOLIST,NODECK,LOAD,NOMAP
PTIONS IN EFFECT*  NAME = DIMAG    , LINECNT =      57
TATISTICS*    SOURCE STATEMENTS =        8,PROGRAM SIZE =      530
TATISTICS*  NO DIAGNOSTICS GENERATED
ORS IN DIMAG
```

AN TERMINAL SYSTEM FORTRAN G(41336) CDSINH 09-19-78 2

```
      COMPLEX FUNCTION CDSINH*16(X)
      COMPLEX*16 X,CDEXP,DCMPLX
      CDSINH=(CDEXP(X)-CDEXP(-X))/DCMPLX(2.D0,0.D0)
      RETURN
      END
```

TIONS IN EFFECT* ID,EBCDIC,SOURCE,NOLIST,NODECK,LOAD,NOMAP
TIONS IN EFFECT* NAME = CDSINH , LINECNT = 57
ATISTICS* SOURCE STATEMENTS = 5,PROGRAM SIZE = 526
ATISTICS* NO DIAGNOSTICS GENERATED
ES IN CDSINH

AN TERMINAL SYSTEM FORTRAN G(41336) CDCOSH 09-19-78 2

```
                COMPLEX FUNCTION CDCOSH*16(X)
                COMPLEX*16 X,CDEXP,DCMPLX
                CDCOSH=(CDEXP(X)+CDEXP(-X))/DCMPLX(2.D0,0.D0)
                RETURN
                END
```

TIONS IN EFFECT* ID,EBCDIC,SOURCE,NOLIST,NODECK,LOAD,NOMAP
TIONS IN EFFECT* NAME = CDCOSH , LINECNT = 57
ATISTICS* SOURCE STATEMENTS = 5,PROGRAM SIZE = 522
ATISTICS* NO DIAGNOSTICS GENERATED
BS IN CDCOSH

GAN TERMINAL SYSTEM FORTRAN G(41336) CDTAN 09-19-78

```
1                COMPLEX FUNCTION CDTAN*16(X)
2                COMPLEX*16 X,CDSIN,CDCOS,DCMPLX
3                IF(DIMAG(X).LE.34.D1)GO TO 1
4                CDTAN=DCMPLX(0.D0,1.D0)
5                GO TO 3
6              1 IF(DIMAG(X).GT.-34.D1)GO TO 2
7                CDTAN=DCMPLX(0.D0,-1.D0)
8                GO TO 3
9              2 CDTAN=CDSIN(X)/CDCOS(X)
0              3 RETURN
1                END
PTIONS IN EFFECT*  ID,EBCDIC,SOURCE,NOLIST,NODECK,LOAD,NOMAP
PTIONS IN EFFECT*  NAME = CDTAN    , LINECNT =      57
TATISTICS*    SOURCE STATEMENTS =       11,PROGRAM SIZE =      628
TATISTICS*  NO DIAGNOSTICS GENERATED
ORS IN CDTAN
```

G. RESULTS OF IN VIVO TESTS ON THE FOREARMS OF SEVEN HUMAN SUBJECTS

The results of the *in vivo* tests performed on Subject TT are presented and discussed in Section VII.A. Similar results from seven other subjects have been obtained and are presented here. Driving-point mechanical impedance plots associated with 400, 500 and 600 gram-force preloads are given for each subject. The corresponding parametric values in each case are listed in Table 7.1.

TABLES

TABLE 2.1

Three Basic Types of Mechanical Elements

	mass	damper	spring
Equation of Motion	$f = m\ddot{x}$	$f = c\dot{x}$	$f = kx$
F/a	m	c/p	k/p^2
Slope on log-log plot	0^o	-45^o	-63.4^o
F/v (impedance)	mp	c	k/p
Slope on log-log plot	45^o	0^o	-45^o
F/δ	mp^2	cp	k
Slope on log-log plot	63.4^o	45^o	0^o

TABLE 3.1

Boundary Conditions

	at $x = 0$	at $z = 0$
1. Simply-supported	$y_1 = 0$	$y_2 = 0$
	$M_1 = 0$	$M_2 = 0$
2. Rotational spring	$y_1 = 0$	$y_2 = 0$
on one end	$k_1\theta_1 - M_1 = 0$	$M_2 = 0$
3. Rotational spring	$y_1 = 0$	$y_2 = 0$
on each end	$k_1\theta_1 - M_1 = 0$	$k_2\theta_2 - M_2 = 0$
4. Translational spring	$k_1 y_1 + V_1 = 0$	$y_2 = 0$
on one end	$M_1 = 0$	$M_2 = 0$
5. Translational spring	$k_1 y_1 + V_1 = 0$	$k_2 y_2 + V_2 = 0$
on each end	$M_1 = 0$	$M_2 = 0$
	at $x = -e$	at $z = 0$
6. Translational spring	$k_3 y_3 + V_3 = 0$	$y_2 = 0$
on an extended beam	$M_3 = 0$	$M_2 = 0$

TABLE 3.2

Non-dimensional Parameter Definitions

Non-dimensional Parameter	Definition in terms of Model Parameters
ζ	$\zeta = \omega\eta/2E$
α	a/L
β	b/L
M	$\mu_f/\mu = L^4/\pi^4\ \mu_f\omega^2/EI$
B	ω/ω_f
ζ_f	$\zeta_f = \omega_f\eta_f/2E_f$
S	$k/K = kL^3/48EI$ [14]
T	$2kL^3/EI$ [15]
R	$kL/2EI$ [16]
ε	e/L
C_T	$c_T\omega/k$
C_R	$c_R\omega/k$

[14] k is the spring constant of the spring in series with the beam.

[15] k is the spring constant of the translational spring at a support.

[16] k is the spring constant of the rotational spring at a support.

TABLE 1

Parametric Values of DPHI Plots

Figure Number	Model Description	Parameters Varied						Constant					
4.1	SS beam	ζ	0.05	0.1	0.2	0.5	1.0						
4.3	SDOFO	ζ	0.05	0.1	0.2	0.5	1.0						
4.4	SS beam	α	0.5	0.6	0.7	0.8		ζ	0.2				
4.5	Rot. Spring on one end	R	.1	1.0	10.0	100.		ζ	0.2	C_R	0.2		
4.6	Rot. Spring on each end	R	0.1	1.0	10.0	100.		ζ	0.2	C_R	0.2		
4.7	Trans. Spring on one end	T	30.0	100.	300.	1000		ζ	0.2	C_T	0.2		
4.8	Trans. Spring on each end	T	30.0	100.	300.	1000		ζ	0.2	C_T	0.2		
4.9	Trans. Spring on an extended beam	T	40E2	40E3	43E4	12E6		ζ	0.2	C_T	0.2	ϵ	0.01
4.10	SS beam							ζ	0.2				
	Rot. Spring on one end							ζ	0.2	R	10.0	C_R	0.2
	Rot. Spring on each end							ζ	0.2	R	10.0	C_R	0.2
	Trans. Spring on one end							ζ	0.2	T	100.	C_T	0.2
	Trans. Spring on each end							ζ	0.2	T	100.	C_T	0.2
4.11	SS beam							ζ	0.2				
	Rot. Spring on one end							ζ	0.2	R	10.0	C_R	0.2
	Rot. Spring on each end							ζ	0.2	R	10.0	C_R	0.2
	Trans. Spring on one end							ζ	0.2	T	100.	C_T	0.2
	Trans. Spring on each end							ζ	0.2	T	100.	C_T	0.2
4.13	SS beam with fixed foundation	H	0.2	0.5	1.0	2.0	5.0	ζ	0.05	ζ_f	0.2	B	2.0
4.14	SS beam with fixed foundation	ζ_f	0.2	0.3	0.4	0.5		ζ	0.05	H	2.0	B	2.0
4.15	SS beam with free foundation	H	0.2	0.5	1.0	2.0	5.0	ζ	0.05	ζ_f	0.2	B	2.0
4.16	SS beam with free foundation	ζ_f	0.2	0.3	0.4	0.5		ζ	0.05	H	1.0	B	2.0
4.18	SS beam with spring in series	ζ	0.05	0.1	0.2	0.5	1.0	S	5.0				
4.19	SS beam with spring in series	S	1.0	2.0	5.0	10.0	20.0	ζ	0.2				

TABLE 4.2

Static Stiffnesses for Beams With Various Boundary Conditions

The stiffness of a beam is

$$K = \phi \, 3EIL/a^2b^2$$

where expressions for ϕ are listed below for several different boundary conditions.

Boundary Conditions	ϕ
1. Simply-supported	1
2. Rotational spring on one end	$\dfrac{6+4R_1}{6+\alpha(3\alpha+4\beta)R_1}$
3. Rotational spring on each end	$\dfrac{6+4R_1+4R_2+2R_1R_2}{6+\alpha(3\alpha+4\beta)R_1+\beta(3\beta+4\alpha)R_2+2\alpha\beta R_1R_2}$
4. Translational spring on one end	$\dfrac{T_1\alpha^2}{6+T_1\alpha^2}$
5. Translational spring on each end	$\dfrac{T_1T_2\alpha^2\beta^2}{6(T_1\alpha^2+T_2\beta^2)+T_1T_2\alpha^2\beta^2}$
6. Translational spring on an extended beam	$\dfrac{24+4\varepsilon^3T_3+4\varepsilon^2T_3}{24+4\varepsilon^3T_3+\alpha(3\alpha+4\beta)\varepsilon^2T_3}$

TABLE 6.1

Parametric Values for the Forearm of Monkey 663

Parameter Name	Symbol	Parametric Value
Ulnar support length	L	17.1 cm
Length-to-probe-location ratio	α	0.6
Ulnar bending stiffness	EI	2.9795×10^9 dyne cm^2
Ulnar fundamental frequency	ω	332.0 Hz
Ulnar damping ratio	ζ	0.0425
Support rotational stiffness	k_1	0.86535×10^9 dyne cm
Support rotational damping	c_1	1.7136×10^5 dyne cm s
Tissue mass per unit length	p_t	1.85 g/cm
Tissue fundamental frequency	ω_t	174.0 Hz
Tissue damping ratio	ζ_t	0.4050
Skin stiffness	k	2.2098×10^8 dyne/cm

Condition	Value of Error Function
Excised ulna	0.0086
Musculature removed	0.0112
Probe on ulna	0.0115
Intact arm	0.0132

TABLE 6.2

Parametric Values for the Forearm of Monkey 665

Parameter Name	Symbol	Parametric Value
Ulnar support length	L	17.2 cm
Length-to-probe-location ratio	α	0.6
Ulnar bending stiffness	EI	5.0311×10^9 dyne cm^2
Ulnar fundamental frequency	ω	350.4 Hz
Ulnar damping ratio	ζ	0.0364
Support rotational stiffness	k_t	4.4382×10^9 dyne cm
Support rotational damping	c_t	2.2225×10^5 dyne cm s
Tissue mass per unit length	μ_f	6.96 g/cm
Tissue fundamental frequency	ω_f	101.0 Hz
Tissue damping ratio	ζ_f	0.0792
Skin stiffness	k	1.1155×10^8 dyne/cm

Condition	Value of Error Function
Excised ulna	0.0228
Musculature removed	0.0127
Probe on ulna	0.0208
Intact arm	0.0653

TABLE 6.3

Parametric Values for the Forearm of Monkey 659

Parameter Name	Symbol	Parametric Value
Ulnar support length	L	17.2 cm
Length-to-probe-location ratio	α	0.6
Ulnar bending stiffness (EU)	EI	5.2498×10^9 dyne cm^2
Ulnar bending stiffness (MR)	EI	7.7120×10^9 dyne cm^2
Ulnar fundamental frequency	ω	377.4 Hz
Ulnar damping ratio	ζ	0.0267
Support rotational stiffness	k_t	3.4682×10^9 dyne cm
Support rotational damping	c_t	4.2095×10^5 dyne cm s
Tissue mass per unit length	p_t	4.02 g/cm
Tissue fundamental frequency	ω_t	145.1 Hz
Tissue damping ratio	ζ_t	0.5827
Skin stiffness-400 gm preload	k	1.3543×10^8 dyne/cm
Skin stiffness-600 gm preload	k	1.3924×10^8 dyne/cm

Condition	Value of Error Function
Excised ulna	0.0094
Musculature removed	0.0179
Probe on ulna	0.0111
Intact arm 400 gm preload	0.0122
Intact arm 600 gm preload	0.0169

TABLE 6.4

Bending Stiffness Measurements on the Ulna of Monkey 659

Test	Bending Stiffness EI (10^9 dyne cm^2)
DPMI test (musculature removed)	7.712
DPMI test (excised ulna)	5.246
Percent difference	32.0%
Three-point bending test (MTS machine)	4.827
Percent difference	37.4%
Repeat bending test on dry bone	4.530
Percent difference	41.3%

TABLE 6.5

Mechanical Properties of the Aluminum Beam

	Bending Stiffness EI (10^9 dyne cm^2)	Fundamental Frequency ω (Hz)
Predicted values	5.587	429.2
Corrected for enlarged ends	5.670	448.2
Percent difference	1.5%	4.4%
Measured values	6.090	489.3
Percent difference	9.0%	14.0%

TABLE 7.1

Parametric Values for the Forearms of Thompson s Subjects

	Measured Quantities					Bone Parameters		Tissue Parameters			Skin Parameters			Calculated
Subject	Sex	Age (years)	Body mass (kg)	Bone mineral content (g/cm)	Ulna support length L (cm)	Bending stiffness EI (10^{10} dyne cm²)	Fundamental frequency ω (Hz)	Mass per unit length μ_t (gm/cm)	Fundamental frequency ω_t (Hz)	Damping ratio γ_t (dimensionless)	Stiffness 400 gm pl k (10^8 dyne/cm)	Stiffness 500 gm pl k (10^8 dyne/cm)	Stiffness 600 gm pl k (10^8 dyne/cm)	Bone mass/length μ (g/cm)
BL	M	21	75	0.53	27.4	4.2731	393.1	12.42	137.8	0.3497	2.3655	3.1712	3.9917	1.21
CDG	M	19	56	0.50	24.2	3.2041	429.1	13.29	162.9	0.3109	3.6611	4.4883	5.6442	1.25
DG	M	30	55	0.55	23.9	2.8459	390.1	13.92	145.3	0.3264	3.7619	5.9957	8.1292	1.41
HB	M	18	67	0.67	26.0	3.5105	405.0	13.28	140.4	0.4453	1.7845	2.7261	4.0319	1.15
HO	M	24	61	0.75	25.2	5.0845	376.0	13.07	168.2	0.3173	2.2745	2.t224	3.3959	2.20
SS	F	25	50	0.44	23.4	2.0772	590.9	14.22	149.0	0.4410	3.1580	3.7947	5.1195	0.49
TT	M	21	59	0.54	23.4	3.1031	390.0	11.76	151.1	0.3512	3.2148	3.8086	4.3268	1.68
VG	F	22	46	0.32	20.5	1.3482	562.2	11.49	128.1	0.5310	2.3305	3.3836	3.7389	0.60

TABLE 7.2

Parametric Values for the Forearms and Legs of Monkeys 2, 16 and 17

Measured Quantities				Bone Parameters			Tissue Parameters			Skin	Calculated	
Monkey	Bone	Bone support length l (cm)	Probe-location ratio α (dimensionless)	Bending stiffness EI	Fundamental frequency ω (Hz)	Damping ratio ζ (dimensionless)	Mass per unit length μ_t (g/cm)	Fundamental frequency ω_t (Hz)	Damping ratio ζ_t (dimensionless)	Stiffness k (10^6 dyne/cm)	Bone stiffness K (10^6 dyne/cm)	Stiffness ratio k/K (dimensionless)
2	Tibia	16.0	0.5	1.1466	701.6	0.0500	2.07	270.1	0.4342	7.1179	1.3437	5.2974
16	Tibia	16.0	0.5	1.9185	672.6	0.0500	5.57	113.8	0.3903	7.6108	2.2482	3.3852
17	Tibia	16.5	0.5	1.5456	637.6	0.0500	3.57	147.2	0.4411	10.4960	1.6515	6.3553
2	Ulna	18.0	0.6	0.4321	431.3	0.5333				4.6291	0.3859	11.9967
16	Ulna	21.0	0.6	0.4684	367.5	1.2557				6.6567	0.2634	25.2714
17	Ulna	19.0	0.6	0.4900	488.2	0.0500	4.62	160.1	0.2346	7.8615	0.3720	21.1304

TABLE C.1

$Z_{min}\omega/K$ as a Function of μ_f and γ_f

Fixed foundation

$\mu_f \backslash \gamma_f$	0.2	0.3	0.4	0.5
0.2	0.135	0.138	0.141	0.144
0.5	0.184	0.191	0.199	0.207
1.0	0.263	0.279	0.297	0.311
2.0	0.418	0.455	0.491	0.517
5.0	0.867	0.988	1.084	1.123

Free foundation

$\mu_f \backslash \gamma_f$	0.2	0.3	0.4	0.5
0.2	0.164	0.184	0.199	0.208
0.5	0.257	0.309	0.346	0.369
1.0	0.413	0.518	0.598	0.643
2.0	0.725	0.938	1.113	1.213
5.0	1.655	2.192	2.670	3.049

TABLE C.2

$f(\mu_f, \zeta_f)$

Fixed foundation

$\mu_f \backslash \zeta_f$	0.2	0.3	0.4	0.5
0.2	0.035	0.038	0.041	0.044
0.5	0.084	0.091	0.099	0.107
1.0	0.163	0.179	0.197	0.211
2.0	0.318	0.355	0.391	0.417
5.0	0.767	0.888	0.984	1.023

Free foundation

$\mu_f \backslash \zeta_f$	0.2	0.3	0.4	0.5
0.2	0.064	0.084	0.099	0.108
0.5	0.157	0.209	0.246	0.269
1.0	0.313	0.418	0.498	0.543
2.0	0.625	0.838	1.013	1.113
5.0	1.555	2.092	2.570	2.949

TABLE C.3

$g(\zeta_f)$

Fixed foundation

$\mu_f \backslash \zeta_f$	0.2	0.3	0.4	0.5
0.2	0.174	0.188	0.206	0.222
0.5	0.168	0.183	0.199	0.213
1.0	0.163	0.179	0.197	0.211
2.0	0.159	0.178	0.196	0.209
5.0	0.153	0.178	0.197	0.206

Free foundation

$\mu_f \backslash \zeta_f$	0.2	0.3	0.4	0.5
0.2	0.319	0.420	0.495	0.539
0.5	0.315	0.417	0.492	0.538
1.0	0.313	0.418	0.498	0.543
2.0	0.312	0.419	0.507	0.557
5.0	0.311	0.418	0.514	0.590

FIGURES

Figure 1.1. Human Long Bones.

(a) Arm and forearm showing relative size, shape and position of its bones. (b) Thigh and leg showing relative size, shape and position of its bones.

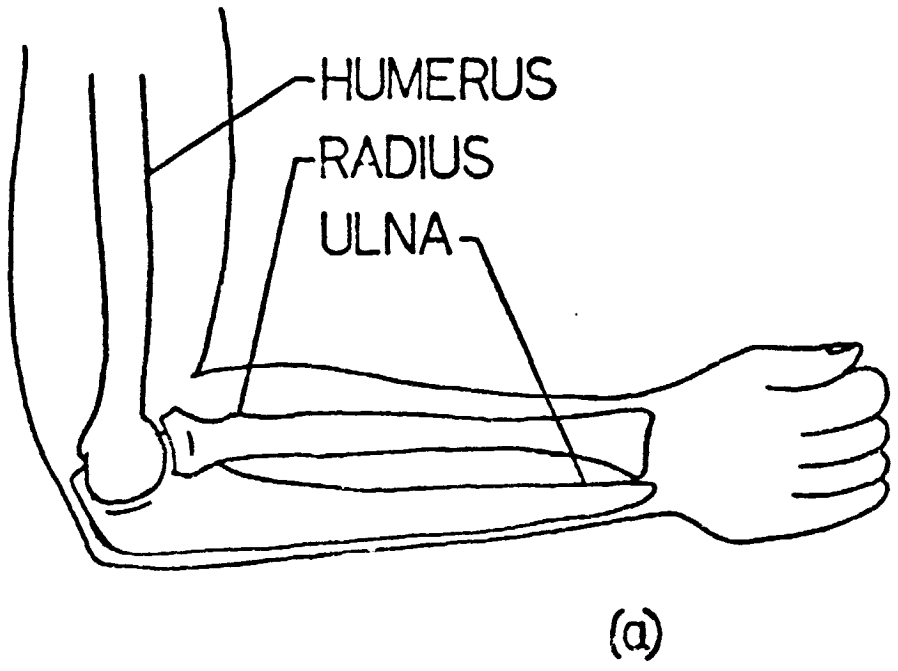

(a)

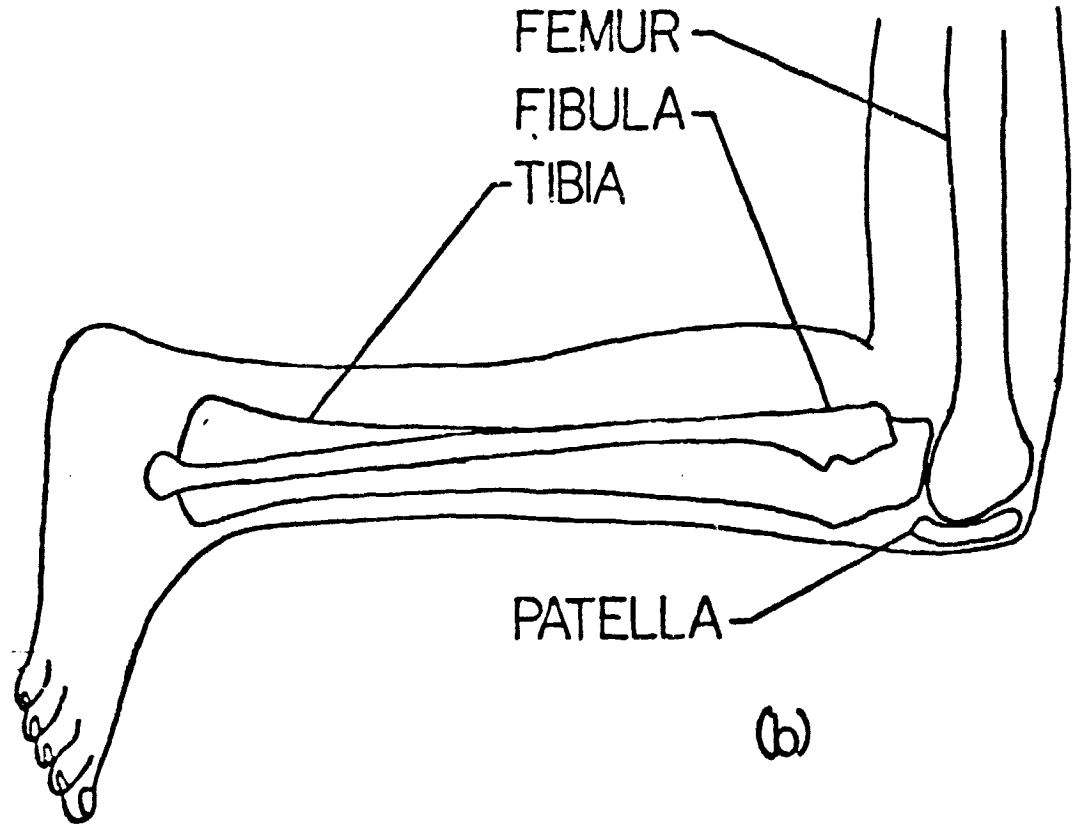

(b)

Figure 1.2. The Test Fixture.

(a) Shown with a human forearm in position. (b) Shown with a monkey leg in position.

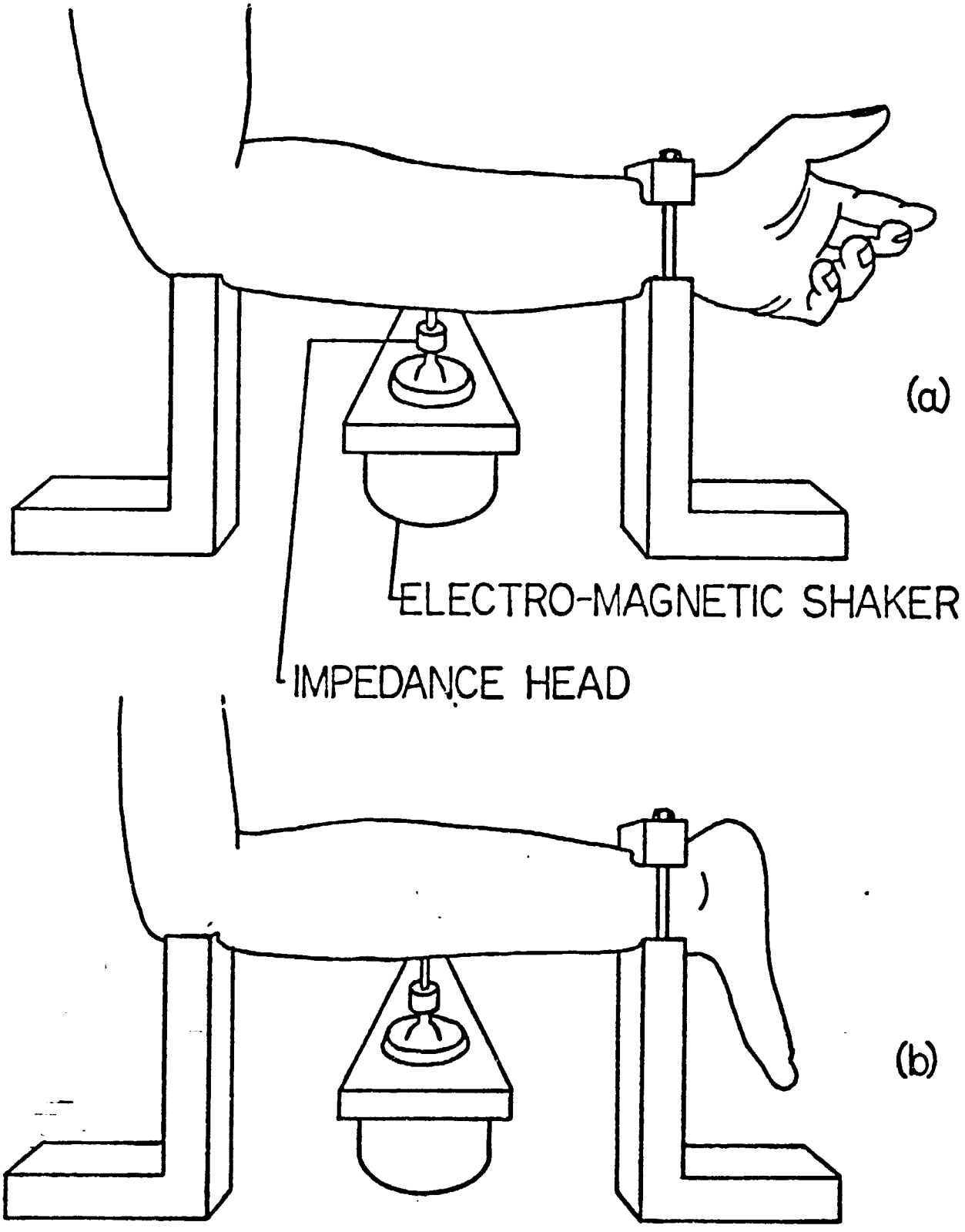

Figure 1.3. Schematic Diagram of the Impedance-measuring System.

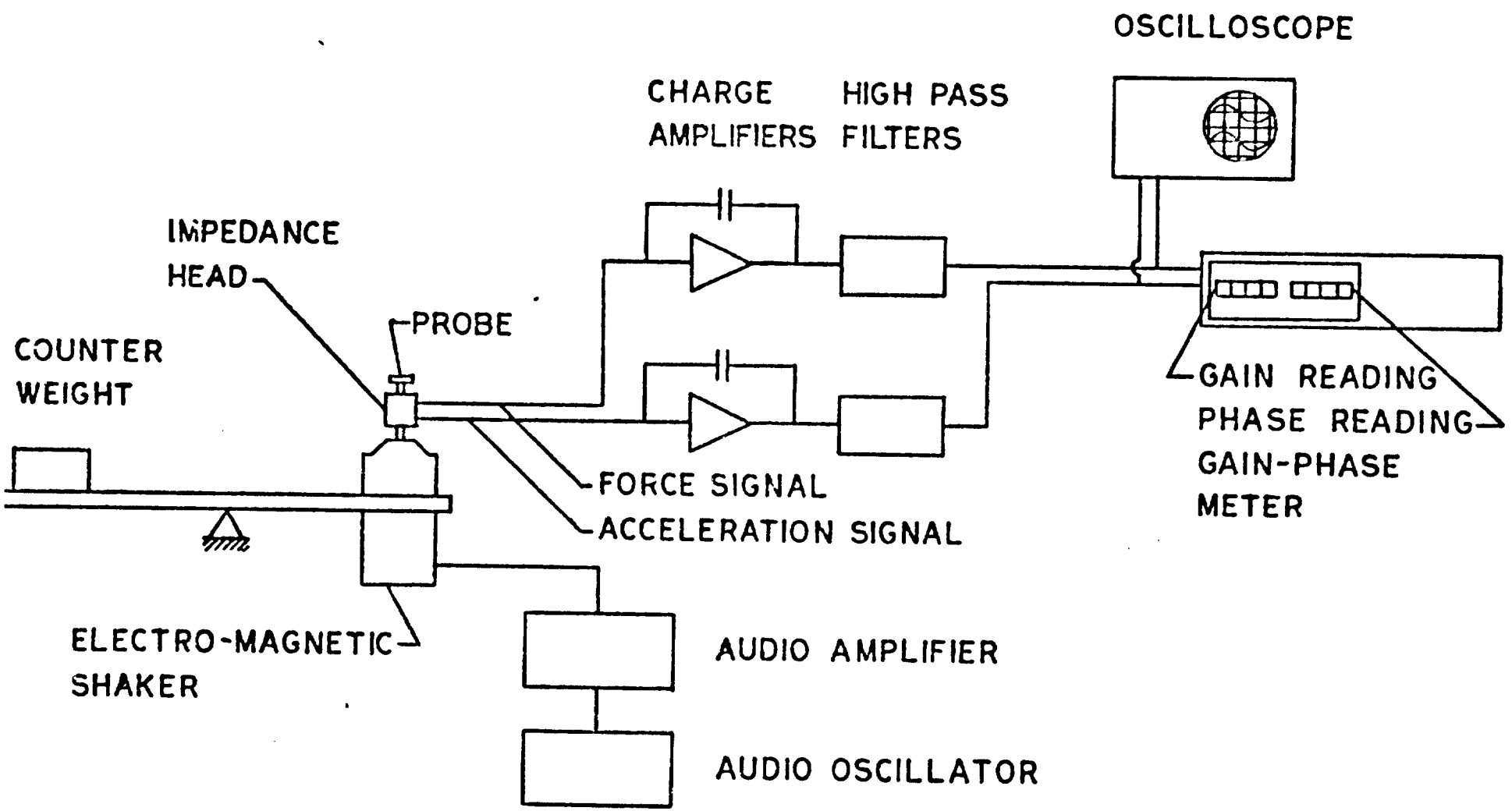

Figure 1.4. Sample Output From Thompson's Program.

EXP 730518 SUBJ T.T.
50-GM-PRELOAD

OUTPUT DATA SUMMARY FOR CASE 2

FREQ	ABS Z	ARG Z	RE Z	IM Z
HZ	DYNE-SEC/CM	DEG	DYNE-SEC/CM	DYNE-SEC/CM
65.	.259E+06 .32E+05	-92. 8.3	-.106E+05 -.37E+05	-.248E+06 .31E+05
70.	.240E+06 .30E+05	-96. 4.8	.157E+05 .19E+05	-.219E+06 .29E+05
80.	.175E+06 .19E+05	-96. 5.1	.127E+05 -.16E+05	-.173E+06 .29E+05
90.	.145E+06 .13E+05	-82. 3.2	.189E+05 .60E+04	-.143E+06 .17E+05
100.	.134E+06 .13E+05	-79. 3.3	.242E+05 .30E+04	-.127E+06 .14E+05
110.	.121E+06 .79E+04	-77. 1.6	.271E+05 .29E+04	-.118E+06 .81E+04
120.	.107E+06 .51E+04	-75. 1.6	.276E+05 .19E+04	-.104E+06 .57E+04
130.	.96 E+05 .40E+04	-73. 1.3	.287E+05 .10E+04	-.926E+05 .50E+04
140.	.897E+05 .61E+04	-70. 1.7	.309E+05 .65E+03	-.841E+05 .60E+04
150.	.7 5E+05 .44E+04	-63. 2.4	.353E+05 .17E+04	-.69 E+05 .7 E+04
160.	.751E+05 .61E+04	-54. 3.4	.429E+05 .64E+04	-.615E+05 .70E+04
170.	.690E+05 .42E+04	-52. 3.0	.431E+05 .43E+04	-.543E+05 .33E+04
180.	.659E+05 .30E+04	-47. 1.2	.449E+05 .21E+04	-.482E+05 .20E+04
190.	.591E+05 .23E+04	-42. 2.1	.437E+05 .25E+04	-.397E+05 .10E+04
200.	.572E+05 .33E+04	-37. 3.6	.460E+05 .44E+04	-.349E+05 .31E+04
210.	.574E+05 .17E+04	-30. 9.1	.498E+05 .19E+04	-.273E+05 .78E+03
220.	.57 E+05 .31E+04	-21. 5.6	.537E+05 .36E+04	-.206E+05 .6 E+03
230.	.61 E+05 .30E+04	-17. 7.6	.581E+05 .32E+04	-.176E+05 .8 E+03
240.	.69 E+05 .36E+04	-8. 5.8	.689E+05 .47E+04	-.94 E+04 .45E+03
250.	.821E+05 .33E+04	-2. 8.0	.815E+05 .36E+04	-.213E+04 .1 E+03
260.	.143E+06 .76E+04	-5. 7.4	.104E+06 .92E+04	-.8 E+04 .12E+03
270.	.127E+06 .71E+04	-15. 5.3	.121E+06 .10E+05	-.309E+05 .19E+03
280.	.164E+06 .14E+05	-31. 9.7	.129E+06 .19E+05	-.76 E+05 .1 E+04
290.	.145E+06 .17E+05	-44. 9.0	.103E+06 .21E+05	-.10 E+05 .13E+04
300.	.114E+06 .18E+05	-62. 9.9	.564E+05 .19E+05	-.11 E+05 .11E+04
310.	.893E+05 .14E+05	-67. 3.6	.357E+05 .11E+05	-.8 E+04 .1 E+04
320.	.831E+05 .13E+05	-60. 1.0	.286E+05 .32E+04	-.7 E+04 .17E+03
330.	.11 E+06 .11E+05	-71. 3.4	.329E+05 .11E+05	-.7 E+04 .12E+03

Figure 1.4. Sample Output From Thompson's Program.

EXP 730510 SUMJ T.T.
50--GM-PRELOAD

OUTPUT DATA SUMMARY FOR CASE 2

FREQ HZ	ABS Z DYNE-SEC/CM	ARG Z DEG	RE Z DYNE-SEC/CM	IM Z DYNE-SEC/CM
65.	.259E+06	.32E+05	-92.	8.3	-.106E+05	-.37E+05	-.240E+04	.31E+05
70.	.223E+06	.30E+05	-95.	4.8	.15?E+05	.19E+05	-.21?E+05	.30E+05
80.	.175E+06	.19E+05	-96.	5.1	.127E+05	-.16E+05	-.173E+04	.21E+05
90.	.145E+06	.13E+05	-82.	3.?	.189E+05	.48E+04	-.143E+05	.17E+05
100.	.1?4E+06	.13E+05	-79.	3.3	.24?E+05	.?2E+04	-.127E+05	.14E+05
110.	.121E+06	.79E+04	-77.	1.6	.271E+05	.29E+04	-.13?E+05	.81E+04
120.	.107E+06	.51E+04	-75.	1.6	-.276E+05	-.19E+04	-.104E+05	.57E+04
130.	.96?E+05	.49E+04	-73.	1.3	.287E+05	.17E+04	-.923E+05	.?2E+04
140.	.807E+05	.61E+04	-73.	1.7	.309E+05	.65E+03	-.841E+05	.6?E+04
150.	.?2?E+05	.54E+04	-63.	2.4	.353E+05	.17E+04	-.697E+05	.?2E+04
160.	.751E+05	.61E+04	-5?.	?.4	-.?2?E+05	-.?4E+04	-.?17E+04	.??E+04
200.	.609E+05	.42E+04	-52.	3.3	.43?E+05	.43E+04	-.5?1E+05	.3?E+04
2?0.	.6??E+05	.30E+04	-47.	1.2	.4?0E+05	.21E+04	-.4?2E+05	.2?E+04
250.	.?0?E+05	.?3E+04	-?2.	2.1	.437E+05	.25E+04	-.307E+05	.1?E+04
275.	.372E+05	.??E+04	-??	?.6	.4?3E+05	.4?E+04	-.?42E+05	.??E+04
300.	.57?E+05	.17E+04	-?0.	9.1	.498E+05	.10E+05	-.?73E+05	.?2E+?
325.	.??2E+0?	.?1E+04	-21.	5.6	-.?37E+0?	-.?3E+04	-.20?E+?	.??E+?
?50.	.?1?E+05	.??E+04	-1?.	?.0	.5?1E+05	.32E+04	-.17?E+??	.?E+??
375.	.?0?E+05	.?3E+04	-8.	5.0	.5??E+05	.47E+04	-.?4?E+??	.??E+??
400.	.??2E+05	.?1E+04	-2.	?.?	.?15E+0?	.?6E+04	-.?13E+??	.?E+??
?50.	.1?3E+06	.??E+04	-5.	7.4	.10?E+06	.?2E+04	-.8?4E+??	.12E+??
500.	.?27E+?6	.?1E+04	-15.	5.?	.?2?E+05	.1?E+??	-.?0?E+??	.1?E+??
?50.	.1??E+06	.1??E+??	-?1.	?.?	.12?E+05	.10E+??	-.?0?E+??	.??E+??
600.	.1?5E+06	.1?E+??	-??	?.?	.133E+??	.?1E+??	-.1?1E+??	.??E+??
?50.	.1??E+06	.?2E-??	-?2.	?.?	.?5?E+0?	.19E+??	-.1??E+??	.??E+??
700.	.??1E+??	.?4E+??	-6?.	3.?	.3?7E+05	.1?E+??	-.?1?E+??	.??E+??
750.	.?1?E+??	.1?E+??	-50.	?.?	.?0?E+0?	.?2E+??	-.?0?E+??	.??E+??
800.	.??1E+??	.??E+??	-??	3.?	.2?0E+0?	.?1E+??	-.?1?E+??	.??E+??

Figure 1.5. Sample Plot From Thompson's Program.

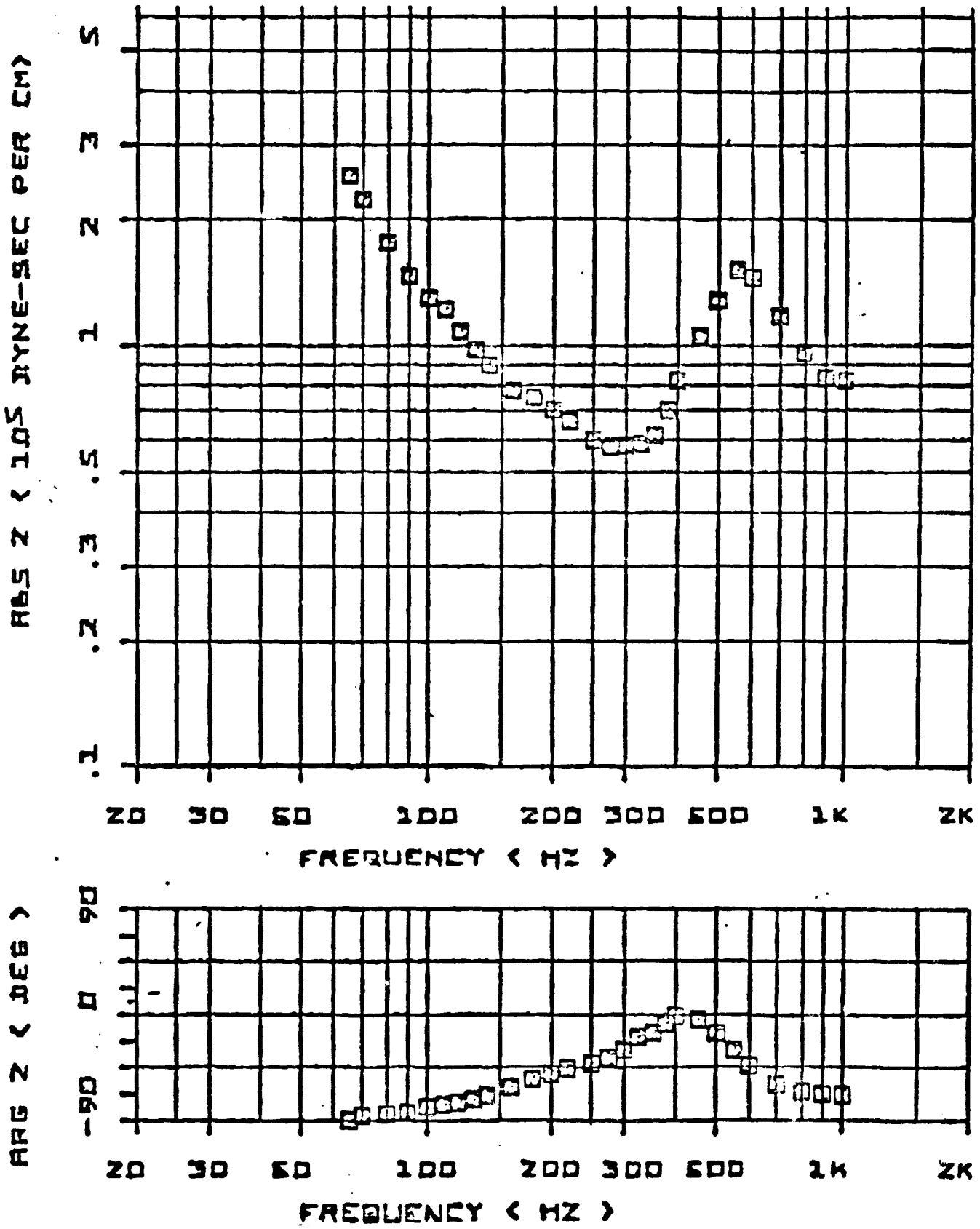

Figure 2.1. Orne's First Model of the Ulra in Thompson's Experimental Procedure.

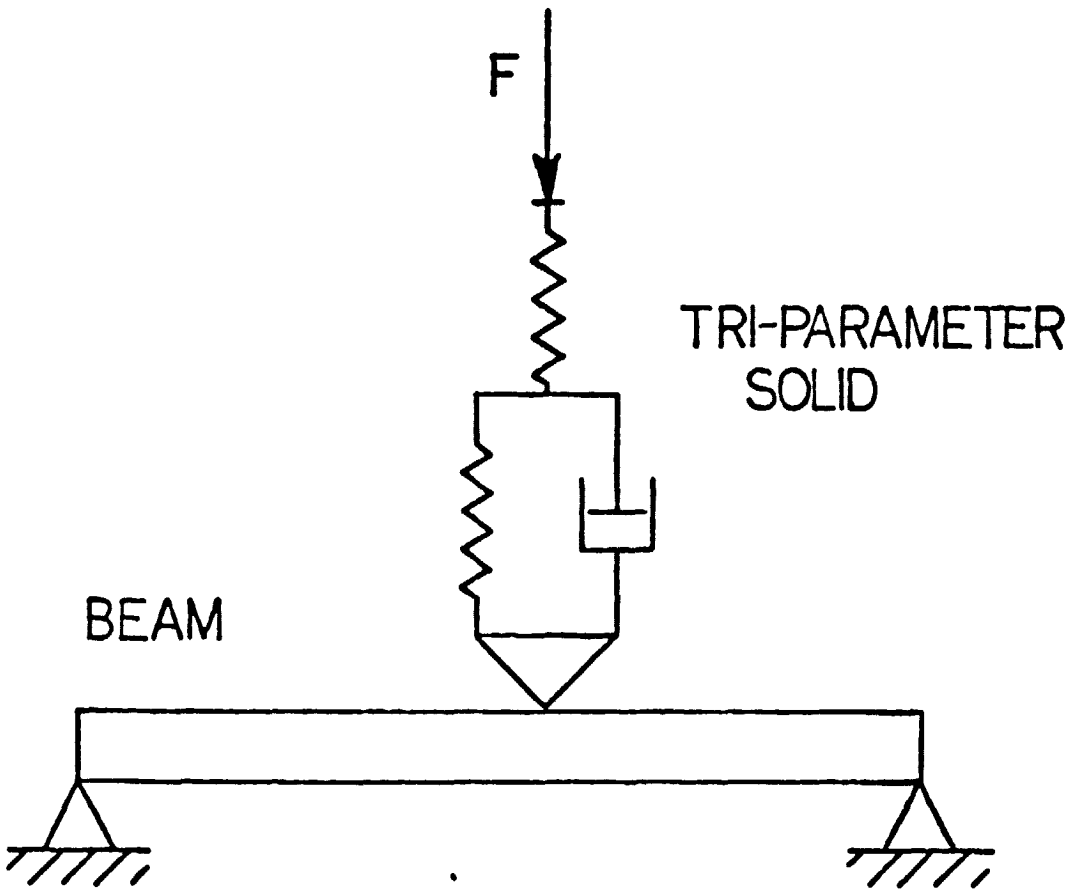

Figure 2.2. Impedance Data From a Piece of Skin.

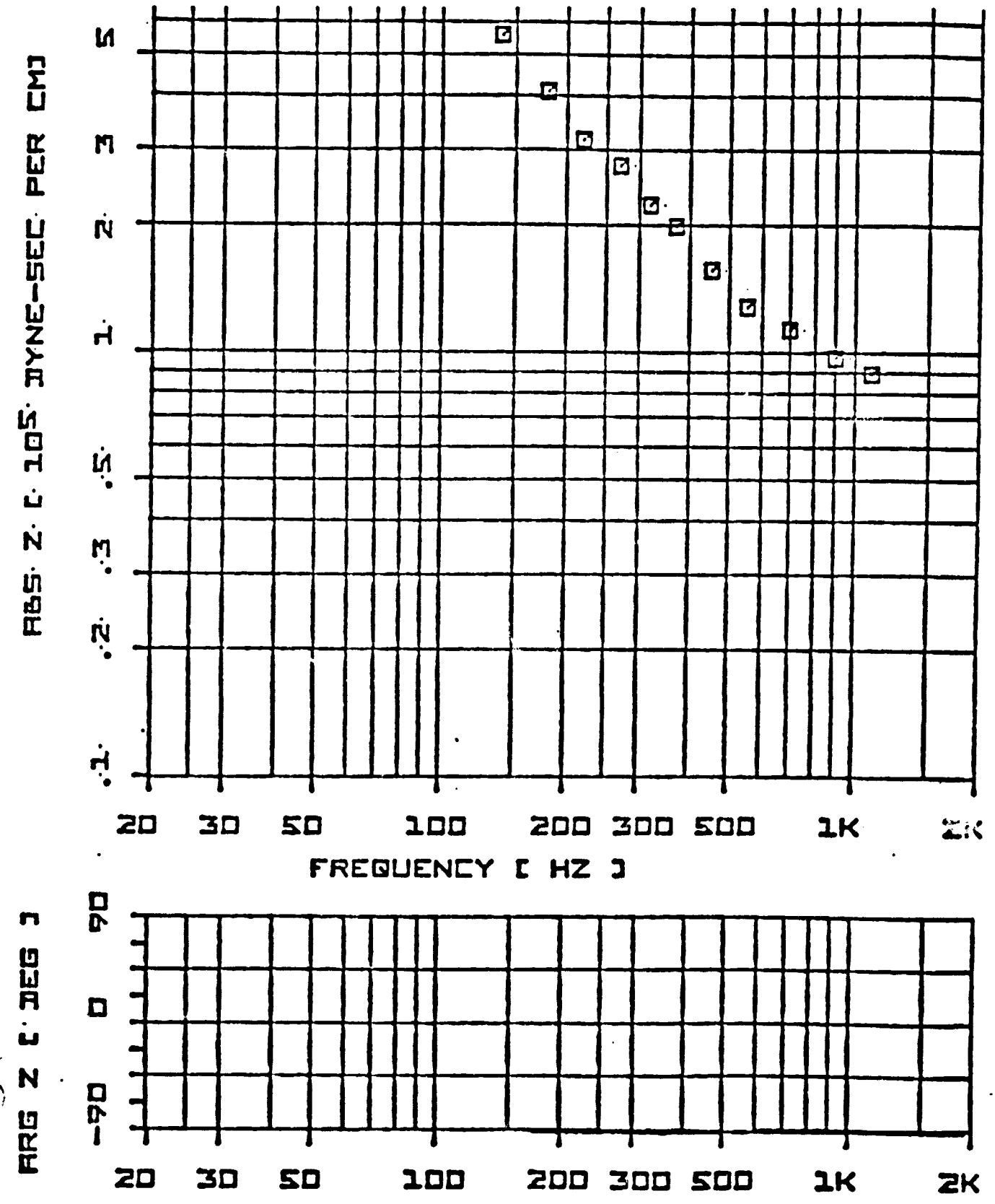

Figure 2.3. Improved Model of the Ulna in Thompson's Experimental Procedure.

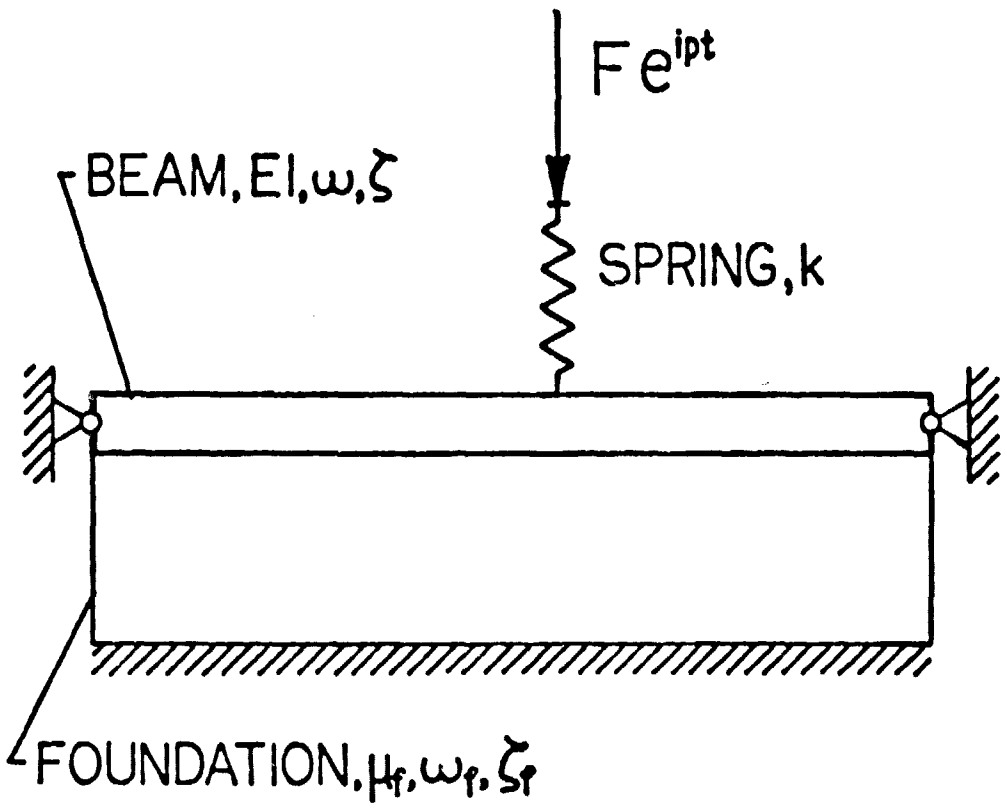

Figure 3.1. Diagrams of Beam Models.

(a) Case 1: simply-supported
(b) Case 2: rotational spring on one end
(c) Case 3: rotational spring on each end
(d) Case 4: translational spring on one end
(e) Case 5: translational spring on each end
(f) Case 6: translational spring on an extended beam

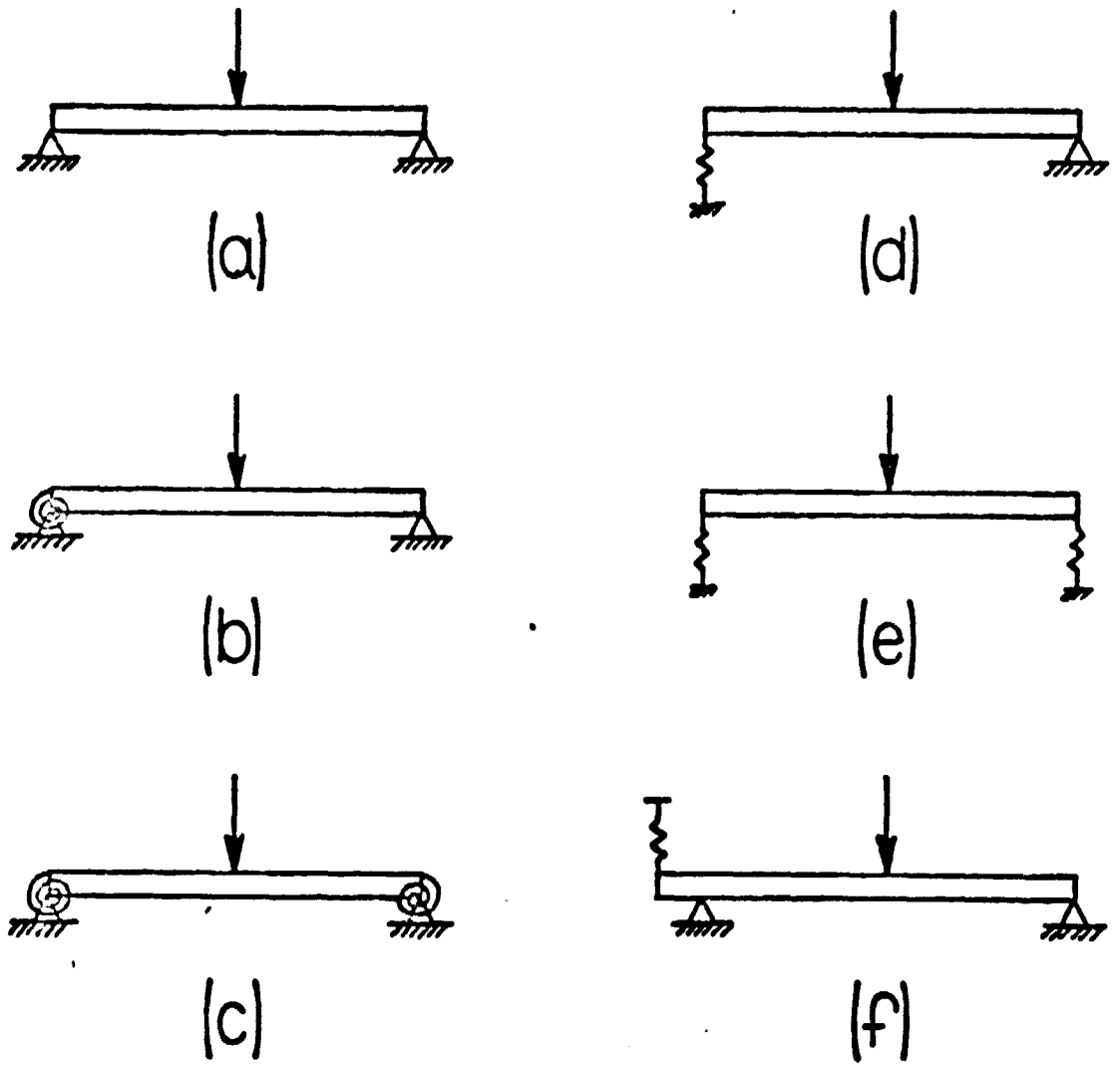

Figure 3.2. The Coordinate System of the Beam.

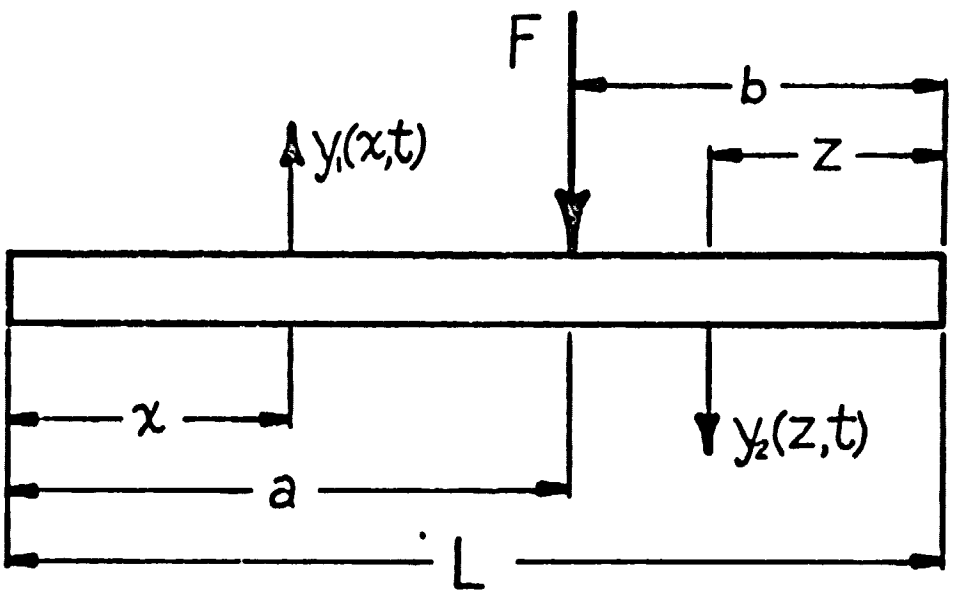

Figure 3.3. The Foundation.

The coordinate system and boundary conditions: (a) fixed, (b) free.

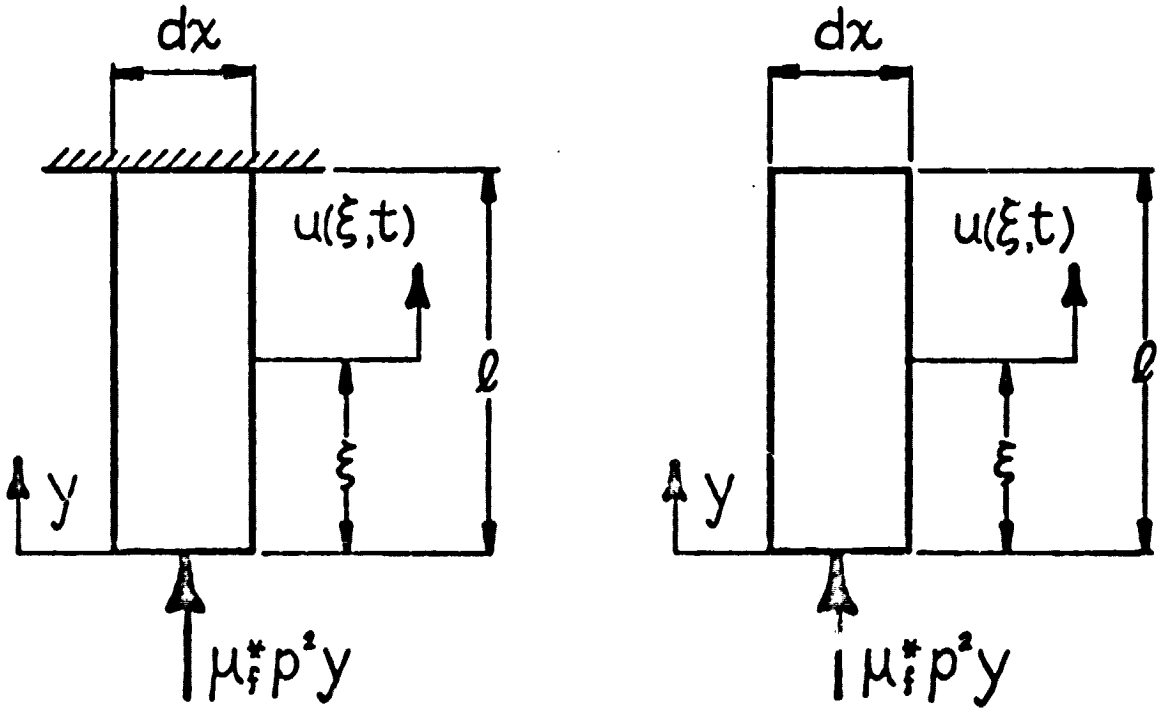

$$u(0,t) = y$$

$$u(\ell,t) = 0$$

$$bE_f^* \frac{\partial u}{\partial \xi}(0,t) = \mu_f^* p^2 y$$

$$u(0,t) = y$$

$$\frac{\partial u}{\partial \xi}(\ell,t) = 0$$

$$bE_f^* \frac{\partial u}{\partial \xi}(0,t) = \mu_f^* p^2 y$$

Figure 4.1. DPMI of a Simply-supported Beam.

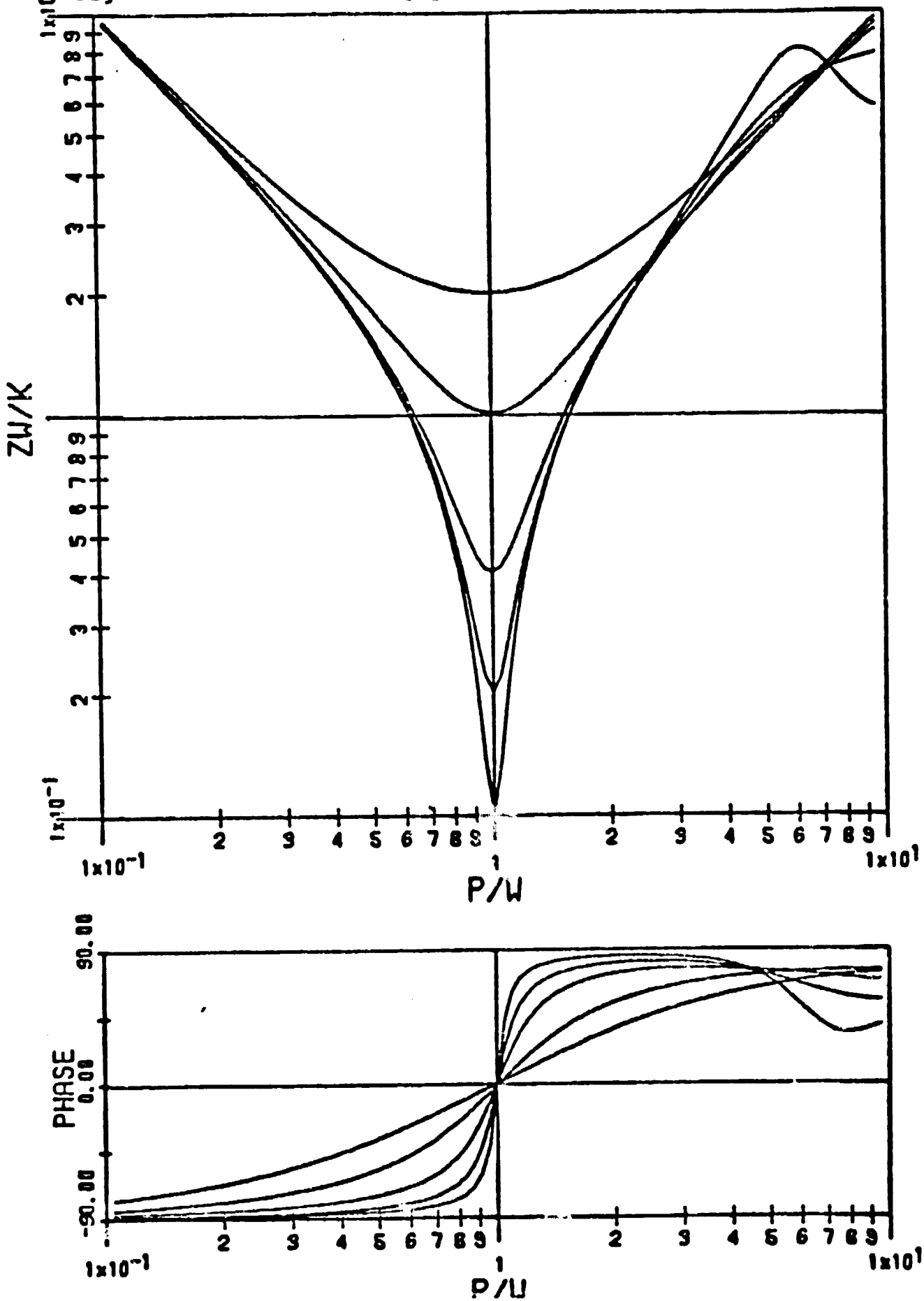

Figure 4.2. Single-degree-of-freedom Oscillator.

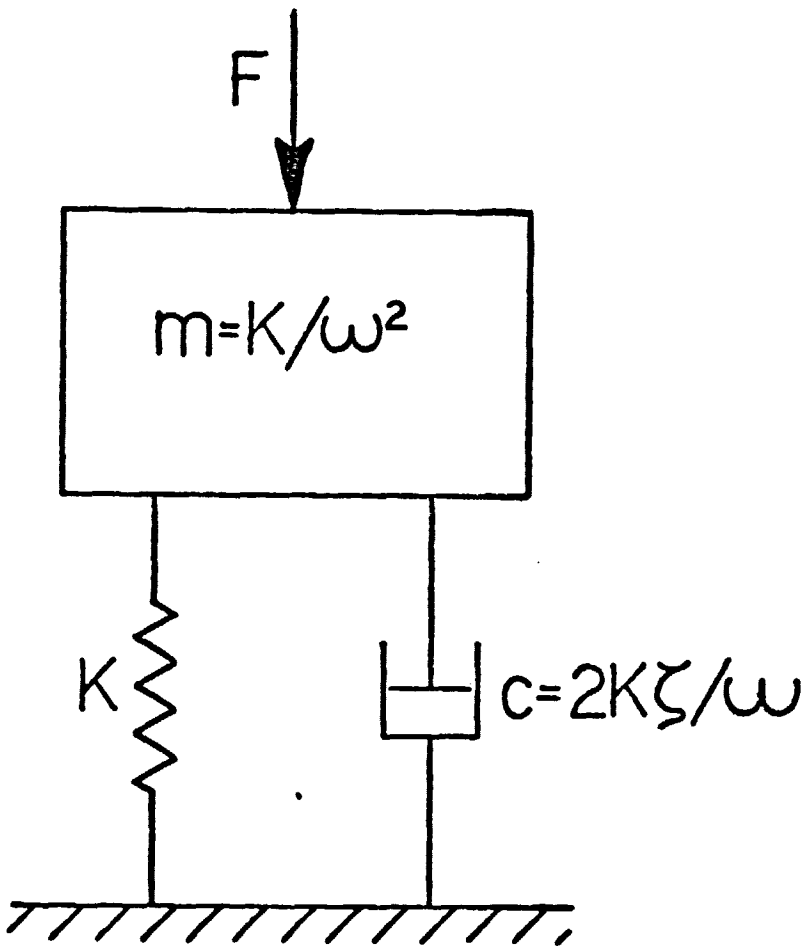

C - 3

Figure 4.3. DPMI of a Single-degree-of-freedom Oscillator.

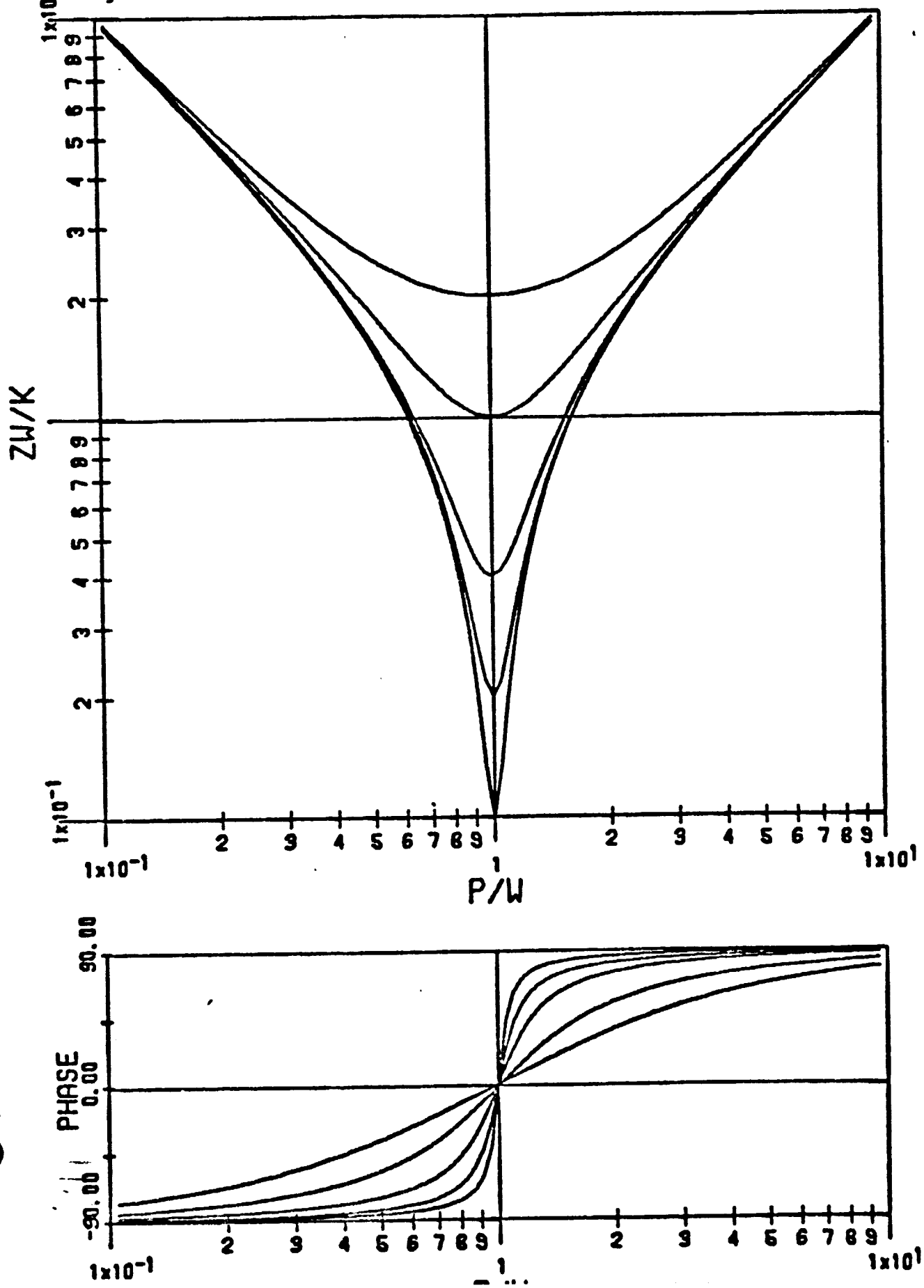

Figure 4.4. DPMI of a Simply-supported Beam Loaded Off Center

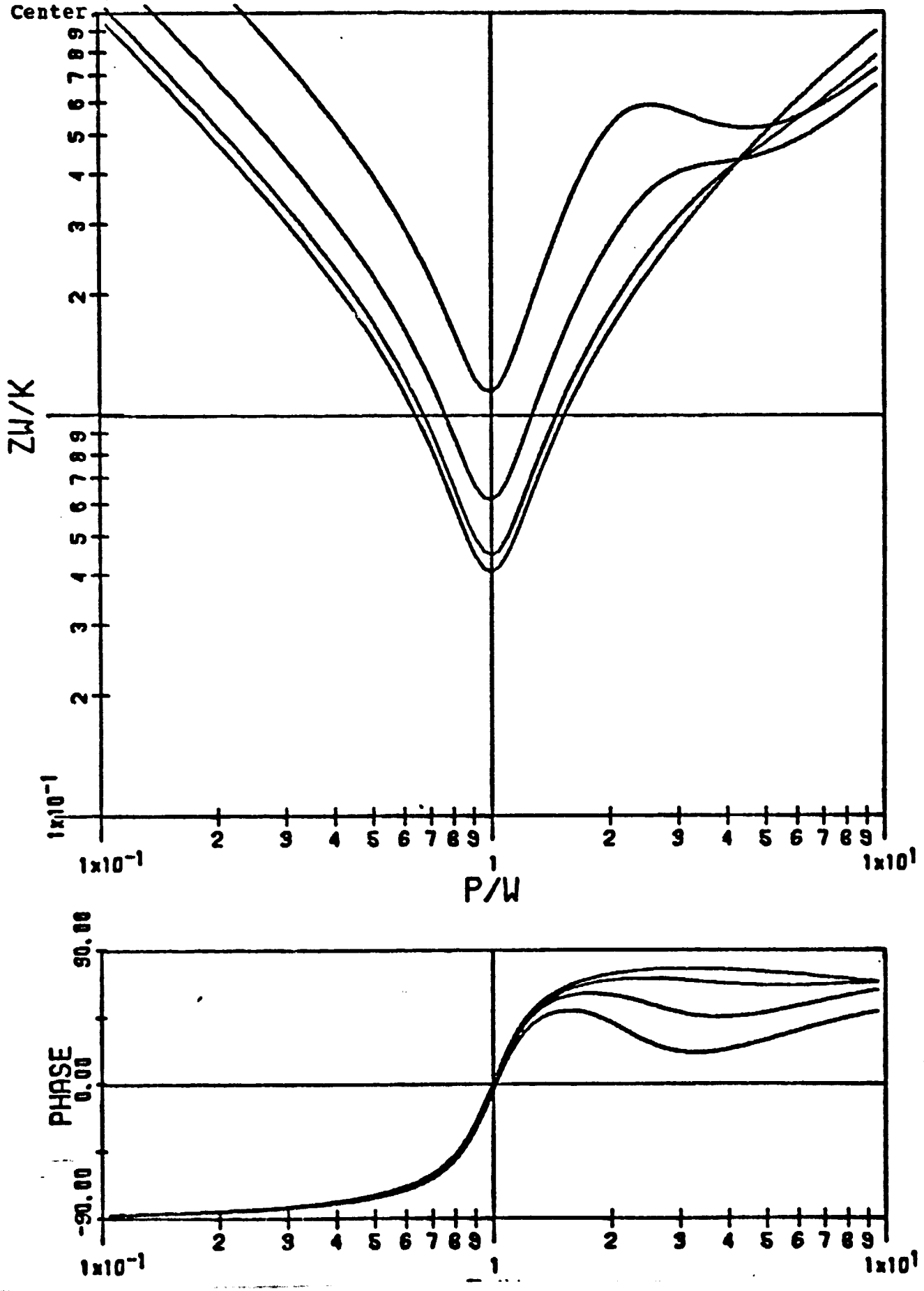

Figure 4.5. DPMI of Case 2: Rotational Spring on One End.

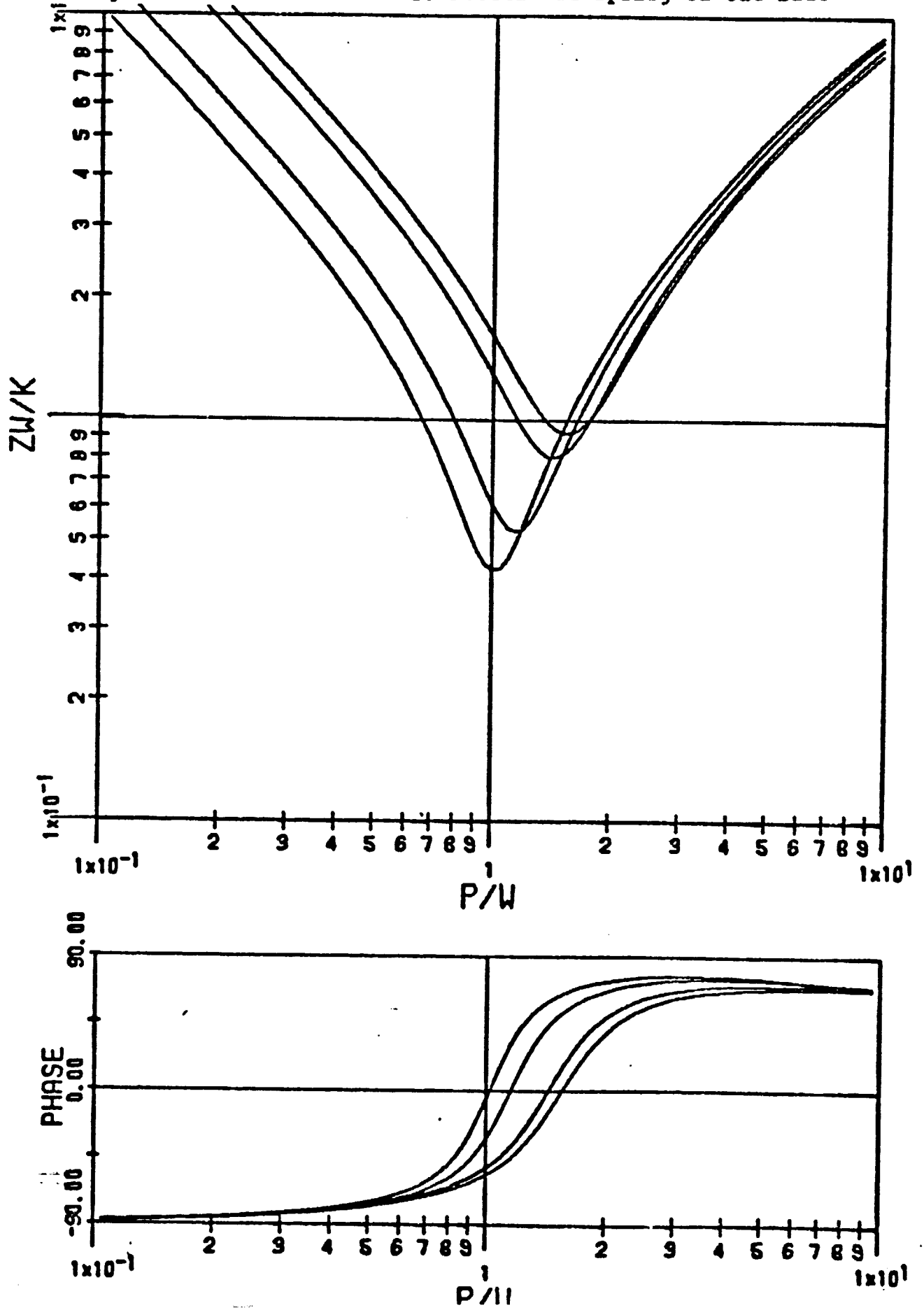

Figure 4.6. DPMI of Case 3: Rotational Spring on Each End.

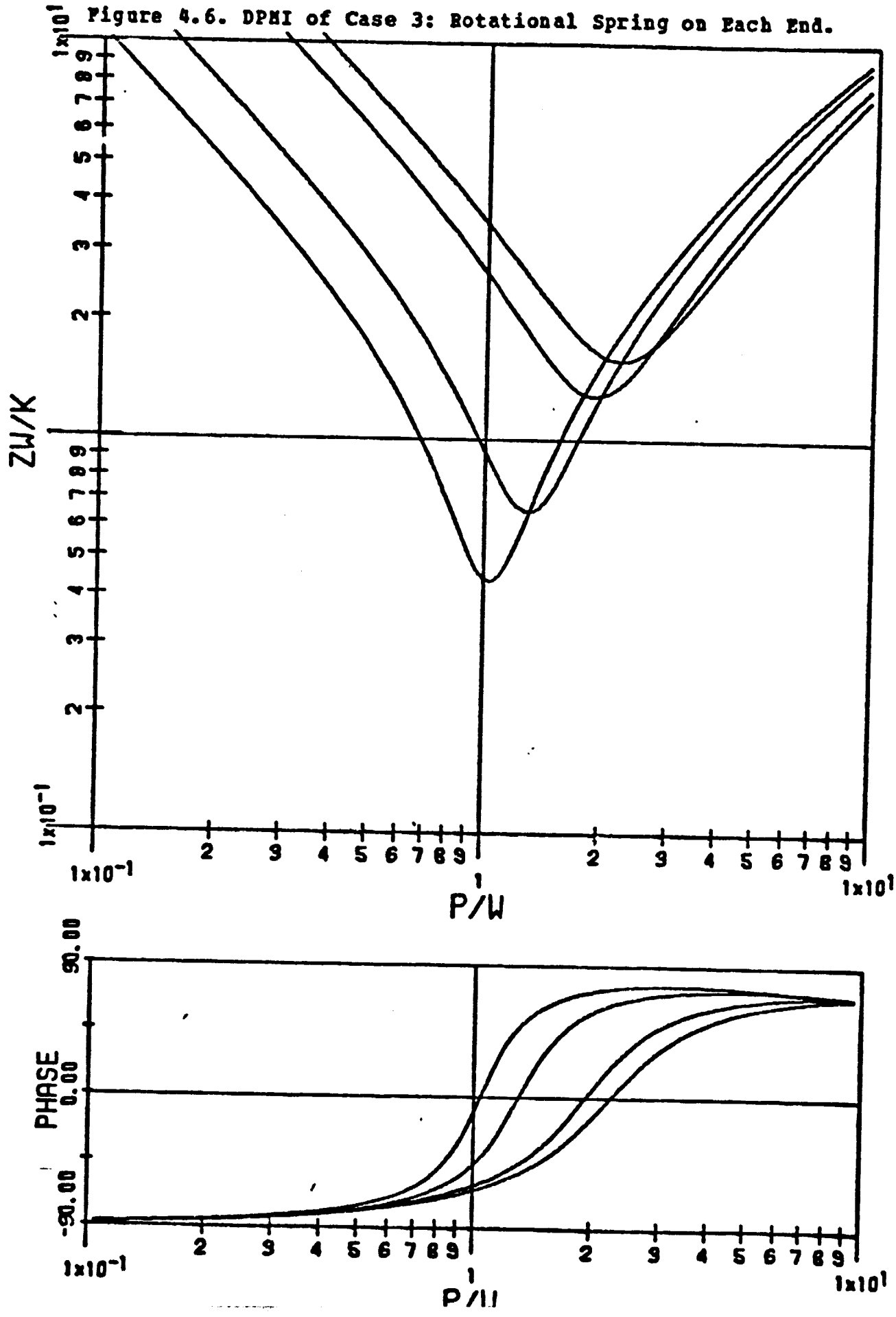

Figure 4.7. DPMI of Case 4: Translational Spring on One End

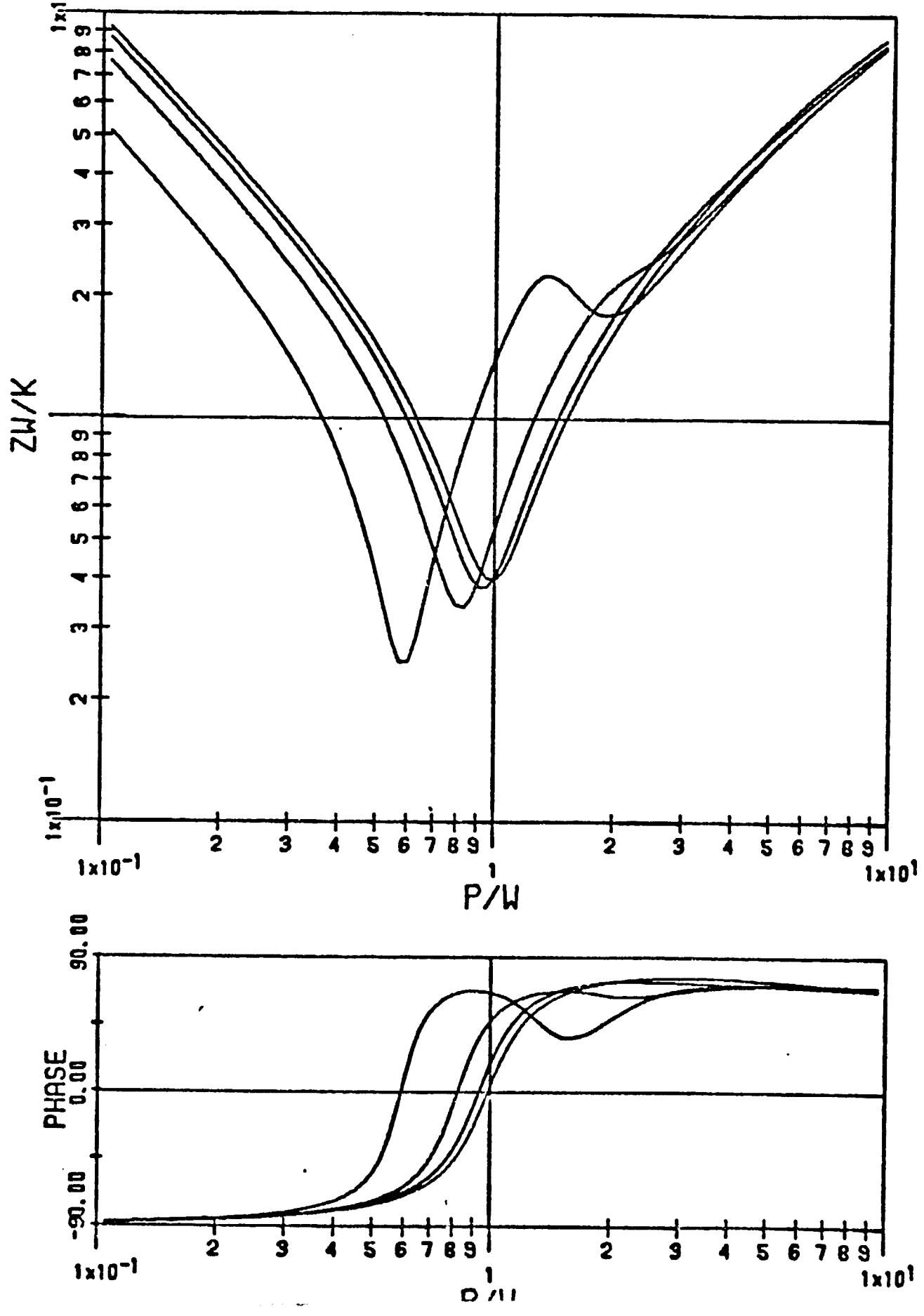

Figure 4.8. DPHI of Case 5: Translational Spring on Each End.

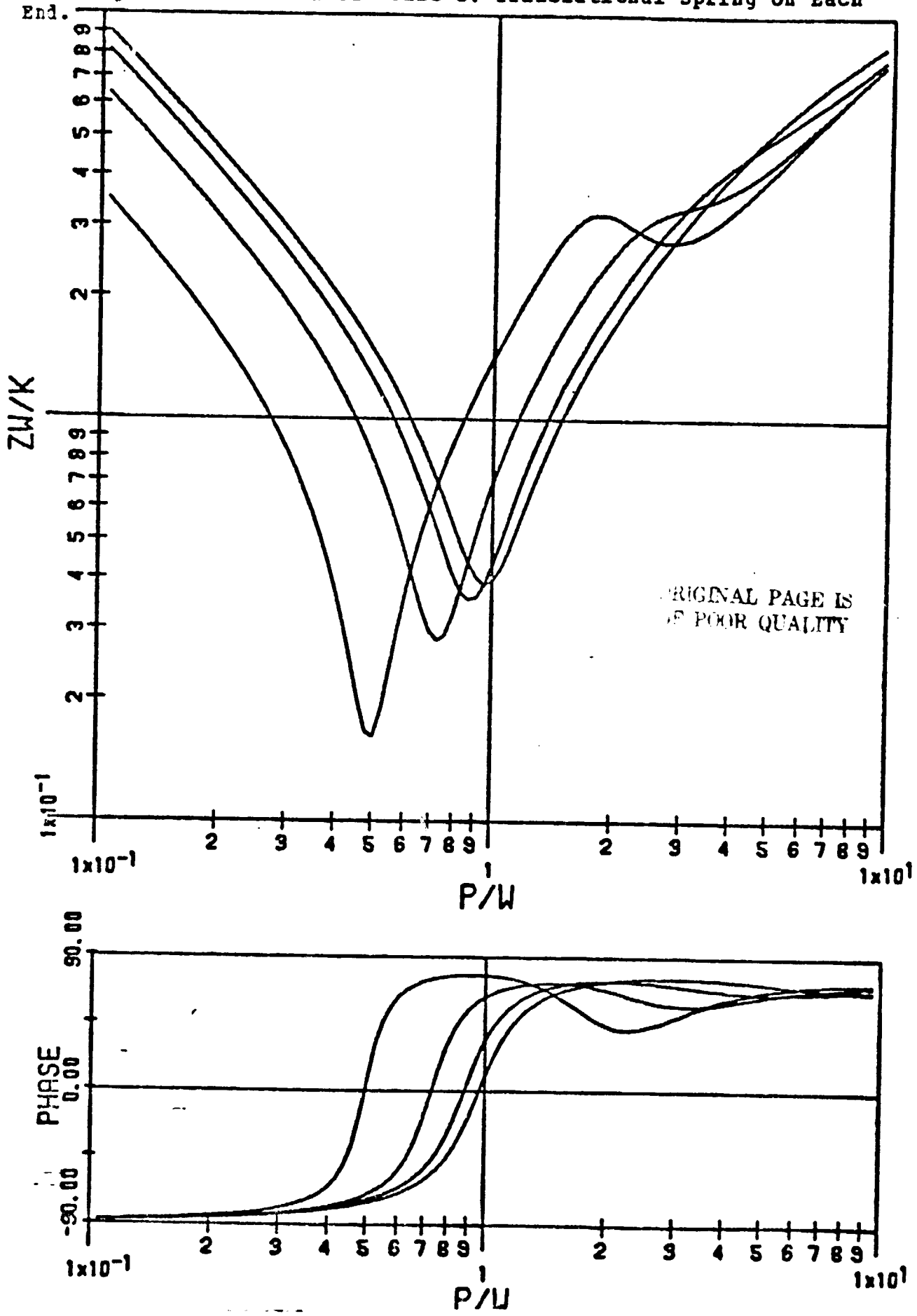

Figure 4.9. DPMI of Case 6: Translational Spring on An Extended Beam.

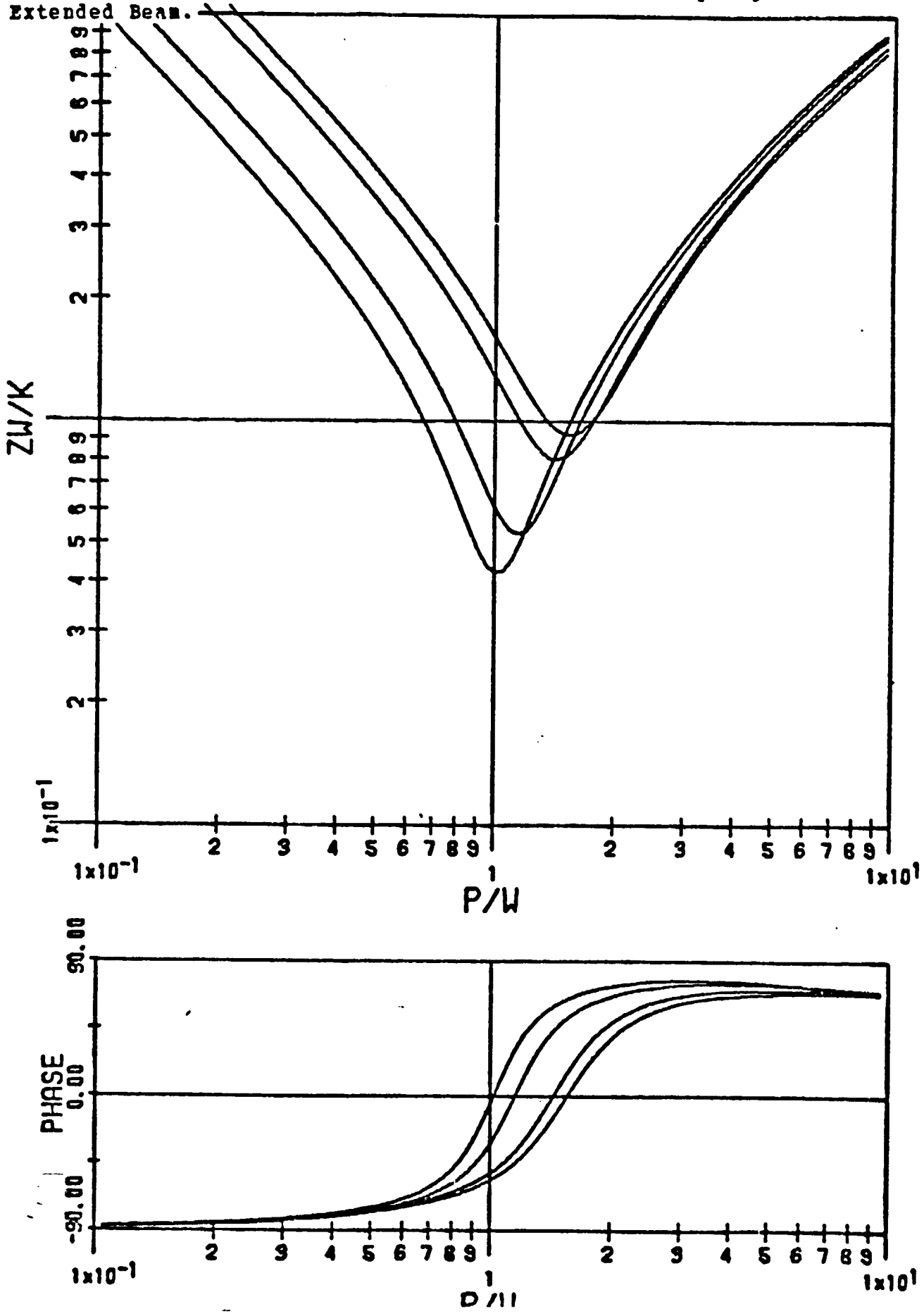

Figure 4.10. DPHI of Cases 1 Through 5, Re-non-dimensionalized.

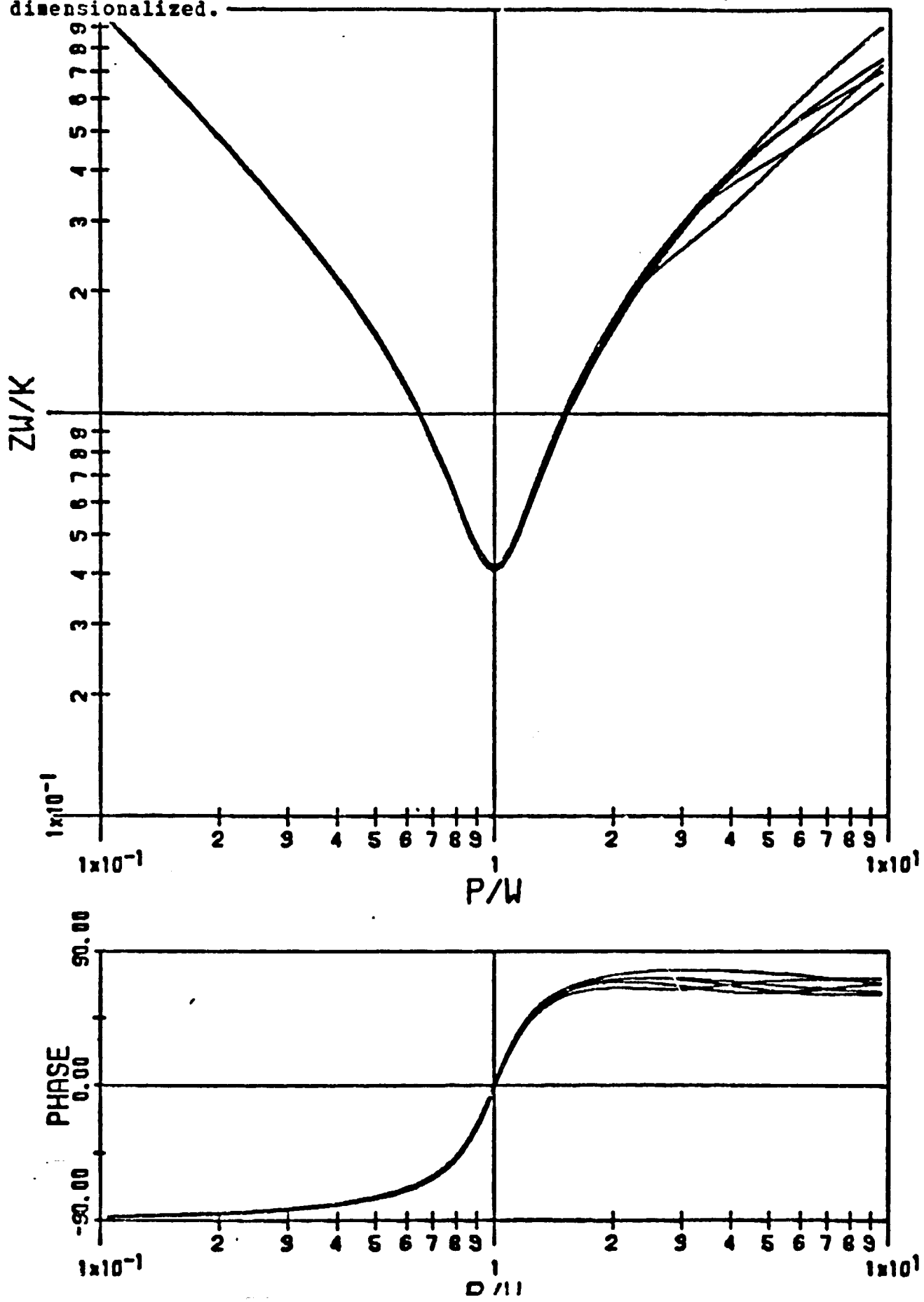

Figure 4.11. DPNI of Cases 1 Through 5, Re-non-dimensionalized.

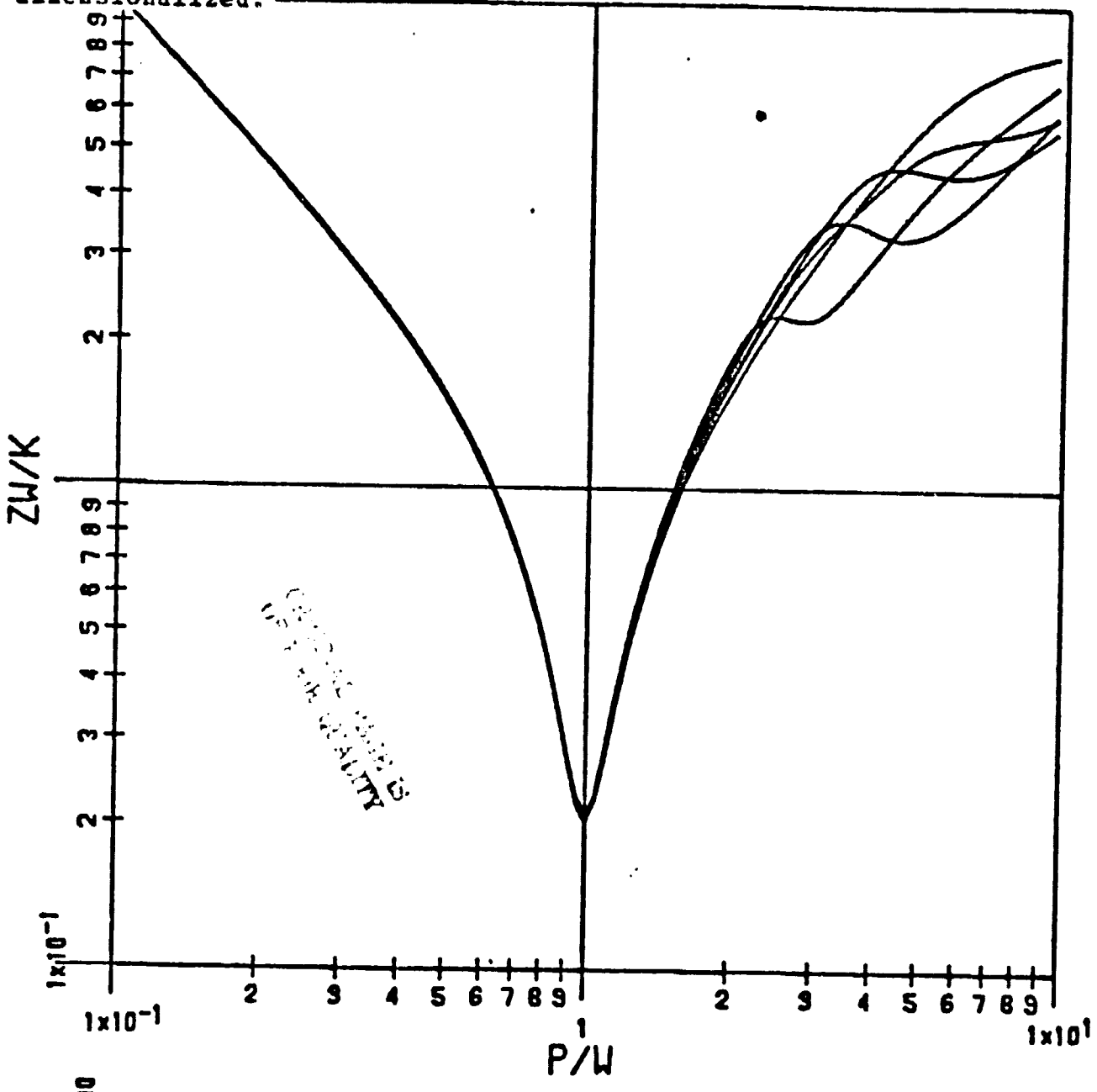

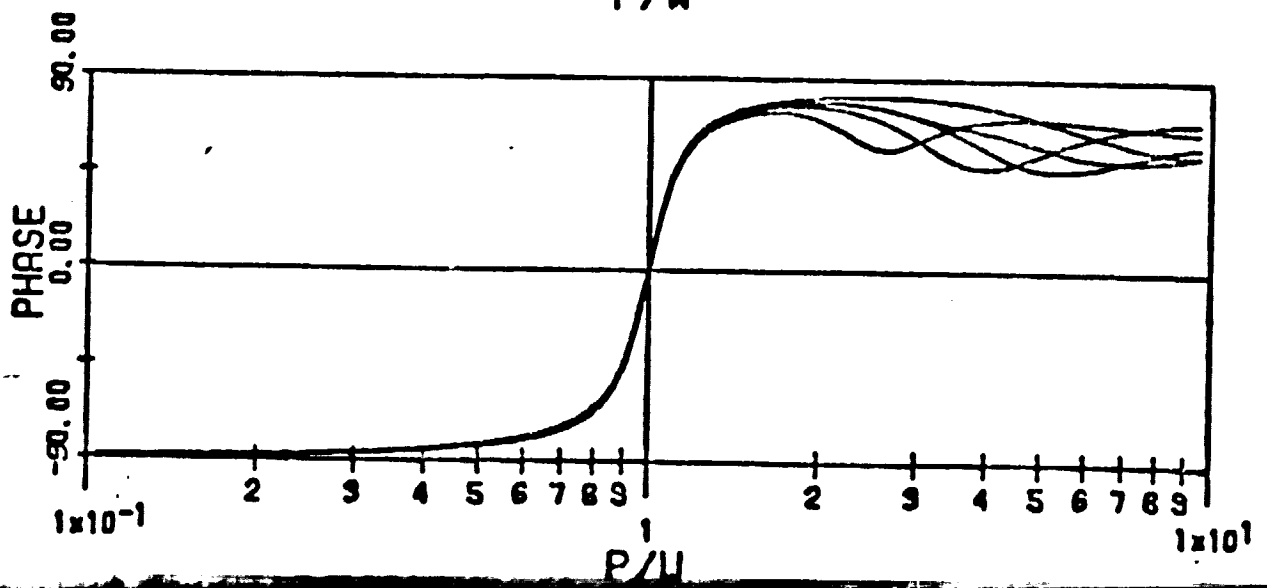

Figure 4.12. Taper.

(a) Linear, (b) quadratic.

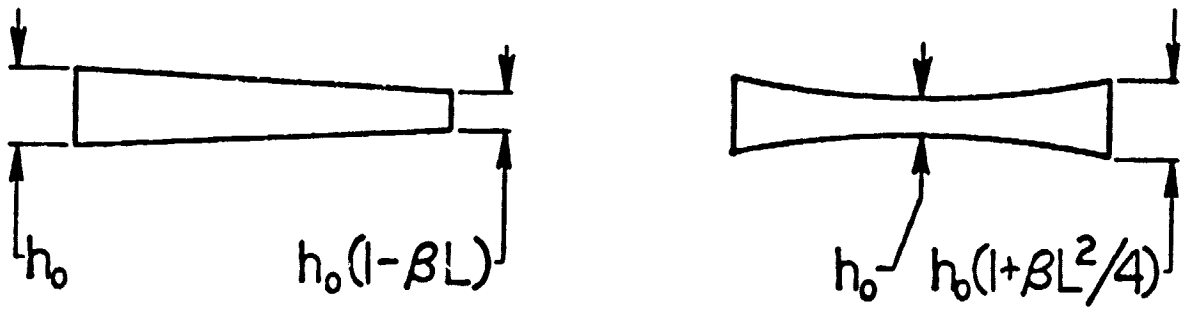

(a)

$$h(x) = h\,(1 - \beta x)$$

$$A(x) = A\,(1 - \beta x)^2$$

$$I(x) = I\,(1 - \beta x)^4$$

(b)

$$h(x) = h\,(1 + \beta x^2)$$

$$A(x) = A\,(1 + \beta x^2)^2$$

$$I(x) = I\,(1 + \beta x^2)^4$$

$h(x)$ = a cross sectional dimension

$A(x)$ = the cross sectional area

$I(x)$ = the cross sectional area moment of inertia

Figure 4.13. DPMI Plot Exhibiting the Dependance of the Mass Per Unit Length of a Fixed Foundation.

(The beam boundary conditions are simply-supported.)

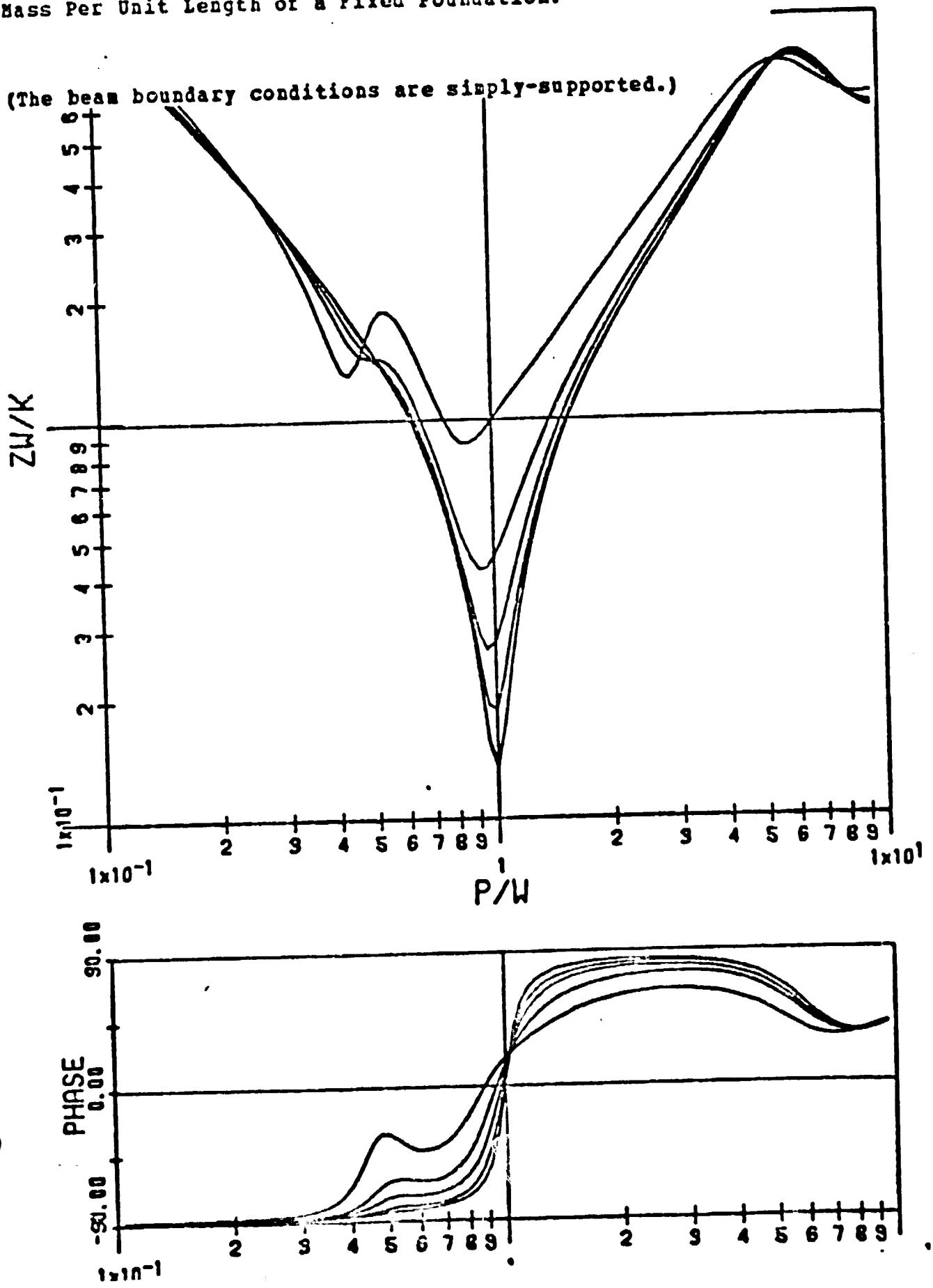

Figure 4.14. DPMI Plot Exhibiting the Dependance of the Damping Ratio of a Fixed Foundation.

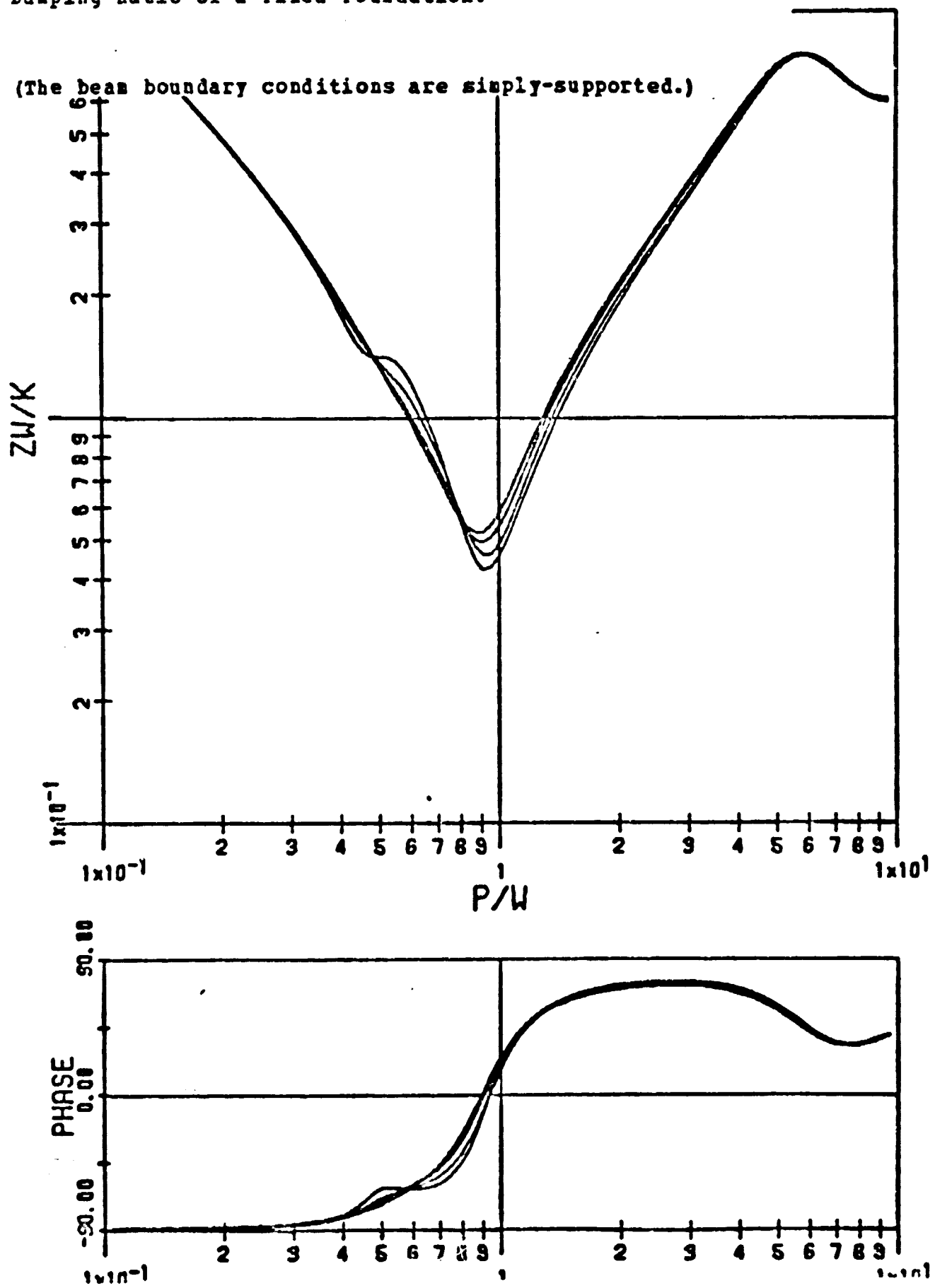

Figure 4.15. DPMI Plot Exhibiting the Dependance of the Mass Per Unit Length of a Free Foundation.

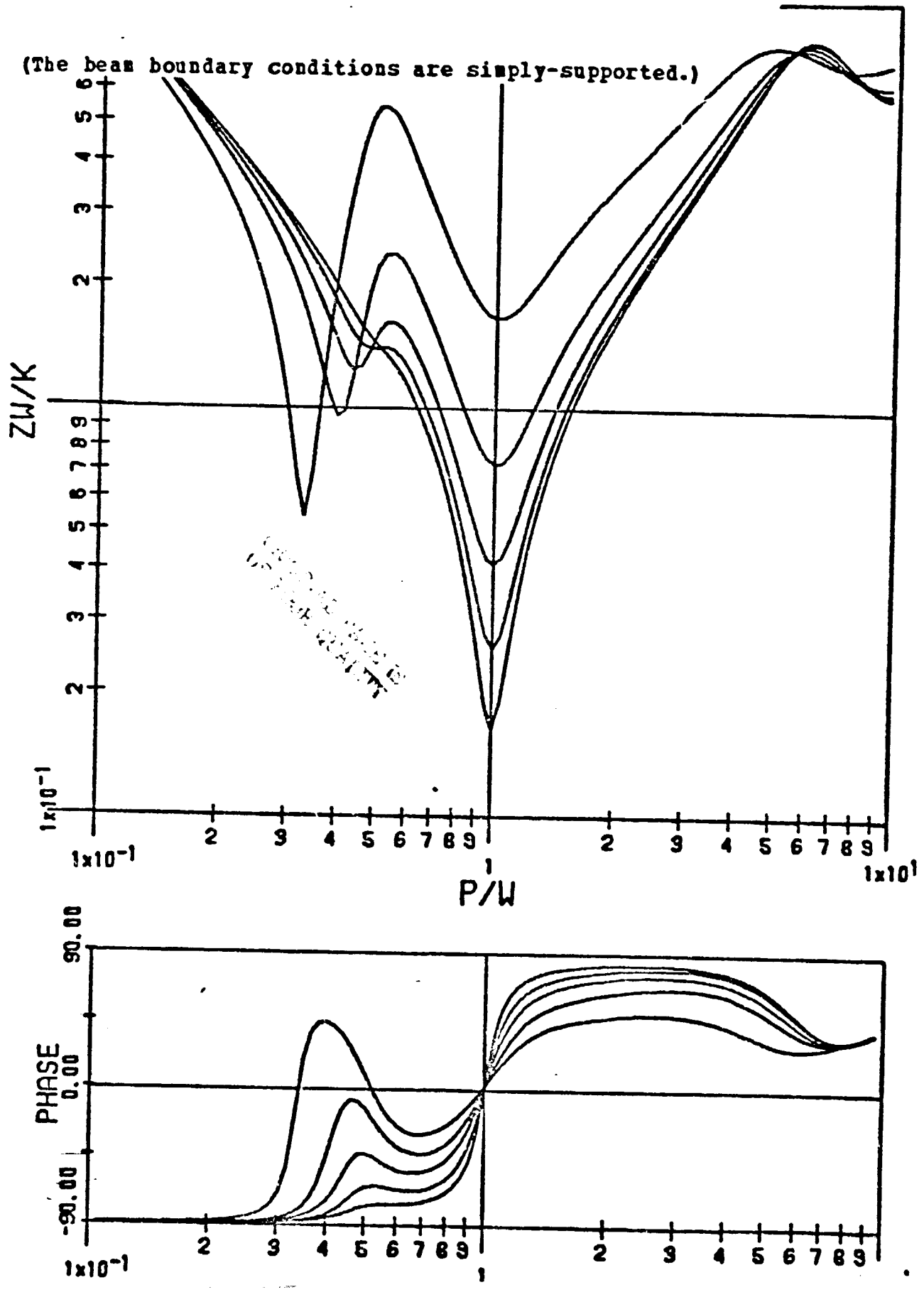

Figure 4.16. DPMI Plot Exhibiting the Dependance of the Damping Ratio of a Free Foundation.

(The beam boundary conditions are simply-supported.)

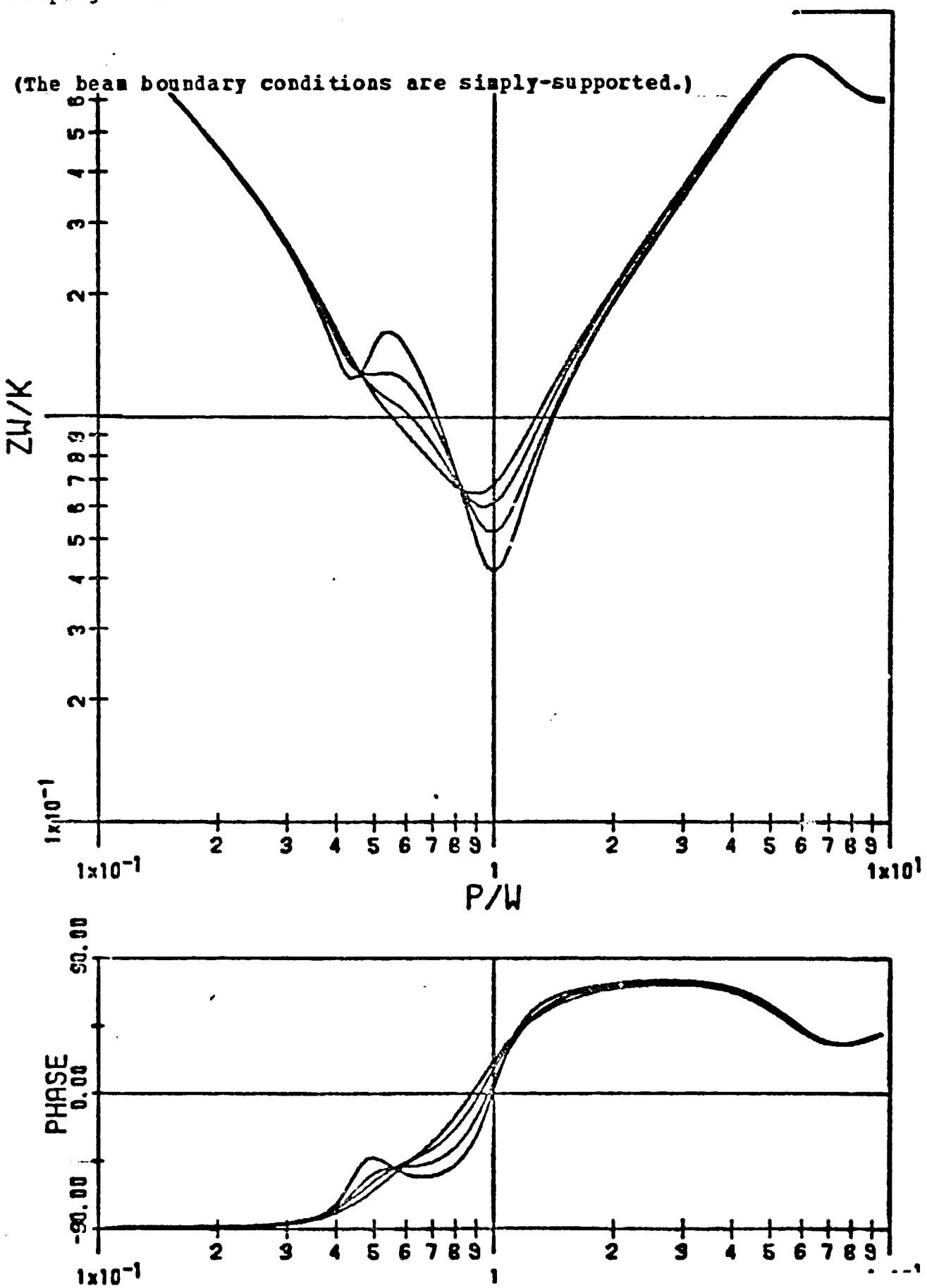

Figure 4.17. Comparison Between Actual Minimum DPMI and Approximate Equations.

(a) Equation (4.17), fixed foundation, (b) equation (4.18), free foundation.

□ Actual minimum DPMI
– Equation (4.17) or (4.18)

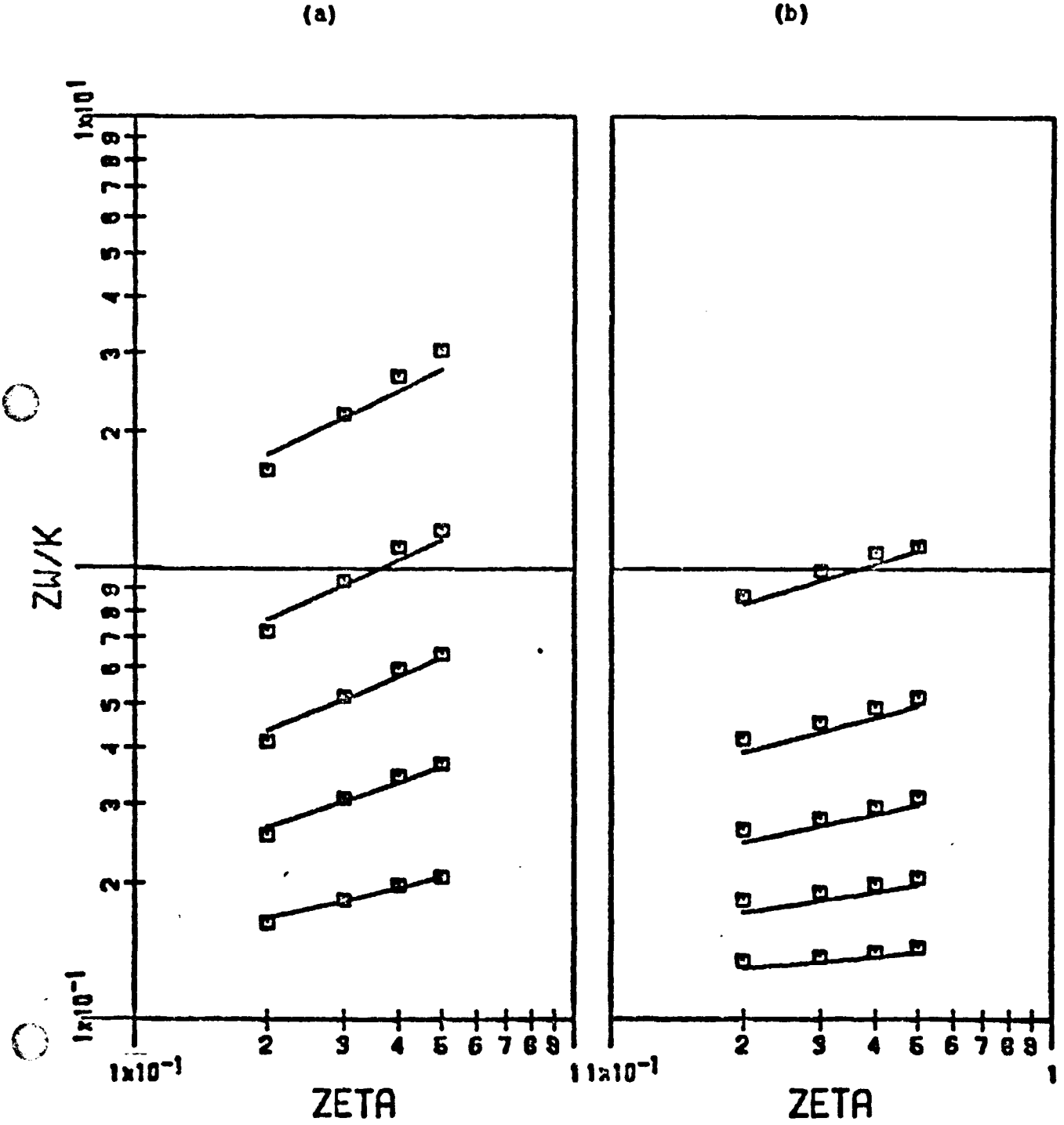

Figure 4.18. DPHI Plot Exhibiting the Dependance of the Spring Constant of a Spring in Series With The Beam.

(The beam boundary conditions are simply-supported.)

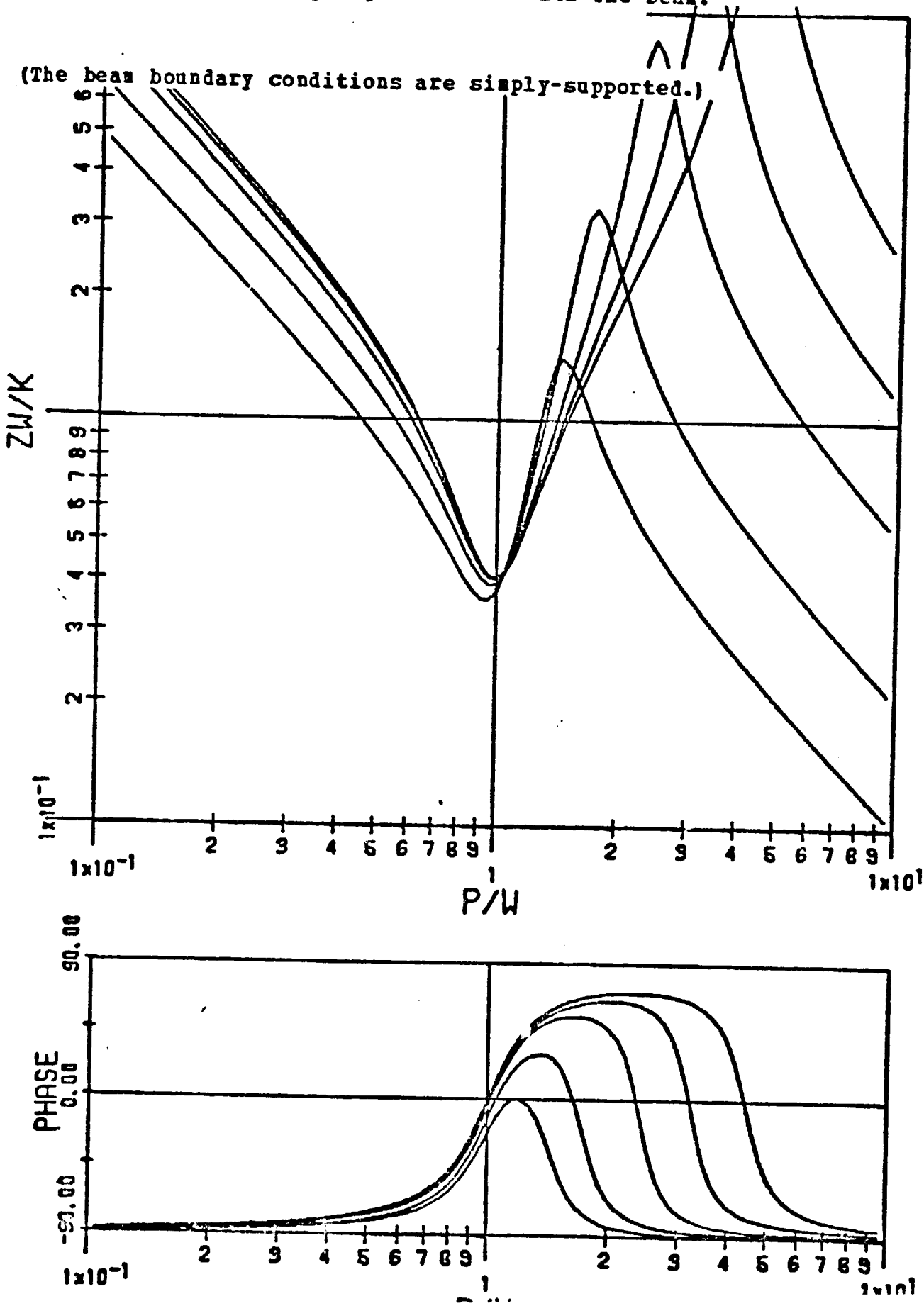

Figure 4.19. DPMI Plot Exhibiting the Dependance of the Beam Damping Ratio in the Presents of a Spring in Series With The Beam.

(The beam boundary conditions are simply-supported.)

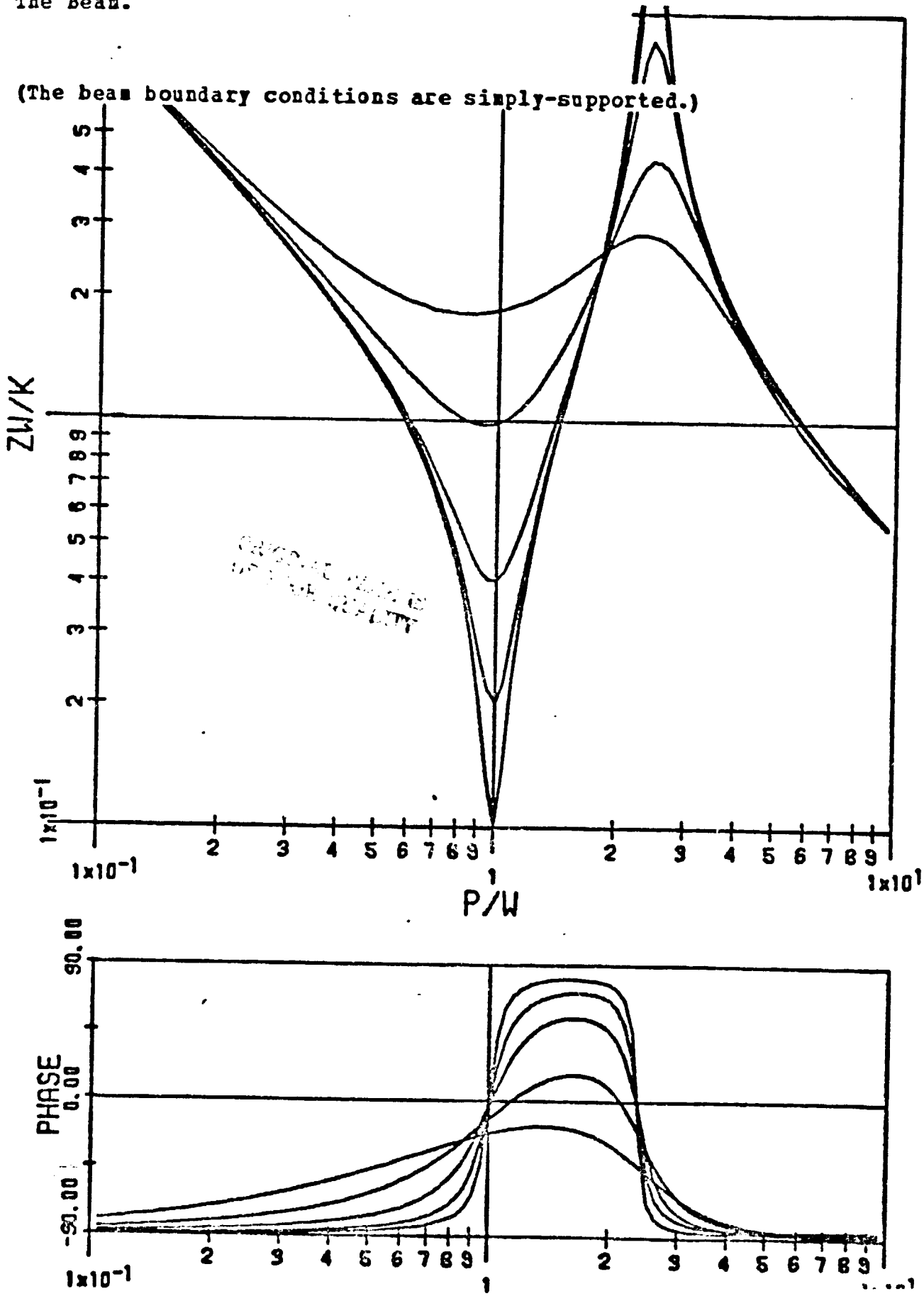

Figure 4.20. A Typical Set of DPMI Data, Indicating Certain Key Points.

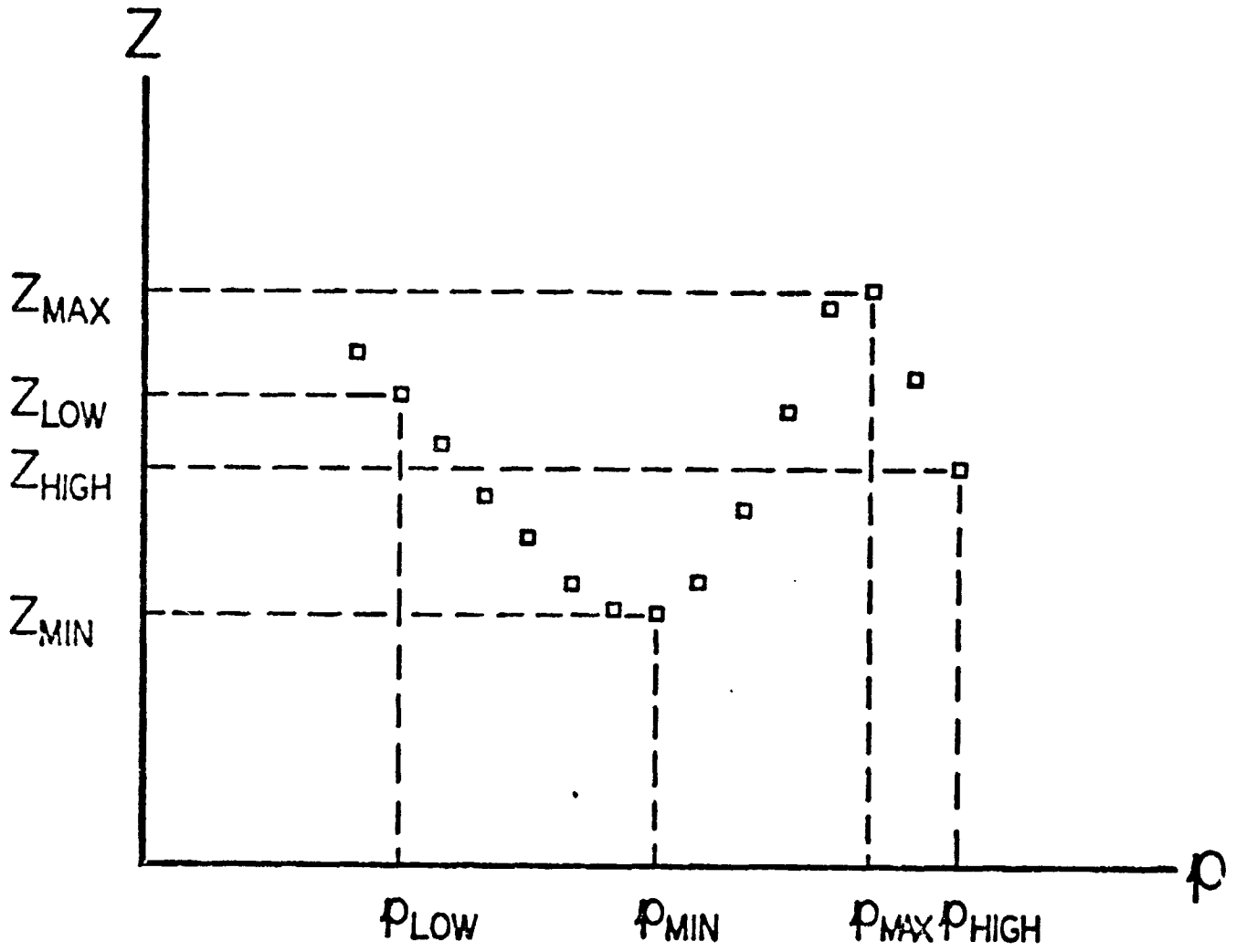

Figure 4.21. Single-degree-of-freedom Oscillator in Series with a Spring.

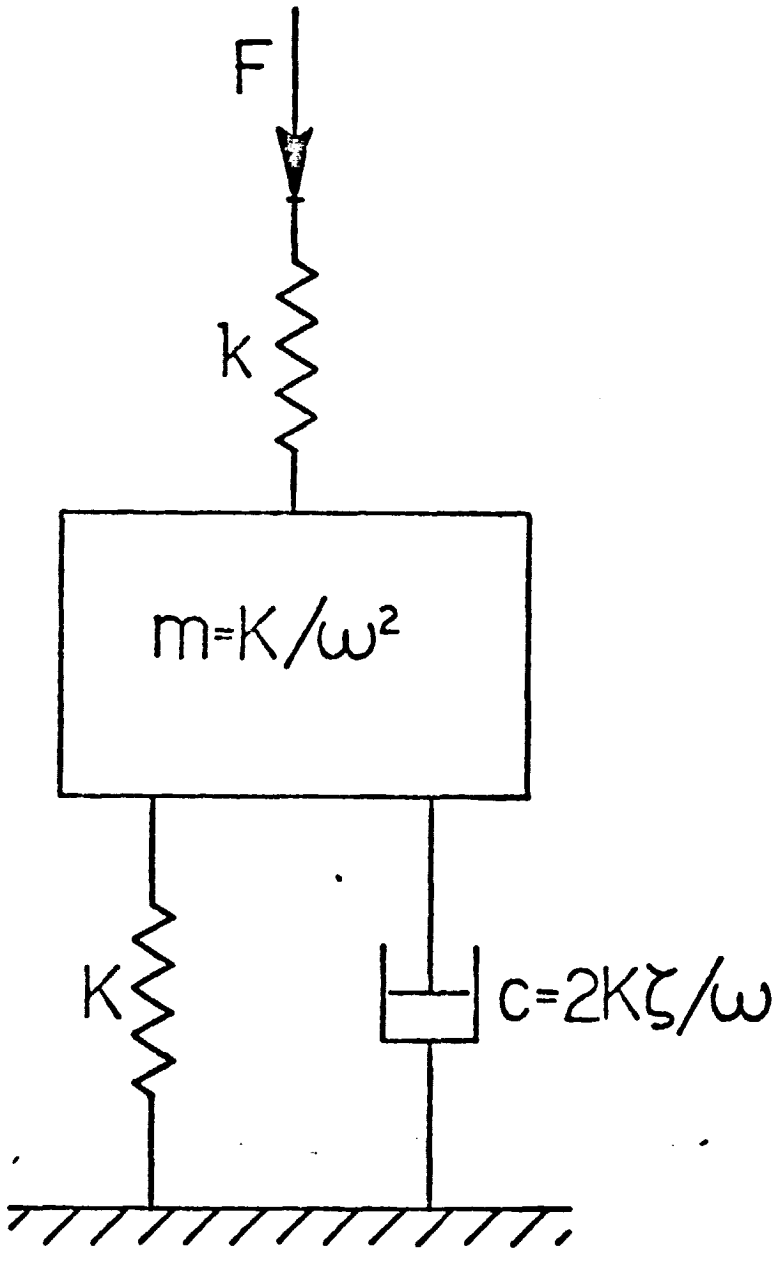

Figure 5.1. (a) Error, (b) Error Function.

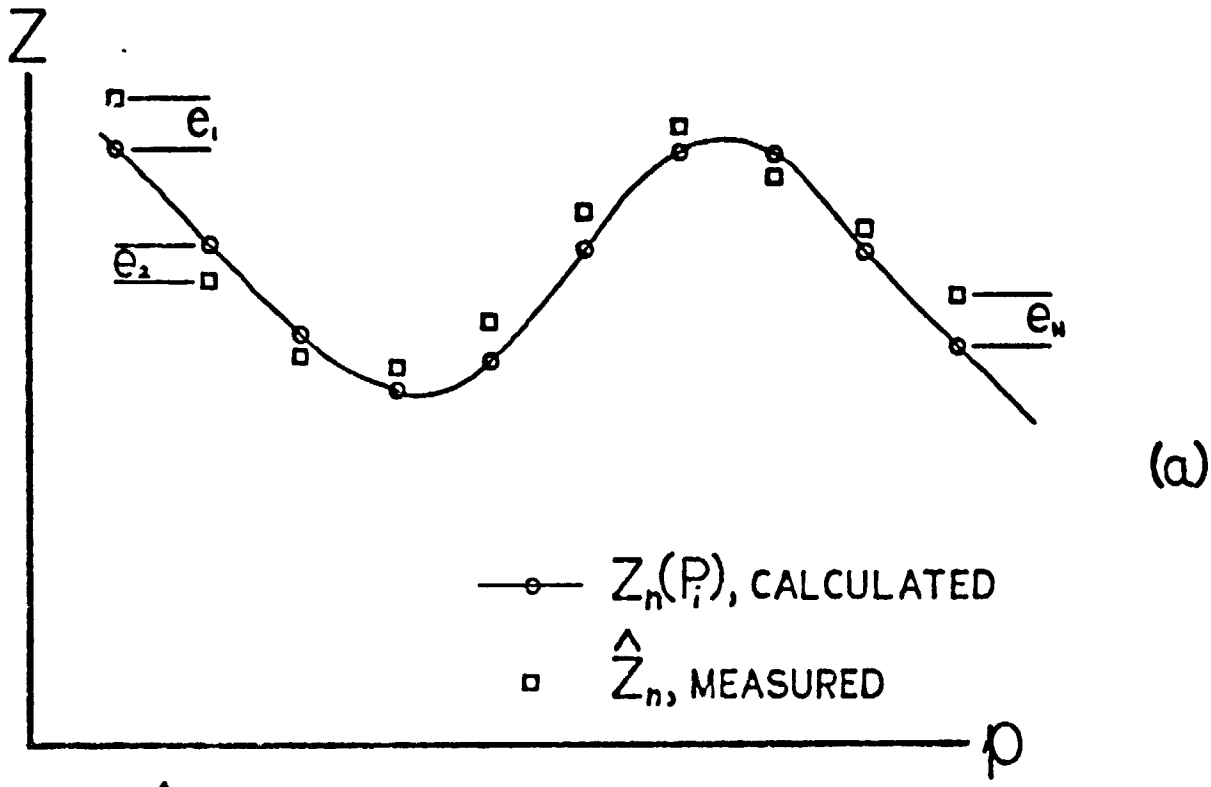

$$e_n = \hat{Z}_n - Z_n(P_i)$$

$$E = \sum_{n=1}^{N} (e_n / \hat{Z}_n)^2 / N$$

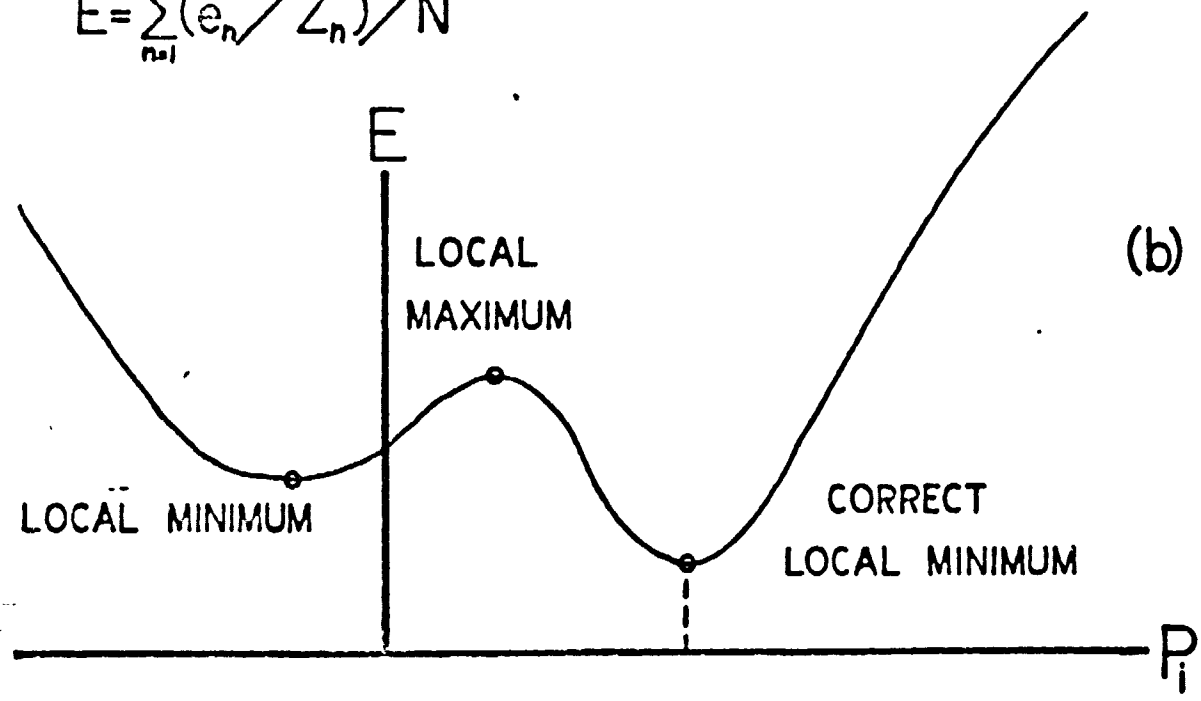

Figure 5.2. Flow Chart of the Computer Program.

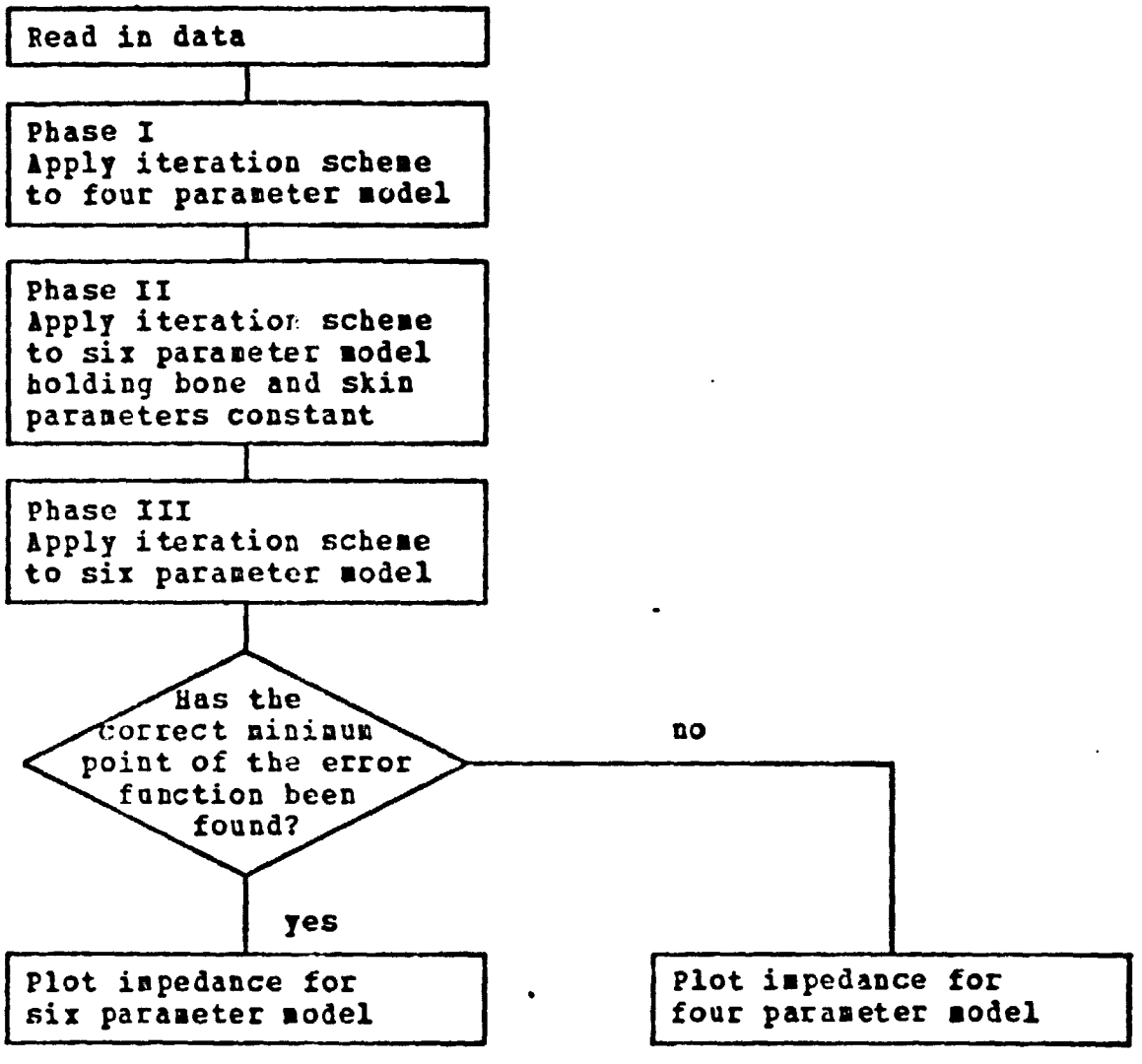

Figure 5.3. Flow Chart of One Phase of the Computer Program

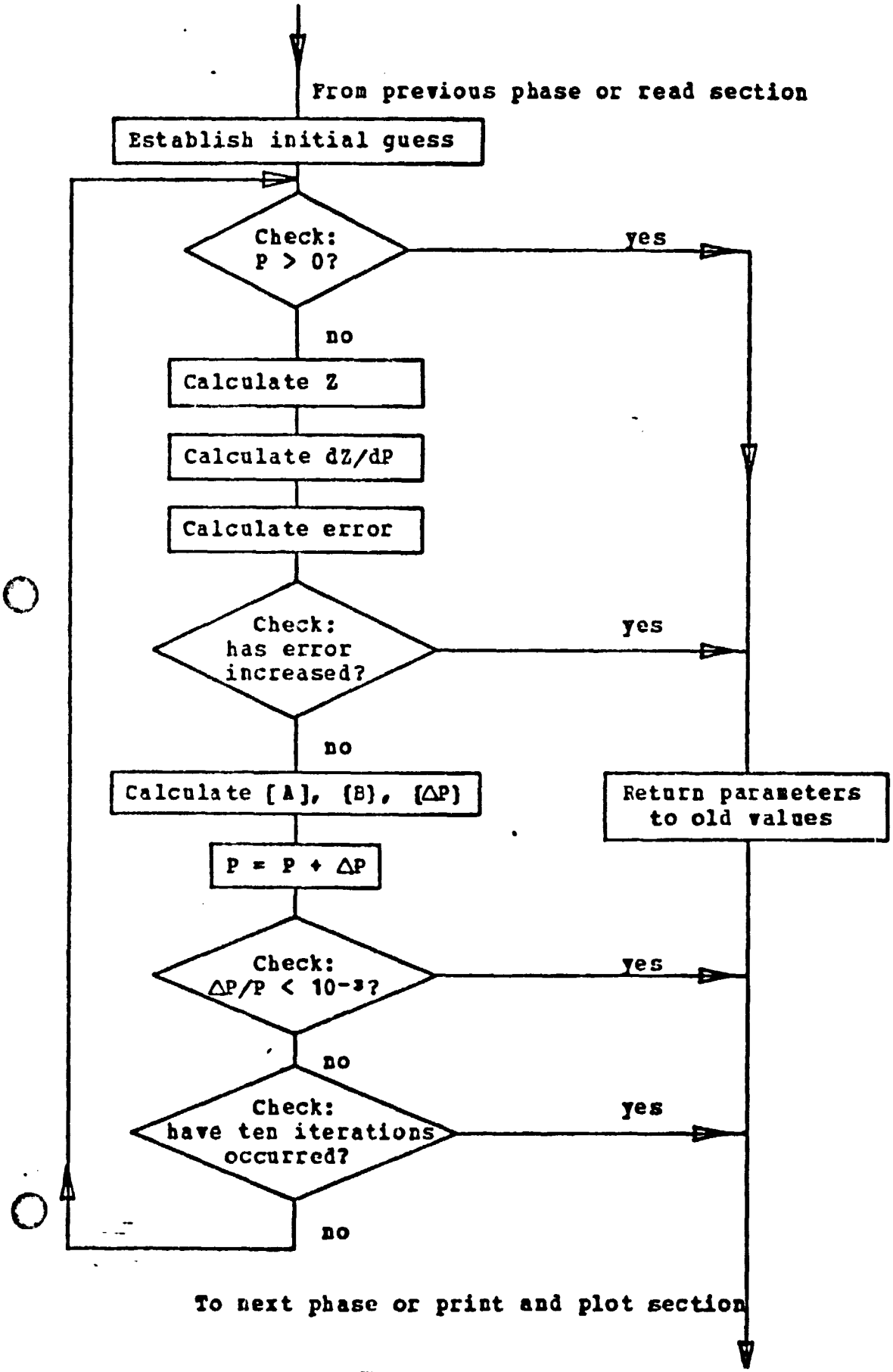

Figure 5.4. Sample Input To Computer Program.

```
$LIST -DATA
     1    SUBJECT TT 500 GM PRELOAD
     2       23.4       .6
     3   -1
     4   28
     5     65.  .250E+06 -92.
     6     70.  .220E+06 -86.
     7     80.  .175E+06 -86.
     8     90.  .145E+06 -82.
     9    100.  .130E+06 -79.
    10    110.  .121E+06 -77.
    11    120.  .107E+06 -75.
    12    130.  .969E+05 -73.
    13    140.  .897E+05 -70.
    14    160.  .778E+05 -63.
    15    180.  .751E+05 -55.
    16    200.  .698E+05 -52.
    17    220.  .658E+05 -47.
    18    250.  .591E+05 -42.
    19    275.  .572E+05 -37.
    20    300.  .574E+05 -30.
    21    325.  .577E+05 -21.
    22    350.  .611E+05 -17.
    23    375.  .698E+05 -08.
    24    400.  .821E+05 -02.
    25    450.  .105E+06 -05.
    26    500.  .127E+06 -18.
    27    550.  .150E+06 -31.
    28    600.  .145E+06 -45.
    29    700.  .116E+06 -62.
    30    800.  .938E+05 -67.
    31    900.  .839E+05 -69.
    32   1000.  .819E+05 -70.
END OF FILE
```

Figure 5.5. Sample Output From Computer Program.

SUBJECT TT 500 GM PRELOAD

BONE LENGTH	PROBE LOCATION
23.4	0.6

BONE STIFFNESS	BONE NAT FREQ	BONE DAMPING	SKIN STIFFNESS
0.31692E+11	400.7	0.0500	0.38004E+09

TISSUE MASS/LENGTH	TISSUE NAT FREQ	TISSUE DAMPING
11.61	152.2	0.3785

		EXPERIMENTAL		THEORETICAL	
	FREQ	IMPEDANCE	PHASE ANGLE	IMPEDANCE	PHASE ANGLE
1	65.00	0.2500E+06	-92.00	0.2372E+06	-87.80
2	70.00	0.2200E+06	-86.00	0.2176E+06	-87.53
3	80.00	0.1750E+06	-86.00	0.1851E+06	-86.83
4	90.00	0.1450E+06	-82.00	0.1589E+06	-85.83
5	100.00	0.1300E+06	-79.00	0.1372E+06	-84.32
6	110.00	0.1210E+06	-77.00	0.1191E+06	-82.00
7	120.00	0.1070E+06	-75.00	0.1044E+06	-78.58
8	130.00	0.9690E+05	-73.00	0.9345E+05	-74.04
9	140.00	0.8970E+05	-70.00	0.8628E+05	-68.94
10	160.00	0.7780E+05	-63.00	0.7962E+05	-60.71
11	180.00	0.7510E+05	-55.00	0.7503E+05	-56.20
12	200.00	0.6980E+05	-52.00	0.6934E+05	-52.61
13	220.00	0.6580E+05	-47.00	0.6361E+05	-48.18
14	250.00	0.5910E+05	-42.00	0.5720E+05	-39.20
15	275.00	0.5720E+05	-37.00	0.5490E+05	-30.22
16	300.00	0.5740E+05	-30.00	0.5563E+05	-21.21
17	325.00	0.5770E+05	-21.00	0.5916E+05	-13.44
18	350.00	0.6110E+05	-17.00	0.6505E+05	-7.65
19	375.00	0.6980E+05	-8.00	0.7283E+05	-4.02
20	400.00	0.8210E+05	-2.00	0.8209E+05	-2.40
21	450.00	0.1050E+06	-5.00	0.1035E+06	-4.43
22	500.00	0.1270E+06	-18.00	0.1251E+06	-12.22
23	550.00	0.1500E+06	-31.00	0.1399E+06	-23.86
24	600.00	0.1450E+06	-45.00	0.1429E+06	-36.53
25	700.00	0.1160E+06	-62.00	0.1238E+06	-56.25
26	800.00	0.9380E+05	-67.00	0.1005E+06	-66.87
27	900.00	0.8390E+05	-69.00	0.8319E+05	-72.15
28	1000.00	0.8190E+05	-70.00	0.7125E+05	-74.74

THE ERROR FUNCTION FOR THIS SET OF PARAMETERS IS 0.00234246.

Figure 5.6. Sample Plot From Computer Program.

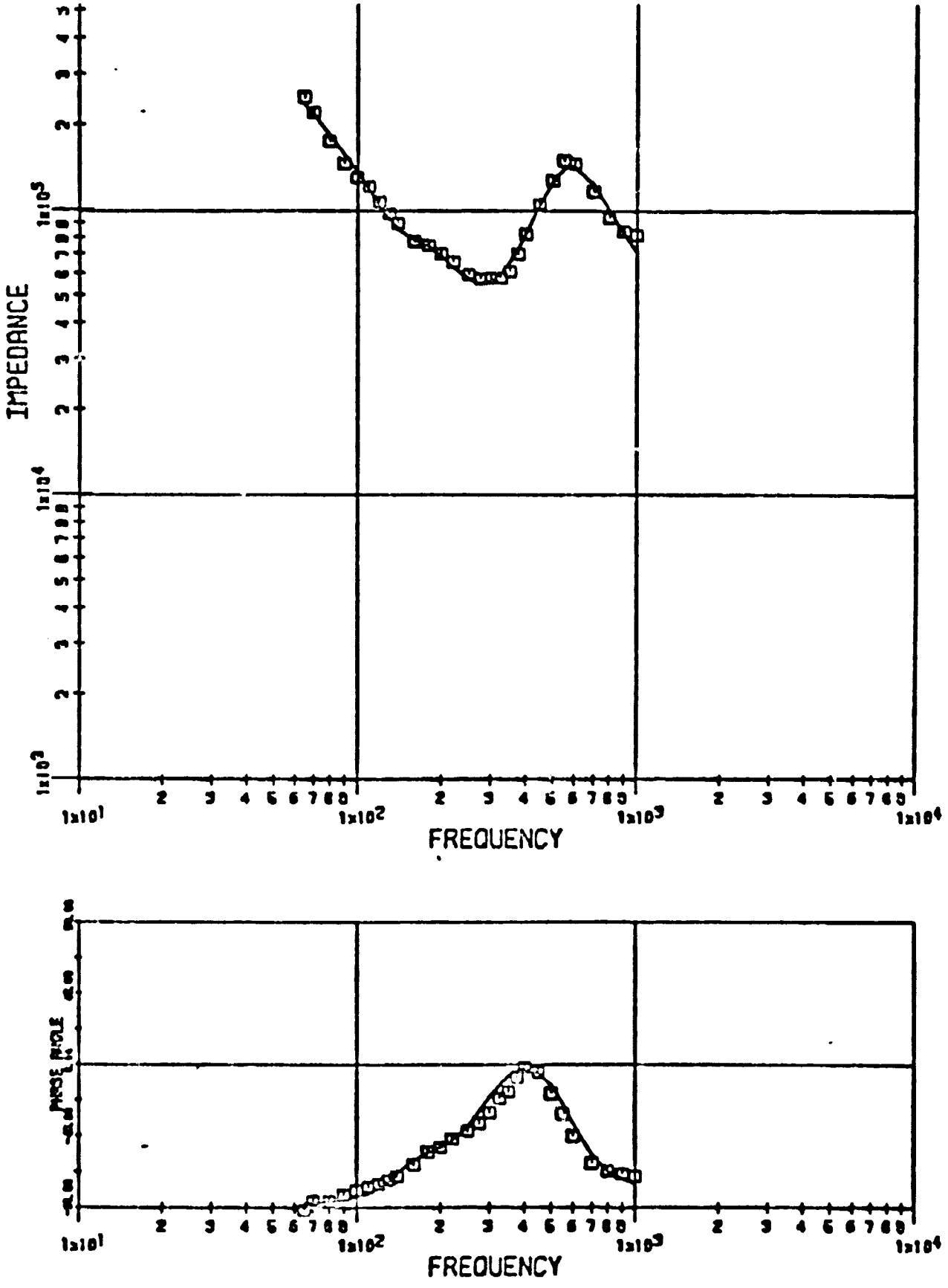

Figure 6.1. Monkey Arm in Test Fixture.

(a) Intact arm, (b) Probe on ulna, (c) Musculature removed, (d) Excised ulna.

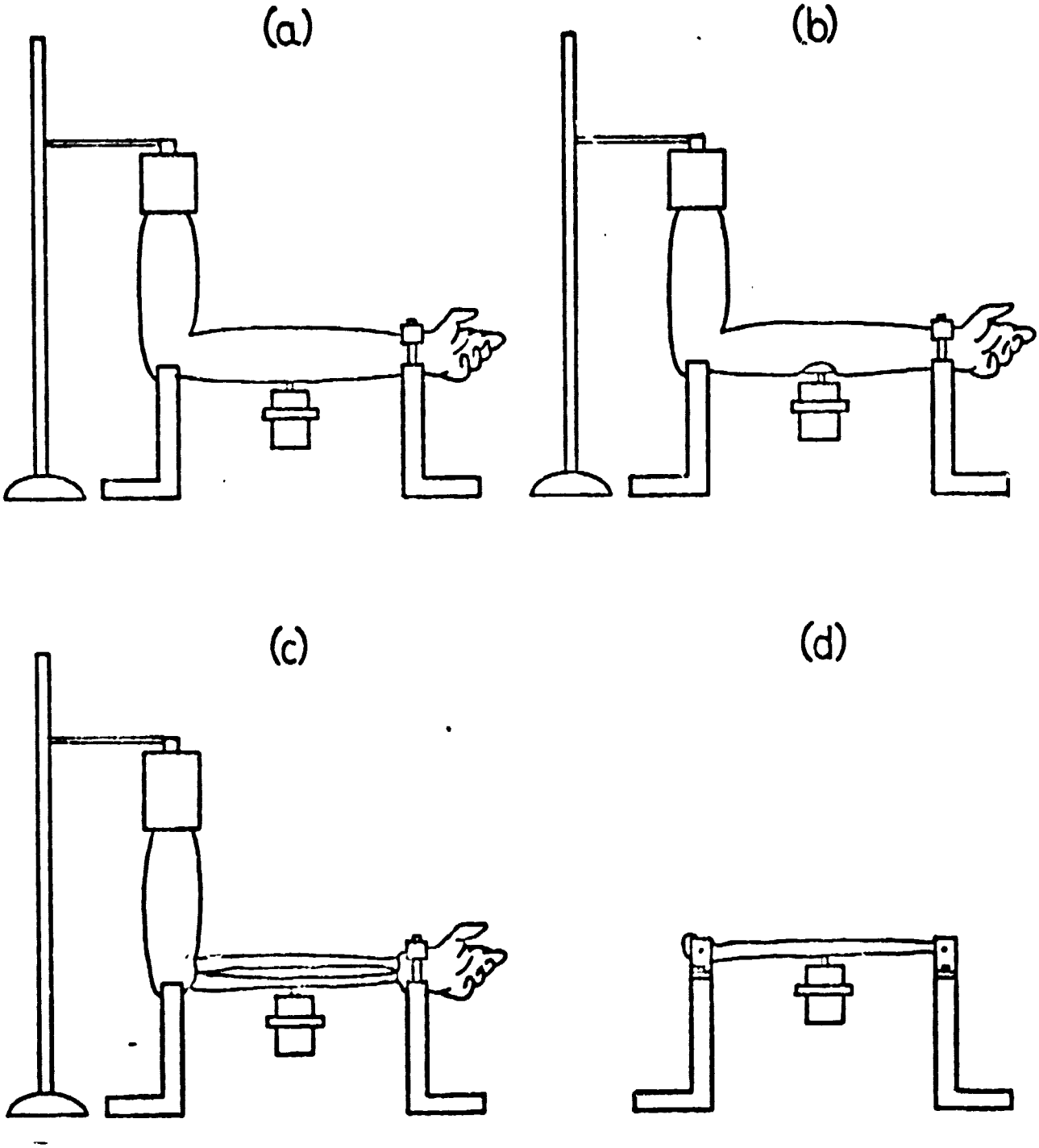

Figure 6.2. DPHI of Monkey 663: Excised Ulna.

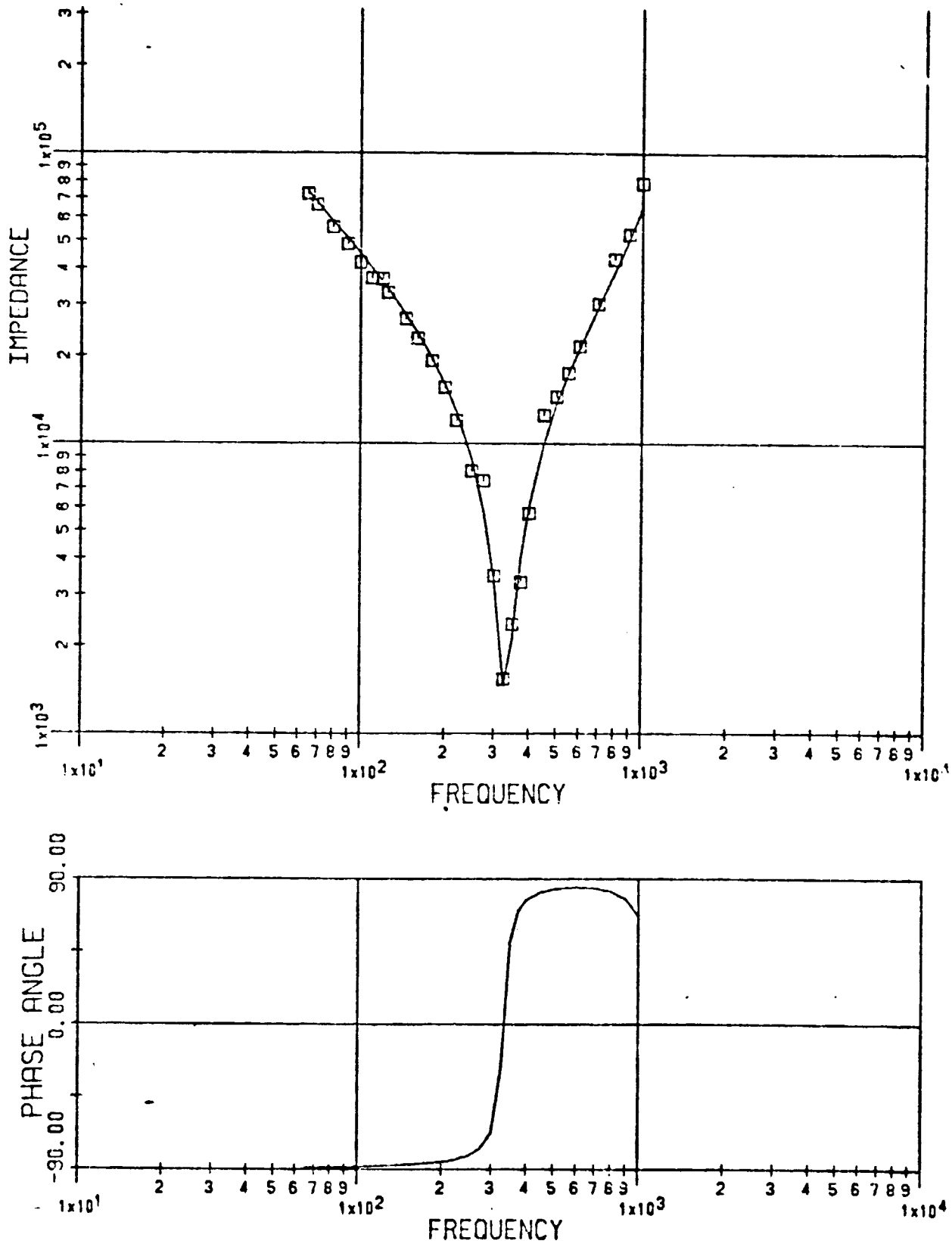

Figure 6.3. DPMI of Monkey 663: Musculature Removed.

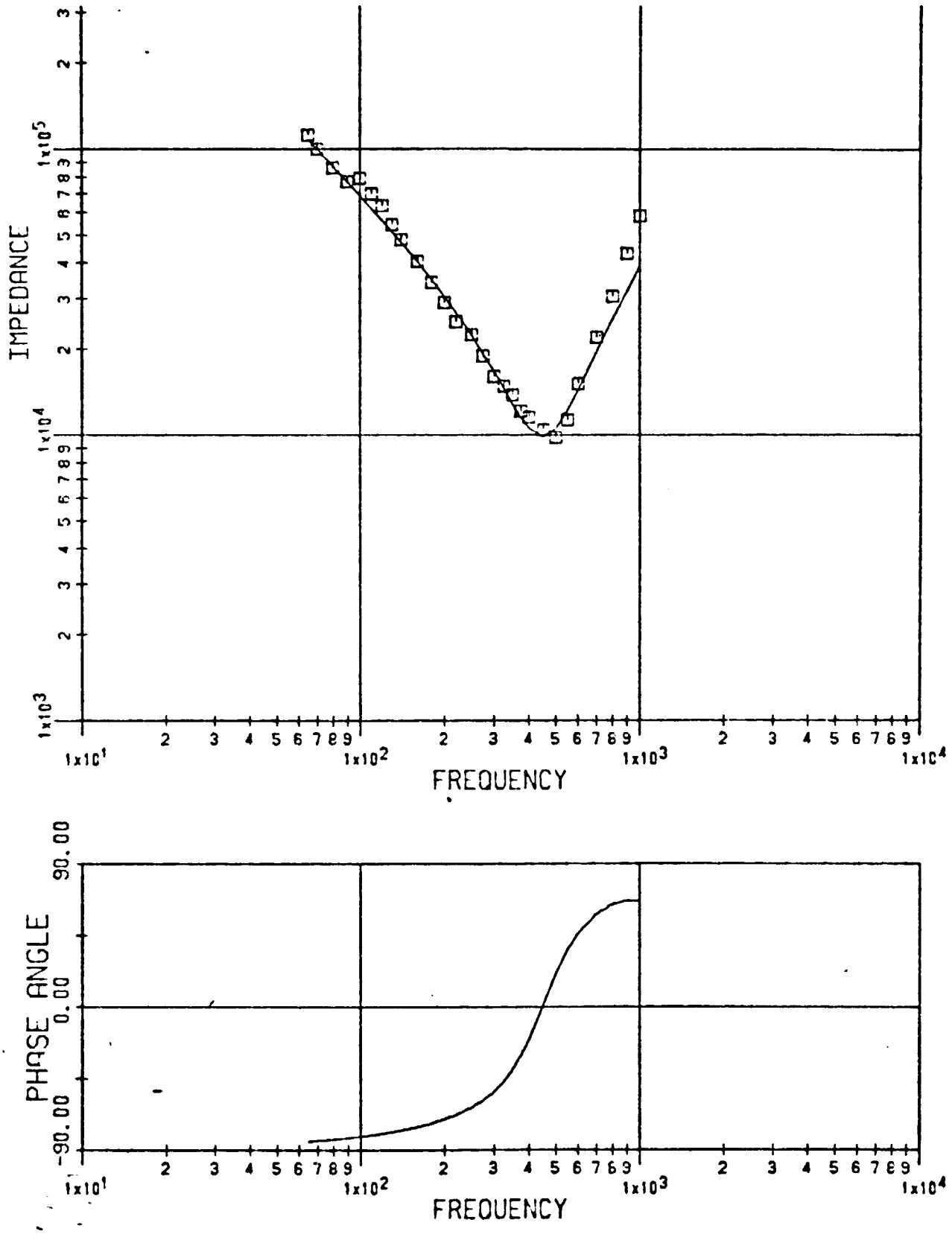

Figure 6.4. DPHI of Monkey 663: Probe on Ulna.

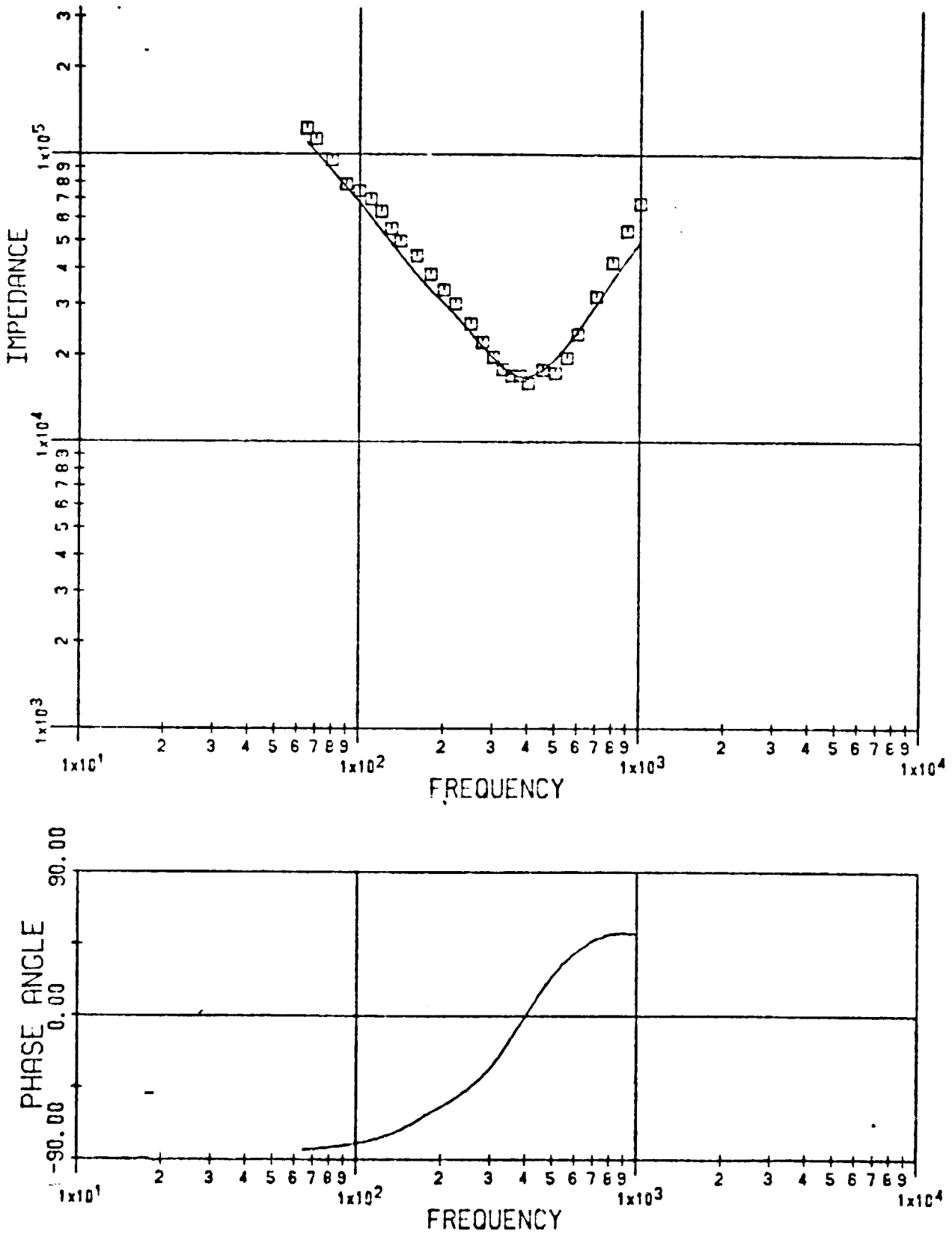

Figure 6.5. DPMI of Monkey 663: Intact Arm.

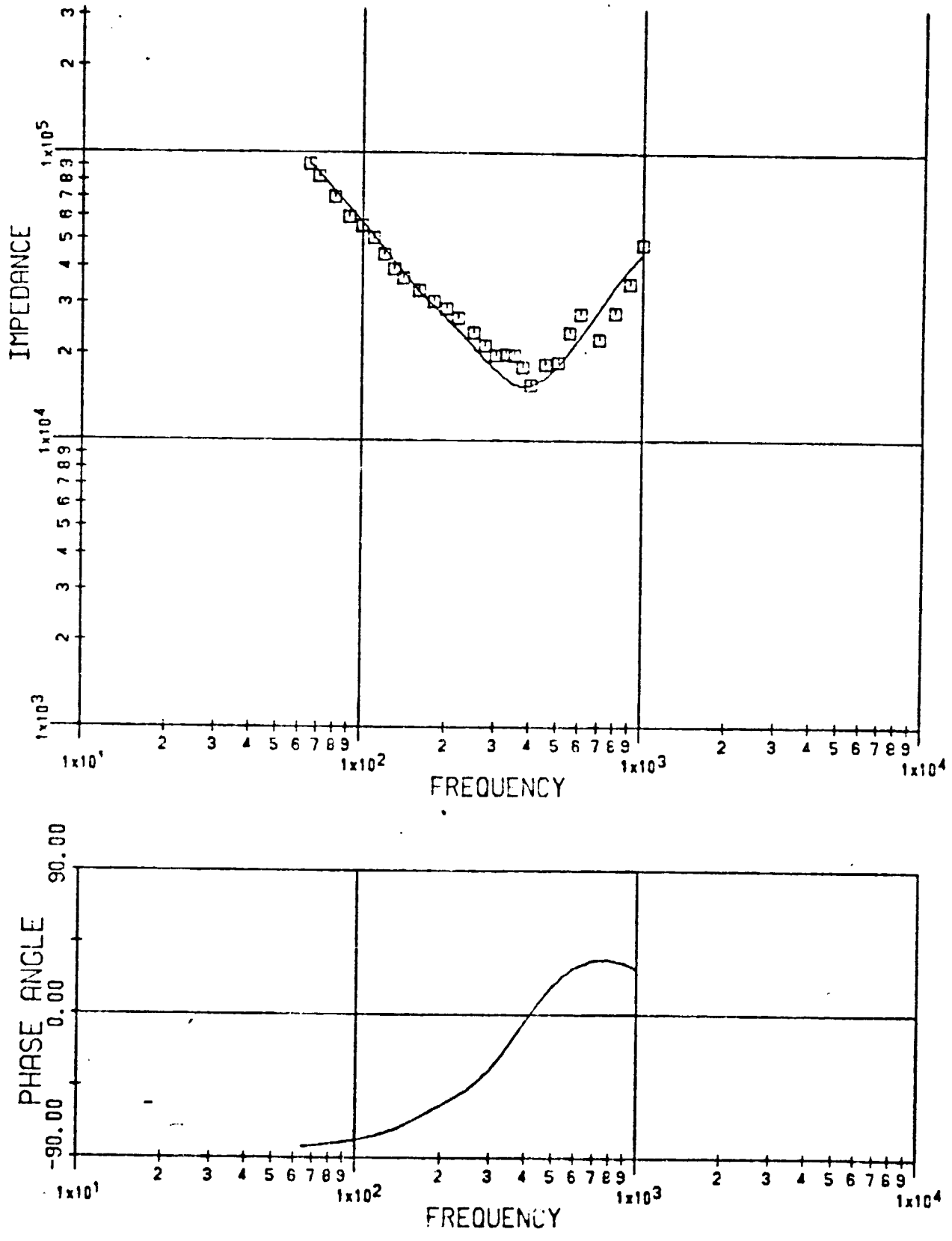

Figure 6.6. Misalignment Between Humerus and Support at the Elbow.

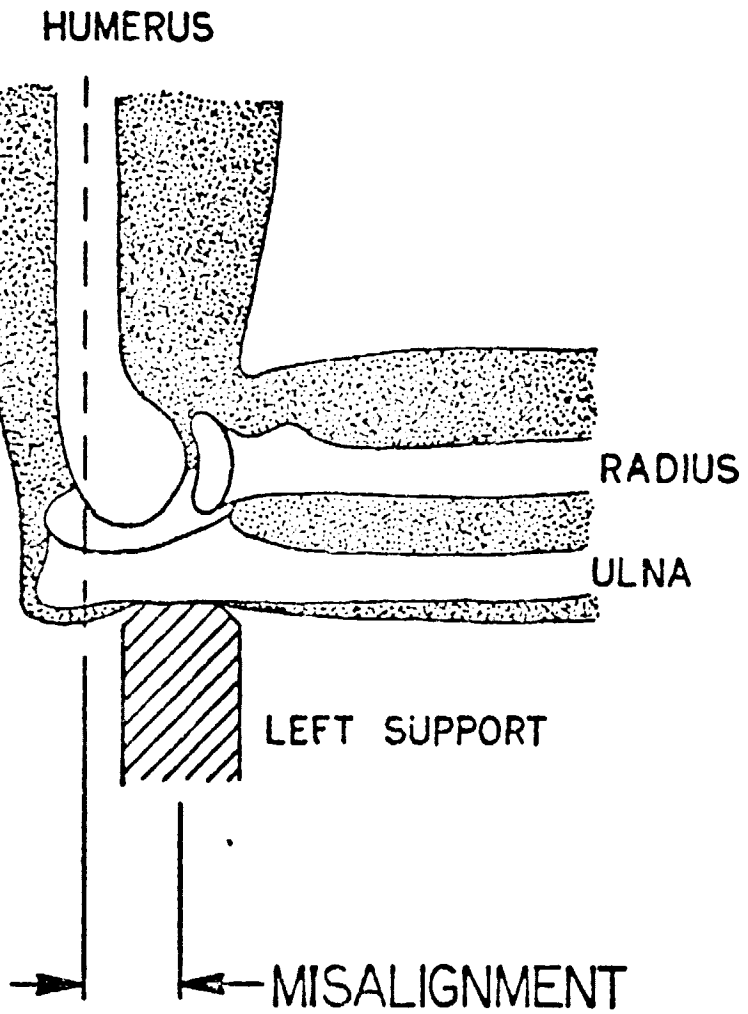

Figure 6.7. DPSI of Monkey 665: Excised Ulna.

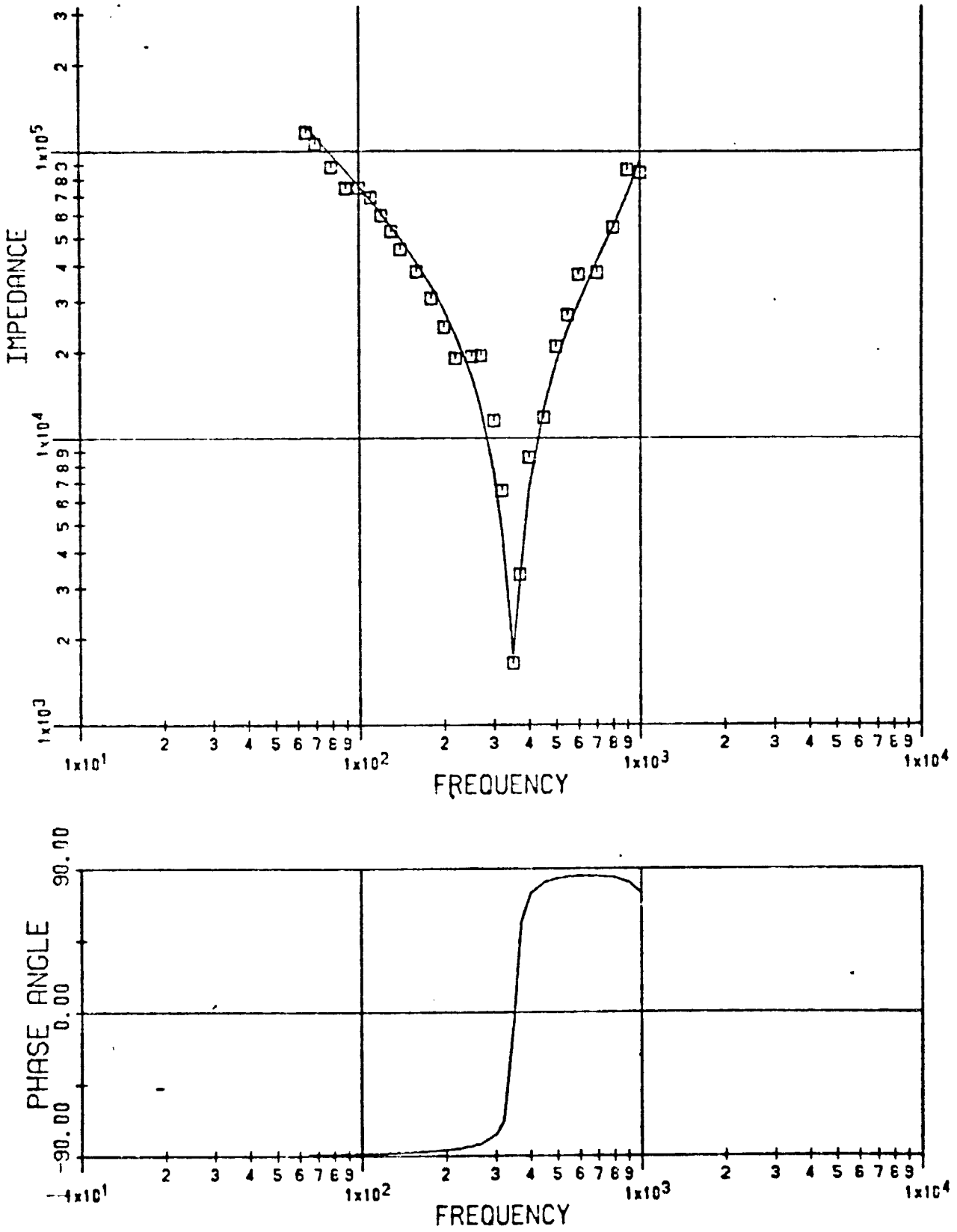

Figure 6.8. DPMI of Monkey 665: Musculature Removed.

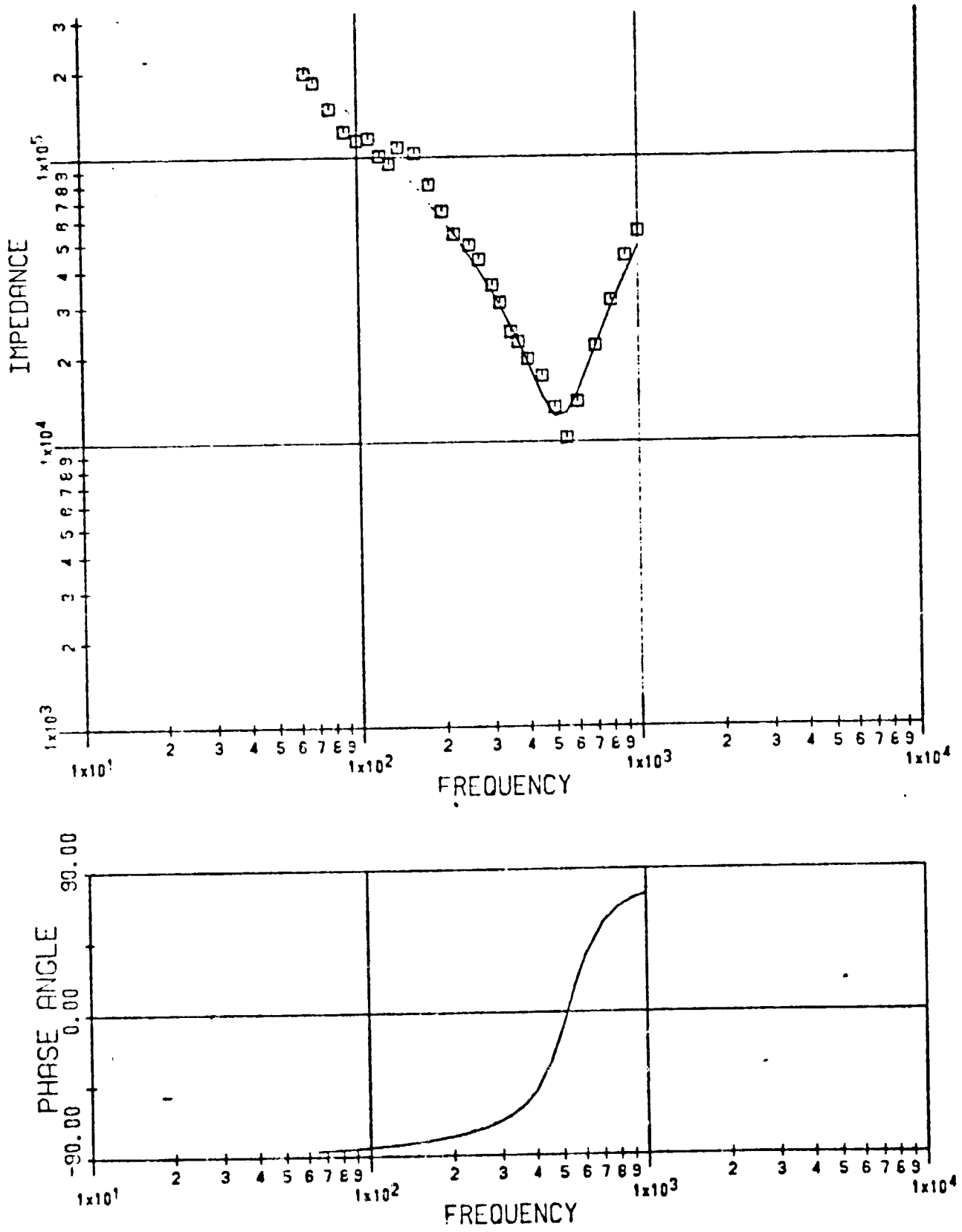

MONK 665 MUSCULATURE REMOVED

Figure 6.9. DPMI of Monkey 665: Probe on Ulna.

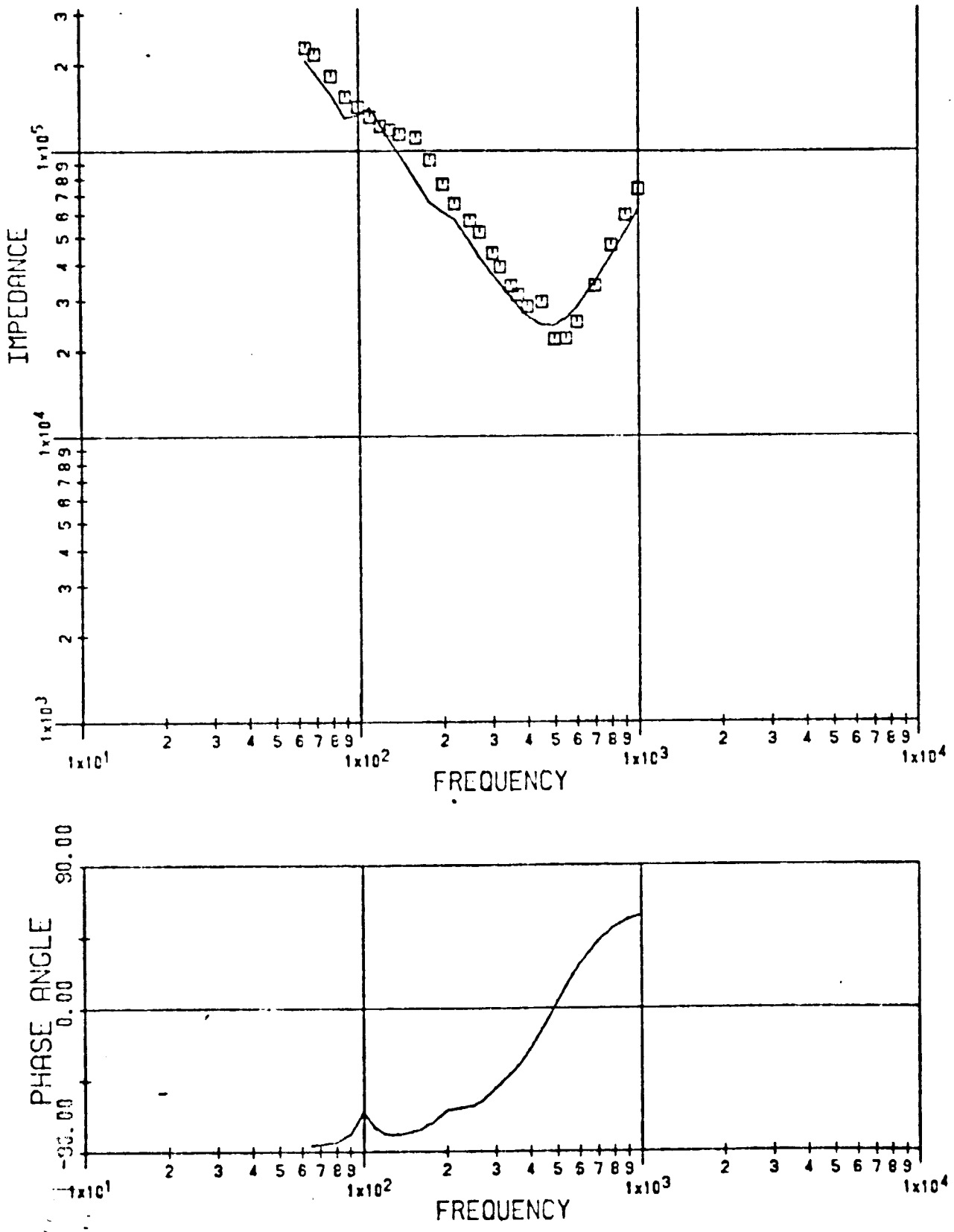

Figure 6.10. DPMI of Monkey 665: Intact Arm.

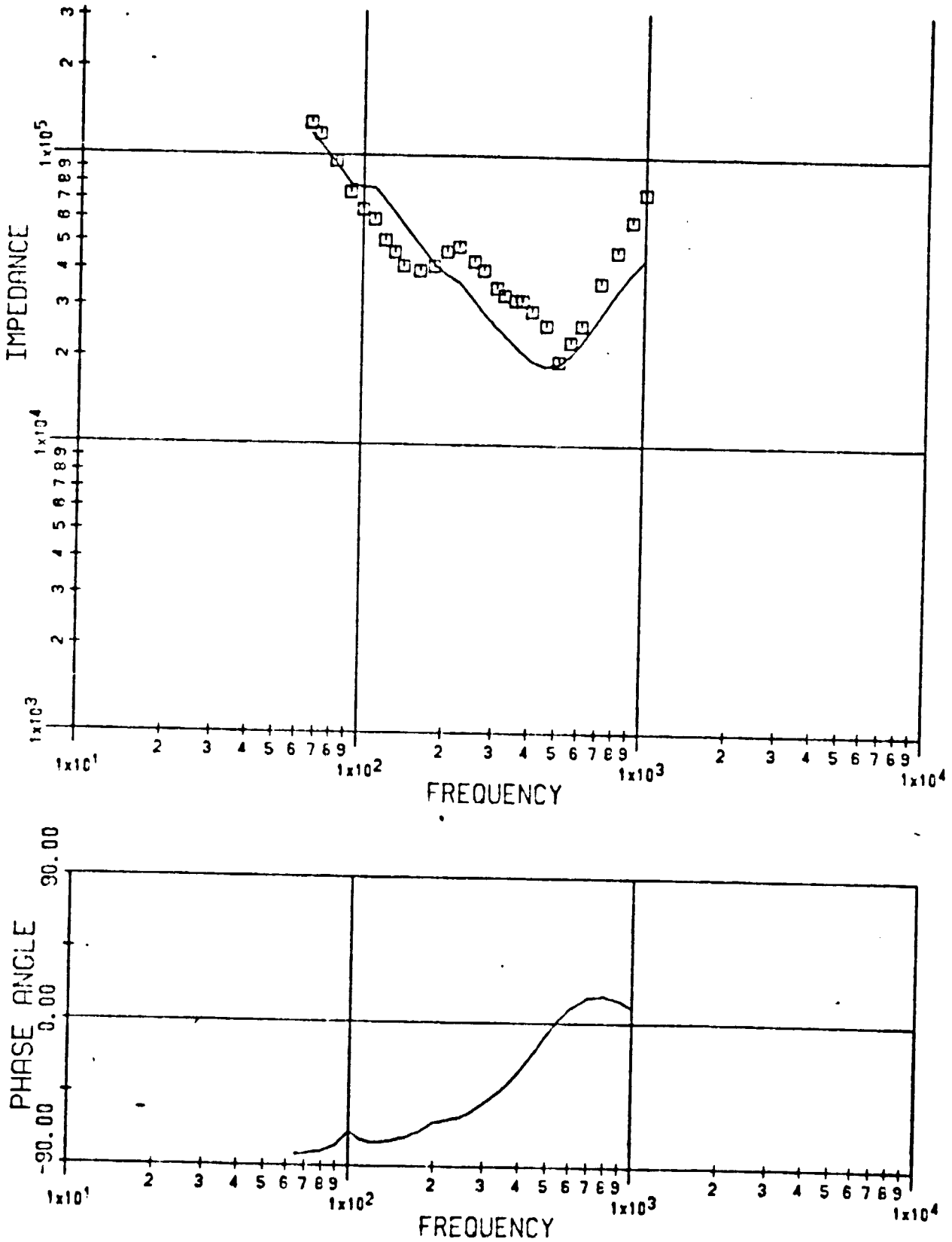

Figure 6.11. DPMI of Monkey 659: Excised Ulna.

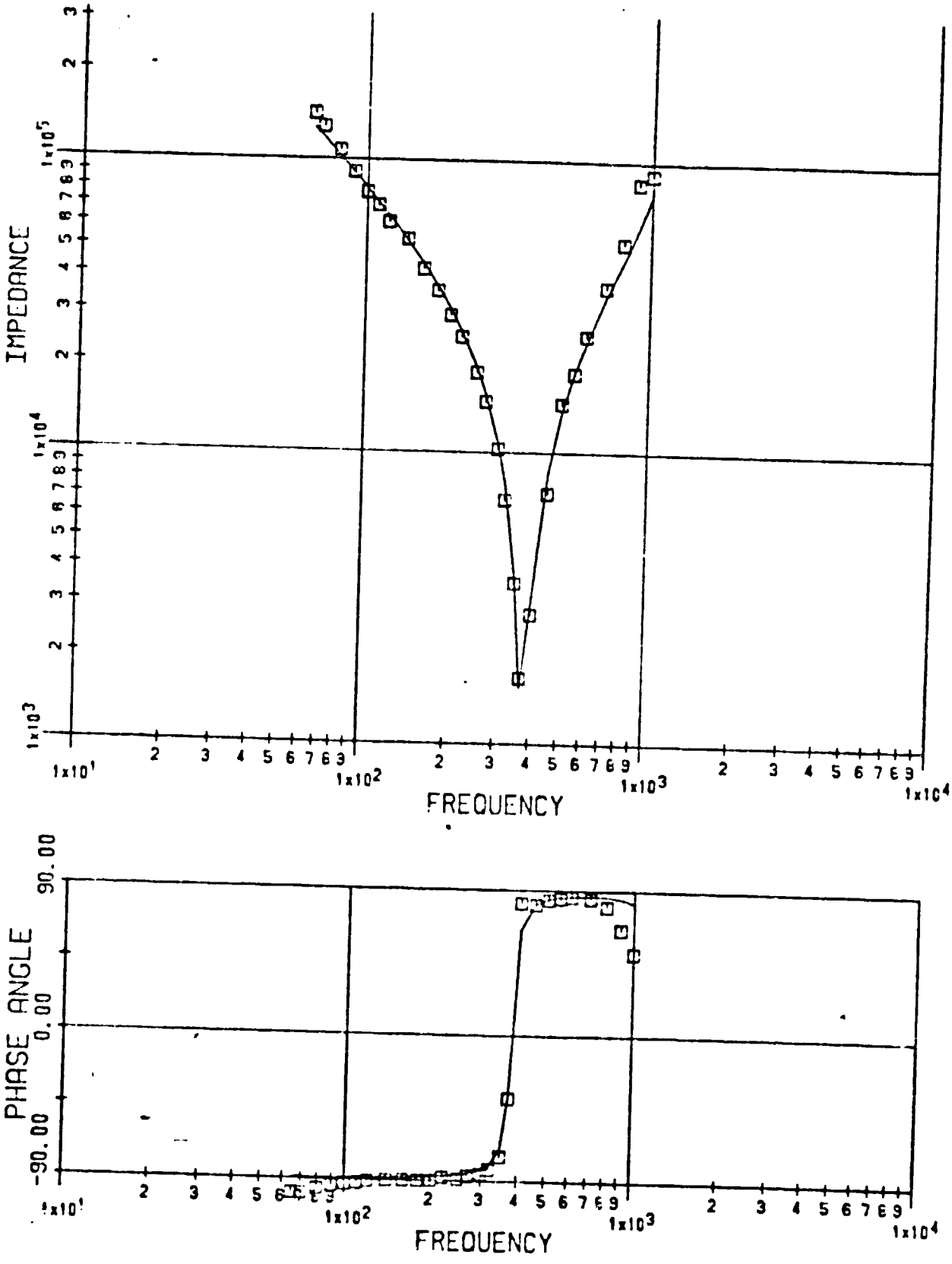

Figure 6.12. DPMI of Monkey 659: Musculature Removed.

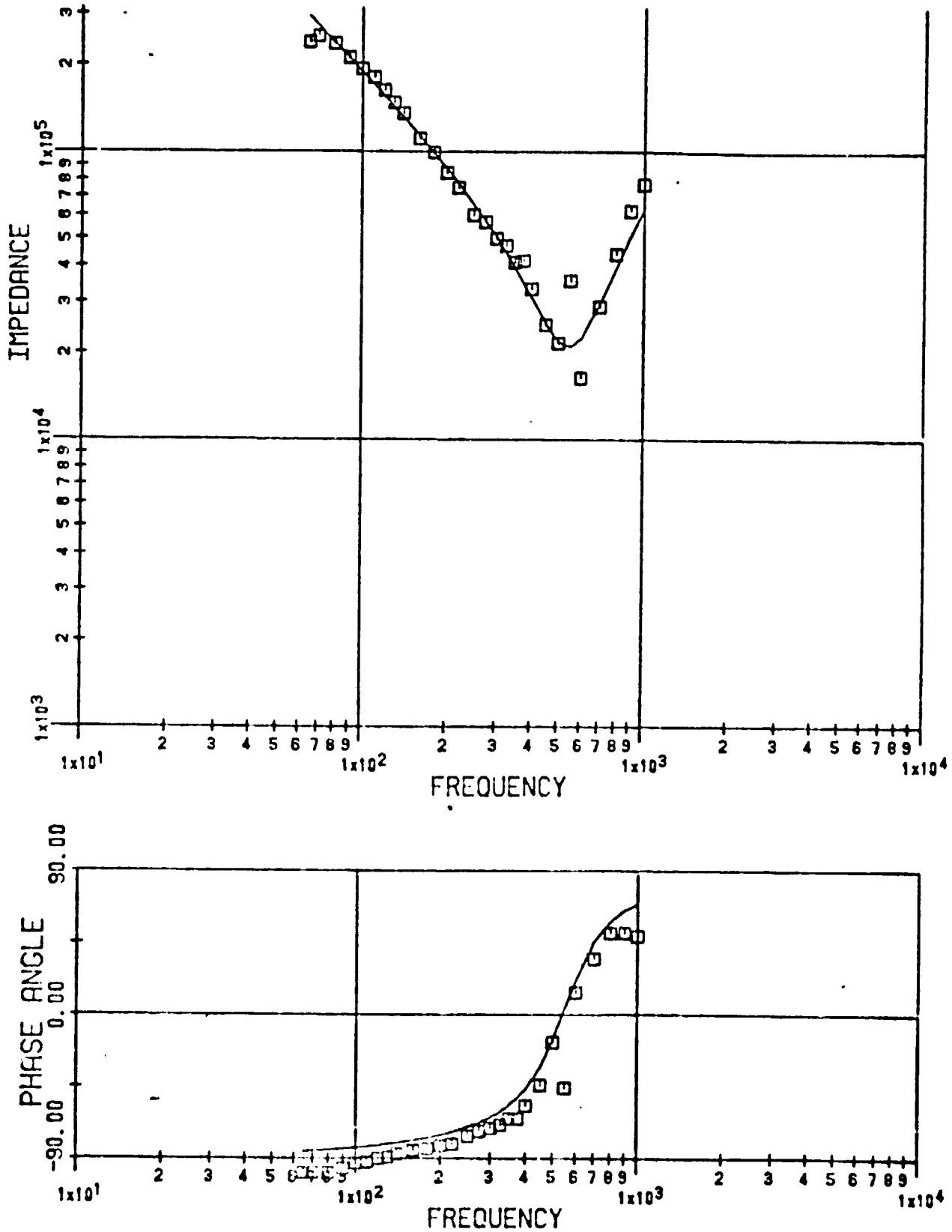

MONK 659 MUSCULATURE REMOVED

Figure 6.13. DPSI of Monkey 659: Probe on Ulna.

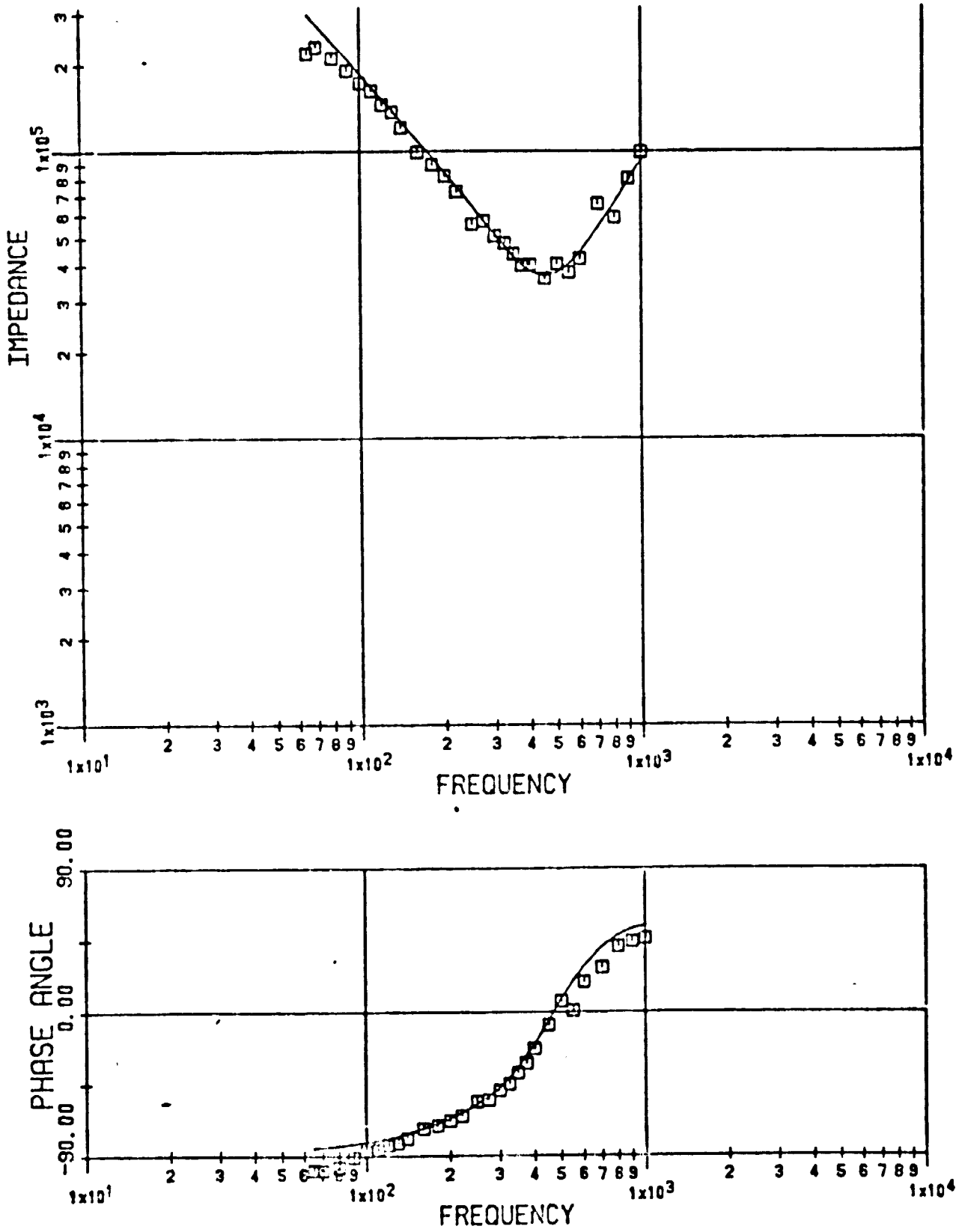

Figure 6.14. DPHI of Monkey 659: Intact Arm, 400 gm Preload

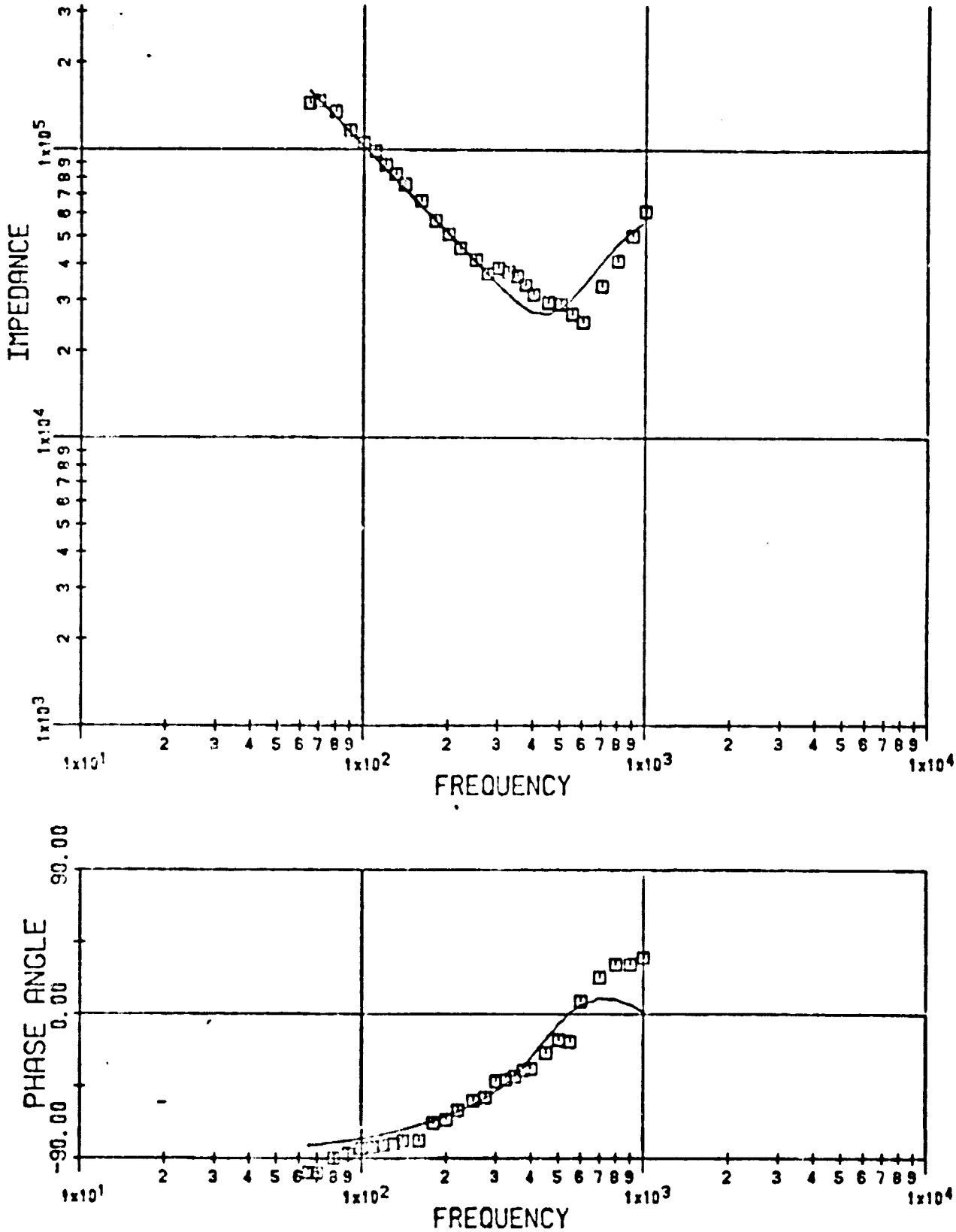

Figure 5.15. DPNI of Monkey 659: Intact Arm, 600 gm Preload

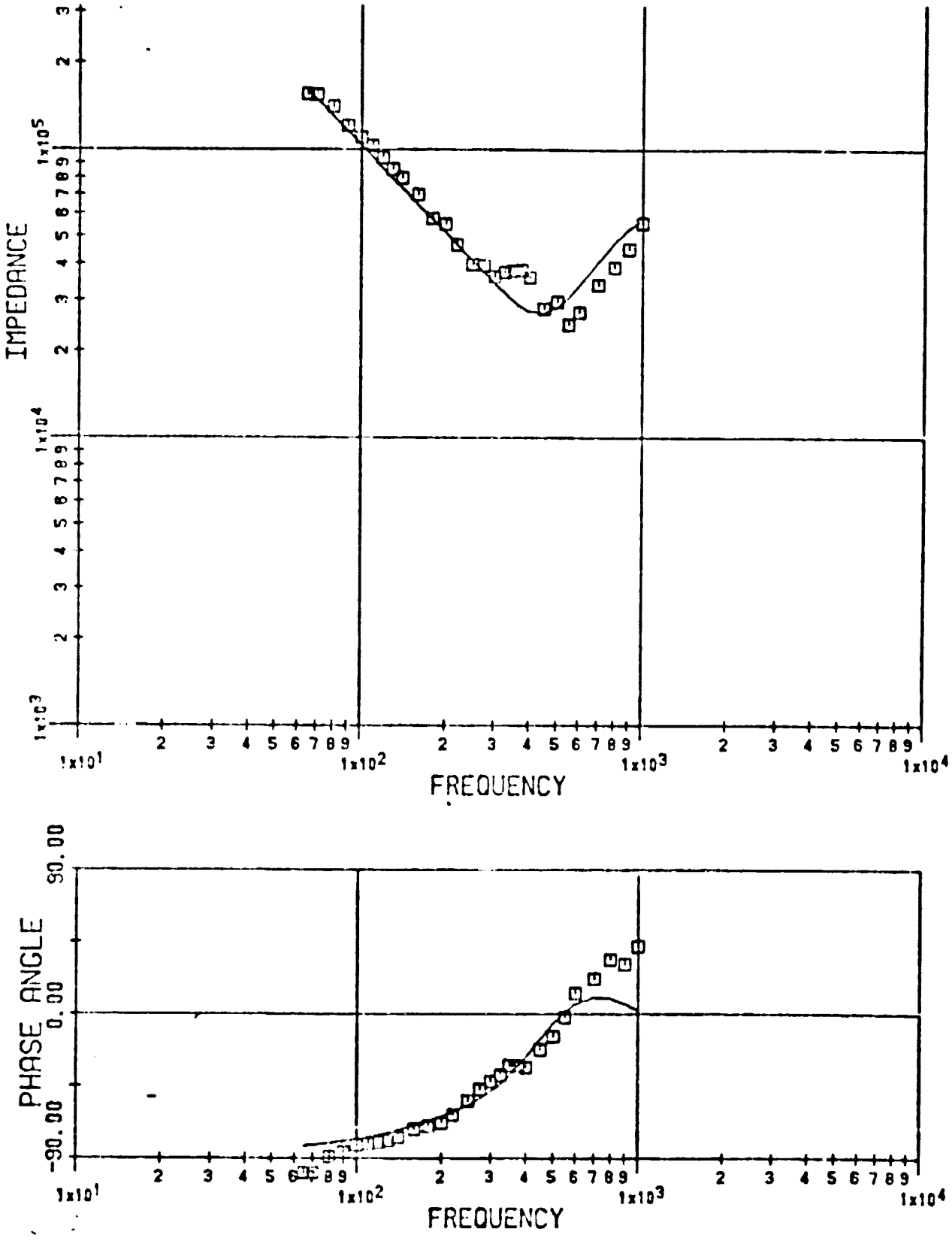

MONK 659 INTACT ARM 600 GM PRELOAD

Figure 6.16. Bending Fixture Used For Three-point Bending Test on the Ulna of Monkey 659.

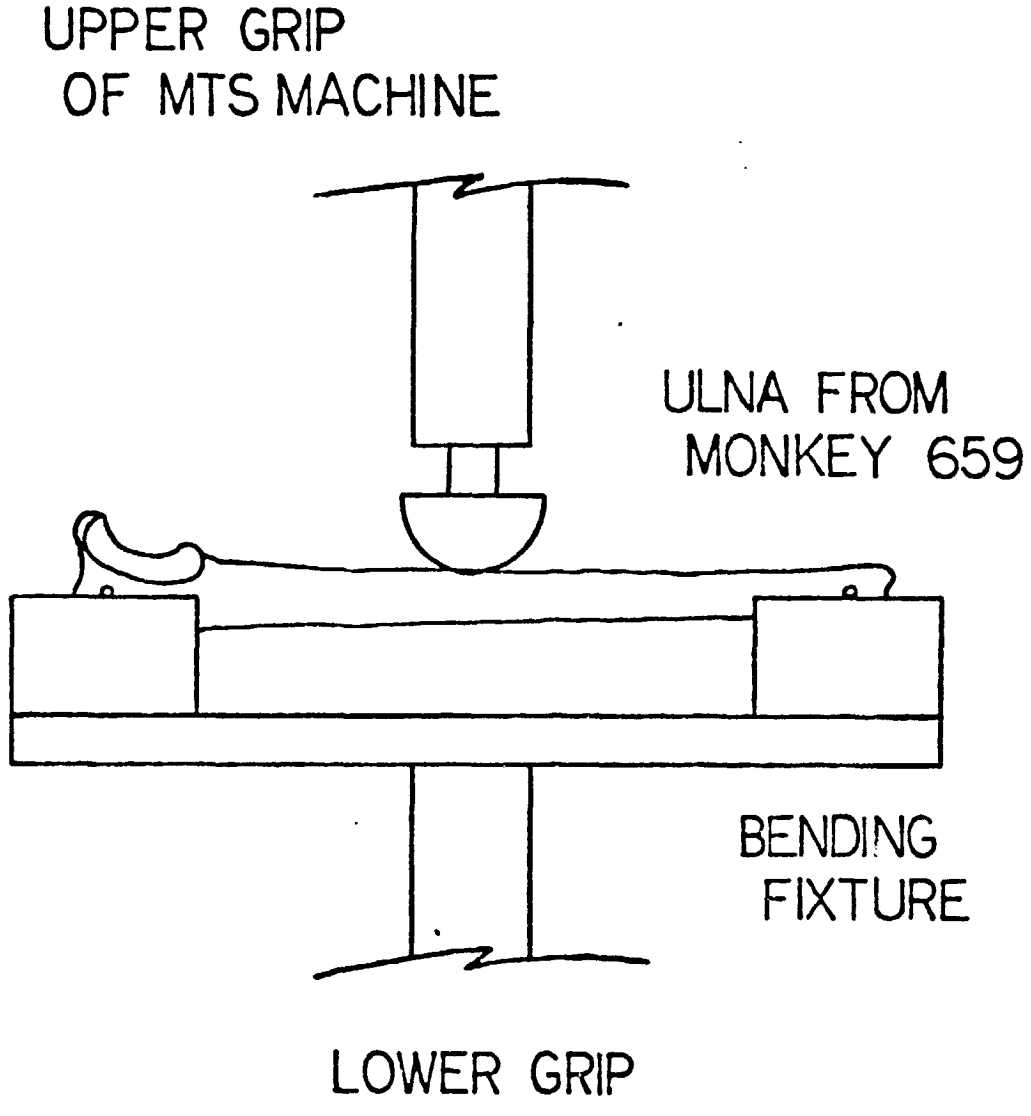

Figure 6.17. Load-deflection Curve From Three-point Bending Test on the Ulna of Monkey 659.

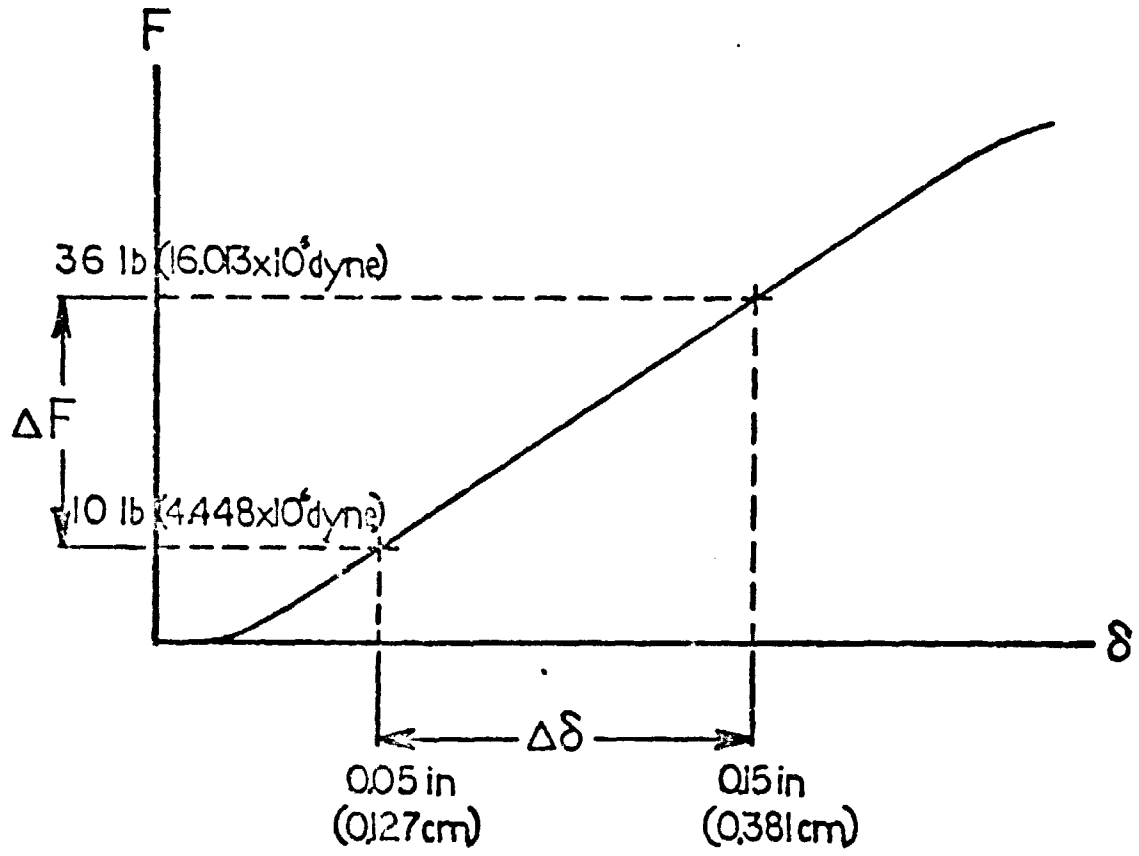

Figure 6.18. DPMI of the Calibration Mass.

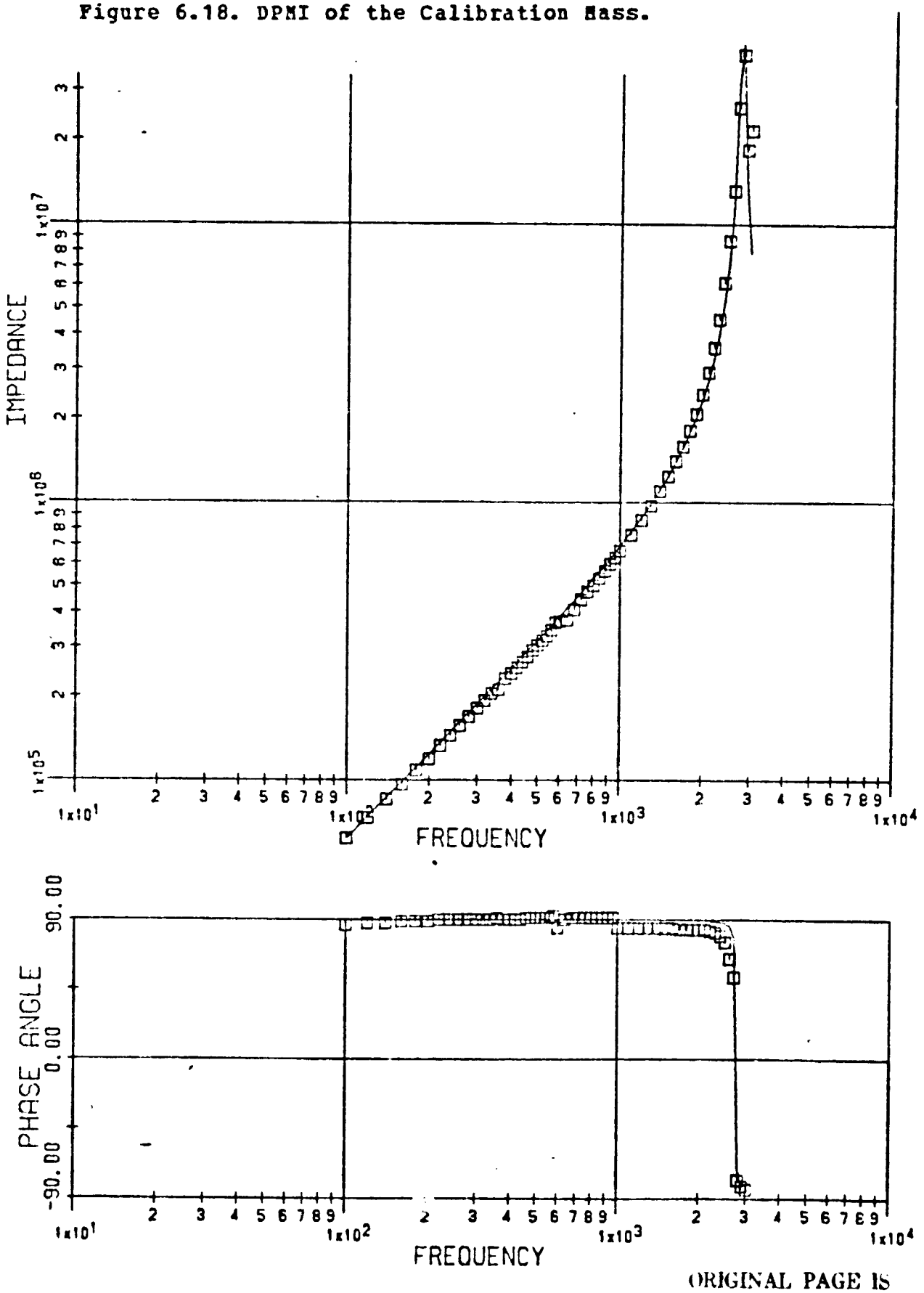

CALIBRATION MASS

Figure 6.19. Dimensions of the Aluminum Beam and its Support Brackets.

Dimensions are given in inches with mm in parentheses.

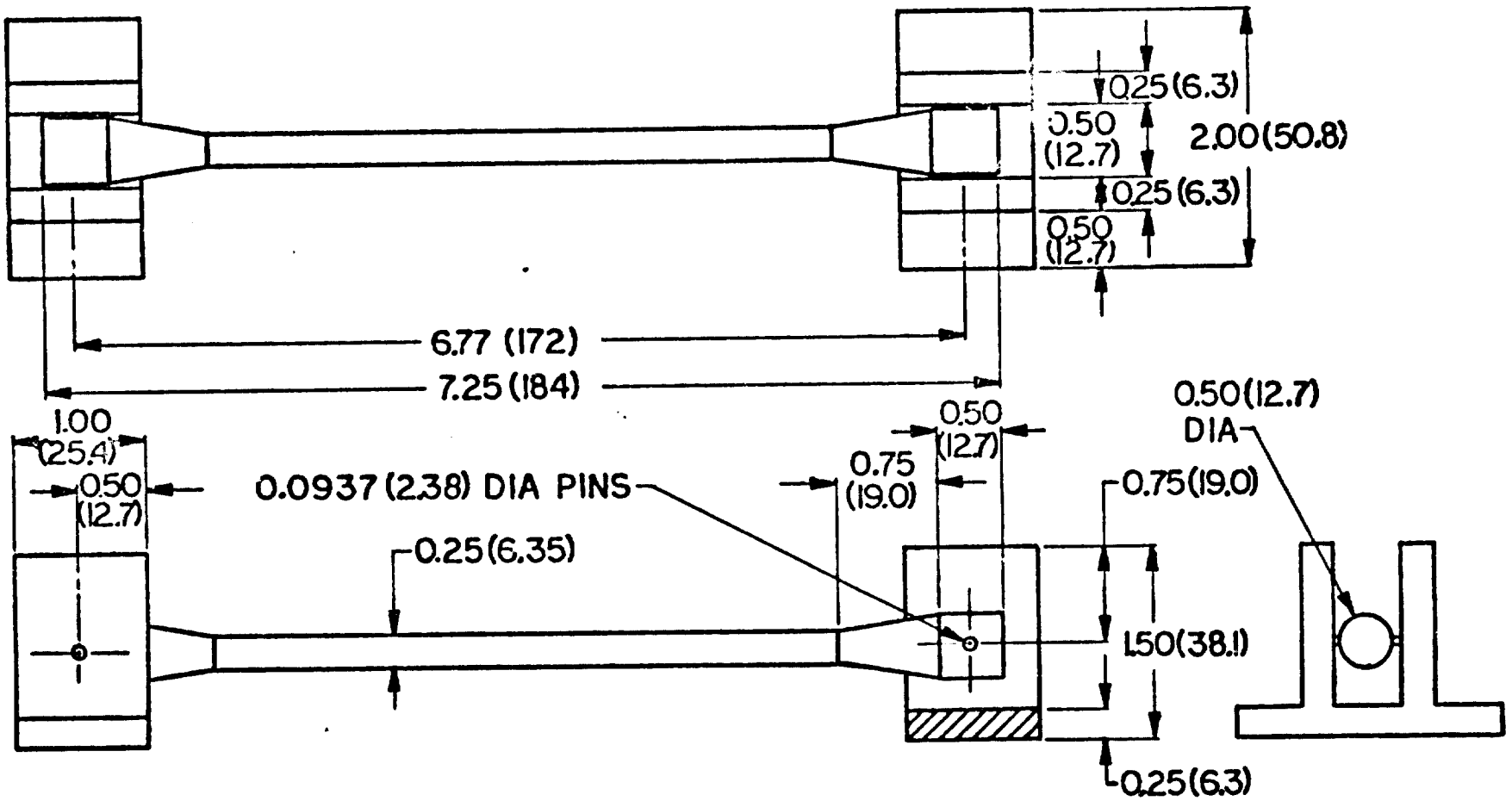

Figure 6.20. DPHI of the Aluminum Beam.

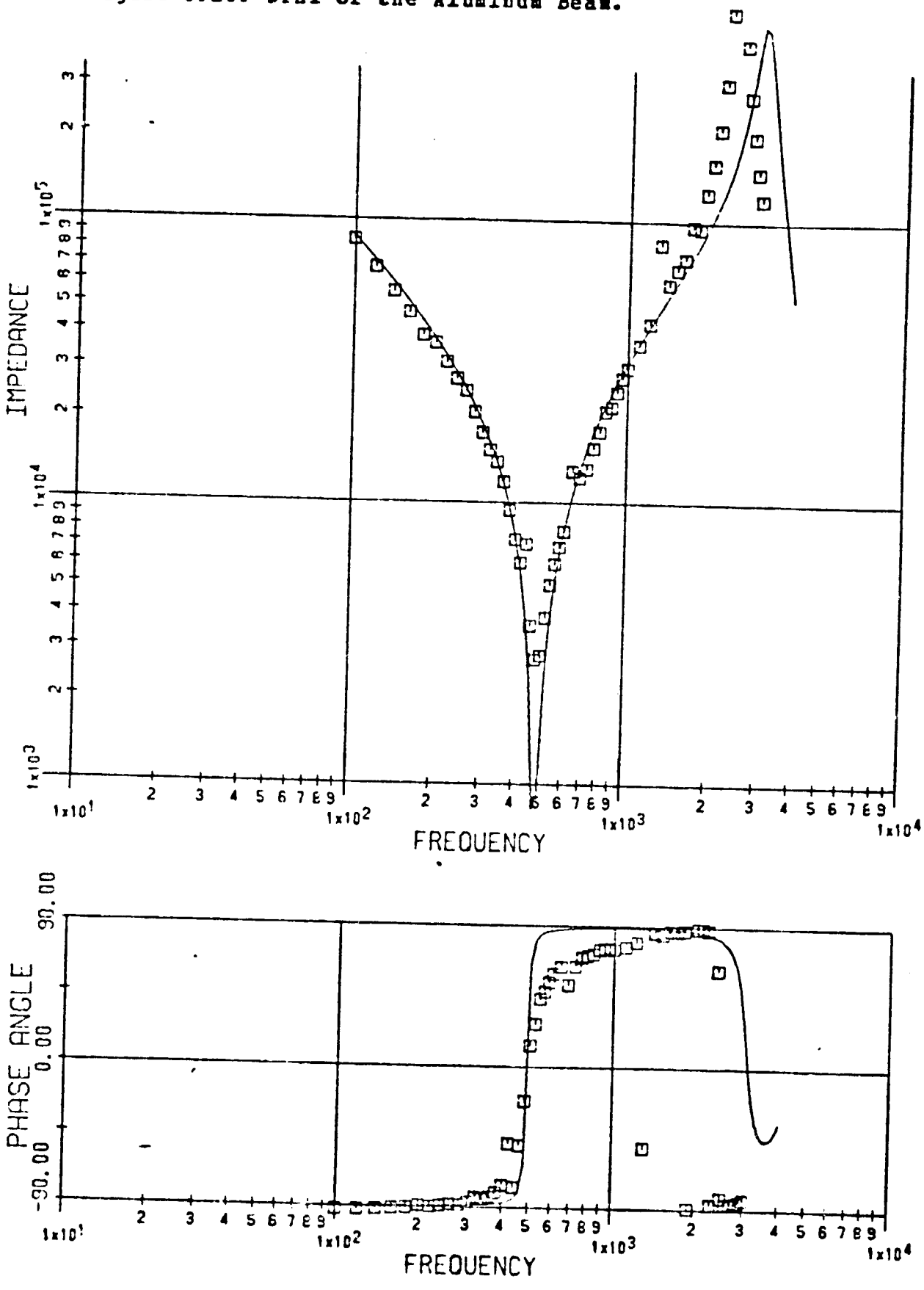

Figure 7.1. DPMI of Subject TT: 400 gm Preload.

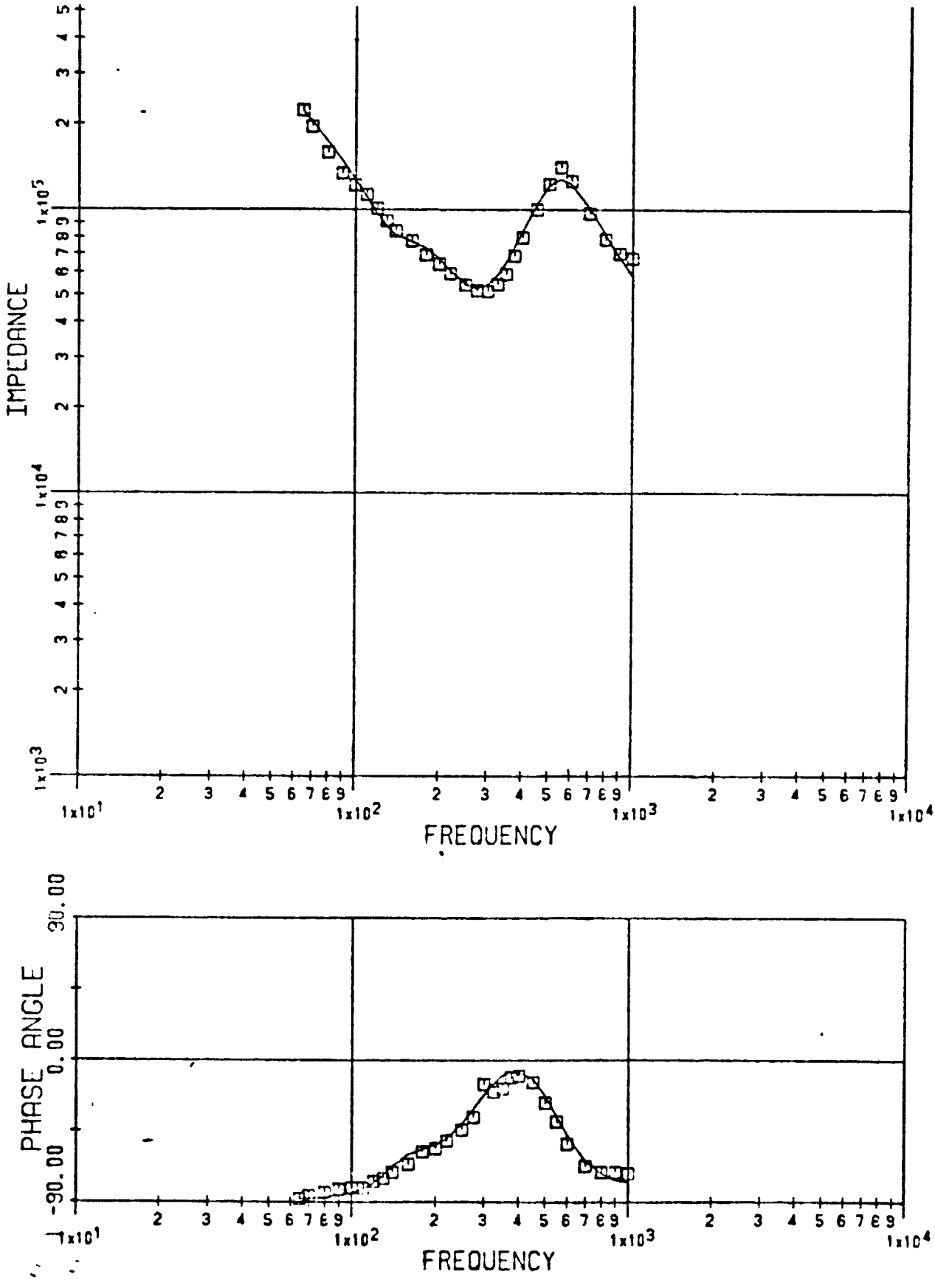

Figure 7.2. DPMI of Subject TT: 500 gm Preload.

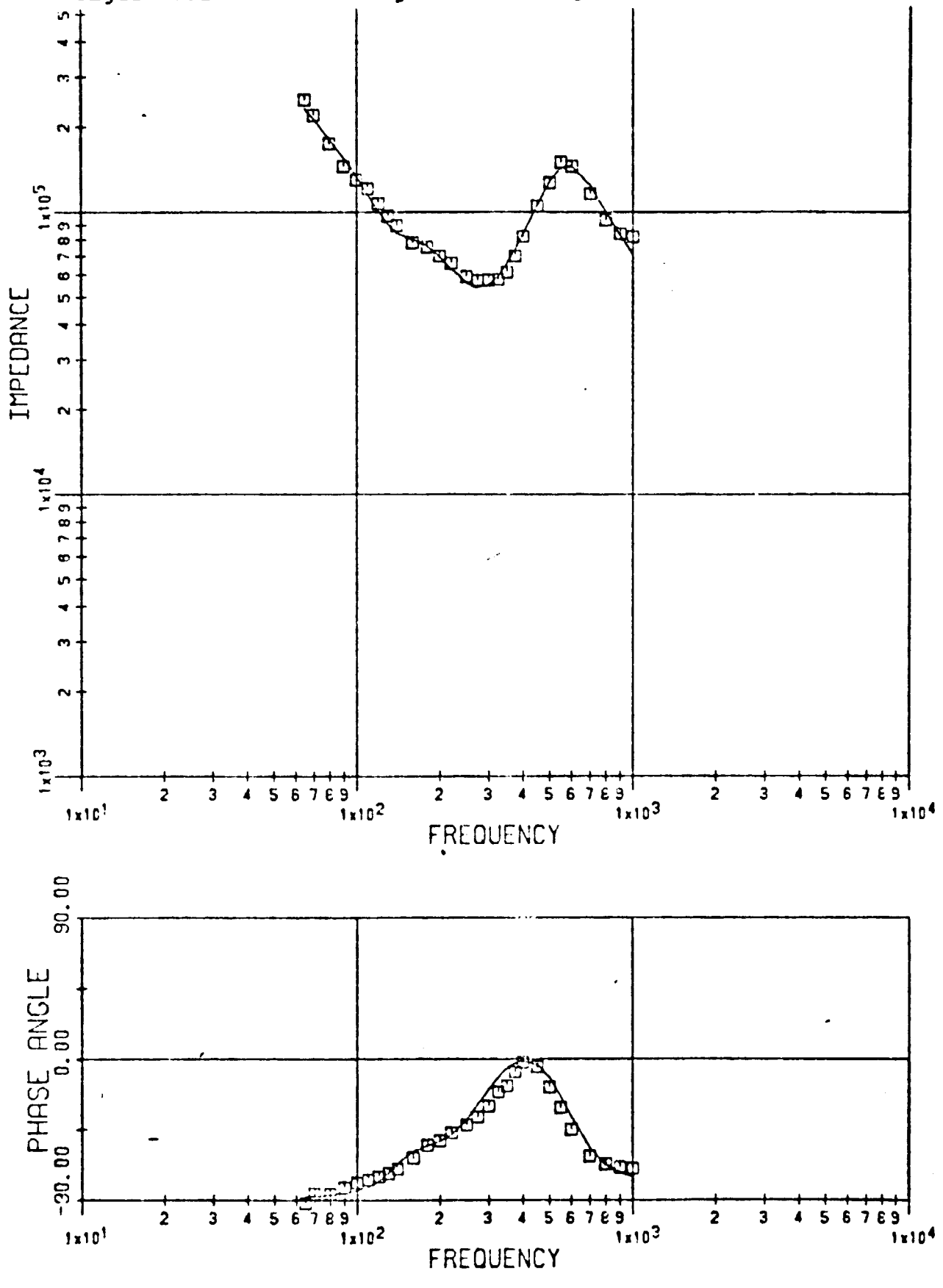

SUBJECT TT 500 GM PRELOAD

Figure 7.3. DPMI of Subject TT: 600 gm Preload.

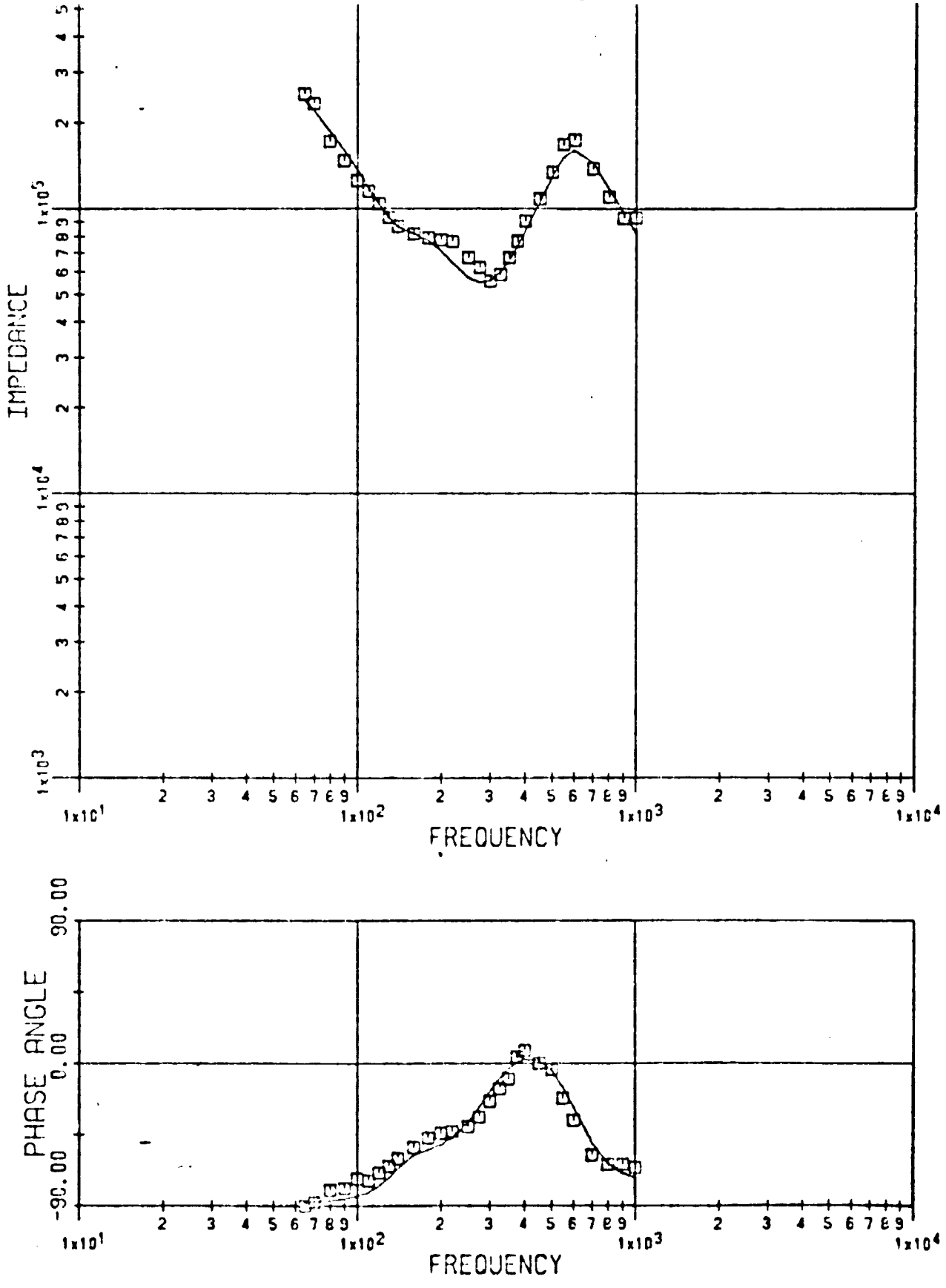

Figure 7.4. DPMI of Monkey 2: Tibia.

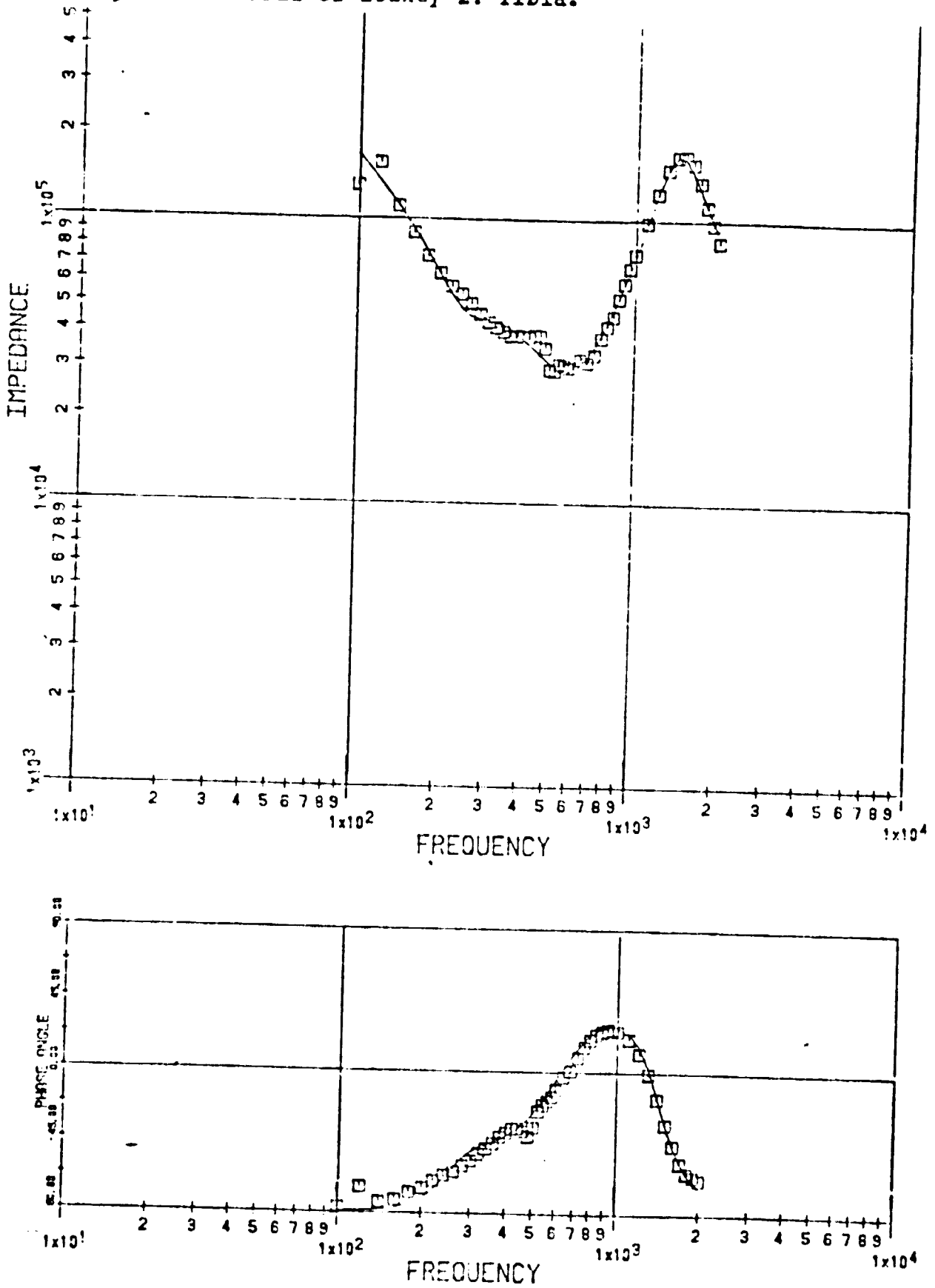

Figure 7.5. DPMI of Monkey 16: Tibia.

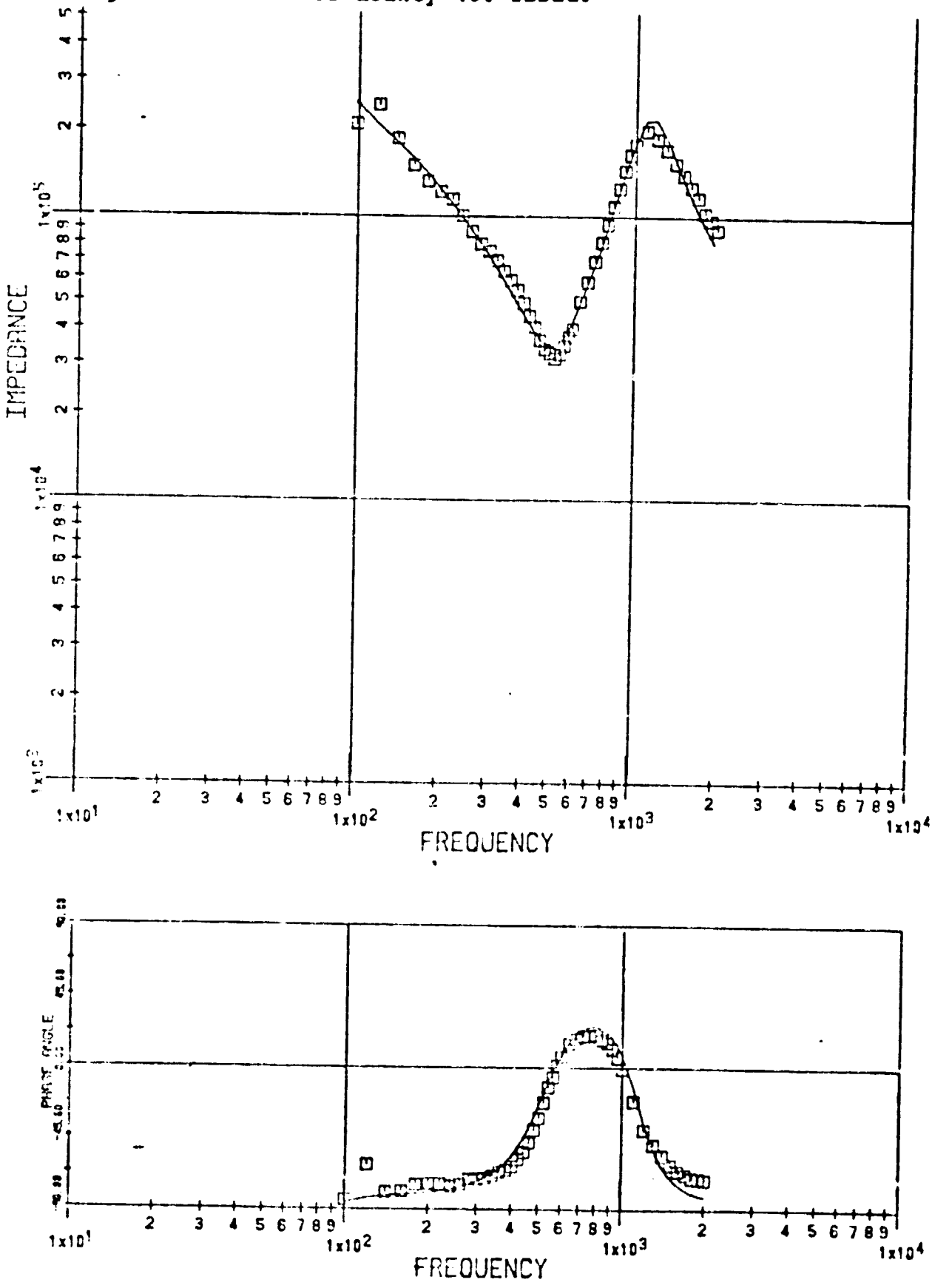

MONK 16 LEFT TIBIA 600 GM PRELOAD

Figure 7.6. DPHI of Monkey 17: Tibia.

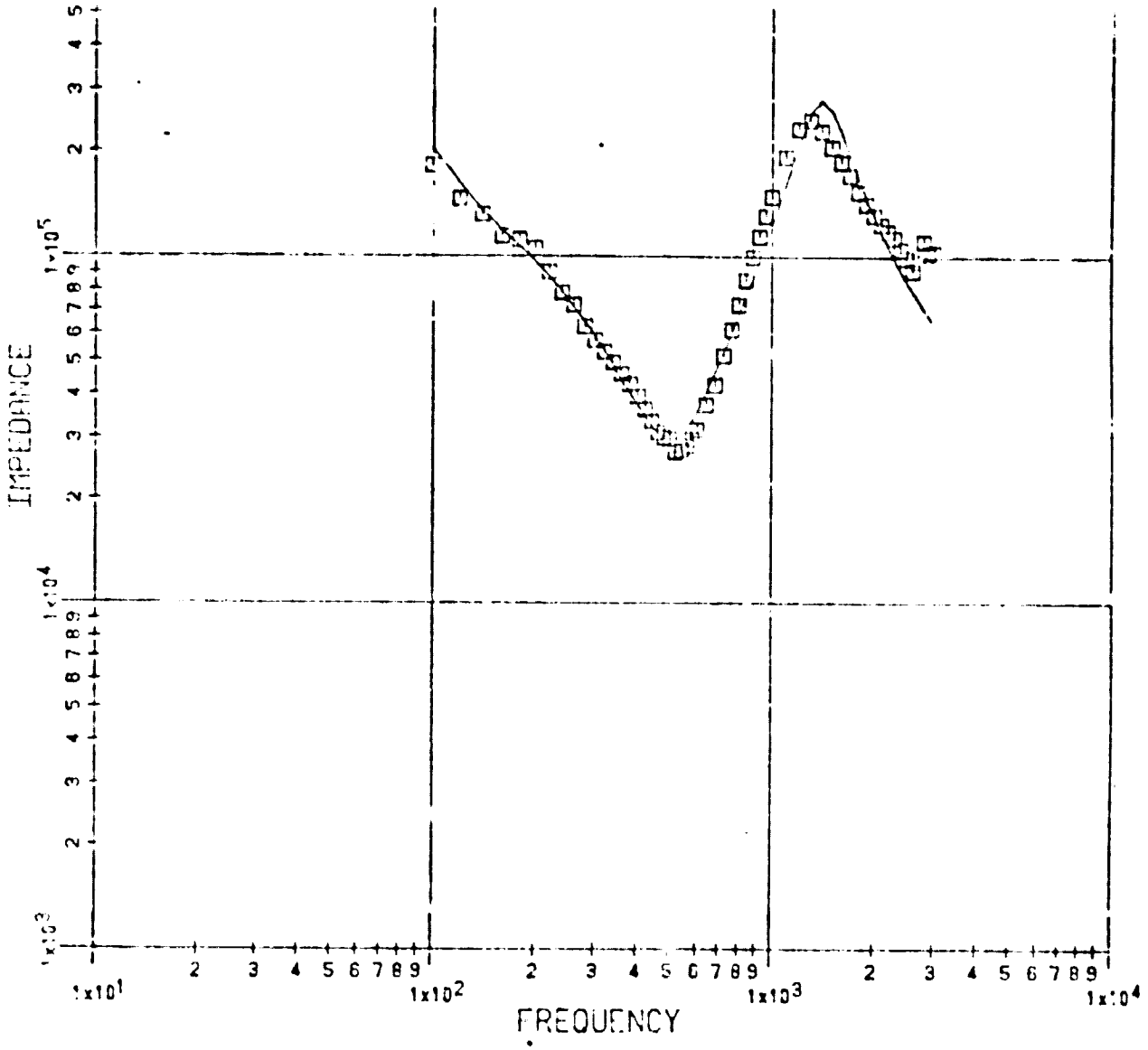

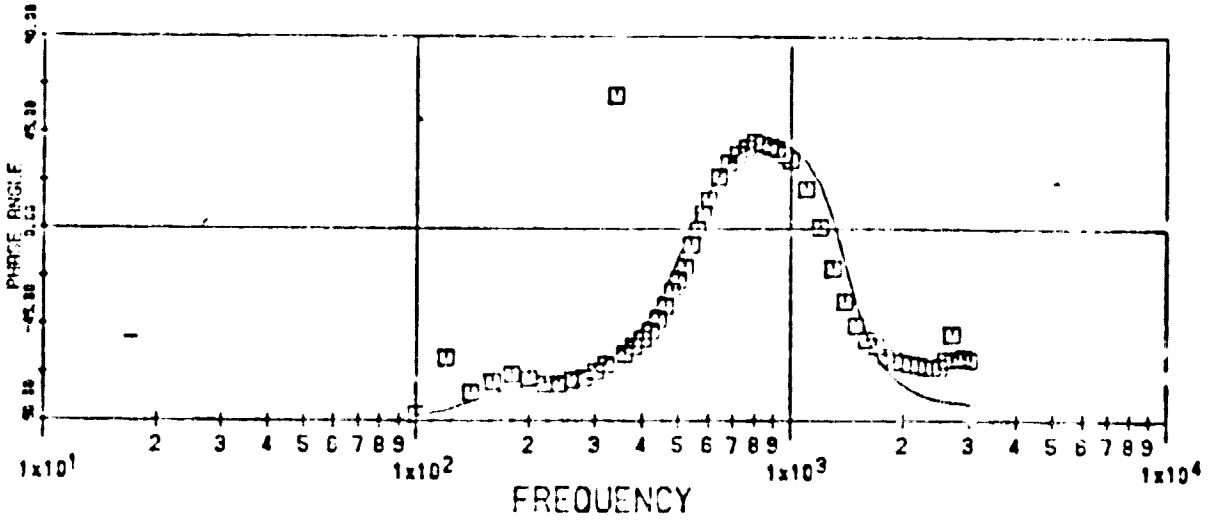

MONK 17 LEFT TIBIA 600 GM PRELOAD

Figure 7.7. DPMI of Monkey 2: Ulna.

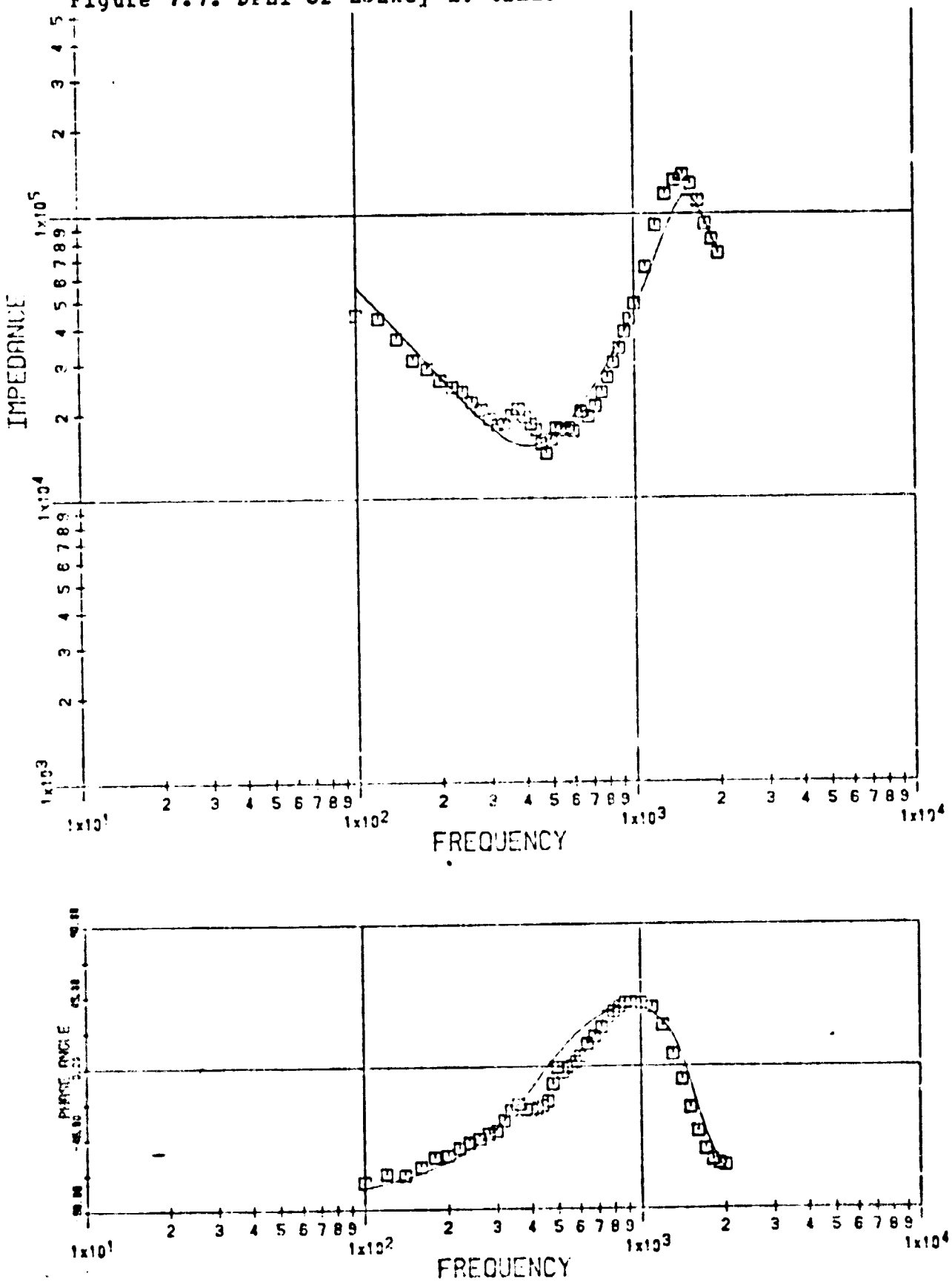

Figure 7.8. DPHI of Monkey 16: Ulna.

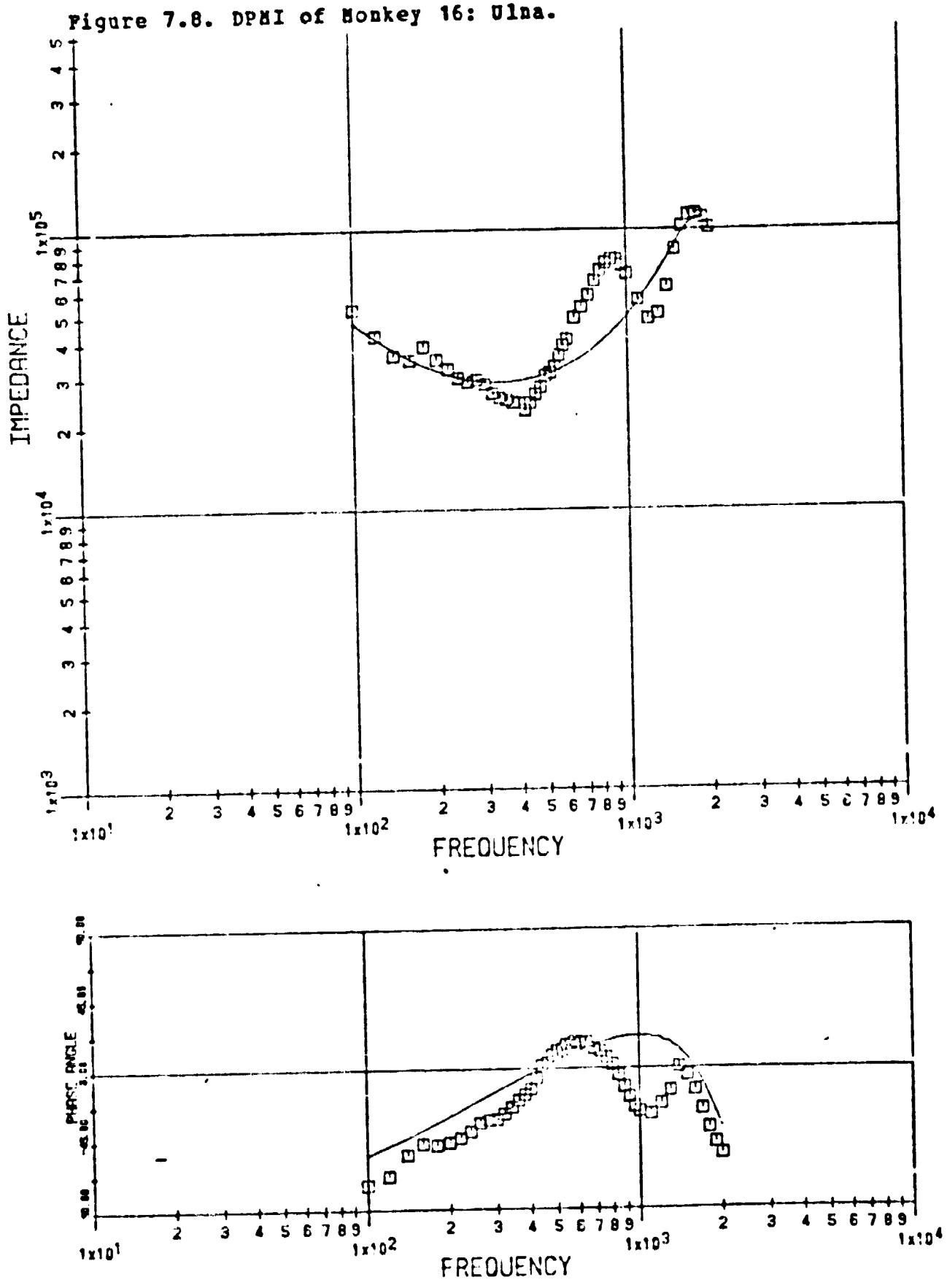

Figure 7.9. DPMI of Monkey 17: Ulna.

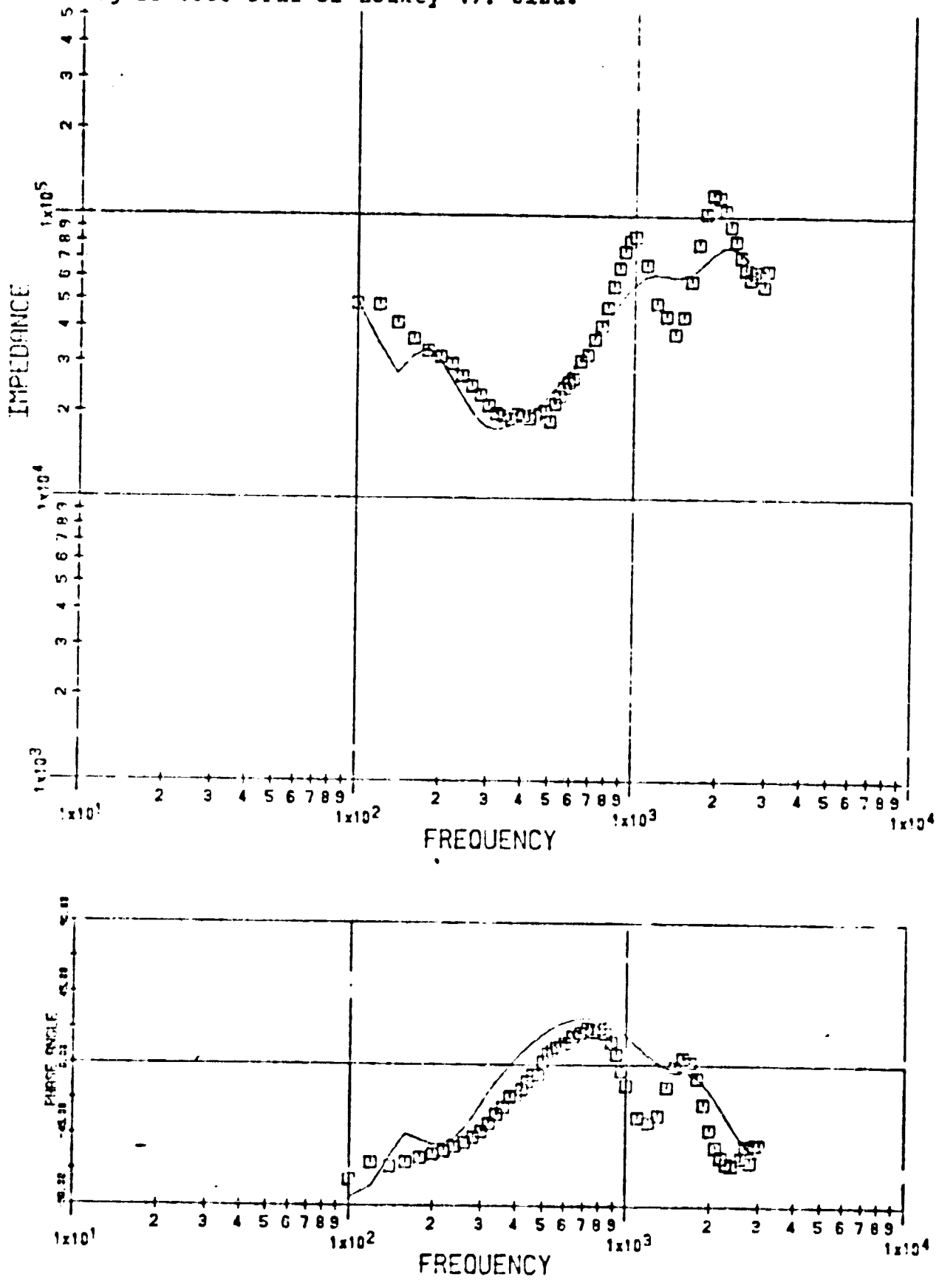

Figure 7.10. DPNI Plot Exhibiting the Effect of Translational Springs and Dampers at the Boundaries.

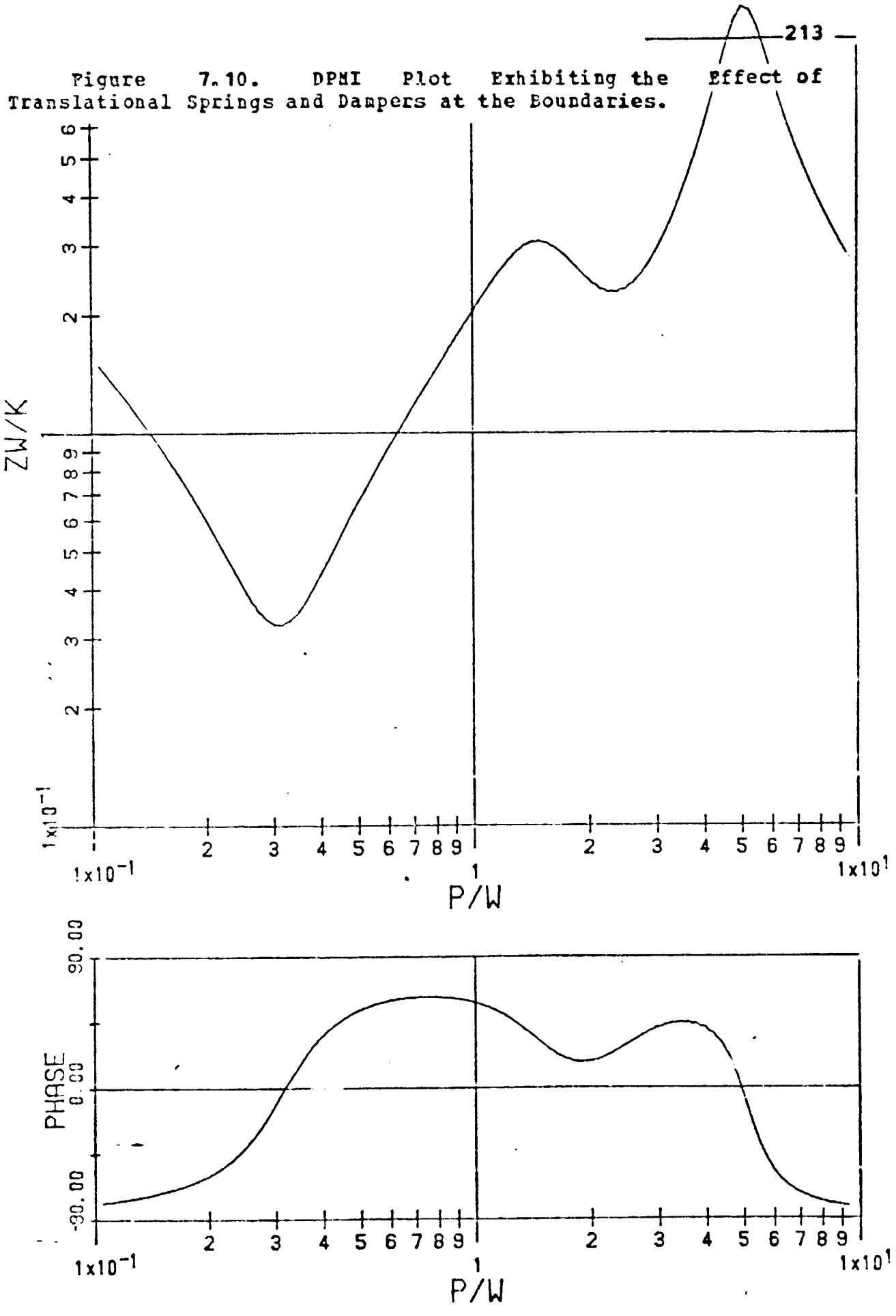

Figure 7.11. DPMI Plot Exhibiting the Masking Effect of the Spring-in-series.

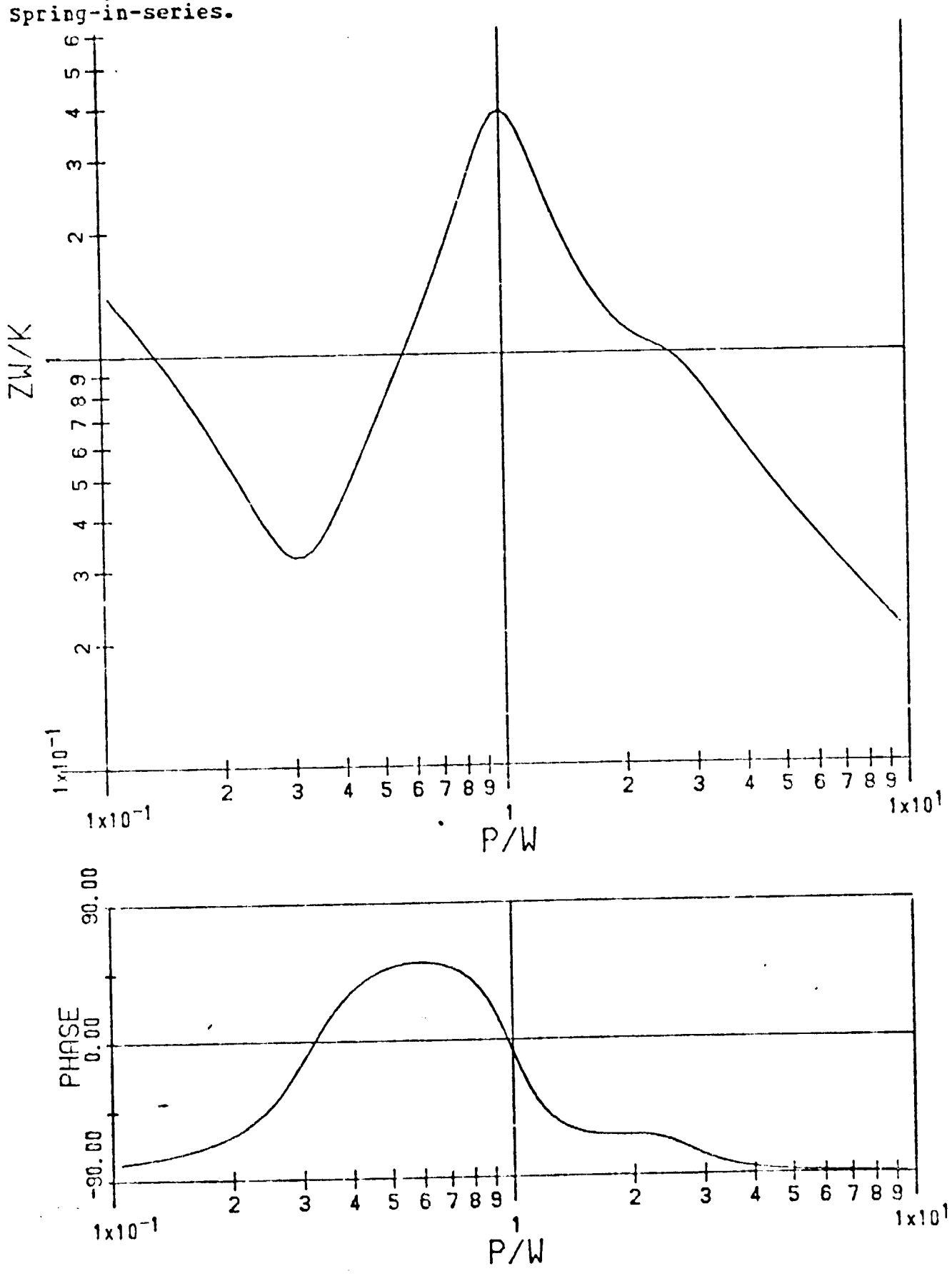

Figure B.1. The Elements of a Tapered Beam.

(a) Linear taper, (b) Quadratic taper

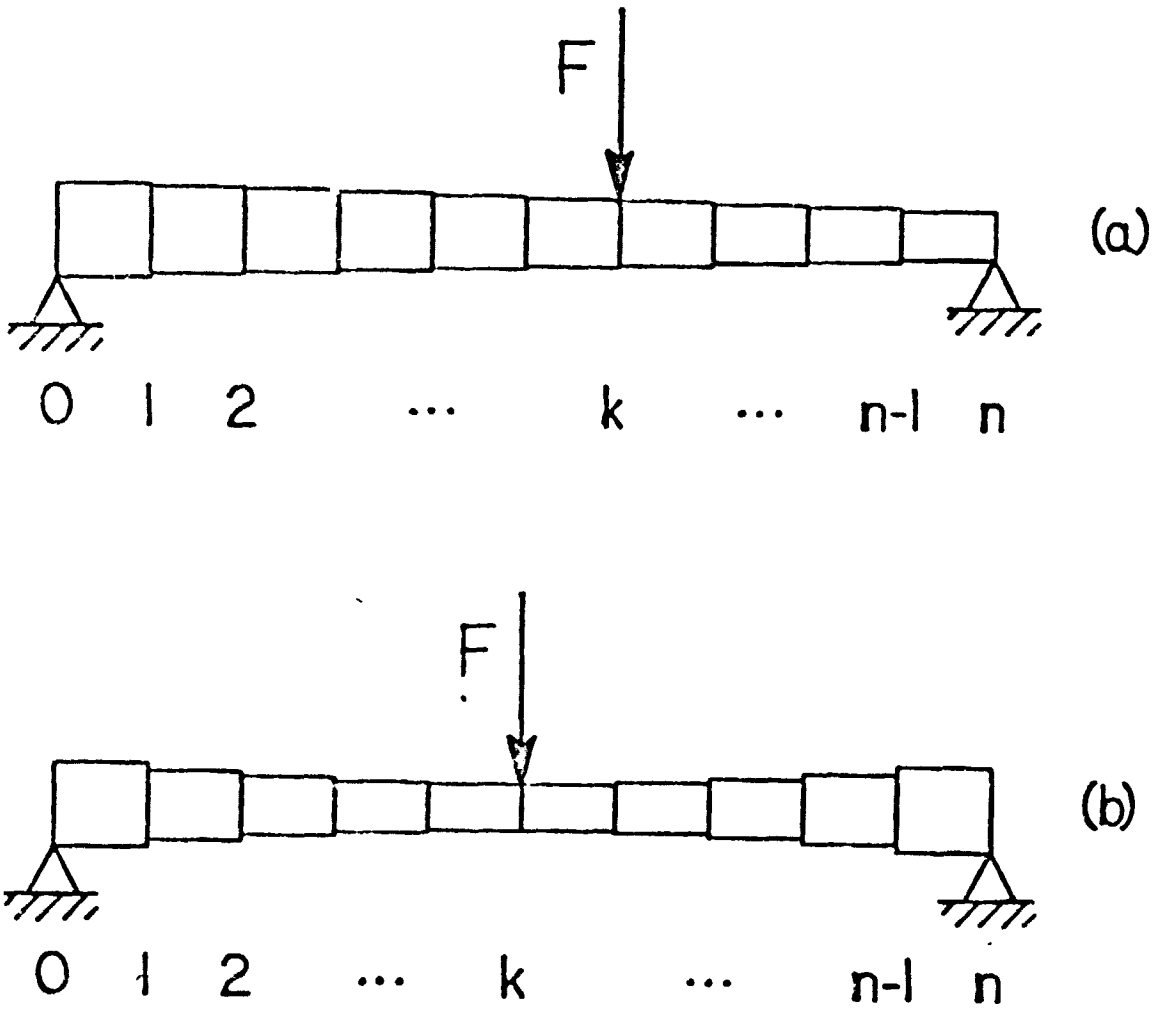

Figure C.1. True Minimum of a Discrete DPMI Plot.

$$x_0 = p_{MIN}/\omega$$

$$y_0 = Z_{MIN}\omega/K$$

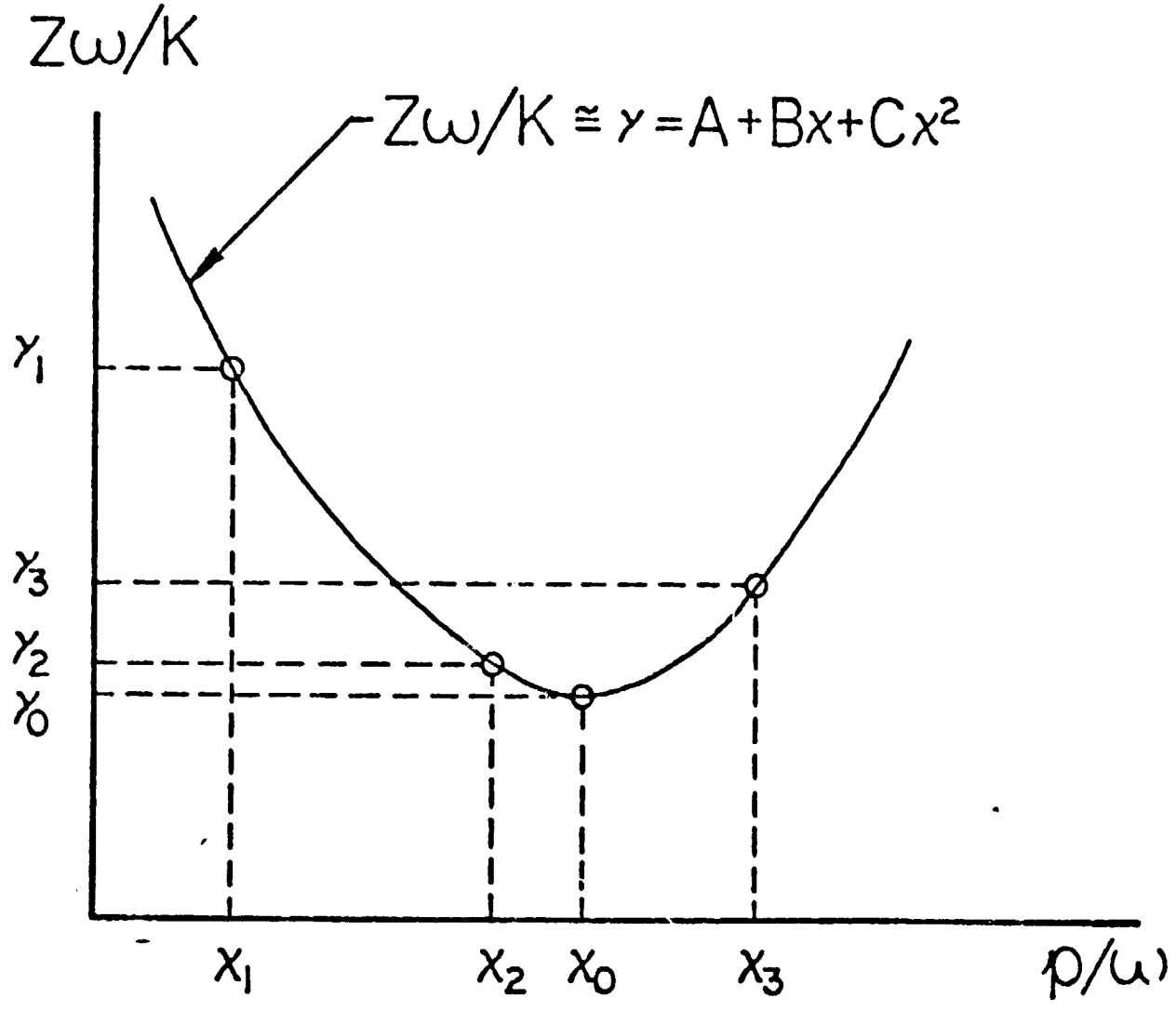

Figure G.1. DPSI of Subject BL: 400 gm Preload.

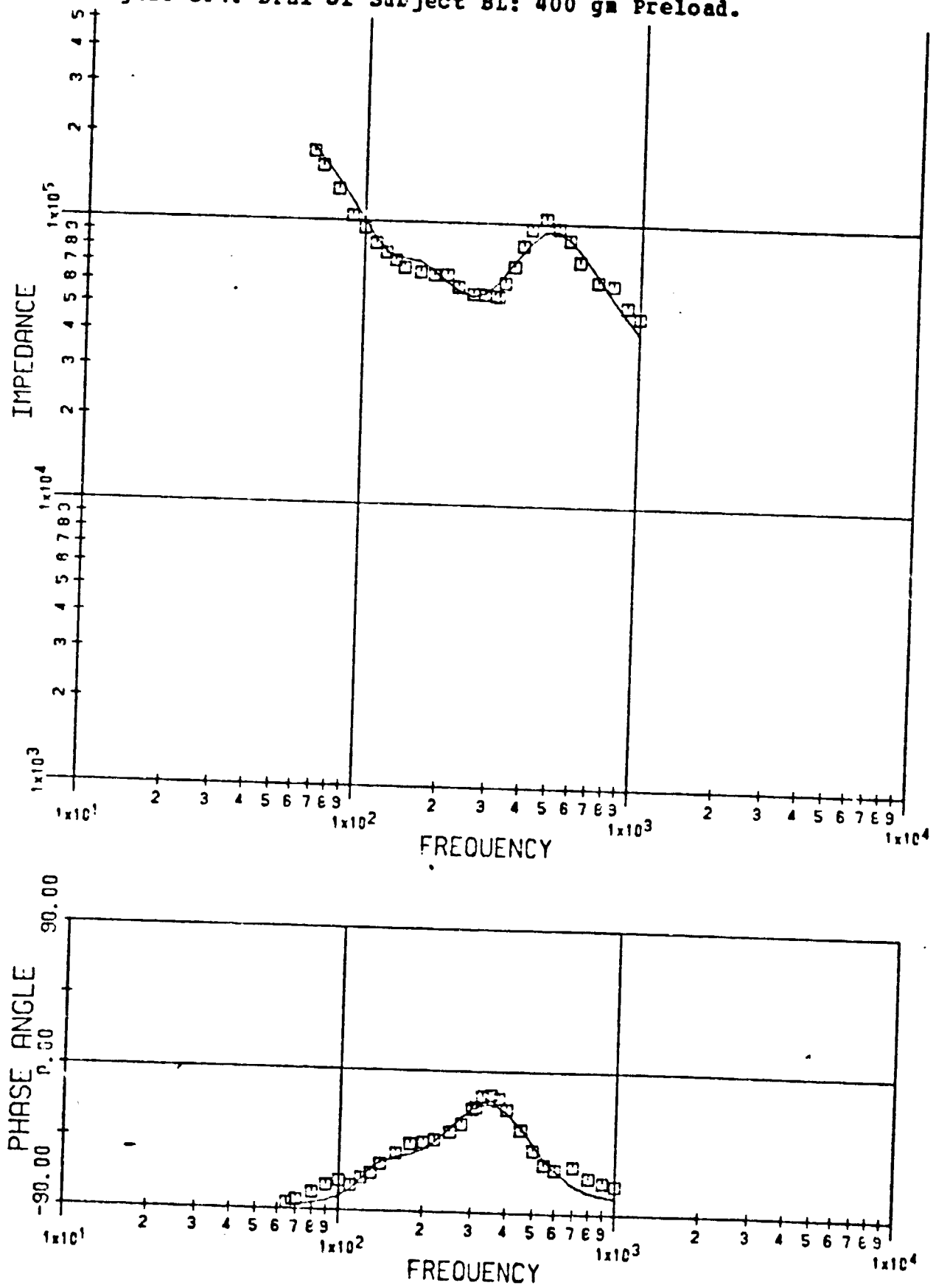

SUBJECT BL 400 GM PRELOAD

Figure G.2. DPMI of Subject BL: 500 gm Preload.

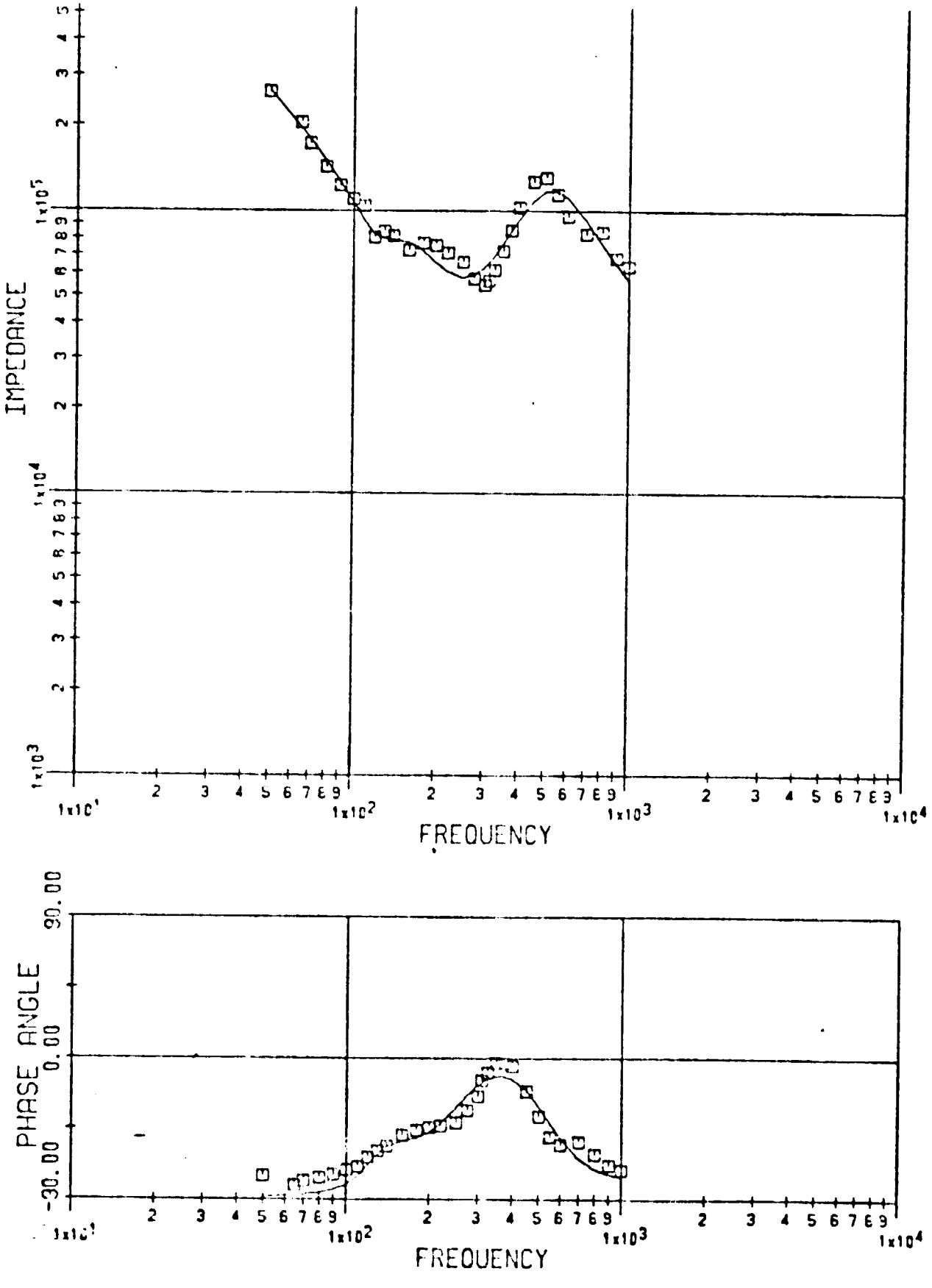

SUBJECT BL 500 GM PRELOAD

Figure G.3. DPM1 of Subject BL: 600 gm Preload.

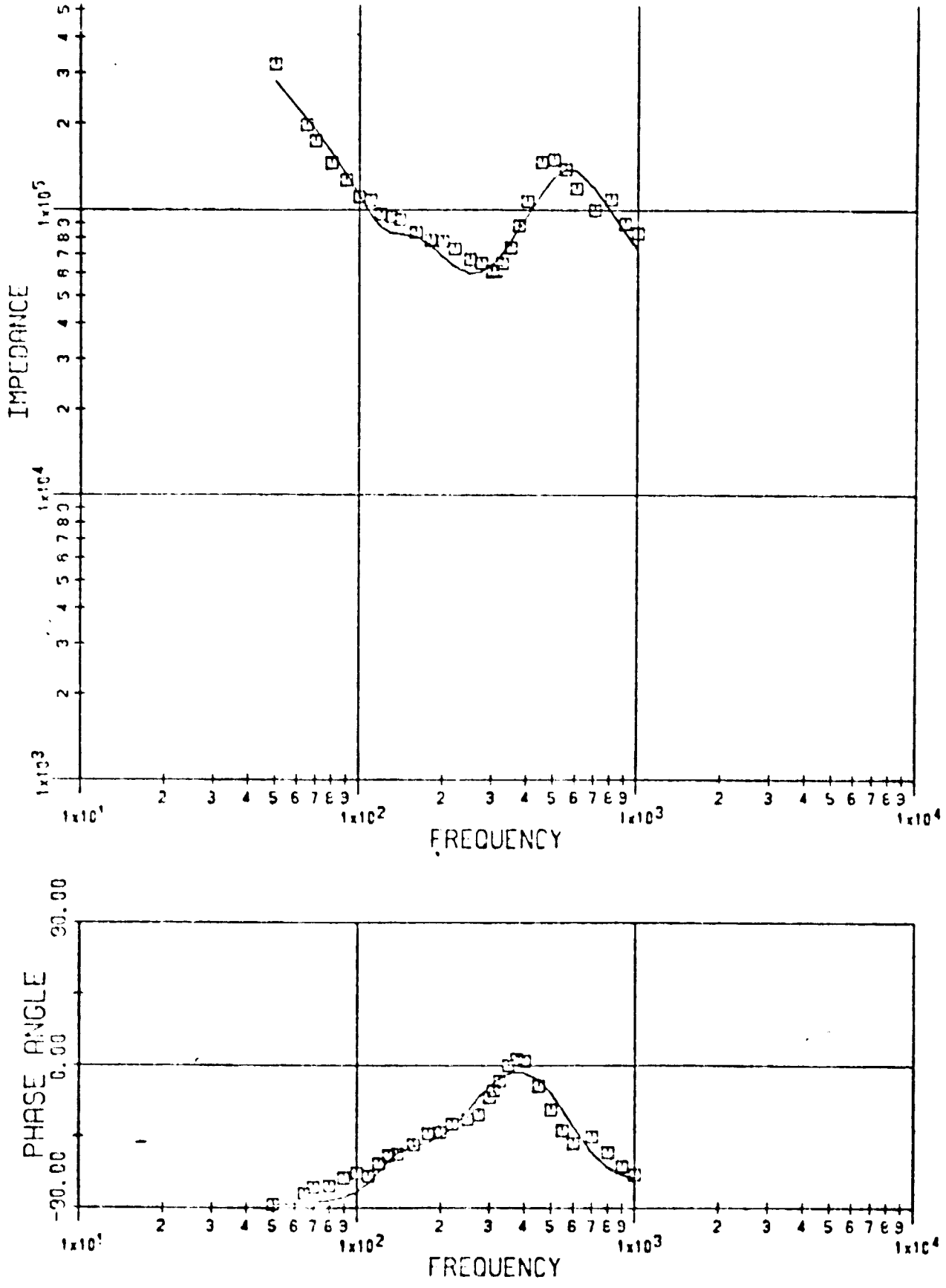

SUBJECT BL 600 GM PRELOAD

Figure G.4. DPMI of Subject CDG: 400 gm Preload.

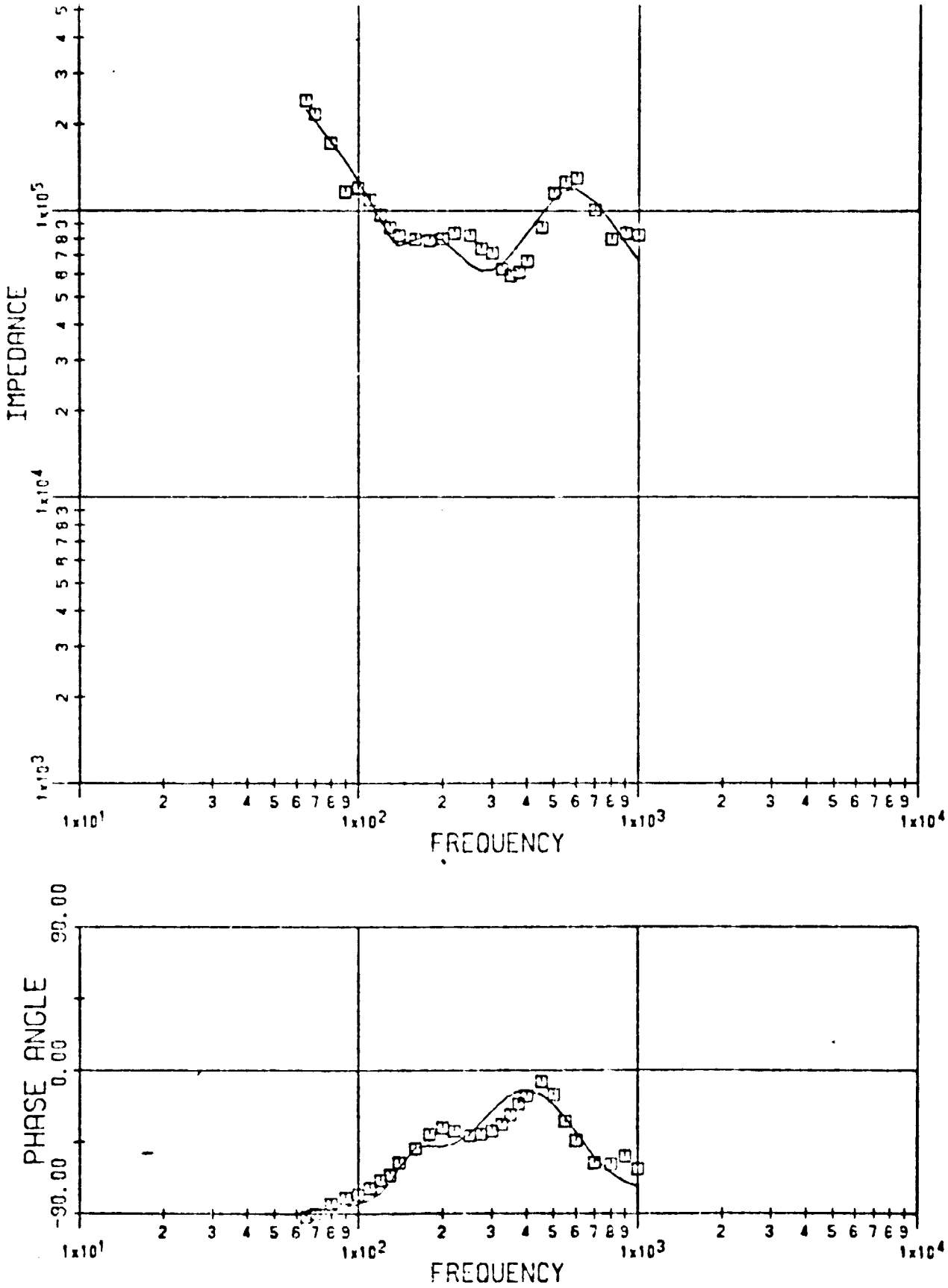

SUBJECT CDG 400 GM PRELOAD

Figure G.5. DPMI of Subject CDG: 500 gm Preload.

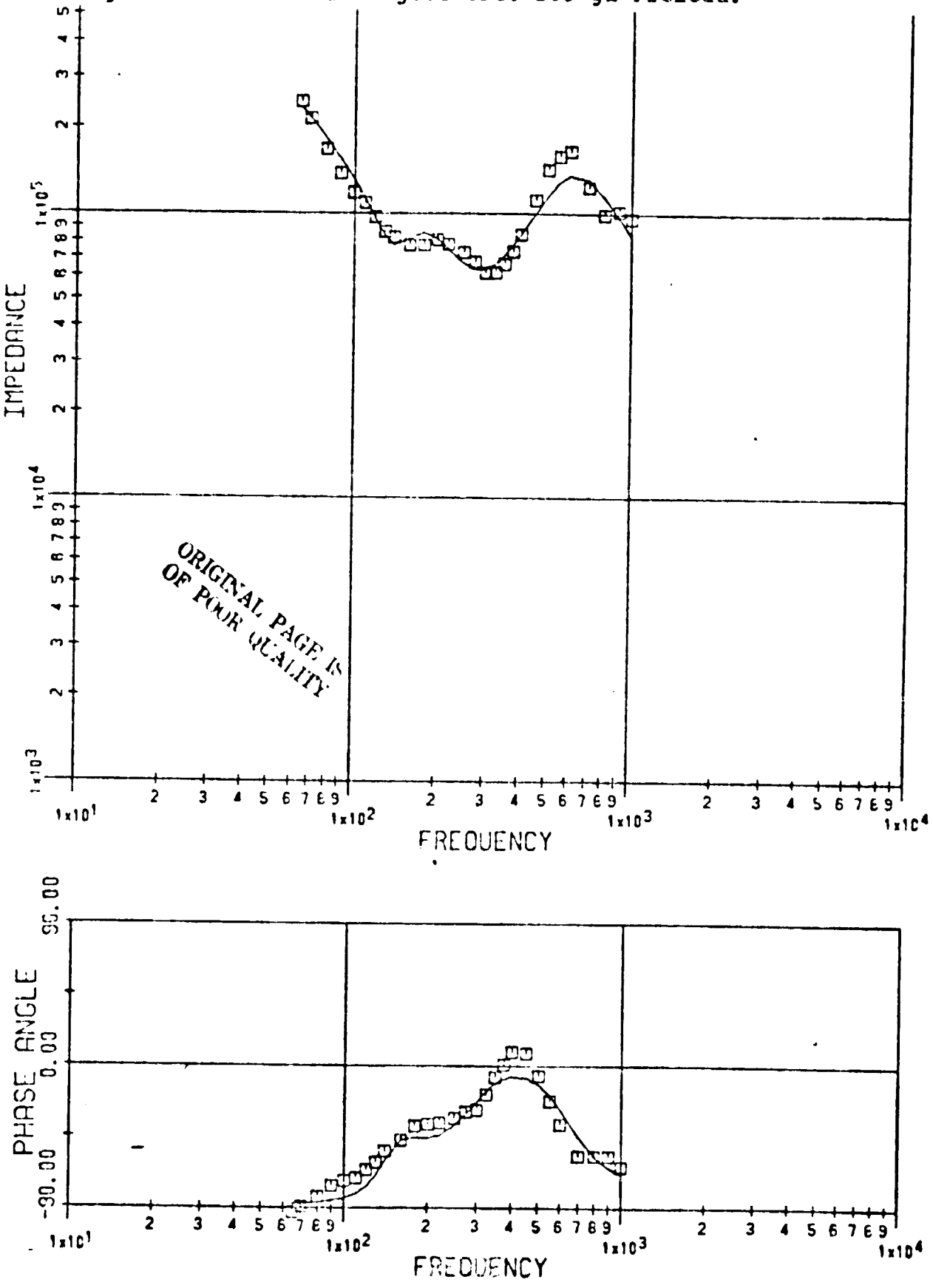

SUBJECT CDG 500 GM PRELOAD

Figure G.6. DPNI of Subject CDG: 600 gm Preload.

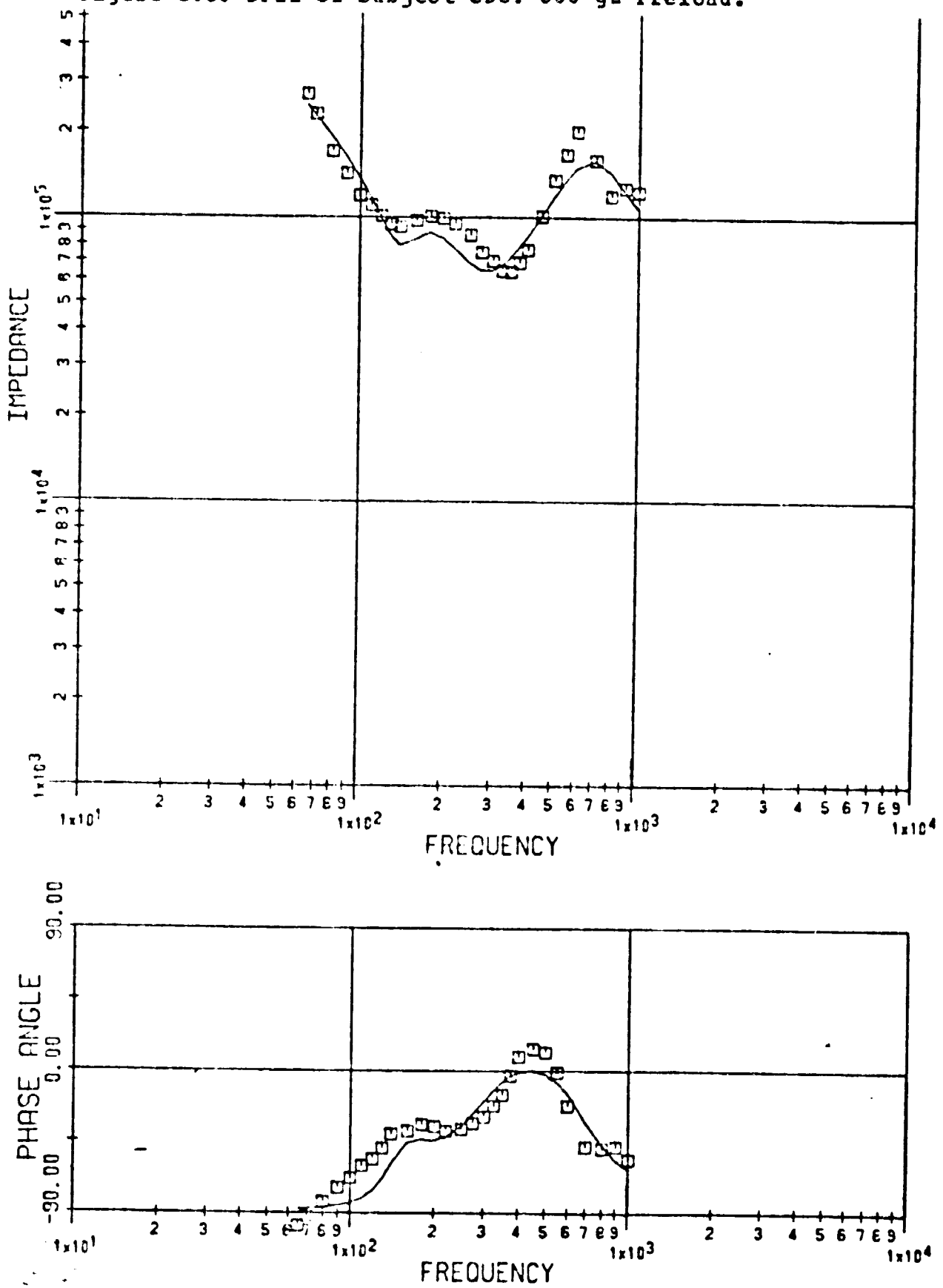

SUBJECT CDG 600 GM PRELOAD

Figure G.7. DPMI of Subject DG: 400 gm Preload.

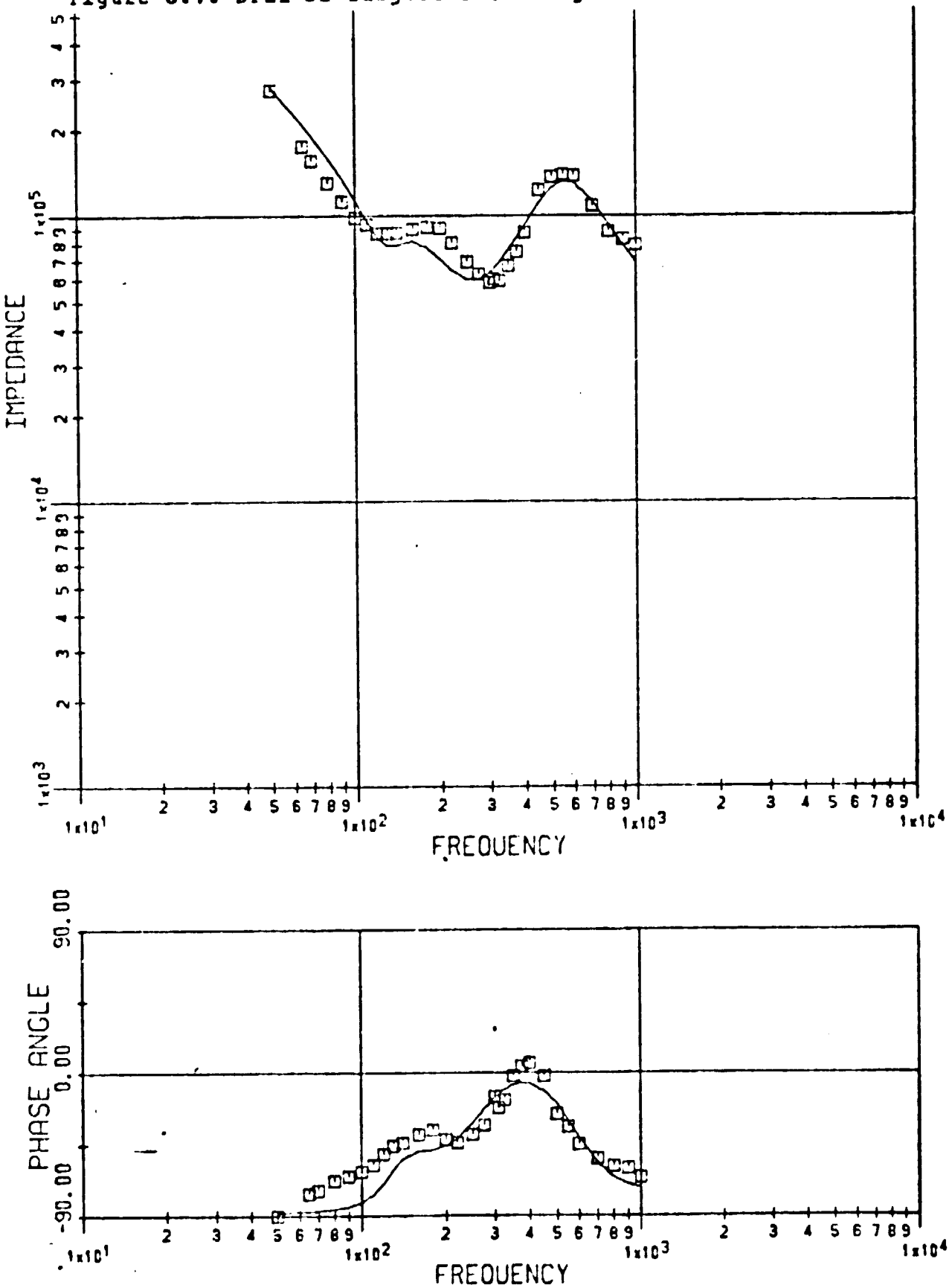

SUBJECT DG 400 GM PRELOAD

Pignre G.8. DPHI of Subject DG: 500 gm Preload.

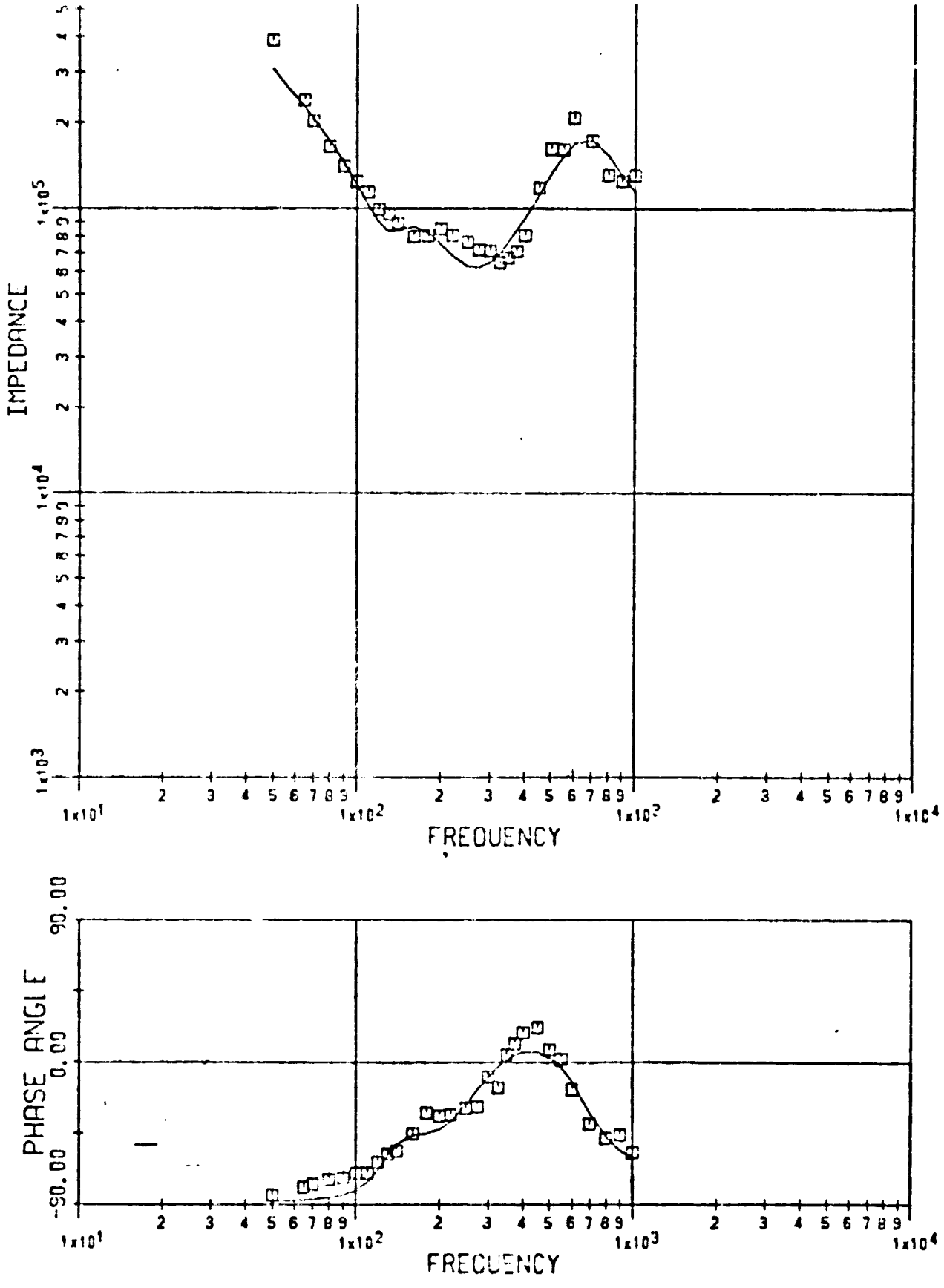

SUBJECT DG 500 GM PRELOAD

Figure G.9. DPMI of Subject DG: 600 gm Preload.

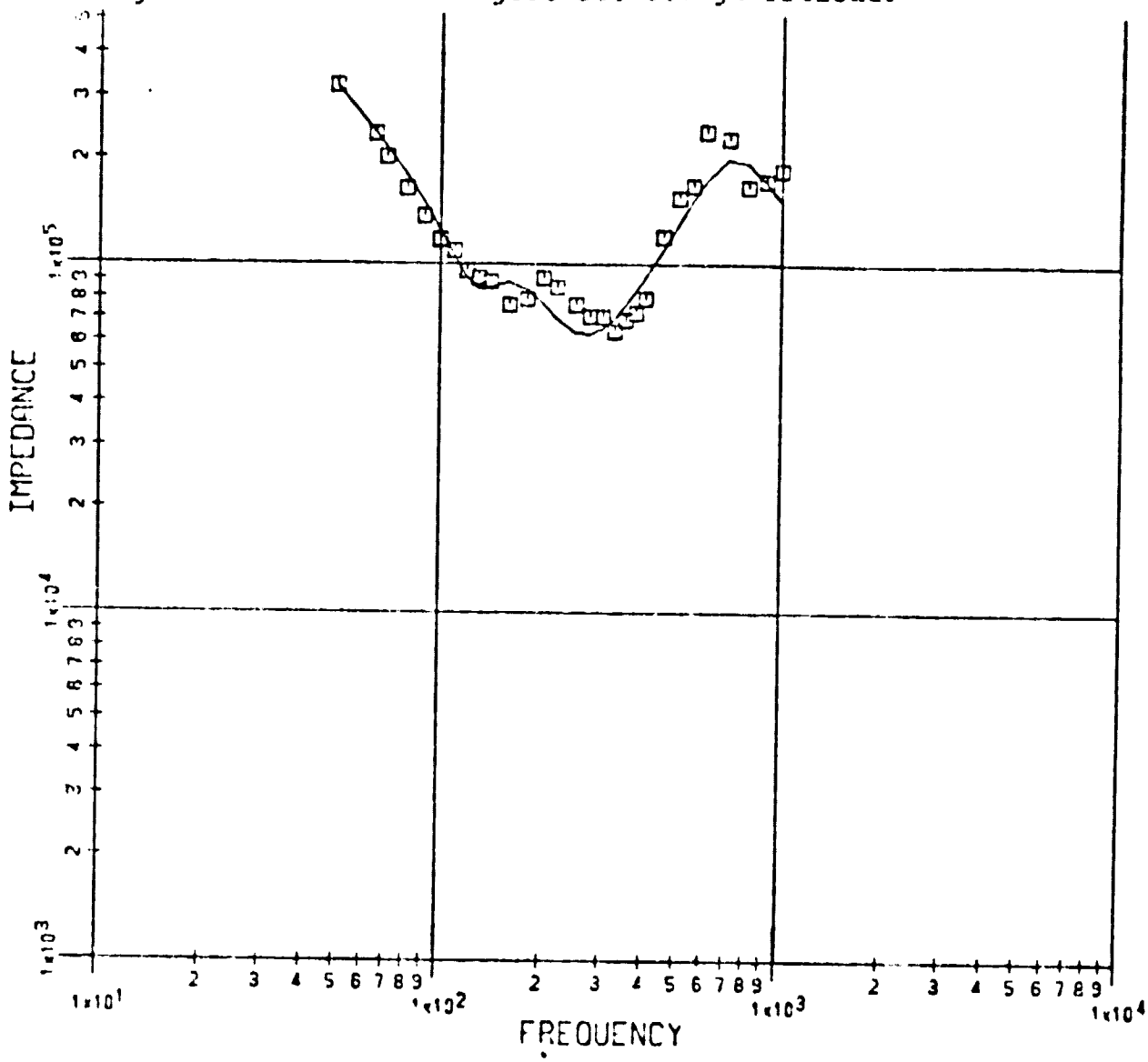

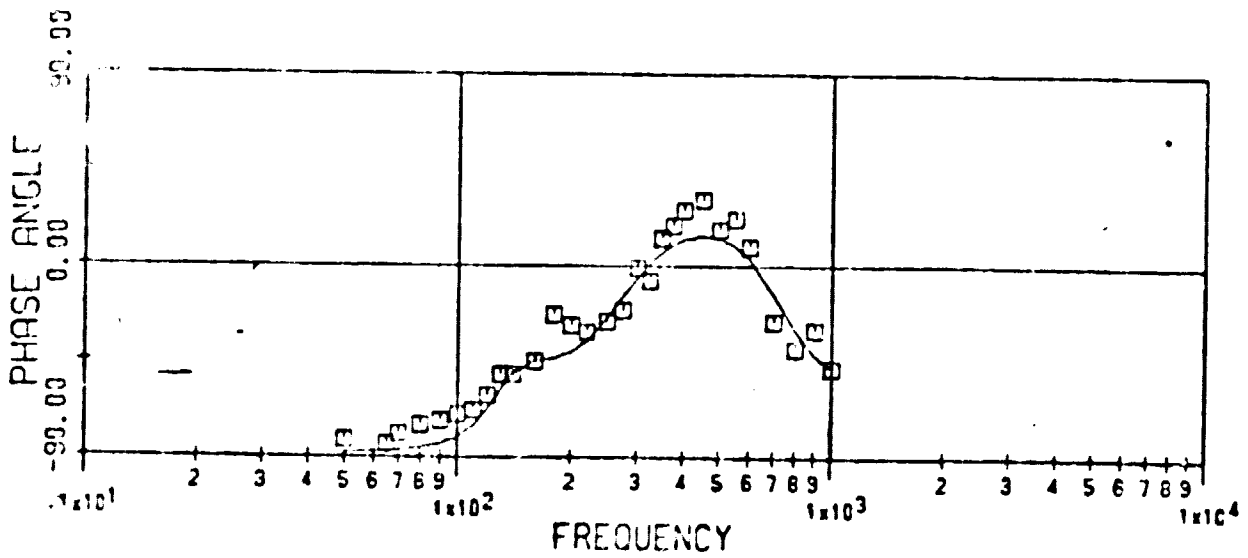

SUBJECT DG 600 GM PRELOAD

Figure G.10. DPMI of Subject MB: 400 gm Preload.

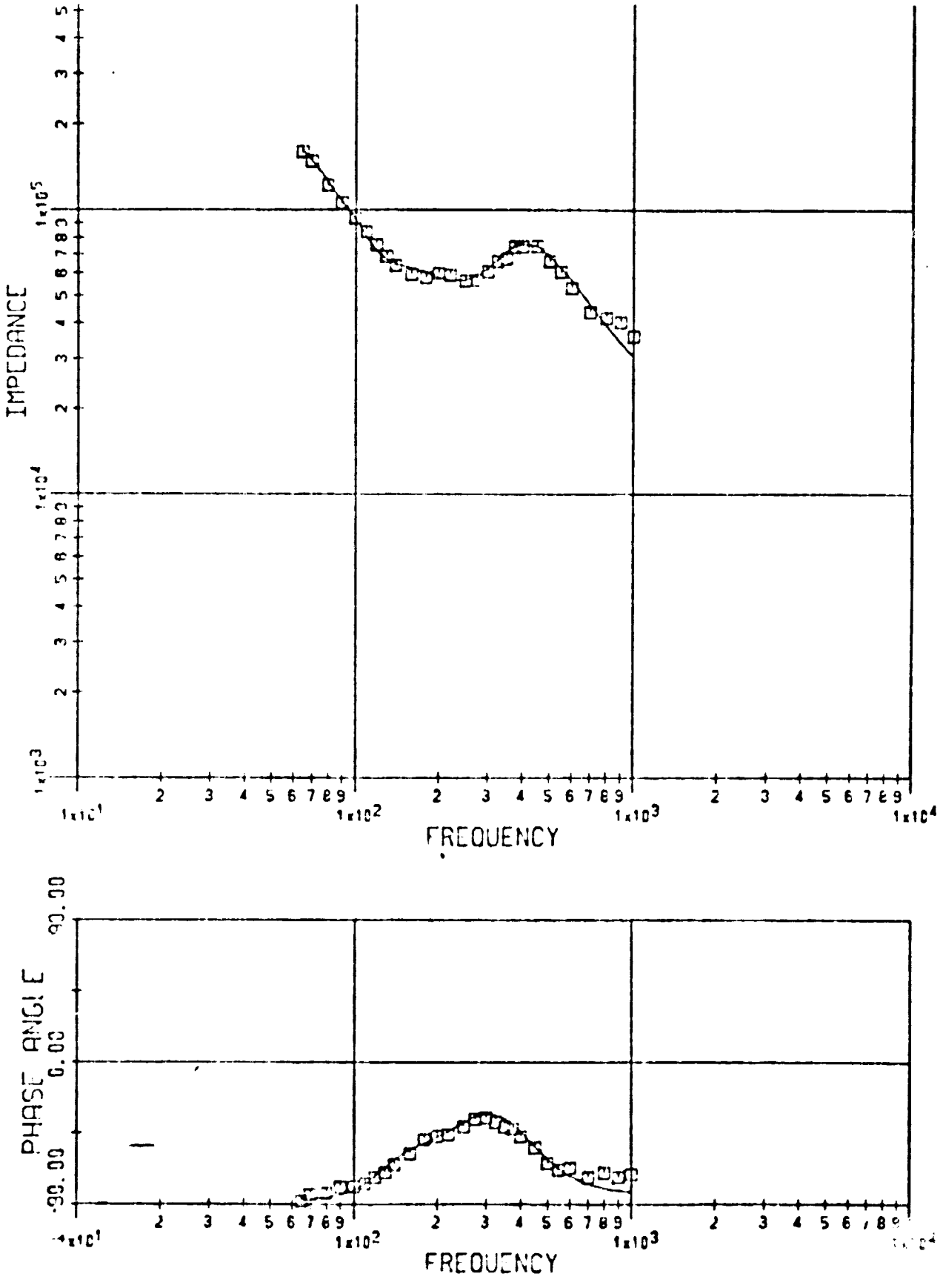

Figure G.11. DPMI of Subject MB: 500 gm Preload.

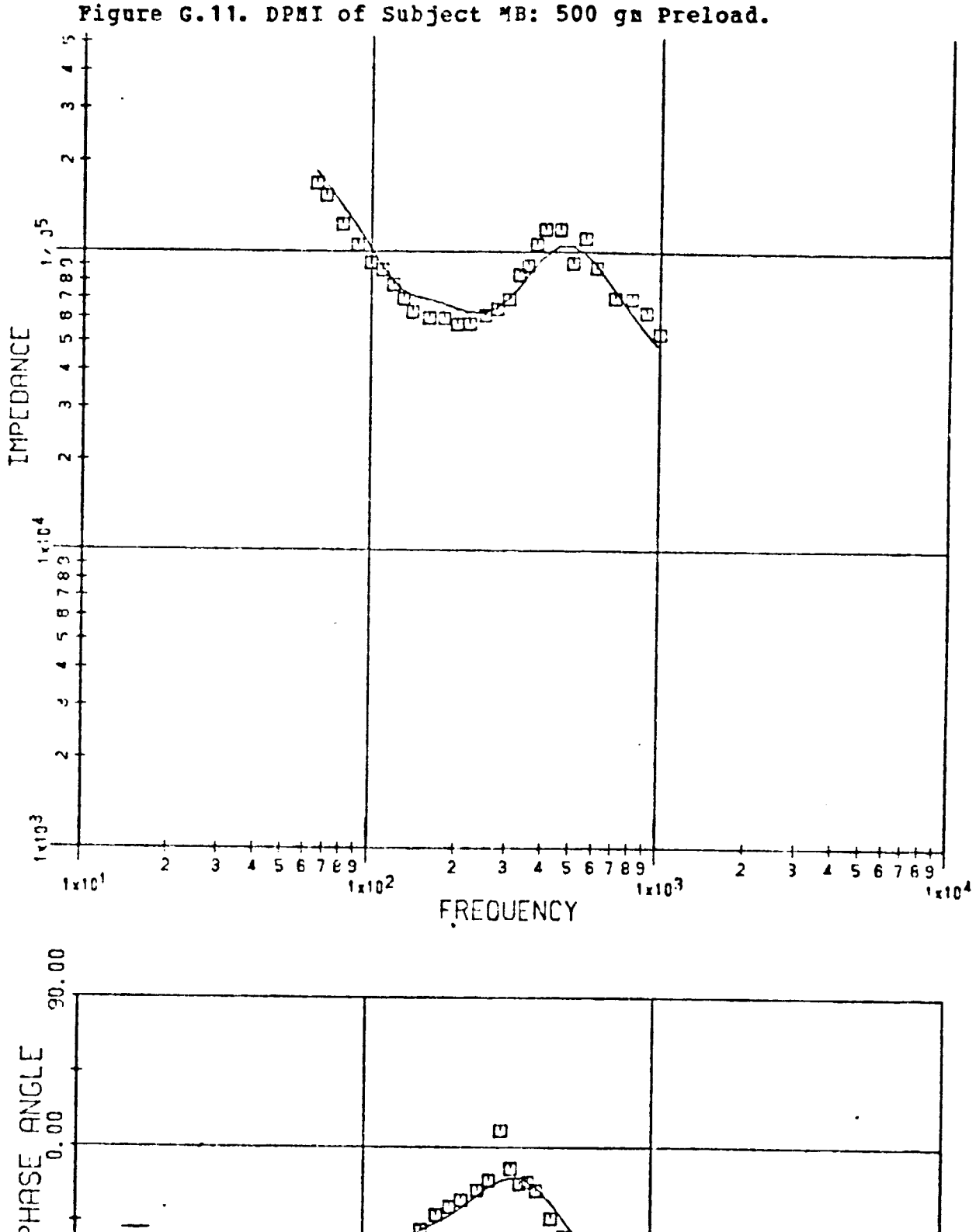

SUBJECT MB 500 GM PRELOAD

Figure G.12. DPMI of Subject MB: 600 gm Preload.

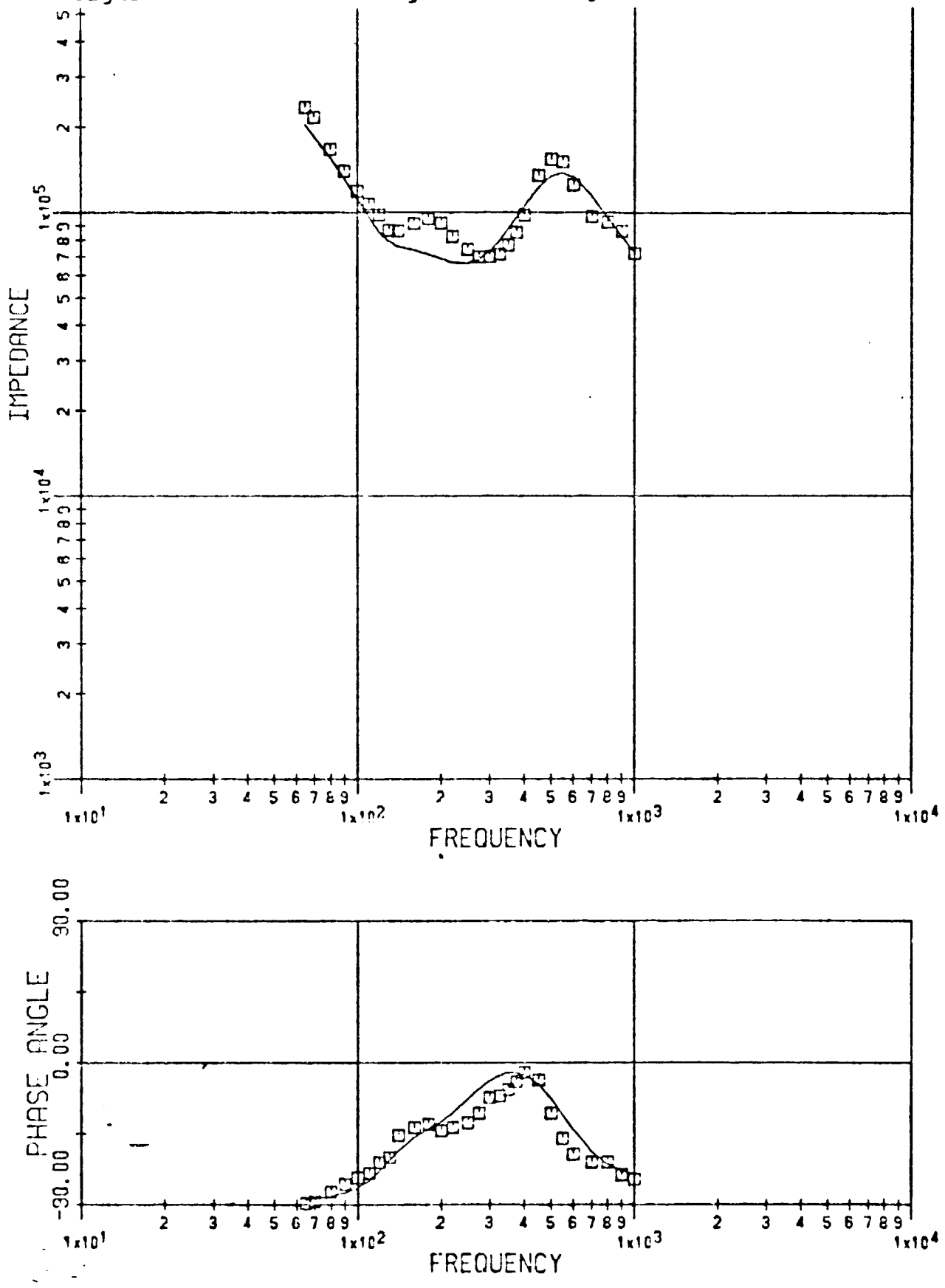

Figure G.13. DPMI of Subject MO: 400 gm Preload.

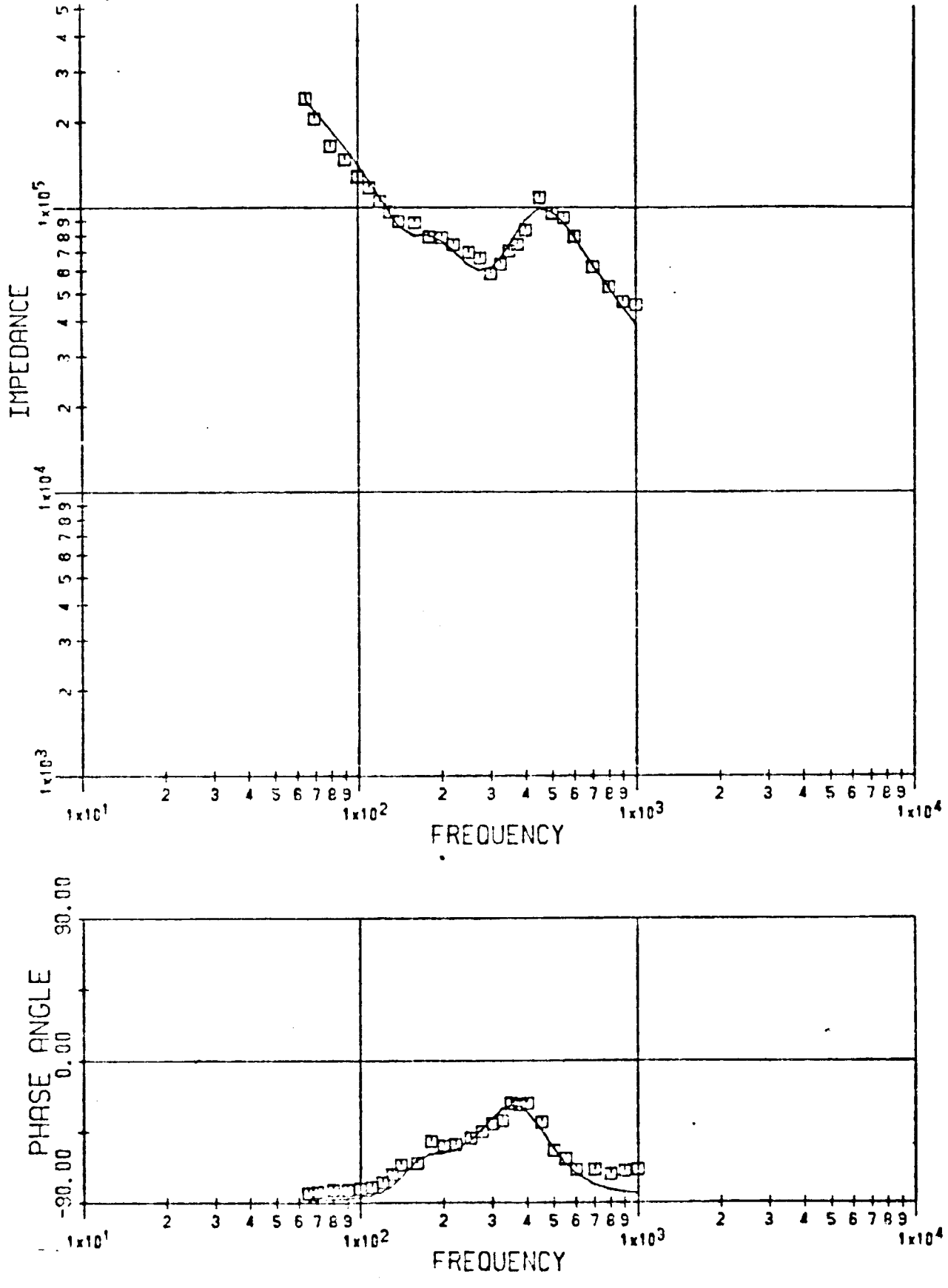

SUBJECT MO 400 GM PRELOAD

Figure G.14. DPMI of Subject MO: 500 gm Preload.

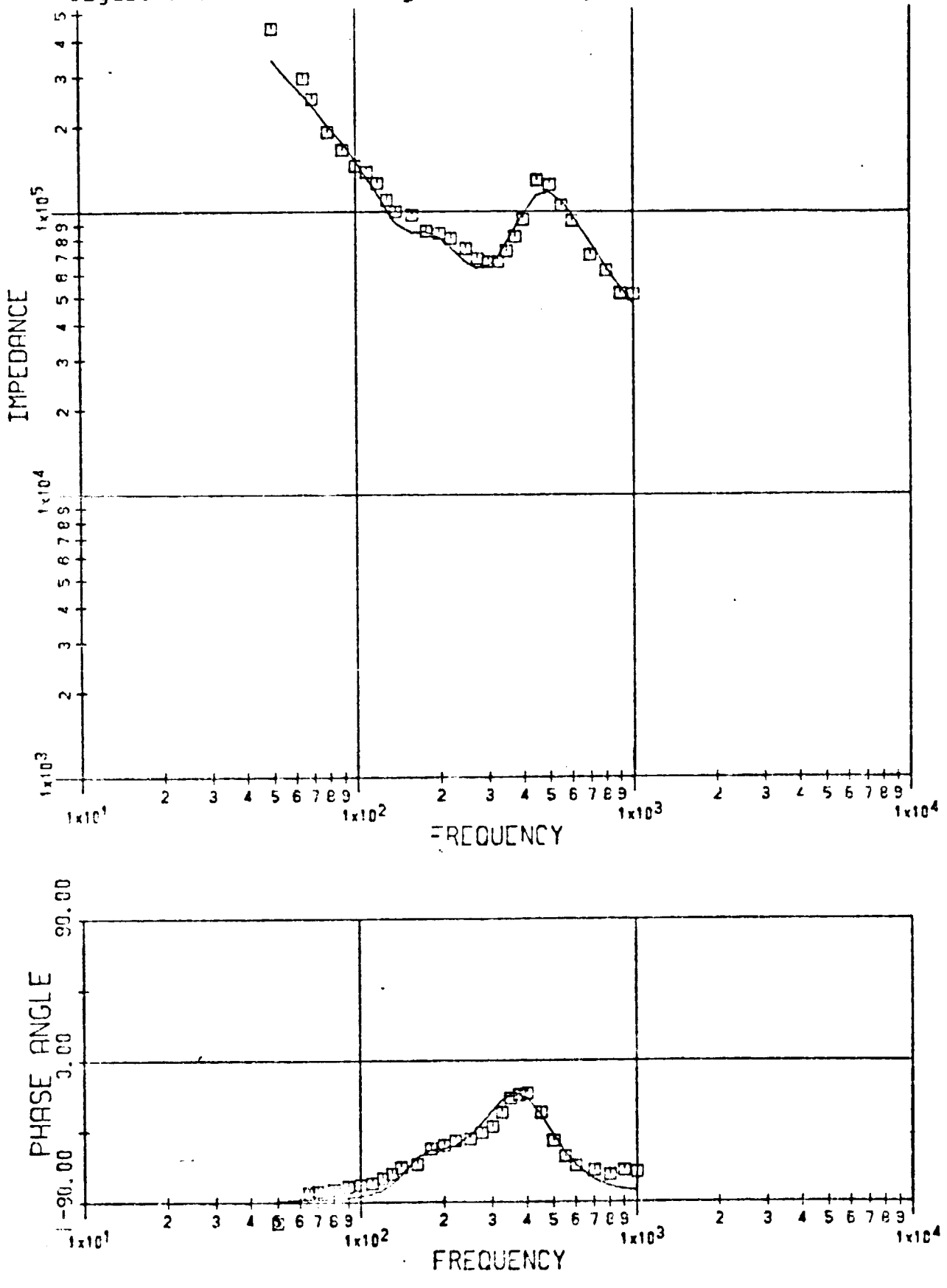

SUBJECT MO 500 GM PRELOAD

Figure G.15. DPMI of Subject MO: 600 gm Preload.

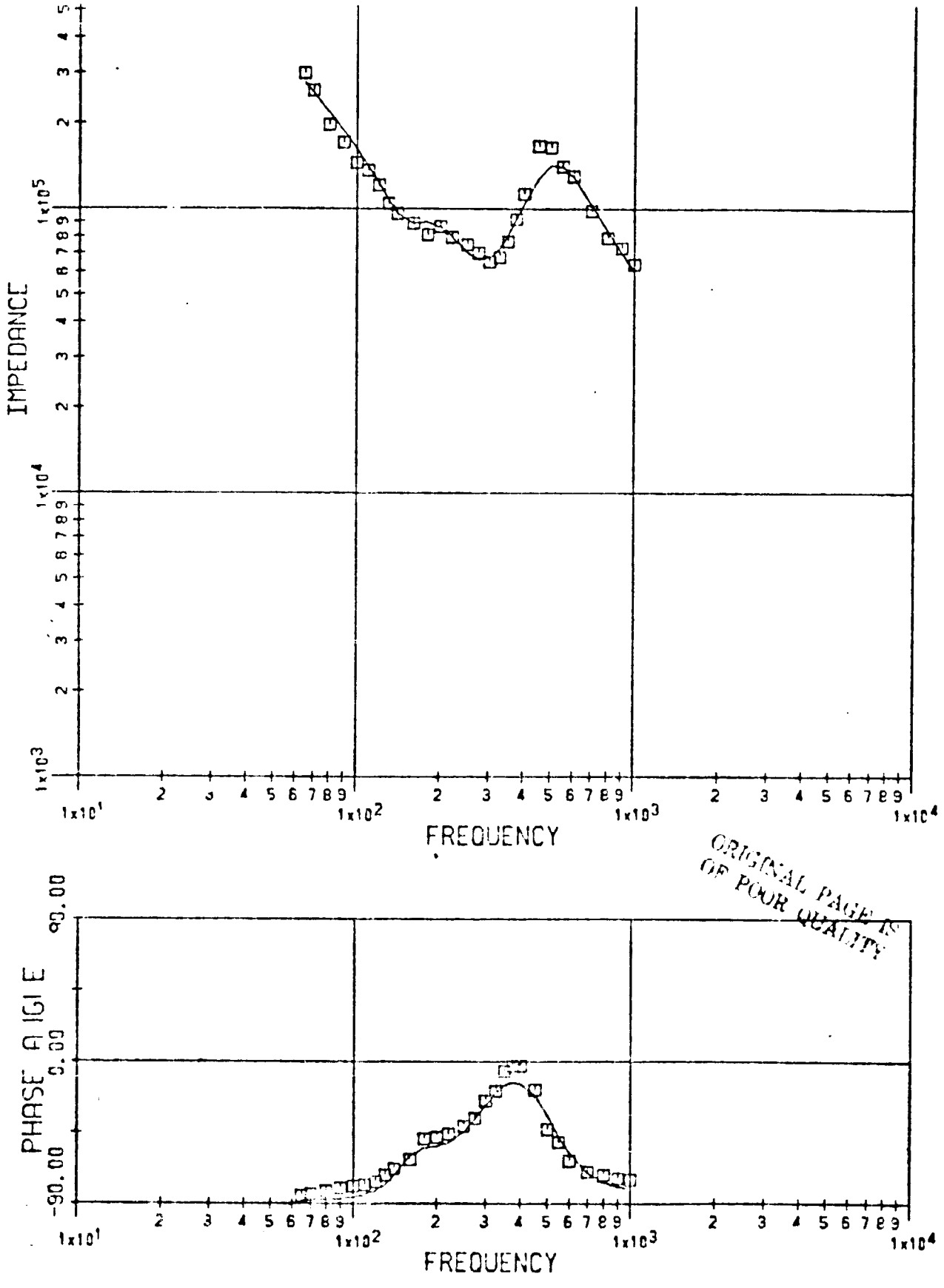

SUBJECT MO 600 GM PRELOAD

Figure G.16. DPMI of Subject SS: 400 gm Preload.

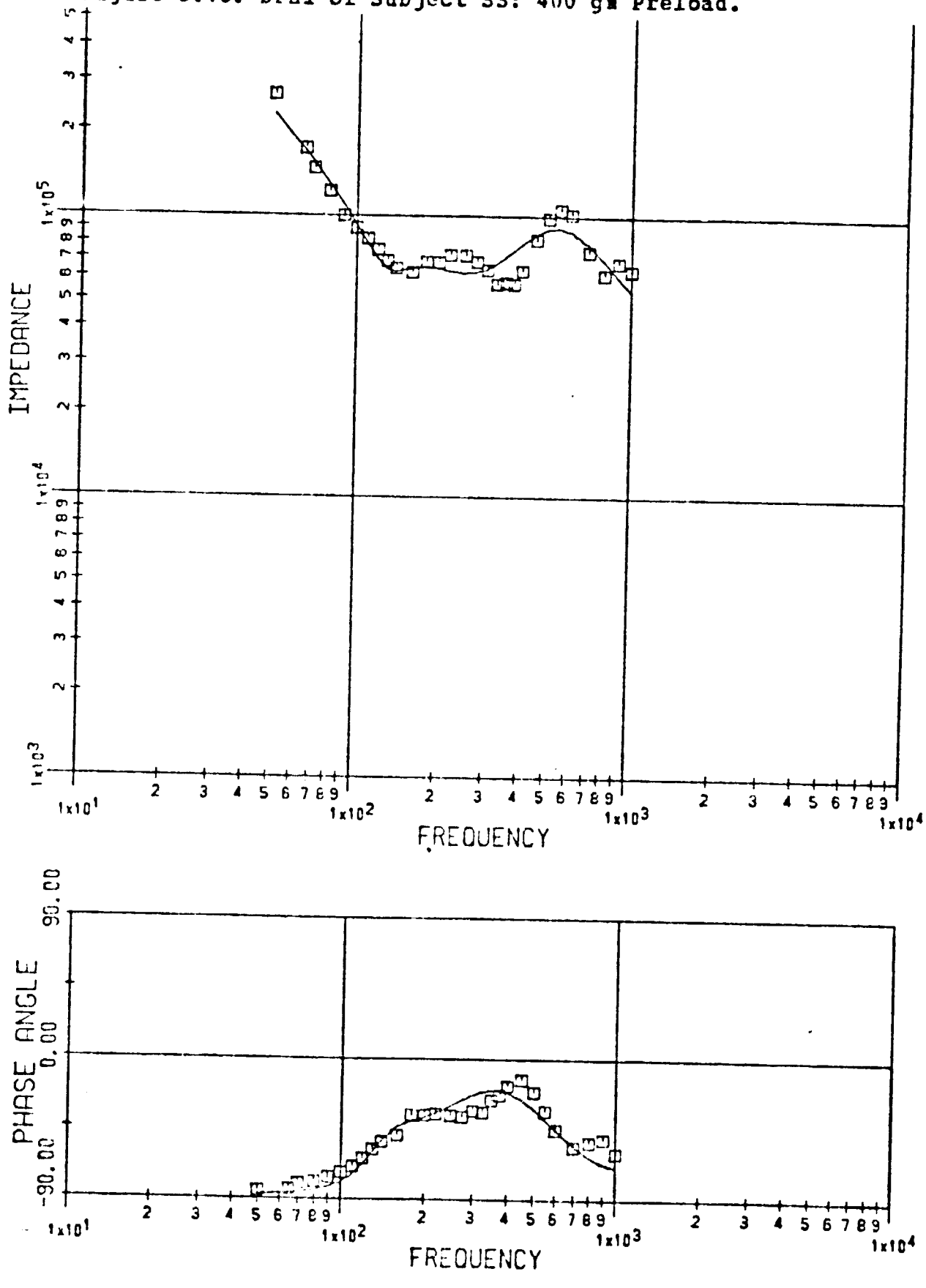

Figure G.17. DPMI of Subject SS: 500 gm Preload.

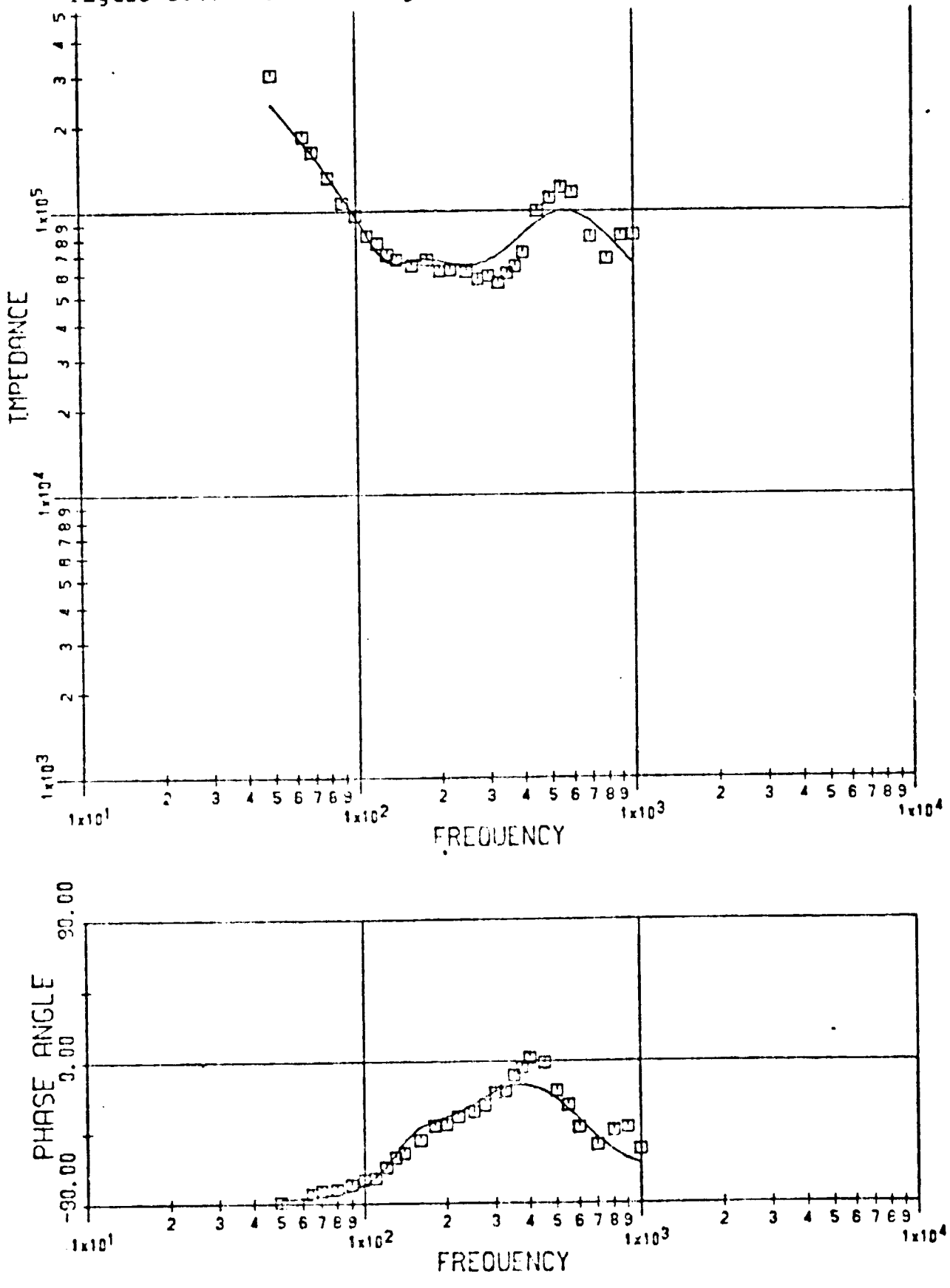

Figure G.18. DPMI of Subject SS: 600 gm Preload.

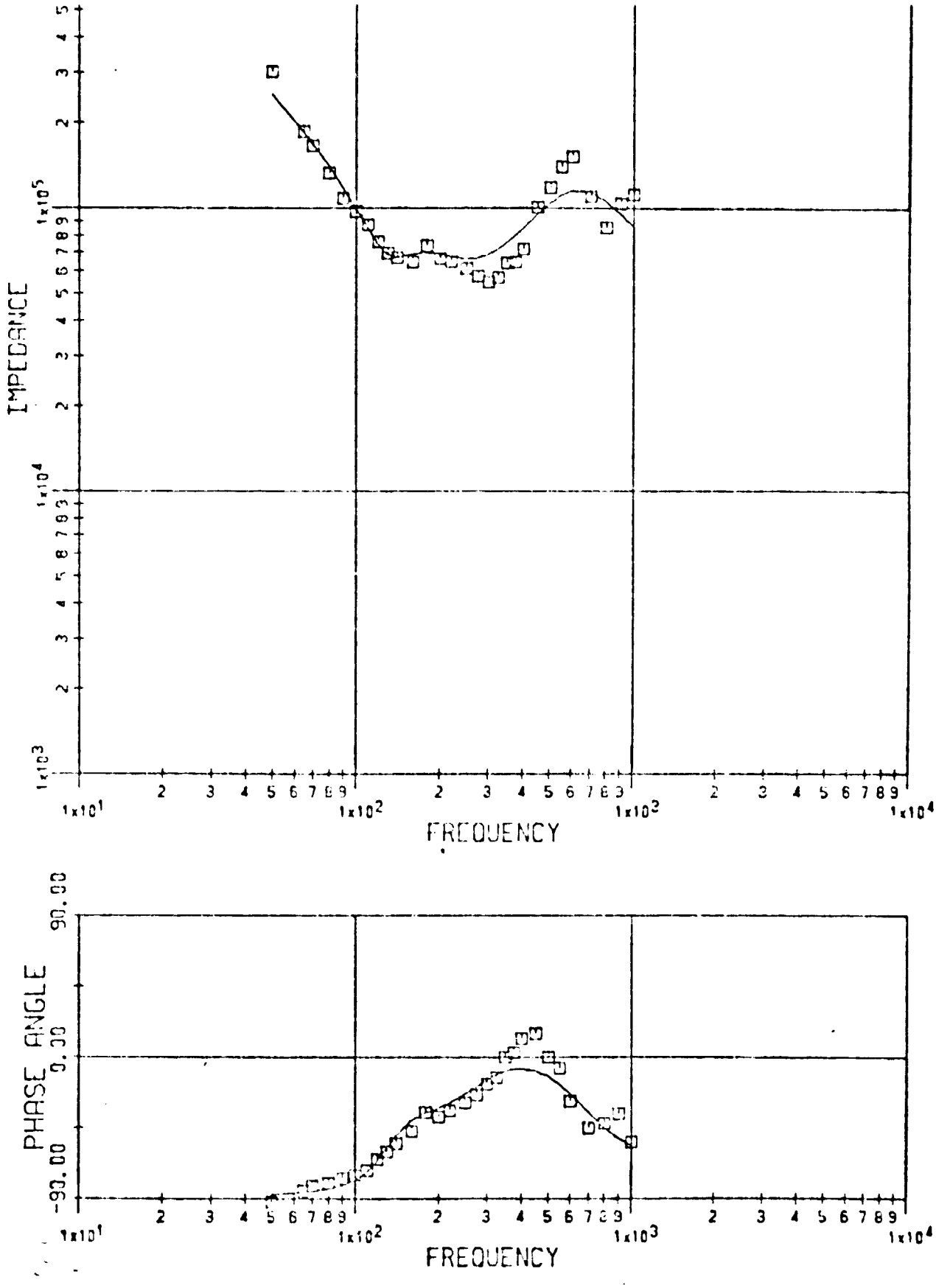

SUBJECT SS 600 GM PRELOAD

Figure G.19. DPMI of Subject VG: 400 gm Preload.

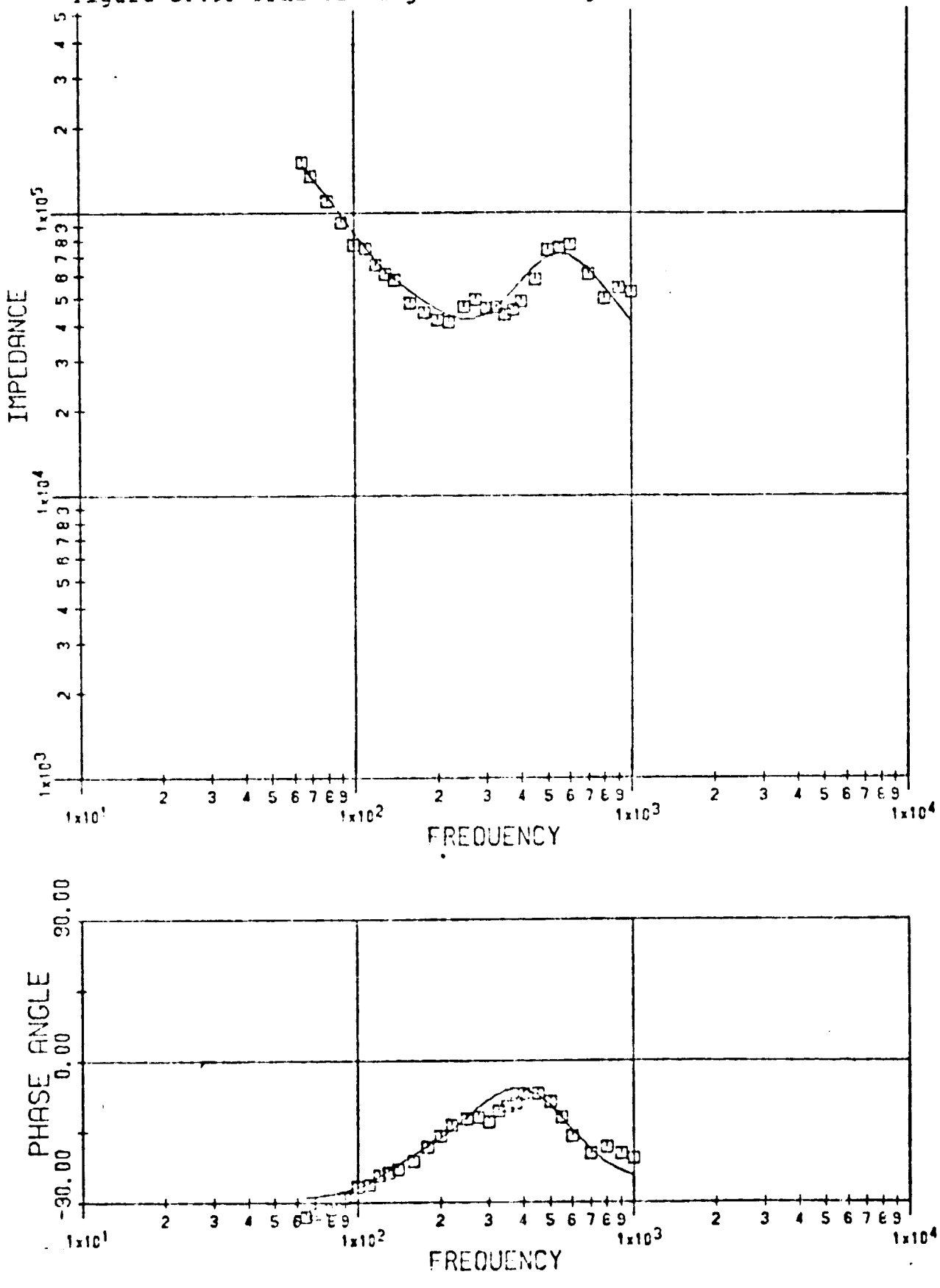

Figure G.20. DPMI of Subject VG: 500 gm Preload.

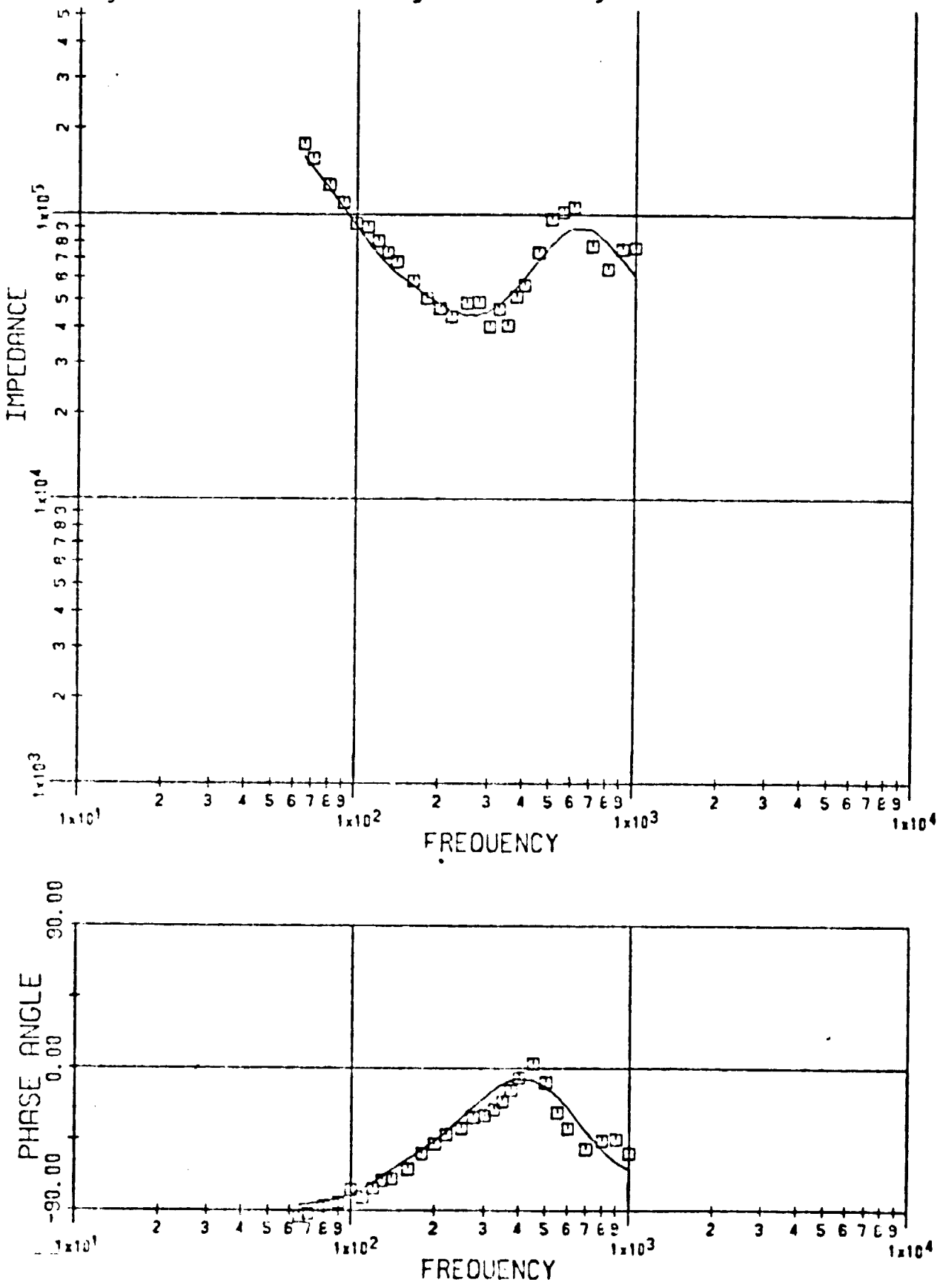

SUBJECT VG 500 GM PRELOAD

Figure G.21. DPHI of Subject VG: 600 gm Preload.

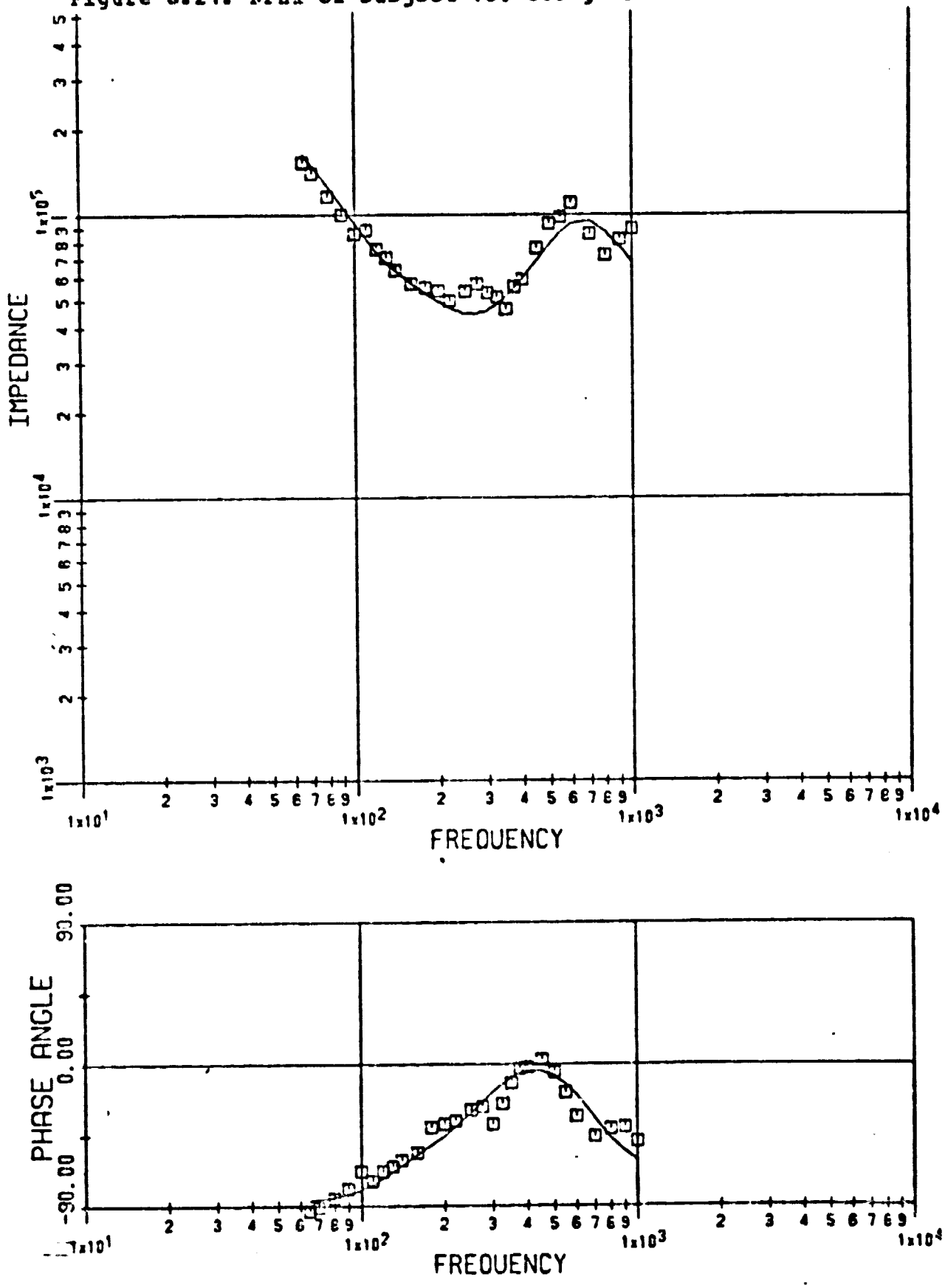

SUBJECT VG 600 GM PRELOAD

REFERENCES

Abendschein, W., and Hyatt, G. W., 1972, "Ultrasonics and Physical Properties of Healing Bone," Journal of Trauma, Vol. 12, pp. 297-301.

Abendschein, W. And Hyatt, G. W., 1970, "Ultrasonics and Selected Physical Properties of Bone," Clinical Orthopaedics and Related Research, Vol. 69, pp. 294-301.

Borders, S., Petersen, K. R., and Orne, D., 1977, "Predictions of Bending Strength of Long Bones from Measurements of Bending Stiffness and Bone Mineral Content," Journal of Biomechanical Engineering, Transactions of A.S.M.E., Vol. 99, pp. 40-44.

Bourgois, R., and Burny, F., 1972, "Measurements of Stiffness of Fracture Callus in Vivo; a Theoretical Study," Journal of Biomechanics, Vol. 5, pp. 85-91.

Cambell, J. And Jurist, J. M., 1971, "Mechanical Impedance of the Femur: A Preliminary Report," Journal of Biomechanics, Vol. 4, pp. 319-322.

Craven, J. D., Costinini, M. A., Greenfield, M. A., and Stern, R., 1973, "Measurement of the Velocity of Ultrasound in Human Cortical Bone and its Potential Clinical Importance," Investigative Radiology, Vol. 8, pp. 72-77.

Deitrick, J. E., Whedon, G. D., and Shorr, E., 1948, "Effects of Immobilization Upon Various Metabolic and Physiologic Functions of Normal Man," American Journal of Medicine, Vol. 4, pp. 3-36.

Doherty, W. P., Bovill, E. G., and Wilson, E. L., 1974, "Evaluation of the Use of Resonant Frequencies to Characterize Physical Properties of Human Long Bones," Journal of Biomechanics, Vol. 7, pp. 559-561.

Entrekin, R. R., and Abrams, C. F., 1976, "In Vivo Determination of the Dynamic Mechanical Properties of Long Bones," 29th A. C. E. M. B., p. 103.

Faires, V. M., 1965 Design of Machine Elements, Fourth Edition, Macmillan Co., New York.

Garner, E. R., and Blackketer, D. O., 1975, "In Vivo Determination of Macroscopic Biological Material Properties," Journal of Engineering Materials and Technology, Transactions of A. S. M. E., Vol. 97, pp. 350-356.

Gorman, D. J., 1975, Free Vibration Analysis of Beams and Shafts, John Wiley & Sons, New York.

Greenfield, M. A., Craven, J. D., Nishko, D. S., Huddleston, A. L., Friedman, R., and Stern, R., 1975, "The Modulus of Elasticity of Human Cortical Bone: An In Vivo Measurement and its Clinical Applications," Radiology, Vol. 115, pp. 163-166.

Hoeksema, H. D., and Jurist, J. M., 1977, "Resonant Frequency and Strength of Healing Dog Femora," presented at the 23rd Annual O. R. S. Convention Center, Las Vegas, p. 109.

International Business Machines Corp., Copyright 1966, 1967, 1968, System/360 Scientific Subroutine Package, Version III, Program Manuel, fifth edition, International Business Machines, pp. 121-124.

Jurist, J. M., 1970, "In Vivo Determination of the Plastic Response of Bone: I. Method of Ulnar Resonant Frequency," Physics in Medicine and Biology, Vol. 15, pp. 417-426.

Jurist, J. M., and Foltz, A. S., 1977, "Human Ulnar Bending Stiffness, Mineral Content, Geometry and Strength," Journal of Biomechanics, Vol. 10, pp. 455-459.

Jurist, J. M., and Kianian, K., 1973, "Three Models of the Vibrating Ulna," Journal of Biomechanics, Vol. 6, pp. 331-342.

Krane, S. M., 1977, "Metabolic Bone Disease," 1977, Harrison's Principles of Internal Medicine, eighth edition, p. 2028, McGraw-Hill Book Co., New York.

Markey, E., and Jurist, J. M., 1974, "Tibial Resonant Frequency Measurements as an Index of the Strength of Fracture Healing," Wisconsin Medical Journal, Vol. 73, pp. 62-65.

Mather, B., 1967a, "Comparison of Two Formulae for In Vivo Prediction of Strength of the Femur," Aerospace Medicine, Vol. 38, pp. 1270-1272.

Mather, B., 1967b, "Correlations Between Strength and Other Properties of Long Bones," Journal of Trauma, Vol. 7, pp. 633-638.

Orne, D., 1974, "The In Vivo, Driving Point Impedance of the Human Ulna - A Viscoelastic Beam Model," Journal of Biomechanics, Vol. 7, pp. 249-257.

Orne, D., 1976, "The Application of Mechanical Impedance Testing and Bone Mineral Measurement to Skeletal Status Evaluation of Human Cadavers," Third Annual International Workshop of Human Subjects for Biomechanical Research, sponsored by U. S. Dept. of Transportation, San Diego, Nov. 1975.

Orne, D., and Mandke, J., 1975, "The Influence of Musculature on the Mechanical Impedance of the Human Ulna, an In Vivo Simulated Study," Journal of Biomechanics, Vol. 8, pp. 143-148.

Petersen, K. R., 1977, Noninvasive Determination of Bone

Stiffness, Ph.D. Dissertation, Department of Applied Mechanics, Stanford University, Palo Alto, Cal.

Piziali, R. L., Wright, T. M., and Nagel, D. A., 1976, "An Extended Structural Analysis of Long Bones - Application to the Human Tibia," Journal of Biomechanics Vol. 9, pp. 695-701.

Rowe, J. W., Wheble, V. M., 1972, Concise Textbook of Anatomy and Physiology, third edition, p. 49, Churchill Livingston, Edinburgh.

Saha, S. And Lakes, R. S., 1977, "The Effects of Soft Tissue on Wave Propagation and Vibration Tests for Determining the In Vivo Properties of Bone," Journal of Biomechanics, Vol. 10, pp. 393-401.

Selle, W. A., and Jurist, J. M., 1966, "Acoustical Detection of Senile Osteoporosis," Proceedings of the Society for Experimental Biology and Medicine, Vol. 121, pp. 150-152.

Speigl, P. And Jurist, J. M., 1975, "Prediction of Ulnar Resonant Frequency," Journal of Biomechanics, Vol. 8, pp. 213-217.

Thompson, G. A., 1973, "In Vivo Determination of Bone Properties from Mechanical Impedance Measurement," abstract in Aerospace Medical Association Annual Science Meeting, Las Vegas, pp. 133-134.

Thompson, G. A., Orne, D., and Young, D. R., 1976, "In Vivo Determination of Mechanical Properties of the Human Ulna by Means of Mechanical Impedance Tests: Experimental Results and Improved Mathematical Model," Medical and Biological Engineerin, Vol. 14, pp. 253-262.

Thomson, W. T., 1972, Theory of Vibration with Applications, p. 47, Prentice Hall, Inc., Englewood Cliffs.

Whedon, G. D., Lutwak, L., Rambaut, P., Whittle, M., Leach, C., Reid, J., Smith, M., 1976, "Effects of Weightlessness on Mineral Metabolism; Metabolic Studies on Skylab Orbital Space Flights," Calcif. Tiss. Res. , Vol. 21, P. 123.

Whedon, G. D., Lutwak, L., Rambart, P. C., Whittle, M. W., Smith, M. C., Reid, J., Leach, C., Stadler, C. R., and Sanford, D. D., 1977, "Mineral and Nitrogen Metabolic Studies," Biomedical Results from Skylab, p. 164, National Aeronautics and Space Administration, Washington.

Young, D. R., Tremor, J. W., 1978, "Effect of Hypodynamic Simulations on the Skeletal System of Monkeys," to be published.

AUTOBIOGRAPHICAL STATEMENT

Stephen Borders
20173 Keating
Detroit, Michigan 48203

Personal

Birthdate: March 31, 1952
Marital Status: Married, no children

Education

Dec. 1979 — Ph.D. Mechanical Engineering (Minor in Mathematics)
Wayne State University
Detroit, Michigan

Dissertation:
Determination of In Vivo Mechanical Properties of Long Bones From Their Impedance Response Curves. Mathematical models of the forearm and leg were developed and a systems identification algorithm was developed to use the mathematical models to determine mechanical properties.

June 1975 — M.S. Mechanical Engineering Sciences
Wayne State University

June 1974 — B.S. Mechanical Engineering Sciences (With Distinction)
Wayne State University

Honors and Awards

University Graduate Fellowship (limit two years) held during academic years of 1974-75 and 1976-77.

Member of Tau Beta Pi, National Engineering Honor Society.

Member of Pi Tau Sigma, Mechanical Engineering Honor Society.

Dean's List (undergraduate).

Grade Point Average: Undergraduate 3.56, Graduate 3.93.

Publications

"Prediction of Bending Strength of Long Bones From Measurements of Bending Stiffness and Bone Mineral Content", Borders, Petersen and Orne, Journal of Biomechanical Engineering, Transactions of the ASME, February, 1977.

Work Experience

June 1974 to June 1979 — Graduate Assistant and Research Assistant
Wayne State University

1974-78 Worked on research project under direction of Prof. David Orne which developed into dissertation topic (see dissertation above). Duties included development of mathematical models and computer programs, including some experience in computer graphics (Cal-Comp plotter and Tektronix graphics terminal). Also wrote computer programs and worked in the labs with other projects.

1978-79 Taught the following courses:

Sprg 78	Statics	
Fall 78	Statics	(two sections)
Wint 79	Statics	Dynamics
Sprg 79	Dynamics	

Duties included preparing and giving lectures, giving and grading exams and grading homework.

1975-76, 1977-78 Graded homework for several different courses.

Apr. 1970 to June 1974 — Machinist
Radar Tool and Manufacturing Co., Detroit, MI
Duties included setting up and running milling machines, drill presses, lathes, etc., part time during undergraduate work and full time during summer.

Aug. 1969 to Jan. 1970 — Draftsman and Blue Print Machine Operator
Dollar Design Co., Madison Heights MI
Duties included making detail drawings from assembly drawings and running a blue print machine, part time during high school.